

**Self-assembled peptide
nanostructures: production,
structural characterization and *in*
vivo application as cancer
vaccine**

Mazda Rad Malekshahi

2015

The printing of this thesis was financially supported by:

Utrecht Institute for Pharmaceutical Sciences, Utrecht, The Netherlands



Self-assembled peptide nanostructures: production, structural characterization and *in vivo* application as cancer vaccine

Mazda Rad Malekshahi

Ph.D. Thesis

Department of Pharmaceutics, Utrecht Institute for Pharmaceutical Sciences (UIPS), Faculty of Science, Utrecht University, the Netherlands

ISBN: 978-90-393-6395-9

Print: Hadafnovin publication service

Copy right © 2015 by Mazda Rad Malekshahi

All rights reserved. No parts of this book may be reproduced in any form or by any means without permission of the author.

**Self-assembled peptide nanostructures:
production, structural characterization and *in vivo*
application as cancer vaccine**

**Zelfassemblerende peptide nanostructuren:
productie, structurele karakterisering en *in vivo*
toepassing als kankervaccin**

(met een samenvatting in het Nederlands)

Proefschrift

ter verkrijging van de graad van doctor aan de Universiteit Utrecht op
gezag van de rector magnificus, prof.dr. G.J. van der Zwaan, ingevolge
het besluit van het college voor promoties in het openbaar te verdedigen
op woensdag 23 september 2015 des middags te 12.45 uur

door

Mazda Rad Malekshahi

Geboren op 19 september 1981, te Kermanshah, Iran

Promotor **Prof. dr. ir. W. E. Hennink**

Copromotoren **Dr. E. Mastrobattista**

Dr. M. Amidi

“The ultimate measure of a man is not where he stands in moments of comfort, but where he stands at times of challenge and controversy”

Martin Luther King, Jr.

To My Family

Table of Contents

Chapter 1.....8

General Introduction

Chapter 2.....15

Biomedical applications of self-assembling peptides

Chapter 3.....51

Optimization of the recombinant production and purification of a self-assembling peptide in *Escherichia coli*

Chapter 4.....67

The supramolecular organization of a peptide-based nanocarrier at high molecular detail

Chapter 5.....106

Synthesis and characterization of Self-Assembling Peptide Epitopes (SAPes) for prophylactic and therapeutic cancer immunotherapy

Chapter 6.....131

Synthesis and characterization of a Self-Assembling Peptide Epitopes (SAPE) for therapeutic cancer immunotherapy in TC-1 tumor-bearing mice

Chapter 7.....147

Summarizing Discussion and Future Perspectives

Appendices158

Nederlandse samenvatting

Acknowledgments

Curriculum Vitae

List of publications

Chapter 1

General introduction

1. Introduction

Molecular self-assembly is a process in which initially disordered molecules spontaneously adopt a defined supramolecular arrangement through local interactions such as hydrogen bonding, metal coordination, π - π interactions, hydrophobic and van der Waals forces. Molecular self-assembly is a key concept in nature¹. To explain, complex quaternary structures of proteins (e.g. viral capsids, apoptosomes), double stranded DNA, bilayer cell membranes and many other biomacromolecules are formed based on self-assembly patterns. In fact it is believed that self-assembly of biomolecules into discrete compartments is the driving force of natural evolution². By comprehensively examining the self-assembly principles found in nature we can now start to design and create new biomaterials with unique features. For example, *de novo* designed peptides have shown to assemble into various structures for applications in materials and biomedical sciences. In addition, peptides can be modified with lipids or synthetic and natural polymers to gain even more flexibility in the self-assembling properties. Because of these features, self-assembling peptides are interesting materials to design discrete nanomaterials for pharmaceutical and biomedical applications.

2. Amphiphilic peptides

Amphiphilic peptides (Aps) are peptides with sequestered hydrophobic and hydrophilic domains. Their amphiphilic nature allows them to self-assemble through hydrophobic clustering into supramolecular structures, such as micelles, nanotubes, belts or vesicles³⁻⁵. Aps are highly versatile molecules that can readily be modified to contain biofunctional domains such as cell attachment sequences, signaling domains, vaccine epitopes and even therapeutic moieties. Many studies have been performed to explore their potential applications in different biomedical fields such as tissue regeneration⁶⁻¹³, drug and vaccine delivery¹⁴⁻¹⁸, and stent coatings¹⁹.

Zhang *et al.* introduced surfactant like peptides (SLPs) as a class of amphiphilic peptides consisting of a short hydrophilic head group of a few amino acids and a hydrophobic tail comprising either 6 alanine, valine or leucine residues (A6D, V6D1/2 or L6D2 respectively). Dispersion of these peptides in an aqueous medium formed supramolecular structures. TEM images indicated open-ended nanotubes with 30–50 nm in diameter and several micrometers in length, and also three-way junctions that linked nanotubes to each other. The proposed model for these peptides to self-assemble into a nanotube is that the monomers first form a bilayer, which then forms a closed ring. Subsequently, these rings stack on top of each other, which causes tube formation. Moreover, in the A6D and V6D aqueous samples interesting budding vesicles from the

nanotube stems were observed. Dynamic light scattering and TEM images revealed a dynamic conformation for these assemblies⁴.

Inspired by this concept, van Hell *et al.* designed a 10-aa amphiphilic peptide with a cone-shaped hydrophobic tail of 8 amino acid residues followed by 2 or 7 glutamic acid residues as charged head groups (SA2: Ac-AAVVLLWEE-COOH; SA7:Ac-AAVVLLWEEEEEE-COOH). When brought into an aqueous solution of pH 7.4 and above a critical concentration, the designed peptides assembled into nanovesicles of approx. 120 nm in diameter. Interestingly, extending the hydrophilic part of these self-assembling peptides from 2 to 7 glutamic acid residues had no effect on the self-assembling behaviour, with no change in vesicular shape and size^{3,20}. This striking features suggests some degree of flexibility in exposing peptide epitopes on the surface of these peptide vesicles.

With an increased understanding of the intricate interplay of forces that drive the self-assembly, we can now start to predict the self-assembling behavior of simple peptides. This is further aided by the development of advanced molecular dynamics simulations that enable researchers to predict the self-assembly behavior *in silico*, thereby offering a tremendous advantage in rational design of such self-assembling peptides.

3. Immunotherapy of cancer and cancer vaccines

Cancer is a group of diseases characterized by abnormal cell growth with the potential of tissue invasion and spread to other parts of the body. It is caused by the accumulation of genetic defects, either inherited or acquired, which together contribute to the malignant phenotype. In some cases, these genetic changes also result in an altered antigenic repertoire. The recognition of these minor changes in antigens by cells of the acquired immune system forms the basis of cancer immunotherapy.

Cancer vaccines aim to evoke a strong adaptive immune response against these tumor antigens²¹⁻²³. To be able to design an efficient vaccine it is essential to understand the mechanisms to elicit an antitumor immune response. The immune response elicited by vaccination is a multistep, complex process that involves the coordinated action of diverse molecular signals and immune cells within lymphoid organs. First, antigen presenting cells (APCs), amongst which dendritic cells (DCs), should internalize the antigens either at the site of injection or in the draining lymph nodes. Next, DCs process the antigen into short peptide fragments within lysosomal vacuoles or cytosol and load the fragments onto major histocompatibility complex (MHC) molecules to activate T cells. The entire process of antigen internalization, fragmentation and loading is called antigen

presentation. DCs play an important function in this by continuously probing the tissue in which they reside for potentially infectious material. Besides uptake of antigen, APCs need other signals such as inflammatory signals to become activated. Typically, adjuvants in vaccine formulations assist to provide these stimulatory signals. Activated DCs change in morphology and upregulate specific cell surface receptors (*i.e.* CCR7, CD86 and CD40), which is called maturation. Mature DCs migrate towards the lymph nodes where they present antigen in an MHC-restricted manner to T cells. If the DCs are appropriately activated, they are able to stimulate antigen-specific T cells to proliferate and differentiate into antigen-specific T cells that directly can kill infected cells (CD8+ “cytotoxic” T cells) or secrete cytokines to promote other immune cells (CD4+ “helper” T cells). In parallel, antigen is also recognized by antigen-specific B cells, that receive promoting signals from primed CD4+ T cells to differentiate into antibody-producing plasma cells that secrete copious amounts of antibody that will bind to pathogens and promote their clearance.

As mentioned above, DCs play a pivotal role in eliciting an efficient immune response. The way antigens are presented to them determines the quality and longevity of the induced immune response.

Several studies demonstrated that delivery of antigens in particulate form is able to induce a much stronger immune response than soluble forms of the same antigen. Such particulate systems have several advantages over soluble form of the antigens such as a) protection of the antigen and adjuvant from premature enzymatic and proteolytic degradation, b) prolongation of the residence time in tissue and thus the chance of internalization by DCs c) increased cellular uptake by APCs to trigger a strong immunostimulatory cascade. d) co-delivery of two or more antigens or adjuvants to DCs for modulating immune responses²⁴⁻²⁶.

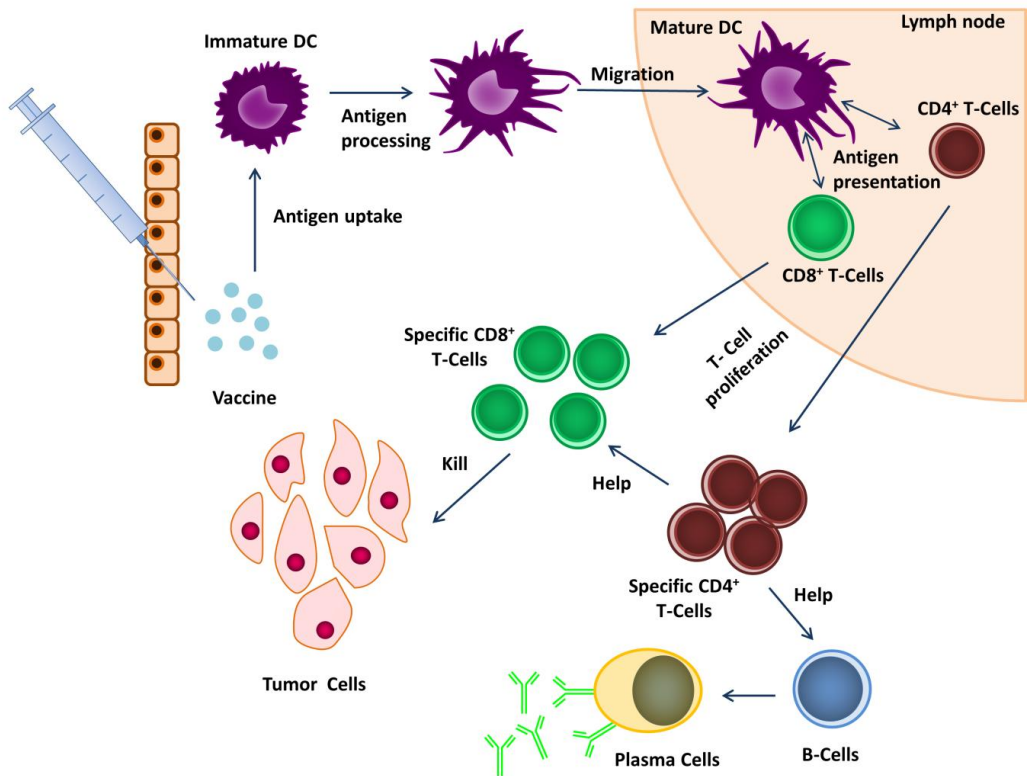


Figure 1. Summary of different steps and main immune cells involved in an anti-tumor immune response. Antitumor immune responses begin with the uptake of cancer vaccines by immature DCs. Next, the DCs process the antigen for (cross)-presentation on MHC class I or class II molecules. In the presence of costimulatory molecules DCs mature while migrating to the draining lymph nodes. In lymph nodes, matured DCs activate T cells, and subsequently activated T cells proliferate and migrate to tumor bed where T cells can recognize and lyse the tumor cells in a MHC class I dependent way.

Since the majority of epitopes used for cancer vaccination are small peptides, the utilization of peptide self-assembly to deliver peptide epitopes in a nanoparticulate form represents an interesting approach, which offers several advantages over existing particulate vaccine delivery systems, such as polymeric and lipidic nanocarriers including ease of production, high density of antigen epitopes and direct conjugation of ligands or adjuvants to the peptides. Moreover, multiple epitopes can be combined at will within these peptide assemblies with preservation of the high loading efficiency^{25–28}.

4. Aim of this Thesis

In this thesis, we capitalize on the previous work done in our group with SA2 peptides and apply peptide self-assembly as a means to obtain peptide nanoparticles that can be used for vaccination.

The main objectives of this thesis are:

- i) To better understand the dynamics of self-assembly of SA2 and characterize the self-assembling structures at the molecular level.
- ii) To utilize self-assembling peptides derived from SA2 to deliver peptide epitopes into antigen presenting cells for tumor vaccination.

In addition to these two main objectives, we also attempted to optimize the recombinant production of SA2 peptides in *E. coli*.

5. Outline

Chapter 2 provides a general overview of self-assembling peptides. The first part of this chapter covers the different secondary structures that peptides can adopt which are important for the further assembly into highly-ordered nanostructures, such as micelles, vesicles, fibrils, and tubes. The second part gives an overview of the recent literature on studies in peptide self-assembly for application in drug delivery, vaccination, and tissue engineering.

Chapter 3 focuses on the optimization of the recombinant production of SA2 peptides in *E. coli* as a cost-effective way to produce large quantities of these peptides for vaccination purposes. First, this chapter describes how the production yields of the SA2 peptide can be improved by using a SUMO fusion construct and a well-balanced auto-induction medium. Second, it describes the optimization of the purification steps by preventing premature self-assembly of the SA2 peptide within the *E. coli* host leading to increased yields during production and less loss of the peptide during purification.

Chapter 4 presents an avenue to the high-resolution structural characterization of peptide-based nanovesicles and their assembly pathway based on the example of the nanocarrier formed by the SA2 peptide. By integrating a multitude of experimental techniques (*i.e.* solid-state NMR, AFM, SLS, DLS, FT-IR, CD) with large- and multi-

scale MD simulations, it is demonstrated that SA2 nanocarriers consist of interdigitated antiparallel β -sheets, which bear little resemblance to phospholipid liposomes.

In **Chapter 5 and 6**, the potential use of the self-assembling peptide as a carrier for peptide-based vaccine in prophylactic and therapeutics models is investigated. **Chapter 5** describes the capability of a designed vaccine based on peptide self-assembly to induce OVA-specific immune responses and to delay tumor growth were tested in mice bearing OVA-expressing B16 melanoma cells both prophylactic and therapeutic setting. To establish and explore the ability of peptide self-assembly as a platform for delivery of minimal soluble epitopes, **Chapter 6** describes the *in vivo* effectiveness another designed self-assembling peptide bearing human papillomavirus antigens (HPV 16 E744-57) in a therapeutic setting.

Chapter 7 is a brief summary of the aforementioned chapters, and future perspectives of self-assembling peptides for biomedical applications are proposed.

6. References:

- (1) Zhang, S. (2002) Emerging biological materials through molecular self-assembly. *Biotechnol. Adv.* 20, 321–339.
- (2) Szostak, J. W., Bartel, D. P., and Luisi, P. L. (2001) Synthesizing life. *Nature* 409, 387–390.
- (3) Van Hell, A. J., Costa, C. I. C. A., Flesch, F. M., Sutter, M., Jiskoot, W., Crommelin, D. J. A., Hennink, W. E., and Mastrobattista, E. (2007) Self-assembly of recombinant amphiphilic oligopeptides into vesicles. *Biomacromolecules* 8, 2753–2761.
- (4) Santoso, S., Hwang, W., Hartman, H., and Zhang, S. (2002) Self-assembly of Surfactant-like Peptides with Variable Glycine Tails to Form Nanotubes and Nanovesicles. *Nano Lett.* 2, 687–691.
- (5) Vauthey, S., Santoso, S., Gong, H., Watson, N., and Zhang, S. (2002) Molecular self-assembly of surfactant-like peptides to form nanotubes and nanovesicles. *Proc. Natl. Acad. Sci. U. S. A.* 99, 5355–5360.
- (6) Hauser, C. A. E., and Zhang, S. (2010) Designer self-assembling peptide nanofiber biological materials. *Chem. Soc. Rev.* 39, 2780–2790.
- (7) Semino, C. E. (2008) Self-assembling Peptides: From Bio-inspired Materials to Bone Regeneration. *J. Dent. Res.* 87, 606–616.
- (8) Cormier, A. R., Pang, X., Zimmerman, M. I., Zhou, H.-X., and Paravastu, A. K. (2013) Molecular structure of RADA16-I designer self-assembling peptide nanofibers. *ACS Nano* 7, 7562–7572.
- (9) Zhang, S., Greenfield, M. A., Mata, A., Palmer, L. C., Bitton, R., Mantei, J. R., Aparicio, C., de la Cruz, M. O., and Stupp, S. I. (2010) A self-assembly pathway to aligned monodomain gels. *Nat. Mater.* 9, 594–601.
- (10) Sargeant, T. D., Guler, M. O., Oppenheimer, S. M., Mata, A., Satcher, R. L., Dunand, D. C., and Stupp, S. I. (2008) Hybrid bone implants: self-assembly of peptide amphiphile nanofibers within porous titanium. *Biomaterials* 29, 161–171.
- (11) Lee, S. S., Huang, B. J., Kaltz, S. R., Sur, S., Newcomb, C. J., Stock, S. R., Shah, R. N., and Stupp, S. I. (2013) Bone regeneration with low dose BMP-2 amplified by biomimetic supramolecular nanofibers within collagen scaffolds. *Biomaterials* 34, 452–459.
- (12) Berns, E. J., Sur, S., Pan, L., Goldberger, J. E., Suresh, S., Zhang, S., Kessler, J. A., and Stupp, S. I. (2014) Aligned neurite outgrowth and directed cell migration in self-assembled monodomain gels. *Biomaterials* 35, 185–195.

- (13) Webber, M. J., Tongers, J., Newcomb, C. J., Marquardt, K.-T., Bauersachs, J., Losordo, D. W., and Stupp, S. I. (2011) Supramolecular nanostructures that mimic VEGF as a strategy for ischemic tissue repair. *Proc. Natl. Acad. Sci. U. S. A.* *108*, 13438–13443.
- (14) Matson, J. B., Newcomb, C. J., Bitton, R., and Stupp, S. I. (2012) Nanostructure-templated control of drug release from peptide amphiphile nanofiber gels. *Soft Matter* *8*, 3586–3595.
- (15) Webber, M. J., Matson, J. B., Tamboli, V. K., and Stupp, S. I. (2012) Controlled release of dexamethasone from peptide nanofiber gels to modulate inflammatory response. *Biomaterials* *33*, 6823–6832.
- (16) Matson, J. B., Webber, M. J., Tamboli, V. K., Weber, B., and Stupp, S. I. (2012) A peptide-based material for therapeutic carbon monoxide delivery. *Soft Matter* *8*, 2689–2692.
- (17) Van Hell, A. J., Fretz, M. M., Crommelin, D. J. A., Hennink, W. E., and Mastrobattista, E. (2010) Peptide nanocarriers for intracellular delivery of photosensitizers. *J. Control. Release* *141*, 347–353.
- (18) Gudlur, S., Sukthankar, P., Gao, J., Avila, L. A., Hiromasa, Y., Chen, J., Iwamoto, T., and Tomich, J. M. (2012) Peptide nanovesicles formed by the self-assembly of branched amphiphilic peptides. *PLoS One* *7*, e45374.
- (19) Kushwaha, M., Anderson, J. M., Bosworth, C. A., Andukuri, A., Minor, W. P., Lancaster Jr., J. R., Anderson, P. G., Brott, B. C., and Jun, H.-W. (2010) A nitric oxide releasing, self assembled peptide amphiphile matrix that mimics native endothelium for coating implantable cardiovascular devices. *Biomaterials* *31*, 1502–1508.
- (20) Van Hell, A. J., Klymchenko, A., Burgers, P. P., Moret, E. E., Jiskoot, W., Hennink, W. E., Crommelin, D. J. A., and Mastrobattista, E. (2010) Conformation and intermolecular interactions of SA2 peptides self-assembled into vesicles. *J. Phys. Chem. B* *114*, 11046–11052.
- (21) Itoh, K., Yamada, A., Mine, T., and Noguchi, M. (2009) Recent advances in cancer vaccines: An overview. *Jpn. J. Clin. Oncol.* *39*, 73–80.
- (22) Cuppens, K., and Vansteenkiste, J. (2014) Vaccination therapy for non-small-cell lung cancer. *Curr. Opin. Oncol.* *26*, 165–170.
- (23) Melero, I., Gaudernack, G., Gerritsen, W., Huber, C., Parmiani, G., Scholl, S., Thatcher, N., Wagstaff, J., Zielinski, C., Faulkner, I., and Mellstedt, H. (2014) Therapeutic vaccines for cancer: an overview of clinical trials. *Nat. Rev. Clin. Oncol.* *11*, 509–524.
- (24) Rudra, J. S., Mishra, S., Chong, A. S., Mitchell, R. A., Nardin, E. H., Nussenzweig, V., and Collier, J. H. (2012) Self-assembled peptide nanofibers raising durable antibody responses against a malaria epitope. *Biomaterials* *33*, 6476–6484.

- (25) Black, M., Trent, A., Tirrell, M., and Olive, C. (2010) Advances in the design and delivery of peptide subunit vaccines with a focus on toll-like receptor agonists. *Expert Rev. Vaccines* 9, 157–73.
- (26) De Temmerman, M.-L., Rejman, J., Demeester, J., Irvine, D. J., Gander, B., and De Smedt, S. C. (2011) Particulate vaccines: on the quest for optimal delivery and immune response. *Drug Discov. Today* 16, 569–582.
- (27) Chen, J., Pompano, R. R., Santiago, F. W., Maillat, L., Sciammas, R., Sun, T., Han, H., Topham, D. J., Chong, A. S., and Collier, J. H. (2013) The use of self-adjuvanting nanofiber vaccines to elicit high-affinity B cell responses to peptide antigens without inflammation. *Biomaterials* 34, 8776–8785.
- (28) Rudra, J. S., Sun, T., Bird, K. C., Daniels, M. D., Gasiorowski, J. Z., Chong, A. S., and Collier, J. H. (2012) Modulating adaptive immune responses to peptide self-assemblies. *ACS Nano* 6, 1557–1564.

Chapter 2

Biomedical applications of self-assembling peptides

Mazda Rad-Malekshahi, Ludwijn Lempsink, Maryam Amidi, Wim E. Hennink and Enrico Mastrobattista

Department of Pharmaceutics, Utrecht Institute for Pharmaceutical Sciences, Utrecht University,
Utrecht, The Netherlands

Submitted for publication

Abstract

Self-assembling peptides have gained increasing attention as versatile molecules to generate diverse supramolecular structures with tunable functionality. Because of the possibility of integrating a wide range of biofunctional domains into self-assembling peptides such as cell attachment sequences, signaling domains, vaccine epitopes and even therapeutic moieties, many studies have been performed to explore their potential applications in different biomedical fields.

The first part of the review covers the different secondary structures and a variety of nanostructures formed by several known self-assembling peptides. Next, an overview of the literature is given that discusses the recent studies in peptide self-assembly for application in drug delivery, vaccination and tissue engineering.

1. Introduction

With our increasing understanding of the mechanisms of protein folding we have now reached a stage that we can begin to build peptides and proteins to assemble into predefined, but complex structures for diverse applications in materials and biomedical sciences. Through rational design and engineering of (poly)peptides many different kinds of assemblies can be formed, all driven by inter- and intramolecular forces such as hydrogen bond formation, hydrophobic and electrostatic interactions, van der Waals forces and π - π stacking. Moreover, peptides can be modified with lipids or synthetic and natural polymers to gain even more flexibility in the self-assembling properties. Because of these features, self-assembling peptides are interesting candidates for pharmaceutical and biomedical applications.

This review will focus on the pharmaceutical applications of self-assembling peptides. First, a tutorial overview will be given of the various secondary structures that peptides can adopt that facilitate the formation of well-defined supramolecular structures. Second, different types of self-assembling peptides will be discussed, focusing on their biomedical applications such as drug carrier systems, vaccine formulation, and tissue engineering. Although the field of self-assembling peptides is rather broad, this review will exclusively focus on unmodified peptides < 30 amino acids or peptides with small chemical modifications at the N- or C-terminus that have an intrinsic capacity to self-assemble into ordered supramolecular architectures. We will not discuss the literature on peptides that are conjugated to large chemical structures (e.g. hydrophobic moieties, polymers) in which these chemical structures dictate self-assembly.

2. Secondary structures

Since the supramolecular self-assembly of peptides is governed by the way these individual peptides fold in aqueous solution, it is important to understand which secondary structures exist and how these can be used for self-assembly.

2.1. α -helix

Alpha helices are a type of protein secondary structure of which the amino acids have a tendency to form hydrogen bonds between the oxygen of the carbonyl group and the hydrogen of every third amide group, providing some stabilisation to the peptide backbone. The side chains of the amino acids extend outward from the outer surface of the α -helix¹. The α -helix is in itself not a thermodynamically stable conformation, but by assembling together with other α -helices, a more stable structure is created^{2,3}. A typical assembly of α -helices is the coiled coil.

2.1.1. Coiled-coil

The coiled-coil structure is a structure that is often found in nature. It consists of two or more α -helices intertwined with each other in a way that the hydrophobic parts are excluded from the aqueous environment⁴. The molecular basis for this structure is the repeated heptad sequence: (abcdefg)_n. In this amino acid sequence, positions a and d are occupied by amino acids with hydrophobic side chains and e and g are often charged amino acid residues. Peptides conforming to these rules will form into a right-handed α -helical shape, assembling into helical bundles with left-handed supercoils. Adequately designed coiled coils can self-assemble into larger supramolecular assemblies such as nanofibrils or nanoparticles, structurally supported by the hydrophobic interactions between the amino acids at positions a and d and the electrostatic interactions between the amino acids at position e and g^{5,6}. A more thorough explanation of coiled-coils can be found in a review by Woolfson⁶.

2.2. β -sheet

Another type of secondary protein structure, apart from the α -helix is the β -strand. In a β -strand, the peptide backbone is stretched, and the hydrogen bonding groups point orthogonally to the direction of the peptide chain. When β -strands are connected laterally through hydrogen bonding, they form a β -sheet⁷. The sheet-like structure is created by the hydrogen bonds between the amino acids in different peptide strands (Figure 1). The interpeptide and interchain bonds add considerably to the rigidity of the structure⁸. Peptides that are prone to form β -sheets and self-assemble into supramolecular structures are usually around 16-20 amino acids long and often feature alternating patterns of hydrophobic and polar amino acids. Most β -sheet forming peptides currently described for self-assembly form indefinite assemblies, i.e. assemblies with no discrete dimensions^{9,10}.

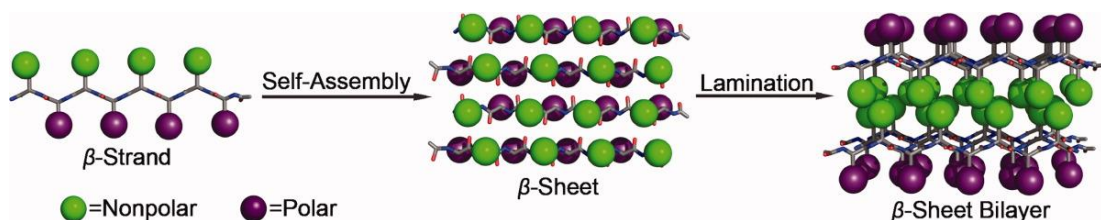


Figure 1. The arrangement of amino acids in amphipathic peptide self-assembly of β -sheets (Courtesy of Bowerman et al.¹⁰)

A different type of the β -strand is the β -hairpin. A 20 amino acid long peptide was designed by Schneider *et al.* and consists of two β -strands with alternating lysine and valine residues and contains a fold in the middle of the molecule¹¹. The β -hairpin will self-assemble, facially or laterally, into a hydrogel, with possible applications such as promoting cell proliferation or as an antimicrobial agent¹²⁻¹⁴.

2.3. poly-L-proline type II (PPII) helices

Apart from the α -helix and β -sheet there is a third, less common type of secondary structure, namely the poly-L-proline type II helix. The poly-L-proline type II (PPII) helix is a left-handed helix with 3 amino acids per turn, having the shape of a triangular prism. While the name suggests it contains many proline residues, this is not necessarily the case. However, proline-rich peptides have a high propensity to assemble into PPII helices¹⁵. The PPII helix might be relevant in the self-assembly of peptides because the backbone of the structure is exposed and available for intermolecular hydrogen bonds, contributing to the stability of oligopeptide vesicles¹⁶. The PPII helix is also an important component of collagen, in which it is assembled into a triple helix, thereby contributing to the stability of collagen¹⁷. Peptides undergoing this assembly might be relevant for tissue regeneration purposes.

3. Supramolecular structures formed by the intermolecular self-assembly

The supramolecular structures formed by the secondary protein structures can be divided into definite assemblies (e.g. micelles and vesicles) and indefinite assemblies (e.g. tubes, fibres, tapes and ribbons). These will be further described below.

3.1. Definite structures

3.1.1. Micelles

Spherical micelles can be formed when building blocks with a hydrophilic head and a hydrophobic tail self-assemble into a definite supramolecular core-shell structure. They can differ in size and shape depending on factors such as the temperature, pH, concentration and interactions between the peptides. Schuster *et al.* designed an all-amino acid peptide that self-assembled into spherical micelles¹⁸. This peptide has a repetitive sequence of the hydrophobic amino acids leucine and tryptophan and three charged lysine residues at the head group (H-K₃-[WL]₃-W-NH₂). Electrostatic repulsion leads to the formation of micelles, possibly created from an intermediary α -helical structure.

To make the hydrophobic effect of the peptides stronger, an acyl chain can be conjugated to the tail instead of hydrophobic amino acid residues, creating so-called peptide amphiphiles¹⁹. Shimada *et al.* designed a peptide, C₁₆-WAAAAKAAAAKAAAAKA, which has an α -helix propensity and self-assembles into spherical micelles into an aqueous solution. After a few days of incubation, however, the conformation changes to a worm-like micelle²⁰. It is likely that this transformation is caused by a change in secondary structure to a more stable β -sheet conformation. This change leads to an enhanced hydrophobicity of the tail part and the subsequent transformation to a worm-like micelle structure²⁰. A particular kind of micelle formation is seen in the so-called ‘nanodonut’ shape (Figure 2). The peptides that generate this assembly are relatively short and cone-shaped (Ac-GAVILRR-NH₂); the hydrophobicity and size of the first five amino acids increase towards the positively charged arginine residues. They first assemble into spherical micelles, which then fuse to form cylindrical micelles or nanotubes. Hydrophobic interactions between the tail parts cause the nanotubes to bend and ultimately form an enclosed nanodonut shape²¹.

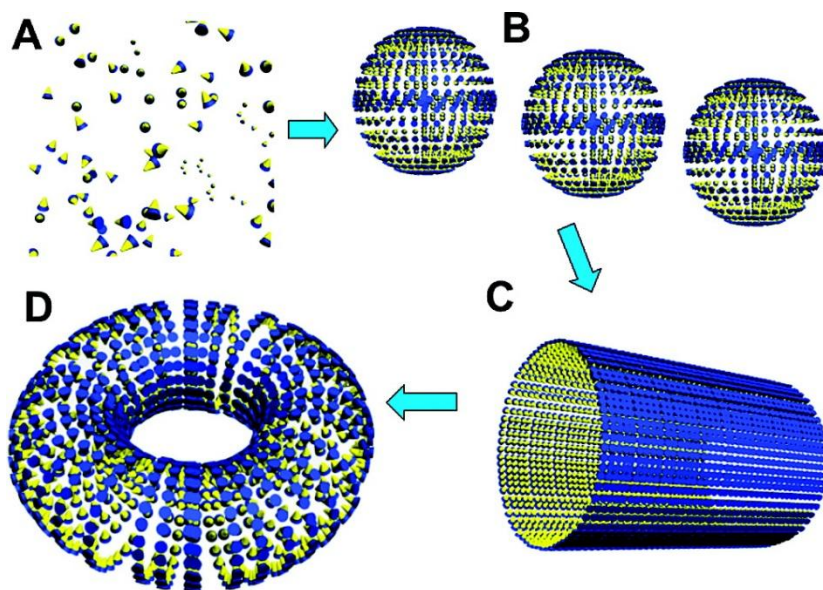


Figure 2. Proposed assembly mechanism of the nanodonut structure. A. Non-assembled peptides at a low concentration. B. Self-assembling into micelles above critical micelle concentration (CMC). C. Elongation of micelles into nanotubes. D. Ultimately, bending of the nanotube into a nanodonut shape (Courtesy of Khoe *et al.*²¹)

Looking at all the studies showing micelle formation by self-assembling peptides, it is clear that the peptide building blocks can be very different from each other²². The common factor, however,

is that there is always a hydrophilic (and most of the time charged) head group and a hydrophobic tail, often conjugated with an acyl group. This design favours the formation of micelles from self-assembling peptides.

3.1.2. Vesicles

Vesicles, contrary to micelles, have an aqueous interior because the amphiphilic building blocks form a bilayer or sheet in which the hydrophilic parts point to both the outer and the inner surface. How the vesicles are exactly being formed from the peptides is not entirely clear at present. It is however suggested that the peptide monomers first create a bilayer by connecting tail to tail and subsequently convert into a spherical or tube-like shape structures due to hydrophobic interactions²³. Some surfactant-like peptides designed by the group of Zhang *et al.* were found to self-assemble into vesicles of about 30-50 nm in diameter²⁴. The hydrophilic head part consisted of 1 or 2 aspartic acid residues and either 6 alanine, valine or leucine residues constitute the hydrophobic tail part (A₆D, V₆D_{1/2} or L₆D₂ respectively). Also, work done by Van Hell *et al.* showed that acetylated oligopeptides of 10 or 15 amino acid residues self-assembled into vesicles²⁵. The sequence of these peptides is Ac-AAVLLLLW-(E)_{n=2-7}-COOH that compared to the sequence of the self-assembling peptides from Zhang *et al.*, the side groups of these amino acids increase in bulkiness nearing the charged glutamate residues at the C-terminus.

For surfactant-like peptides, it is suggested that the hydrophobic domain arrangement has more influence on the final self-assembly structure rather than the differences in ratios between the hydrodynamic volumes of the hydrophobic and hydrophilic domains as is the case for hydrocarbon surfactants. For example in A6D2 and A6D or SA2 and SA7, each set containing the same hydrophobic domain but with hydrophilic domains that differ in size, the obtained supramolecular structures are the same. These examples may indicate some deviations in behavior compared to hydrocarbon surfactants whose self-assembly can be well described by Israelachvil's packing parameter equation²⁴⁻²⁷. Shorter peptides, consisting of only two amino acid residues, phenylalanine coupled with either lysine or glutamic acid, are also able to self-assemble and form nanovesicles²⁸. Furthermore, they were proteolytically and thermally stable and were able to trap molecules inside, making these nanovesicles potentially appealing for drug delivery applications²⁹.

3.2. Indefinite structures

3.2.1. Fibres

Fibres can be very similar to micelles in the way that the hydrophobic tails of the peptide monomers are attracted towards the centre of the structure, and the surface is hydrophilic. Fibres, however, are not spherical, but cylindrical and can, therefore, be seen as elongated micelles (Figure 3). It is, therefore, not surprising that peptides that are able to form micelles are very similar to the peptides that form fibres.

An example of a well-designed peptide amphiphile is the molecule made by the group of Stupp *et al.*³⁰. This peptide has an alkyl tail, 4 cysteine residues for forming disulphide bonds, 3 glycine residues functioning as a flexible linker, a phosphorylated serine residue to interact with calcium ions and finally arginine-glycine-aspartic acid (RGD), a cell adhesion ligand. These peptides self-assemble in a tightly packed nanofibre that can direct mineralisation of hydroxyapatite that eventually create a bone-like composite material. A much shorter peptide (C₁₂-VVAGK) also self-assembles into fibres³¹.

However, amphiphilicity of a peptide is not a prerequisite to forming a fibre. Peptides that will form a β -sheet can also assemble into fibres, depending on the concentration. The peptide Ac-RADARADARADA-CONH₂, for example, forms fibres as well³². Fibres are also not restricted to a certain definition, making it difficult to state a conclusive rule about the properties of fibre forming peptides.

3.2.2. Tubes

In the same way that fibres are basically elongated micelles, tubes are elongated vesicles. The structure is open-ended, has a hollow inside, and the monomers are linked together by their hydrophobic tail parts and their hydrophilic head parts are directed outwards. Generally, the same peptides that are capable of forming vesicles can also form tubes. In fact, Yan *et al.* showed that dipeptide nanotubes can be rearranged into nanovesicles upon dilution and can then be used as a carrier of oligonucleotides³³. The aforementioned peptides designed by Zhang *et al.* are also able to self-assemble into nanotubes²³. The proposed model for these peptides to self-assemble into a nanotube is that the monomers first form a bilayer, which then forms a closed ring. Subsequently, these rings stack on top of each other, which causes tube formation²². For drug delivery purposes, a vesicle might be more preferable than a tube since it is able to encapsulate the drug. However, it can still work as a carrier system for bigger structures such as proteins and genes³⁴.

3.2.3. Tapes

Tapes are micrometre-long β -sheets in a helical or twisted shape. The helical twist is caused by the intrinsic chirality of the amino acids (Figure 3). Since the tape is essentially a β -sheet, it has one side that is predominantly hydrophobic and one that is mainly hydrophilic. The most studied tape structures have been designed by the group of Aggeli *et al.* First, the peptide K24 (NH₂-KLEALYVLGFFGFFTLGIMLSYIR-COOH) was found to assemble into a tape and form a gel when dissolved in methanol³⁵. Later, peptides P₁₁-I (CH₃CO-QQRQQQQEQQ-NH₂) and P₁₁-II (CH₃CO-QQRFQWQFEQQ-NH₂) were designed. These peptides are shorter, but due to the electrically charged residues they are still able to interact electrostatically with each other, resulting in again a tape structure and a gel-like substance when dissolved³⁶. Another tape-like structure based on the β -sheet, but without a helix is the ‘nanobelt’ designed by Cui *et al.* This large one-dimensional structure consists of peptides of only four amino acids (VEVE) coupled to an aliphatic C₁₆H₃₁O group³⁷.

For tape(-like) structures, it is especially necessary to have an amino acid sequence that tends to form β -sheets, for example by incorporating the negatively charged glutamate between hydrophobic amino acid residues. The length of the monomer does not seem to be a very crucial factor, as proven by Cui *et al.* Most tapes will form a gel-like substance and can be used in tissue engineering and cell cultures³⁸.

3.2.4. Ribbons

Ribbons are described as two stacked tapes. Because both sides of the tape have different surfaces, in an aqueous environment the hydrophobic parts will be shielded off by the conjoining of two tapes (Figure.3). The peptide structure does not change, only the supramolecular structure. This was demonstrated with the P₁₁-1 and P₁₁-2 peptides from Aggeli *et al.*³⁹. Above certain concentration of the peptides, ribbons started to form instead of tapes. When the concentration increased further, first fibrils (several ribbons stacked together) and subsequently fibres were formed. An interesting phenomenon was observed when ribbons were kept in solution at 25 °C for 4 weeks. A morphological transformation occurs when the peptide (C₁₆O-F₃E₃) assembly switches from a twisted ribbon to a helical ribbon⁴⁰. In a twisted ribbon conformation, the β -sheets near the outside can be less twisted than those near the centre; the helical ribbon conformation is, therefore, more energetically stable since all β -sheets make the same twist⁴⁰.

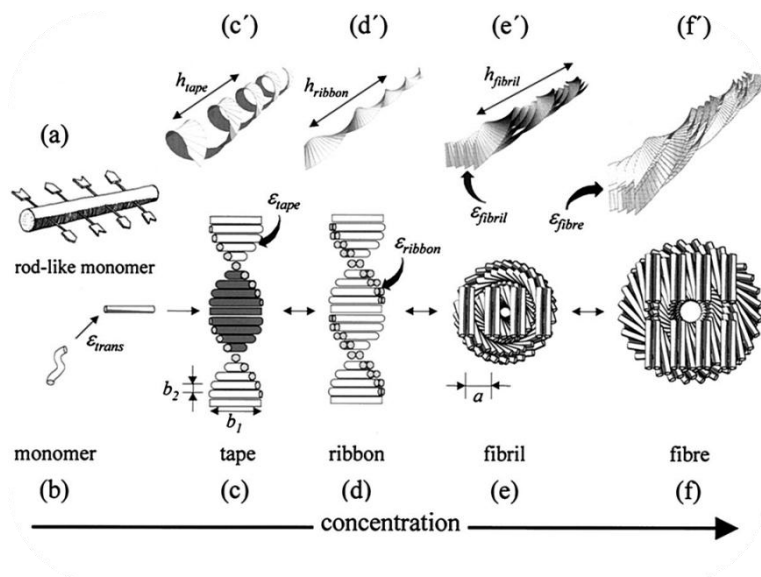


Figure 3. Schematic representation of β -sheet forming supramolecular structures. Peptides are depicted as chiral rod-like units (a, b). Arrows show the complementary donor and acceptor groups. The monomers interact to form a tape (c), these tapes, can stack together with their hydrophobic side to form a ribbon (d). When the concentration increases, monomers can assemble into fibrils (e) or fibers (f), both show the front view of the edges. c'-f' represent the global equilibrium conformations corresponding to c-f respectively (Courtesy of Aggeli et al.³⁹)

In conclusion, driven by various molecular forces peptides can self-assemble in different supramolecular structures. The combinations of all these forces make it difficult to predict the behaviour of self-assembling peptides. Peptides that have an electrostatically charged (or hydrophilic) head and a hydrophobic tail part will likely self-assemble in spherical micelles or vesicles. From these structures on, elongation into fibres or tubes respectively is possible. Peptides with a β -sheet propensity tend to assemble into flat structures such as tapes or ribbons. However, when the concentration of the peptides increases these tapes and ribbons will stack on each other and form more tightly packed fibres. More knowledge of how all the molecular forces interact is essential to design more efficient, chemically stable and practical peptide self-assemblies.

4. Self-assembling peptides for drug delivery applications

Supramolecular structures compiled entirely from synthetic peptides can be used for drug delivery applications. Peptides can be engineered to enable controlled self-assembly, contain therapeutic activity and cell targeting capacity in a single polypeptide molecule. This is from a pharmaceutical point of view attractive as it obviates the need for complex formulation work or chemical reactions to obtain a multifunctional nanoparticles as is often the case with drug delivery systems consisting

of synthetic polymers or lipids. With the current knowledge of how antigenic epitopes generated from proteins and peptides are being presented to the immune system, it has become possible to engineer proteins and peptides in such a way that they are poor substrates for MHC class I and II presentation⁴¹⁻⁴³. Such combinatorial deimmunization can also be applied to self-assembling peptides with the aim to reduce potential immune responses without losing the self-assembling capacity. Nevertheless, the repetitive nature of the surface of supramolecular structures formed by self-assembling peptides may trigger T-cell-independent antibody formation as has been shown for protein aggregates⁴⁴. Therefore, immunogenicity of the peptide scaffolds should be monitored at all times.

Different supramolecular architectures have been studied for drug delivery applications. Self-assembling peptides that form definite nanostructures, such as micelles, rods or vesicles, can be used for the generation of nanocarriers for local or systemic drug delivery. Alternatively, self-assembling peptides forming fibrils or hydrogels may be used as macroscopic drug depots for sustained drug release. Since the majority of self-assembling peptides that have been reported so far form indefinite nanofibers, the application of such peptides has been focussed on the formation of hydrogels for sustained release applications or tissue engineering. There are only a few studies describing the use of self-assembling peptides forming discrete nanoparticles for the delivery of drugs into cells (Table1).

In this section we will divide the self-assembling peptides that have been developed for drug delivery into 3 categories : a) peptides consisting of natural amino acids with no or minor N- or C-terminal modifications b) lipidated peptides and c) polymer-peptide conjugates. Self-assembling peptides with unnatural amino acids and peptide-conjugates in which the peptide part does not contribute to self-assembly will not be discussed.

4.1. Self-assembly based on unmodified peptide

The majority of peptides used for engineering structures driven by self-assembly consist of natural L-amino acids with or without standard N-(acetylation) or C-terminal (amidation) modifications to remove unwanted terminal charges. Self-assembly of such peptides is entirely driven by the properties of the amino acid sequence. The main advantage of this class of self-assembling peptides is that they can be easily synthesized using standard solid phase synthesis techniques without the need for laborious chemical modifications. The majority of unmodified peptides used for self-assembly form indefinite structures such as fibers or hydrogel-based networks. The best example of a self-assembling peptide that form hydrogels is RADA16-I (PuraMatrixTM).

RADA 16-I comprises of 4 repetitive units of arginine (R), alanine (A), aspartic acid (D) and alanine (A). In aqueous solution, hydrophobic interactions of the alanines among 2 peptide molecules expose the negatively charged aspartate residues and positively charged arginine residues towards the exterior face. Consequently, complementary charge interactions between the formed pieces result in nanofiber formations with a width between 3-8 nm. At high concentrations, such large number of nanofibers generate nanoporous hydrogels (Figure 4)⁴⁵⁻⁴⁷. Hydrogels because of their tailorable properties like crosslink density, water content and degradability are frequently studied as matrices for the controlled release of proteins⁴⁸.

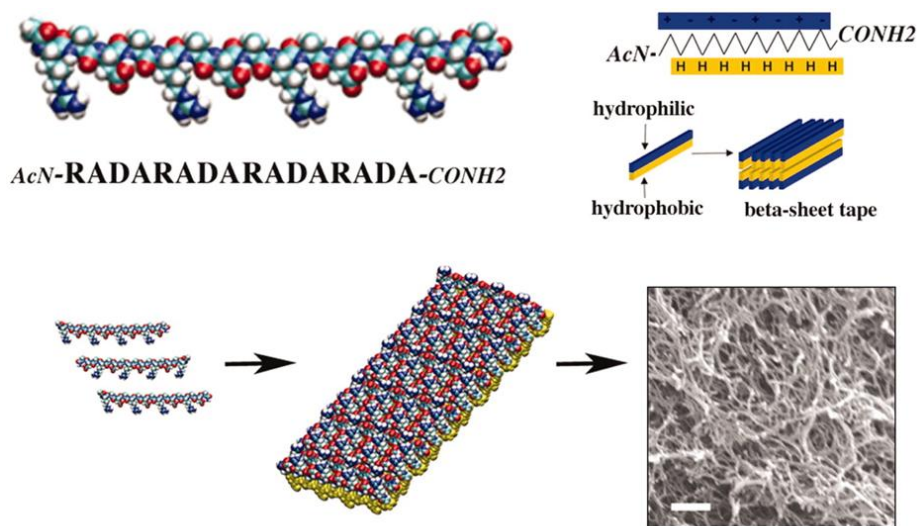


Figure 4. Illustration of RADA 16-I hydrogel formation by parallel β -sheet alignment of peptides (Courtesy of Semino *et al.*⁴⁶).

RADA-16 has been developed for commercial use as cell matrix for tissue engineering and sustained drug delivery, which is called PuraMatrix^{TM49-51}.

Koutsopoulos *et al.* studied the release profile of different proteins with different molecular weights which were loaded in RAD 16-I hydrogels. They found that the release was governed by diffusion which the diffusion coefficients are dependent on the molecular weight of proteins and the concentration of peptide used to form the geometrically uniform hydrogel. For example, IgG (MW:150 kD) was released slower than lysozyme (MW: 14.5 kD) when using hydrogels with the same peptide densities. By a 1% (wt/vol) peptide hydrogel, 40% of embedded IgG was released over 60 hrs of incubation, compared to >60% of lysozyme after 10 hrs of incubation.

Charge interaction between proteins and peptidic scaffold did not play a major role on the release kinetics of entrapped proteins, since the isoelectric point of the peptidic scaffold was very close to

physiological pH, with a slightly negative charge at pH 7.4. However, electrostatic interaction of entrapped proteins with the peptide matrix and thereby the release kinetics of such proteins can be tailored by changing the pI of the scaffold⁴⁹.

There are few designed peptides that are able to form discrete nanoparticles which could in principle be used for intravenous drug delivery. Surfactant-like peptides have shown to form vesicular structures, depending on the primary sequence, peptide concentration pH and ionic strength of the dispersing media^{25,52,53}. Van Hell *et al.*, reported a number of surfactant-like peptides (SLPs) which can form nanovesicles^{16,25,53}. One of these self-assembling peptides is the SA2 peptide (Ac-AAVVLLWEE-COOH), which form discrete nanovesicles with a radius of 60 nm when dispersed in aqueous media at physiological pH. The formed peptide vesicles precipitated out of solution at pH values below the pKa of the glutamic acid side groups, which could be fully reversed when pH was raised again to 7.4²⁵.

SA2 peptide vesicles could be loaded with a photosensitizer with virtually no water solubility. Incubation of this photosensitizer loaded into SA2 peptide vesicles with different cells (HUVECS, COS-7 and C26) in culture resulted in accumulation inside the cells. Upon illumination to excite the delivered photosensitizer, concentration-dependent cytotoxicity was observed which was absent if the cells were not illuminated⁵³.

Tomich and co-workers designed and synthesized two types of branched self-assembling peptides to mimic phospholipid structure⁵². The hydrophobic part (FLIVIGSII and FLIVIGS) is a segment of a transmembrane helix of the human dihydropyridine sensitive L-type calcium channel and the hydrophilic part comprised 5 lysines. In order to branch out the molecule, hydrophobic segments were conjugated to the α and ϵ -amine of the N-terminal of the oligo-lysine. The amphipathic nature of this peptide resulted in the formation of nanovesicles with 50-200 nm in diameters and a positive surface charge in water. These nanovesicles were loaded by 5(6)-carboxyfluorescein and rhodamine 6G as the model drugs and showed internalization in N/N 1003A rabbit lens epithelial cells in culture media⁵². An overview of the literature describing the use of peptide nanostructures for drug delivery is given in the table 1. Most of these studies report *in vitro* data, and only few studies were performed *in vivo*. Alam *et al.* synthesized a dipeptide, methionine - dehydrophenylalanin (M Δ F), which self-assembled into spherical nanoparticles. Delivery of curcumin encapsulated inside these nanoparticles increased the anti tumor activity of curcumin on L-929 cells grown in culture and decreased the mortality rate of tumour-bearing Balb/c mice. Biocompatibility, single step dipeptide synthesis and low risk for immunogenicity were mentioned to be the main advantageous for these dipeptide systems⁵⁴.

Table 1. A selection of *in vitro* characterized self-assembling peptides as drug delivery vehicle

Composition/Sequence	Supramolecular structure	Secondary structure	Cargo		Ref.
L-diphenylalanine (FF)	Microtubes	----	Rhodamine B	P	55
Fmoc-FF	Hydrogel Nanoparticles	---	5-fluorouracil (5-Fu), Doxorubicin	P	29
8 {cyclo-[(D-Trp-L-Leu)5]} , 8 {cyclo-[(L-Ala-D-Gln-L-Ala-D-Glu)2-L-Ala-D-Gln]}	Cyclic peptide nanotubes	Antiparallel beta sheet	5-fluorouracil (5-Fu),	P	56
Ac-(RADA) ₄ -CONH ₂ , Ac-(KLDL) ₃ -CONH ₂	Nanofiber hydrogel	----	Human IgG	P	57
(Ac-FLIVI) ₂ K-KKKK-CONH ₂ (Ac-FLIVIGSII) ₂ K-KKKK-CONH ₂	NanoVesicles	β -sheet	5(6)-carboxyfluorescein, rhodamine 6G carboxytetramethylrhodamine (Covalently)	p/c	52
VKVKVKVK-V ^D PPT-KVEVKVKV-NH ₂	fibrils	β -hairpin	curcumin	p	58
SA ₂₋₇ : Ac-AAVLLLLW(E) ₂₋₇ SA ₂ C ₃ :Ac-ACVCLCLWEE	Nanovesicles	PPII	zinc-phthalocyanine (TT-ZnPcNH ₂)	p	53
Ac-RADARADARADARADA-CONH ₂ : RAD16-I (Ac-RADARADARADARADAGGDGEA-CONH ₂) (Ac-RADARADARADARADAGGPFSSTKT-CONH ₂)	Nanofiber hydrogel	β -sheet	Cytokines: β FGF BDNF VEGF	p	50
Ac-(RADA) ₄ -CONH ₂	Nanofiber hydrogel	β -sheet	lysozyme, trypsin inhibitor, BSA, IgG	p	49
N-Pro-Ser-Phe-Cys-Phe-Lys-Phe-Glu-Pro-C	“beads-on-a-thread” type nano fibers	β -sheet	pyrene	p	59
VKVKVKVK-V ^D PPT-KVEVKVKV-NH ₂	fibrils	β -hairpin	lysozyme, α -lactalbumin, myoglobin, lactoferrin, bovine serum albumin (BSA), human immunoglobulin G (IgG),	p	60

AEAEAKAKAEAEAKAK : EAK16-II AEAEAEAEAKAKAKAK : EAK16-IV FEFEFKFKFEFEFKFK : EFK16-II	EAK16-II : nanofibers EAK16-IV: globular nanostructures , short nanofibers EFK16-II: nanofibers	EAK16-II : β -sheet EAK16-IV: β -turn EFK16-II: Not reported	ellipticine	p	61
-------------------------------------------------------------------------------------------------	-------------------------------------------------------------------------------------------------------------------------	---------------------------------------------------------------------------------------------	-------------	---	----

4.2. Self-assembly based on chemically modified peptides

Peptide self-assembly can be greatly influenced by chemical modifications of the amino acid side groups or the N- and C-terminus. For example, the addition of alkyl tails to N- or C- terminus can drive the self-assembly of such lipopeptides, which would otherwise be soluble. Other modifications have been described of which a few examples will be highlighted in this section.

4.2.1. Lipidated self-assembling peptides

Stupp and co-workers have developed a series of lipid-peptide molecules comprised of a hydrocarbon chain (e.g. palmitoyl) covalently attached to an amphiphilic peptide (e.g. $V_nA_nE_n$) which is able to form beta sheet-rich supramolecular structures. These peptide amphiphiles (PAs) when dispersed in water form hydrogels at concentrations as low as 1% (w/v) in the presence of calcium ions that triggered gelation through charge screening. Interestingly, these PAs kept their hydrogel-forming capacity even after covalently conjugation of dexamethason or prodan to the peptide moieties via acid-cleavable hydrazone bond^{62,63}. This striking feature makes these PAs a versatile system for sustained release of a wide range of medicines.

Table 2. A selection of peptide amphiphiles used as a drug delivery carrier.

Composition/Sequence	Supramolecular structure	Secondary structure	Cargo	Chemically(C)/ Physically(P)	Ref
C16V2A2E2K(Hyd) C16V2A2K(Hyd)E2 C16V2K(Hyd)A2E2 C16K(Hyd)V2A2E2 (Hyd)= hydrazone	Nanofiber hydrogel	β -sheet	6-propionyl-2-dimethylaminonaphthalene (Prodan)	C	62
C16V3A3E3K(β D) β D indicates that the Asp residue was attached to its side chain carboxylic acid)	Nano fiber gels	β -sheet	[Ru(CO)3Cl]2 for CO delivery	C	64

C16V2A2E2	Nanofiber gels	β -sheet	Nabumetone	c	65
C16V2A2E2	Nanofiber gels	β -sheet	Dexamethasone	c	63
C16A4G3E3	Nanofiber gels	β -sheet	Camptothecin	p	66
C16V3A3E3	Nanofiber gels	β -sheet	Sonic hedgehog (SHH) protein	p	67

4.2.2. Polymer-peptide conjugates

Many studies have been conducted on polymer-peptide conjugates (PPC), in which the polymer part was responsible for forming supramolecular structures and the peptide part comprising bioactivity.

Here, we focus only on those PPC in which the peptide part contribute to the self-assembly behaviour of the PPC.

Self-assembled peptides grafted to poly(ethylene glycol) (PEG) have gained increasing attention because of the high water solubility and well-characterized physicochemical properties of this polymer⁶⁸. Peptide-PEG conjugates can form a wide range of supramolecular structures, e.g., micelles, vesicles, fibers, primarily driven by the length of the PEG and the nature of the peptide⁶⁹⁻⁷².

A series of amphiphilic PLL-PEG-PLL copolymers (PLL:poly L-leucine, PEG:polyethylene glycol) were synthesized by Hua *et al.* These PPCs with critical micelle concentration(CMC) equal 95 mg/L predominantly formed flower-like micelles with a diameter 30-50 nm as similar structure reported by de Graaf *et al.*⁷³. The hydrophobic core of these micelles consisted of PLL in the α -helical conformation in which hydrophobic drug molecules such as paclitaxel and prednisone could be loaded (Figure 5). The prednisolone-loaded micelles (35 nm) showed a slower release of the drug in comparison to paclitaxel loaded particles (90 nm) which was ascribed to a more densely packed core of the smaller particles⁷⁴.

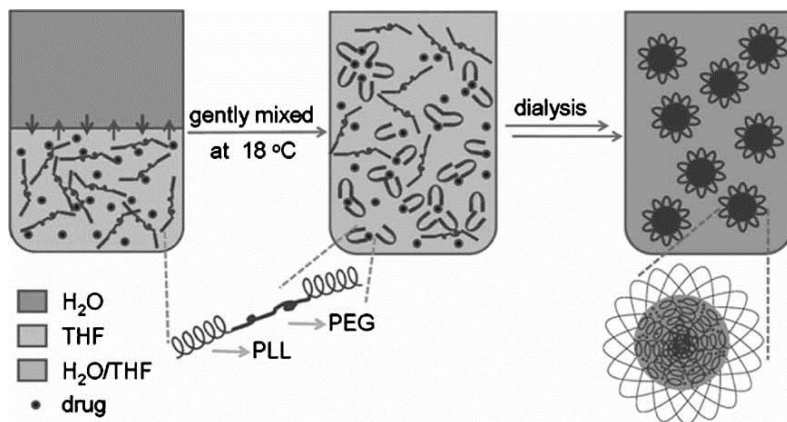


Figure 5. Schematic representation of formation the self-assembled particles of PLL-PEG-PLL copolymer (Courtesy of Hua *et al.*⁷⁴).

Xu *et al.* designed a micellar structure that consisted of 4 components : i) A 3-helix bundle forming coiled-coil peptide ii) poly(ethylene glycol) polymers conjugated to the side chains of the coiled-coil peptides iii) hydrophobic tails (e.g. stearic acid) coupled to the N-terminus of the coiled coil-forming peptide and iv) PEG or targeting ligands that can be attached at the C-terminus (Figure 6).

These 3-helix micelles were approximately 30 nm in size and were loaded with the anticancer drug doxorubicin (8 wt %) for systemic drug delivery. These nanocarriers exhibited notable stability *in vivo* with circulation half-life of 29.5 h and low accumulation in the liver and spleen. Interestingly, proteolytic degradation of the helix is able to sustain drug liberation and subsequently reduce side effects^{75,76}.

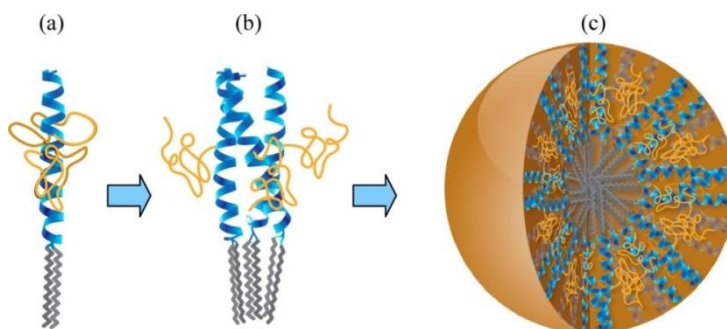


Figure 6. (a) Schematic illustration of the designed unimer of the short amphiphile peptide helix conjugated to a PEG chain; (b) subunit formation with three amphiphile unimers; (c) Micelle formation by subunits assembly with a hydrophobic core containing aliphatic chains and a hydrophilic shell composed of 3-helix bundles (Courtesy of Dong *et al.*⁷⁵)

In another example, Jabbari *et al* conjugated the VVVVVVKK peptide to a low molecular weight poly-L-lactic acid (PLA) with a $\overline{Mn} = 5.1$ kDa resulting in the formation of micelles in which PLA was present in the micellar core. These PLA-V6K2 micelles were compared with PEG-PLA micelles as nanocarrier for cellular delivery of doxorubicin and paclitaxel both *in vitro* and *in vivo*. PLA-V6K2 micelles were smaller in size (100 ± 20 nm) as compared to PEG-PLA ($\overline{Mn} = 8.1$ kDa) micelles (130 ± 50 nm) and showed a slower release for doxorubicin and paclitaxel. Authors propose that the interaction of valine residues in peptide segments made a strong shield around the hydrophobic core of PLA in PLLA-V6K2 nanoparticles which effected the release of loaded molecules and interfacial energy between the nanoparticles and water. Because of the positive surface charge of PLA-V6K2, enabling efficient attachment to cell membranes, a higher cell uptake by 4T1 mouse breast carcinoma cells was observed. Doxorubicin loaded PLA-V6K2 micelles demonstrated an incremental tumor toxicity compared to Dox loaded PLA-PEG and consequently lower host toxicity than the free DOX⁷⁷.

5. Application of self-assembling peptides for vaccination

The way antigens are presented to the immune system determines to a great extent the quality and longevity of the evoked immune response. As such, proper presentation of antigens is of utmost importance in the development of effective vaccines. Although the trend in vaccine formulation is towards “clean” and well-defined systems making use of well characterized synthetic antigens, such as peptide epitopes, these synthetic systems suffer from poor immunogenicity since the antigen presentation far resembles the antigen as part of a living pathogen and the uptake by professional antigen-presenting cells (APC) is suboptimal. Many studies showed that administration of soluble peptides with adjuvants may not necessarily result in induction of efficient immune responses⁷⁸⁻⁸². This is partly because of poor antigen uptake by APCs, *e.g.*, dendritic cells (DCs) and inefficient activation of DCs. Self-assembling peptide systems have been investigated for vaccination purposes with the aim to reconstruct virus-like structures making use of β -sheet or alpha helical coiled-coil forming peptides for assembly into well-defined nanostructures^{78,83}. In general, self-assembling peptide particles have several advantages over other antigen carrier systems such as ease of production, biodegradability, high density of surface-exposed antigen epitopes, control on particle size, direct conjugation of ligands or imaging probes to the peptides⁸⁰ and, most importantly, increasing of antigen uptake by APCs⁷⁹⁻⁸². Moreover, in contrary to virus-like-particles (VLPs) and genetic vaccines based on viruses, self-assembling peptide particles have shown hardly any cytotoxicity⁸⁴. Due to the simplicity and using databases to avoid immunogenic sequences, the self-assembly domain of the peptide vector itself would not

be immunogenic so that any evoked immune reactions will be directed against the incorporated antigenic epitopes. This is in contrast to the use of VLPs where the viral proteins themselves are sometimes very immunogenic causing problems with pre-existing antibodies against the vaccine carrier or leading unwanted immune responses^{85–87}. In the following section, we highlight some examples of self-assembling peptides for vaccination, limiting the discussion to all-peptide systems or to bioconjugates in which the peptide moiety is critical for self-assembly.

Boato *et al.* constructed a synthetic virus-like particle (SVLP), which comprised a lipo-peptide having a coiled-coil sequence. Peptide monomers formed a trimeric coiled-coil helical structure, which in turn formed micelles with a mean diameter of about 20-30 nm (Figure 7)⁸³.

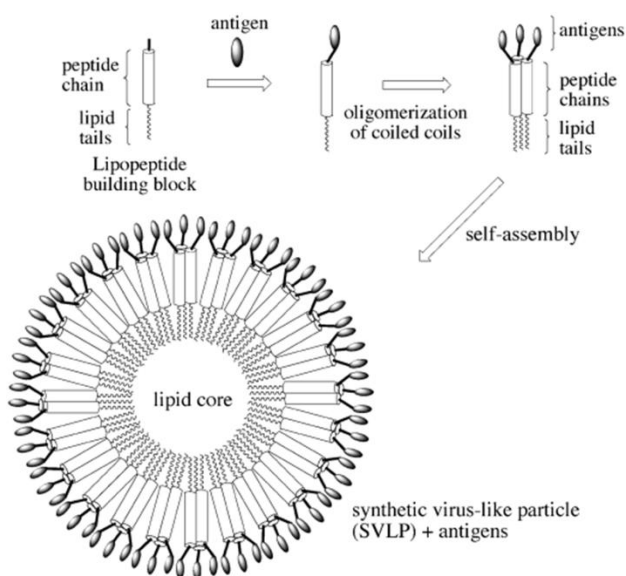


Figure 7. Synthetic virus-like particle (SVLP) formation through self-assembly of a trimeric coiled-coil helical structure and hydrophobic interaction of lipophilic tails (Courtesy of Boato *et al.*⁸³).

The immunogenicity of the synthetic VLPs fused to a sequence derived from the V3 region of gp120 from HIV-1 was tested *in vivo*. The synthetic VLP vaccines showed high antigen specific antibody titers, in vaccinated New Zealand white rabbits without the need for additional adjuvants. The authors suggest that in these systems, the lipid tail can be either a phospholipid or a toll-like

receptor (TLR) ligand (e.g. Pam2Cys or Pam3Cys), which can be coupled to the N-terminus of the self-assembling peptide⁸³. In another study, the same authors showed that these synthetic VLP vaccines were efficiently taken up by DCs mainly through caveolin-independent lipid raft macropinocytosis and subsequent antigen processing and MHC-restricted presentation by DCs⁸⁸.

Rudra *et al.* evaluated the ability of a self-assembling peptide (Q11: Ac-QQKFQFQFEQQ-am) for vaccination. This peptide is able to form β -sheet fibrillar structures of approx. 5-10nm wide and 100-1000nm in length in salt-containing aqueous solutions⁷⁸. They showed that these peptide fibers are non-immunogenic and did not elicit detectable immune response even co-administered with complete Freund's adjuvant (CFA). However, nanofibers fused to OVA₃₂₃₋₃₃₉ peptide (containing T-helper and B-cell epitope) at the N-terminus of Q11 peptide elicited a high level of IgG1, IgG2a and IgG3 antibodies against OVA epitope (Figure 8). The antibody levels were comparable to those induced by the peptide formulated in CFA adjuvant^{80,86}. The effectiveness of this adjuvant-free nanofiber vaccine in induction of humoral immune response against *plasmodium falciparum* circumsporozoite was shown in animals immunized with (NANP)₃ malaria peptide coupled to Q11. The vaccinated mice showed strong antibody responses up to 40 weeks without the necessity for regular boosts. The authors also showed that two different epitope-bearing Q11 peptides could co-assemble without decreasing of the immune response to either epitope⁸⁶.

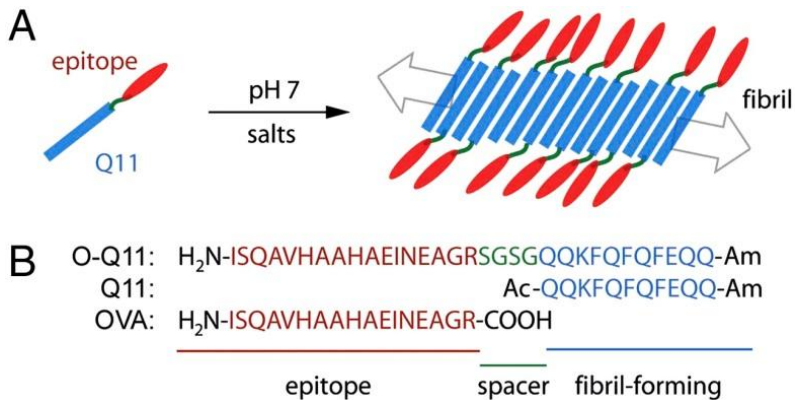


Figure 8. A) alignment the self-assembled Q11-epitope to form fibres B) sequences of the self-assembled Q11-OVA (O-Q11), Q11 and ovalbumin epitope (OVA₃₂₃₋₃₃₉) (Courtesy of Rudra *et al.*⁷⁸).

In another study by Rudra *et al.* it was shown that the immunogenicity of the self-assembled peptide vaccines is T-cell dependent and strongly associated with the self-assembling structure. The fibril-formation and thereby the immunogenicity of the vaccine was fully demolished by mutating key amino acid residues in the self-assembling domain⁸⁰. The authors also tested another self-assembling peptide domain (KFE8: FKFEFKFE-Am) and proved that the adjuvant effect was not limited to a specific self-assembling peptide sequence⁸⁰. In a followup study, Rudra *et al.* investigated the mechanism of immunological activity and adjuvanticity of the self-assembled vaccines *in vivo*⁸⁶. They hypothesized that the fibril structures resemble bacterial flagellin and thus might activate innate immune system through interacting with TLRs or activate inflammasomes due to their particulate structures. They demonstrated that the antigen specific immune response was T-cell and MyD88 dependent, but they could not find any specific interactions with TLR2 and TLR5 as well as NALP3, as an inflammasome activation marker⁸⁰. Recently Chen *et al.* evaluated the cytotoxicity and reactogenicity of the above nanofiber vaccines⁸¹. They proved in contrary to alum-adsorbed OVA₃₂₃₋₃₃₉ vaccine, OVA₃₂₃₋₃₃₉-Q11 nanofibers did not induce any swelling and local inflammation at the site of injection and did not recruit inflammatory cells after intraperitoneal (i.p.) administration. *In vitro* studies showed that OVA-Q11 was safe and did not cause any cell death in a range of concentrations, whereas the alum formulation elicited a dose-dependent cell death. They also demonstrated that fluorescently labelled OVA-Q11 nanofibers were taken up by APCs 10 fold higher than labelled OVA protein and the isolated DCs from mice with positive fluorescent signal had significantly increased expression DCs activation markers (CD80 and CD86). Further, it was shown that OVA-Q11 nanofibers elicited formation of B-cell germinal center and high-titer, high-affinity neutralizing IgG responses in an *in vitro* flu model⁸¹. Rudra and co-workers, recently demonstrated that a self-adjuvanting nanofiber vaccine based on Q11 peptide was able to mount a robust specific OVA₂₅₇₋₂₆₄ CD8+ T cell response in OT-I transgenic mice. Taken together, the results indicate that these self-adjuvanting vaccines not only can elicit CD4+ T cell responses but also rise CD8+ T cells which are playing a pivotal role in immunotherapy of viral infections and cancers⁸⁹.

6. Self-assembling peptides for tissue regeneration

Advances in the field of stem cell research and the technical possibilities to revert differentiated cells back to pluripotent stem cells, makes it in principle possible to regrow damaged tissue using

the patient's own cells. However, this requires a good understanding of the organizational and signaling events that govern the growth and differentiation of (pluripotent) stem cells in a complex 3D microenvironment, with subsequent translation of these principles into man-made engineered scaffolds.

3D cell cultures require sophisticated scaffolds onto which the cells can adhere and, in addition, can provide the necessary signals for growth and differentiation. Scaffolds can be formed from natural components, such as decellularized extracellular matrix components. However, such biological scaffolds have the risk of potential disease transmission, limited range of mechanical properties, complex structures which make them difficult for manipulation and to obtain reproducible manufacturing results. As a consequence, scaffolds composed of synthetic polymeric networks or peptide scaffolds, have gained increasing attention as well-characterized scaffold with tailor-made properties such as mechanical properties, stimuli-responsiveness and degradation rate.

Compared to polymeric scaffolds, peptide scaffolds have the added benefit that biological functionalities, such as cell adherence or growth stimulating factors can be easily incorporated as an intrinsic component of the peptide scaffold. They show excellent biocompatibility and can be metabolized through a series of enzyme reactions *in vivo*. In order to construct a 3D scaffold, self-assembling peptides should form indefinite structures upon the self-assembly. Self-assembling peptides most frequently used for tissue engineering are β -structured peptides that form hydrogelating fibrous scaffolds, thereby mimicking the extracellular matrix (ECM). Peptide sequences can be derived from natural protein sequences or designed *de novo*.

6.1. Self-assembling peptides derived from natural protein sequences

6.1.1. Beta sheets

A well-known example of self-assembling peptides copying natural protein sequences is the EAK-16 peptide⁹⁰. Zhang *et al.* derived the sequence from the yeast protein zootin, a putative nucleic acid binding protein, with a repetitive sequence AEAEAKAKAEAEAKAK which forms fibrous hydrogels upon addition of salts and is stable at high temperatures. A striking feature is that once the hydrogel has been formed the peptides show remarkable resistance to proteolytic degradation, despite the presence of protease recognition sequences⁹⁰. The EAK16 peptide and several variants derived from it, amongst which the RAD16 peptide, were used for cell attachment and were shown to be a suitable scaffold for a variety of cell types⁹¹. Competition experiments using soluble RGD indicated that cell attachment was not integrin-specific. These hydrogels successfully promote the

culture of chondrocytes, bone, nerves, and other cell types in *in vitro* and *in vivo* models⁹². To improve the weak mechanical stability of EAK16 and RAD16 to apply as a scaffold for cartilage repair, self-assembling peptide KLD12 was designed by the same group^{93,94}.

6.1.2. Beta Hairpins

The MAX peptide series consist of *de novo* designed peptides that can form thermally reversible hydrogels^{11,95}. Pochan and colleagues have shown that these peptides have a random coil conformation at room temperature and high pH, but form β -hairpin structures upon heating, which in turn leads to self-assembly into a hydrogel network. Upon cooling, complete dissolution of the hydrogel occurs. By changing the hydrophobicity of the peptides, the temperature at which hydrogel formation occurs can be tuned between 25-60 °C⁹⁵.

Since MAX1 gelation rate was too slow, MAX8 was designed by the same group to improve the gelation kinetics. This amendment led to better spreading of cells within the MAX8 hydrogel network. They demonstrated that MAX8 and MAX1 were able to recover back to its measured elastic modulus when shear was applied. Cell viability results in majority of viable cells in the MAX8 gel – cell construct which injected into a well plate by a syringe. These features of MAX peptides make them suitable for cell-delivery applications⁹⁶.

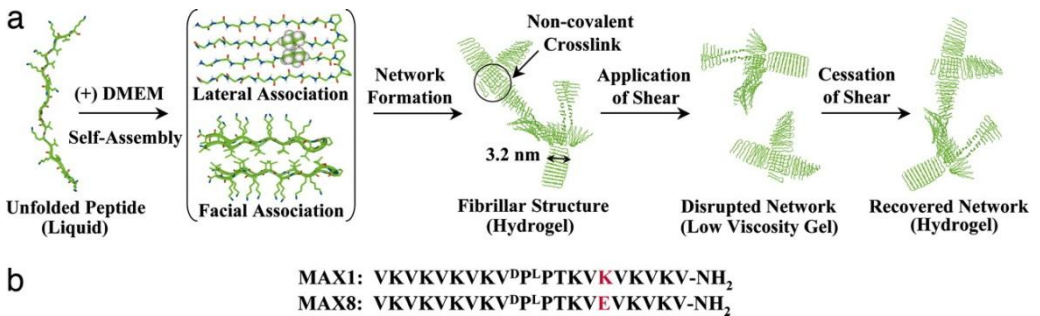


Figure 9. (a) Schematic illustration of triggered self-assembly of β -hairpin peptides by adding the culture medium (DMEM). Shear-thinning and self-healing property of the hydrogel make the system suitable for biomedical applications such as cell delivery. (b) Amino acid sequences of Max1 and Max8 (Courtesy of Haines-Butterick et al.⁹⁶).

6.1.3. Coiled coils

Woolfson *et al.* have developed and studied α -helical coiled-coil peptides that self-assemble into hydrogelating self-assembling fibers (hSAFs). Hydrogel properties can be altered by modifying the peptide sequences^{6,97,98}. For example, hSAFQQQ peptide formed a hydrogel at low temperature but melted by heating, whereas the more hydrophobic peptide hSAFAAA showed an opposite behavior. Such coiled coil-forming peptide hydrogels have been used to support growth and differentiation of rat adrenal pheochromocytoma cells (PC12) for 2 weeks⁹⁹.

6.2. *De novo* designed self-assembling and semi synthetic peptides

Besides natural sequences, many groups have explored *de novo* designed peptides to optimize self-assembly and viscoelastic properties of peptide scaffolds.

6.2.1. P11 and Q11

The P₁₁ series of peptides are an example of such *de novo* β -sheet forming peptides. They were designed to keep both the chemical complexity of the primary structure and the conformational complexity to a minimum¹⁰⁰. They consist of 11-mer peptides with alternating polar and aromatic amino acids, typically incorporating several glutamine residues to drive the formation of β -sheets which, dependent on the peptide concentration, can form higher order structures such as tapes, fibrils and fibers. An interesting feature of these peptides is that they can undergo pH and ionic strength-triggered self-assembly. These properties enable the injection of the peptides in a liquid form, prior to peptide self-assembly. For tissue engineering, gels of P₁₁ peptides can be conveniently prepared by adding the lyophilized peptide directly to the cells in culture, leading to cell incorporation into the peptide matrix. These peptides are currently being tested as a scaffold for enamel regeneration in patients with carious lesions¹⁰¹.

A peptide derived from the P₁₁ series of peptides, which allows chemical end-modification or fibril elongation is the Q11 peptide. This peptide has an N-terminal cysteine residue and a C-terminal thioester to join individual peptide fibrils or to functionalize peptide fibrils with cell adhesion ligands via native chemical ligation (NCL). Hydrogels in which the individual peptide fibrils were ligated with NCL showed increased stiffness compared to the nonligated hydrogel, which resulted in better growth of HUVECs¹⁰².

6.2.2. Aromatic peptides derivatives

Short peptides with strategically positioned aromatic groups can self-assemble in aqueous solutions through π - π stacking in addition to hydrogen bonding interactions. Gazit and co-workers reported one of the shortest self-assembling peptide. They demonstrated that diphenylalanine (FF) peptides and lately Fmoc-FF formed linear nanotubes, amyloid fibers and cylindrical architectures in aqueous solution. They exploited these nanofibers for casting and fabrication of metallic nanowires and nano-cables³⁸.

Ulijn and colleagues showed the usefulness of such diphenylalanine peptides for forming hydrogel scaffolds peptides Boc-FF-COOH, Nap-FF-COOH and Fmoc-FF-COOH all generated hydrogels with a nanofibrous network with diameter 10-100 nm under physiological conditions^{103,104}. In addition, the group has shown that Fmoc di-phenylalanine peptides increased survival of the chondrocytes and human dermal fibroblasts in 2D and 3D cell culture media^{105,106}.

6.2.3. Peptide amphiphile

Stupp and co-workers designed a series of peptide amphiphiles consisting of an alkyl tail and a peptide head group with increasing hydrophilicity towards the C-terminus such as C16-VVAAEE-NH₂¹⁰⁷. Hydrophobic interaction between alkyl chains and hydrogen bonding through beta-sheet formation between the peptide head groups assisted in peptide self-assembly forming elongated fibers with a diameter of approximately 5-7 nm and a length of several micrometers that assembled into hydrogels above a critical concentration. The formed hydrogels showed promising results for tissue engineering such as neuronal repair (see table 3).

6.3. Functionalization for proper cell differentiation:

To improve the functionality of the designed scaffolds including cell adhesion, growth and differentiation, several active motifs have been studied and applied mainly in 2 forms, either conjugated or mixed with the self-assembled peptides^{92,93,108-110}. Gelain *et al.* conjugated several bioactive motifs, including cell adhesion, differentiation and bone marrow homing motifs, to the RADA16-I peptide and evaluated their effects on the bio-functionality of the scaffold. They showed that these peptide scaffolds containing bone marrow homing motifs not only significantly increased the survival of neural stem cell, but also promoted cell differentiation in the absence of any added growth and neurotrophic factors to the cell culture media¹¹¹. Wang *et al.* functionalized the RADA16-I with "Link N" peptide (AcN-(RADA)4-GGRLNSDNYTLDHDRAIH-COHN₂)

and evaluated bone marrow stem cells in the obtained scaffold by mixing RADA16-I and RADA16-Link N (1:1). Though this modification could not stimulate cell proliferation, however, it increased cell adhesion and promoted the production and deposition of type II collagen and aggrecan¹¹². Stupp *et al* also designed several amphiphile peptides conjugated to the bioactive motifs such as VEGF-mimetic epitope and TGF-binding domain which elevated regenerative functionality of *in vivo* tested scaffolds (table3).

6.4. *In vivo* applications

Although still mostly of designed peptide scaffolds are in the research and *In vitro* phase, a number of self-assembling peptide hydrogels are tested in animal models and some systems even undergo clinical translation (table3). Amongst all peptide based scaffolds, RAD16 has been extensively studied *in vivo* due to its well characterized physicochemical properties which are promising for *in vivo* applications. For instance, applied RAD 16-I hydrogel on the deep transection of the optic tract in the Syrian hamster could regenerate the axons and rejoined the injured brain tissue together and eventually with functional return of vision¹¹³. In another study, the injured spinal cord was reconnected through migration of host cells, growth of blood vessels, and axons into the RAD 16-I scaffold, consequently, with recovery of locomotor functions in the subjected rats¹¹⁴. Several *in vivo* studies also have been conducted on peptide amphiphile hydrogels. Designed constructs including active ligands such as IKVAV (a neurite-promoting laminin epitope), RGDS (integrin binding sequence) showed to promote the re-growth of seeded nerve cells in animal models¹¹⁵. Substance P (SP) (an 11-mer neuropeptide) has been indicated for its efficacy in wound healing. Kim *et al.* exploited this motif in conjugation with KLD12 peptide for bone tissue regeneration without cell transplantation. A coated PLA (poly-L-lactide) scaffold with beta-tricalcium phosphate (β -TCP) which was filled with a mixture of KLD12/KLD12-SP showed a chemoattraction for mesenchymal stem cells (MSCs) followed by bone tissue formation and regeneration¹¹⁶.

Hydrogels of P11-4 peptide are now available on the market as Curodont™ and used to repair early dental caries. The results showed that mineral deposition in the dental lesions significantly augmented due to increased remineralization and inhibition of demineralization^{101,117}.

Table 3. *In vivo* studies on self-assembled peptide hydrogels for tissue engineering applications.

Peptide sequence	Binding moieties	2nd structure	animal (spices)	organ	Ref .
RADA16-I	N/A	β -sheets	Syrian hamster	nervous system (optic tract)	113
RADA16-I	N/A	β -sheets	rat	N ervous system(spi nal cord)	114
RADA16-I	N/A	β -sheets	rat	brain (cortical tissue)	118
RADA16-I	N/A	β -sheets	Syrian hamster	brain, spinal cord, femoral artery, liver, or skin (hemostasi s)	119
RADA16-I	N/A	β -sheets	rat	Kidney (hemostasi s)	120
RAD16-II	biotin (to bind to IGF-1 - streptavidin complex)	β -sheets	mouse	heart	121
RADA16-I, RAD16-II	PDGF-BB (platelet-derived growth factor) loaded into the hydrogel	β -sheets	rat	heart	110
RADA16-I	N/A	β -sheets	rat	Skin(woun d healing)	122
KLD 12: Ac-KLDLKLKLDL-NH ₂	TGF- β 1, dexamethasone, and IGF-1 as chondrogenic factors (CF) mixed with the hydrogel	β -sheets	rabbit	joints (cartilage)	93
KLD12 mixed with KLD12-SP: AcKLDLKLKLDLGRPKPQQFFGLM-NH ₂	Substance P (SP): RPKPQQFFGLM	β -sheets	mouse	bone	116
C16-AAAAGGGLRKKLGKA	heparin-binding domain (LRKKLGKA)	β -sheets	at	bone	123
C16-V2A2K3GKLTWQELYQLKYKGI-NH ₂	VEGF-mimetic epitope(KLTWQELYQLKYKGI)	β -sheets	mouse	ischemic tissues (angiogene sis)	124
HSNGLPLGGGSEEEAAAVV V(K)-CO(CH ₂)10CH ₃	TGF-binding domain(NH ₂ -HSNGLPL-COOH)	β -sheets	rabbit	joints (cartilage)	125

C16-VVAAEEEEGIKVAV-COOH, C16-VVAAEERGDS	a neurite-promoting laminin epitope(IKVAV), Integrin binding sequence(RGDS)	β -sheets	rat	spinal cord	115
16C-4xCys-3xGly-1Xphosphorylated serine	phosphoserine (an inducer of mineralization)	β -sheets	rat	bone	126
P11-4	N/A	β -sheets	human	dental caries	^{101,1} 17

Although many peptide scaffolds showed safety *in vitro* and *in vivo*, there are some concerns about their short and long term adverse effects. For instance, Westermarck *et al.* showed that there is a possibility that synthetic fibrils may act as nucleating seeds for pathologic amyloid formation and deposition¹²⁷. They showed some amyloid deposits in some of the subjected mice with designed peptides including RAD16-I and silver nitrate (that can induce AA-amyloidosis) while no amyloid deposits were seen in the control group that only received silver nitrate. However, further studies are needed to confirm these findings¹²⁷.

7. Conclusions

A variety of studies on peptide self-assembly in the different fields of science including medicine and engineering indicate the capacity of such peptides to generate well-defined nano- architectures with unique functionalities. Since many different functionalities can be incorporated into the peptide sequence, including self-assembly domains, cell-attachment or signaling domains, versatile, multifunctional structures can be generated from a single molecular entity. This, combined with ease of production (recombinant or chemical synthesis) makes self-assembling peptides attractive for various biomedical applications. In this paper, we reviewed the structural features of peptide self-assembly and reported recent advances in their applications in drug delivery, vaccination and tissue regeneration. Although very useful examples have appeared in the literature on how self-assembling peptides can be used for drug delivery, tissue engineering or vaccination, there are still some hurdles that need to be overcome.

First, many publications on self-assembling peptides are descriptive, meaning the researchers describe how their self-assembling peptides behave under specific conditions, without being able to predict their self-assembling properties in advance or to make changes to obtain a desired supramolecular structure. Moreover, since self-assembly is influenced by many factors, some of which seem trivial and are therefore not always well described, it is very difficult to reproduce results from laboratory to laboratory. Nevertheless, with an increased understanding of the

intricate interplay of forces that drive the self-assembly, we can now start to predict the self-assembling behavior of simple peptides. This is further aided by the development of advanced molecular dynamics simulations that enable researchers better to predict the self-assembly behavior of self-assembling peptide candidates in advance^{128,129}.

Secondly, for commercial use of peptide-based biomaterials, cost-effective and scalable production methods are needed. Although, synthetic methods (solid and liquid phase peptide synthesis) cover most aspects of short peptide synthesis, the cost of raw materials (protected amino acids) and producing large amount of harmful waste set limitations to this production method. Proper adjustment of recombinant production in combination with site specific reaction for modification can be a good alternative for large-scale production of most self-assembling peptides¹³⁰.

Finally, an aspect, hardly addressed in the literature so far is the potential toxicity and immunogenicity of these peptide-based self-assembling systems. As reviewed in this paper, most self-assembling peptides consist of novel sequences or are derived from naturally existing amino acid sequences with a repetitive nature. Such repetitive, self-assembling polypeptides are generally suitable substrates for innate immune activation and subsequent activation of adaptive immune responses. Not many studies have looked into the immune activating potential of biomaterials based on self-assembling peptides, and this is a point of concern for future development. Furthermore, exposed hydrophobic patches often present in SA peptides may cause toxicity to cells by directly interacting with cell membranes. These issues should be considered and tested when developing self-assembling peptides for biomedical use.

In the coming decade many of these hurdles will without doubt be tackled and more sophisticated self-assembly designs will be created, which will pave the way for widespread applications of peptide-based drug delivery systems for a variety of biomedical applications.

8. References:

- (1) Dieckmann, G. R., Dalton, A. B., Johnson, P. A., Razal, J., Chen, J., Giordano, G. M., Muñoz, E., Musselman, I. H., Baughman, R. H., and Draper, R. K. (2003) Controlled assembly of carbon nanotubes by designed amphiphilic Peptide helices. *J. Am. Chem. Soc.* *125*, 1770–1777.
- (2) Liu, J., Wang, D., Zheng, Q., Lu, M., and Arora, P. S. (2008) Atomic structure of a short alpha-helix stabilized by a main chain hydrogen-bond surrogate. *J. Am. Chem. Soc.* *130*, 4334–4337.
- (3) Orner, B. P., Salvatella, X., Sánchez Quesada, J., De Mendoza, J., Giralt, E., and Hamilton, A. D. (2002) *De novo* protein surface design: use of cation-pi interactions to enhance binding between an alpha-helical peptide and a cationic molecule in 50 % aqueous solution. *Angew. Chem. Int. Ed. Engl.* *41*, 117–119.
- (4) Dong, H., Paramonov, S. E., and Hartgerink, J. D. (2008) Self-assembly of alpha-helical coiled coil nanofibers. *J. Am. Chem. Soc.* *130*, 13691–13695.
- (5) Woolfson, D. N. (2005) The design of coiled-coil structures and assemblies. *Adv. Protein Chem.* *70*, 79–112.
- (6) Papapostolou, D., Smith, A. M., Atkins, E. D. T., Oliver, S. J., Ryadnov, M. G., Serpell, L. C., and Woolfson, D. N. (2007) Engineering nanoscale order into a designed protein fiber. *Proc. Natl. Acad. Sci. U. S. A.* *104*, 10853–10858.
- (7) Toksöz, S., and Guler, M. O. (2009) Self-assembled peptidic nanostructures. *Nano Today* *4*, 458–469.
- (8) Fairman, R., and Akerfeldt, K. S. (2005) Peptides as novel smart materials. *Curr. Opin. Struct. Biol.* *15*, 453–463.
- (9) Lee, N. R., Bowerman, C. J., and Nilsson, B. L. (2013) Effects of varied sequence pattern on the self-assembly of amphipathic peptides. *Biomacromolecules* *14*, 3267–3277.
- (10) Bowerman, C. J., and Nilsson, B. L. (2012) Self-assembly of amphipathic β -sheet peptides: insights and applications. *Biopolymers*, *98*, 169-184.
- (11) Schneider, J. P., Pochan, D. J., Ozbas, B., Rajagopal, K., Pakstis, L., and Kretsinger, J. (2002) Responsive Hydrogels from the Intramolecular Folding and Self-Assembly of a Designed Peptide. *J. Am. Chem. Soc.* *124*, 15030–15037.
- (12) Rajagopal, K., and Schneider, J. P. (2004) Self-assembling peptides and proteins for nanotechnological applications. *Curr. Opin. Struct. Biol.* *14*, 480–486.
- (13) Kretsinger, J. K., Haines, L. A., Ozbas, B., Pochan, D. J., and Schneider, J. P. (2005) Cytocompatibility of self-assembled beta-hairpin peptide hydrogel surfaces. *Biomaterials* *26*, 5177–5186.

- (14) Salick, D. A., Kretsinger, J. K., Pochan, D. J., and Schneider, J. P. (2007) Inherent antibacterial activity of a peptide-based beta-hairpin hydrogel. *J. Am. Chem. Soc.* *129*, 14793–14799.
- (15) Adzhubei, A. A., Sternberg, M. J. E., and Makarov, A. A. (2013) Polyproline-II helix in proteins: structure and function. *J. Mol. Biol.* *425*, 2100–2132.
- (16) Van Hell, A. J., Klymchenko, A., Burgers, P. P., Moret, E. E., Jiskoot, W., Hennink, W. E., Crommelin, D. J. A., and Mastrobattista, E. (2010) Conformation and intermolecular interactions of SA2 peptides self-assembled into vesicles. *J. Phys. Chem. B* *114*, 11046–11052.
- (17) Shoulders, M. D., and Raines, R. T. (2009) Collagen structure and stability. *Annu. Rev. Biochem.* *78*, 929–958.
- (18) Schuster, T. B., de Bruyn Ouboter, D., Bordignon, E., Jeschke, G., and Meier, W. (2010) Reversible peptide particle formation using a mini amino acid sequence. *Soft Matter* *6*, 5596–5604.
- (19) Zhao, X., Pan, F., Xu, H., Yaseen, M., Shan, H., Hauser, C. A. E., Zhang, S., and Lu, J. R. (2010) Molecular self-assembly and applications of designer peptide amphiphiles. *Chem. Soc. Rev.* *39*, 3480–3498.
- (20) Shimada, T., Lee, S., Bates, F. S., Hotta, A., and Tirrell, M. (2009) Wormlike micelle formation in peptide-lipid conjugates driven by secondary structure transformation of the headgroups. *J. Phys. Chem. B* *113*, 13711–13714.
- (21) Khoe, U., Yang, Y., and Zhang, S. (2009) Self-assembly of nanodonut structure from a cone-shaped designer lipid-like peptide surfactant. *Langmuir* *25*, 4111–4114.
- (22) Hamley, I. W. (2011) Self-assembly of amphiphilic peptides. *Soft Matter* *7*, 4122–4138.
- (23) Vauthey, S., Santoso, S., Gong, H., Watson, N., and Zhang, S. (2002) Molecular self-assembly of surfactant-like peptides to form nanotubes and nanovesicles. *Proc. Natl. Acad. Sci. U. S. A.* *99*, 5355–5360.
- (24) Santoso, S., Hwang, W., Hartman, H., and Zhang, S. (2002) Self-assembly of Surfactant-like Peptides with Variable Glycine Tails to Form Nanotubes and Nanovesicles. *Nano Lett.* *2*, 687–691.
- (25) Van Hell, A. J., Costa, C. I. C. A., Flesch, F. M., Sutter, M., Jiskoot, W., Crommelin, D. J. A., Hennink, W. E., and Mastrobattista, E. (2007) Self-assembly of recombinant amphiphilic oligopeptides into vesicles. *Biomacromolecules* *8*, 2753–2761.
- (26) Jacob N. Israelachvili . (2011) Soft and Biological Structures. Intermolecular and Surface Forces. 3rd ed. pp 535-76, Chapter 20, Elsevier Science Publisher, San Diego, CA.
- (27) Luo, Z., Åkerman, B., Zhang, S., and Nordén, B. (2010) Structures of self-assembled amphiphilic peptide-heterodimers: effects of concentration, pH, temperature and ionic strength. *Soft Matter* *6*, 2260–2270.

- (28) Mishra, A., Panda, J. J., Basu, A., and Chauhan, V. S. (2008) Nanovesicles based on self-assembly of conformationally constrained aromatic residue containing amphiphilic dipeptides. *Langmuir* 24, 4571–4576.
- (29) Ischakov, R., Adler-Abramovich, L., Buzhansky, L., Shekhter, T., and Gazit, E. (2013) Peptide-based hydrogel nanoparticles as effective drug delivery agents. *Bioorg. Med. Chem.* 21, 3517–3522.
- (30) Hartgerink, J. D., Beniash, E., and Stupp, S. I. (2001) Self-assembly and mineralization of peptide-amphiphile nanofibers. *Science* 294, 1684–1688.
- (31) Bulut, S., Erkal, T. S., Toksoz, S., Tekinay, A. B., Tekinay, T., and Guler, M. O. (2011) Slow release and delivery of antisense oligonucleotide drug by self-assembled peptide amphiphile nanofibers. *Biomacromolecules* 12, 3007–3014.
- (32) Nagai, A., Nagai, Y., Qu, H., and Zhang, S. (2007) Dynamic Behaviors of Lipid-Like Self-Assembling Peptide A6D and A6K Nanotubes. *J. Nanosci. Nanotechnol.* 7, 2246–2252.
- (33) Yan, X., He, Q., Wang, K., Duan, L., Cui, Y., and Li, J. (2007) Transition of cationic dipeptide nanotubes into vesicles and oligonucleotide delivery. *Angew. Chem. Int. Ed. Engl.* 46, 2431–2434.
- (34) Seabra, A. B., and Durán, N. (2013) Biological applications of peptides nanotubes: an overview. *Peptides* 39, 47–54.
- (35) Aggeli, A., Bell, M., Boden, N., Keen, J. N., Knowles, P. F., McLeish, T. C., Pitkeathly, M., and Radford, S. E. (1997) Responsive gels formed by the spontaneous self-assembly of peptides into polymeric beta-sheet tapes. *Nature* 386, 259–262.
- (36) Fishwick, C. W. G., Beevers, A. J., Carrick, L. M., Whitehouse, C. D., Aggeli, A., and Boden, N. (2003) Structures of Helical β -Tapes and Twisted Ribbons: The Role of Side-Chain Interactions on Twist and Bend Behavior. *Nano Lett.* 3, 1475–1479.
- (37) Cui, H., Muraoka, T., Cheetham, A. G., and Stupp, S. I. (2009) Self-assembly of giant peptide nanobelts. *Nano Lett.* 9, 945–951.
- (38) Gazit, E. (2007) Self-assembled peptide nanostructures: the design of molecular building blocks and their technological utilization. *Chem. Soc. Rev.* 36, 1263–1269.
- (39) Aggeli, A., Nyrkova, I. A., Bell, M., Harding, R., Carrick, L., McLeish, T. C., Semenov, A. N., and Boden, N. (2001) Hierarchical self-assembly of chiral rod-like molecules as a model for peptide beta-sheet tapes, ribbons, fibrils, and fibers. *Proc. Natl. Acad. Sci. U. S. A.* 98, 11857–11862.
- (40) Pashuck, E. T., and Stupp, S. I. (2010) Direct observation of morphological transformation from twisted ribbons into helical ribbons. *J. Am. Chem. Soc.* 132, 8819–8821.

- (41) Tangri, S., Mothé, B. R., Eisenbraun, J., Sidney, J., Southwood, S., Briggs, K., Zinckgraf, J., Bilsel, P., Newman, M., Chesnut, R., LiCalsi, C., and Sette, A. (2005) Rationally engineered therapeutic proteins with reduced immunogenicity. *J. Immunol.* *174*, 3187–3196.
- (42) Onda, M. (2009) Reducing the Immunogenicity of Protein Therapeutics. *Curr. Drug Targets* *10*, 131–139.
- (43) King, C., Garza, E. N., Mazor, R., Linehan, J. L., Pastan, I., Pepper, M., and Baker, D. (2014) Removing T-cell epitopes with computational protein design. *Proc. Natl. Acad. Sci. U. S. A.* *111*, 8577–8582.
- (44) Van Beers, M. M. C., Jiskoot, W., and Schellekens, H. (2010) On the role of aggregates in the immunogenicity of recombinant human interferon beta in patients with multiple sclerosis. *J. Interferon Cytokine Res.* *30*, 767–75.
- (45) Hauser, C. A. E., and Zhang, S. (2010) Designer self-assembling peptide nanofiber biological materials. *Chem. Soc. Rev.* *39*, 2780–2790.
- (46) Semino, C. E. (2008) Self-assembling Peptides: From Bio-inspired Materials to Bone Regeneration. *J. Dent. Res.* *87*, 606–616.
- (47) Cormier, A. R., Pang, X., Zimmerman, M. I., Zhou, H.-X., and Paravastu, A. K. (2013) Molecular structure of RADA16-I designer self-assembling peptide nanofibers. *ACS Nano* *7*, 7562–7572.
- (48) Vermonden, T., Censi, R., and Hennink, W. E. (2012) Hydrogels for protein delivery. *Chem. Rev.* *112*, 2853–2888.
- (49) Koutsopoulos, S., Unsworth, L. D., Nagai, Y., and Zhang, S. (2009) Controlled release of functional proteins through designer self-assembling peptide nanofiber hydrogel scaffold. *Proc. Natl. Acad. Sci. U. S. A.* *106*, 4623–4628.
- (50) Gelain, F., Unsworth, L. D., and Zhang, S. (2010) Slow and sustained release of active cytokines from self-assembling peptide scaffolds. *J. Control. Release* *145*, 231–239.
- (51) Nagai, Y., Unsworth, L. D., Koutsopoulos, S., and Zhang, S. (2006) Slow release of molecules in self-assembling peptide nanofiber scaffold. *J. Control. Release* *115*, 18–25.
- (52) Gudlur, S., Sukthankar, P., Gao, J., Avila, L. A., Hiromasa, Y., Chen, J., Iwamoto, T., and Tomich, J. M. (2012) Peptide nanovesicles formed by the self-assembly of branched amphiphilic peptides. *PLoS One* *7*, e45374.
- (53) Van Hell, A. J., Fretz, M. M., Crommelin, D. J. A., Hennink, W. E., and Mastrobattista, E. (2010) Peptide nanocarriers for intracellular delivery of photosensitizers. *J. Control. Release* *141*, 347–353.
- (54) Alam, S., Panda, J. J., and Chauhan, V. S. (2012) Novel dipeptide nanoparticles for effective curcumin delivery. *Int. J. Nanomedicine* *7*, 4207–4222.

- (55) Silva, R. F., Araújo, D. R., Silva, E. R., Ando, R. A., and Alves, W. A. (2013) L-diphenylalanine microtubes as a potential drug-delivery system: characterization, release kinetics, and cytotoxicity. *Langmuir* 29, 10205–10212.
- (56) Vijayaraj, R., Van Damme, S., Bultinck, P., and Subramanian, V. (2013) Theoretical studies on the transport mechanism of 5-fluorouracil through cyclic peptide based nanotubes. *Phys. Chem. Chem. Phys.* 15, 1260–1270.
- (57) Koutsopoulos, S., and Zhang, S. (2012) Two-layered injectable self-assembling peptide scaffold hydrogels for long-term sustained release of human antibodies. *J. Control. Release* 160, 451–458.
- (58) Altunbas, A., Lee, S. J., Rajasekaran, S. A., Schneider, J. P., and Pochan, D. J. (2011) Encapsulation of curcumin in self-assembling peptide hydrogels as injectable drug delivery vehicles. *Biomaterials* 32, 5906–5914.
- (59) Ruan, L., Zhang, H., Luo, H., Liu, J., Tang, F., Shi, Y.-K., and Zhao, X. (2009) Designed amphiphilic peptide forms stable nanoweb, slowly releases encapsulated hydrophobic drug, and accelerates animal hemostasis. *Proc. Natl. Acad. Sci. U. S. A.* 106, 5105–5110.
- (60) Branco, M. C., Pochan, D. J., Wagner, N. J., and Schneider, J. P. (2009) Macromolecular diffusion and release from self-assembled beta-hairpin peptide hydrogels. *Biomaterials* 30, 1339–1347.
- (61) Fung, S. Y., Yang, H., and Chen, P. (2008) Sequence effect of self-assembling peptides on the complexation and *in vitro* delivery of the hydrophobic anticancer drug ellipticine. *PLoS One* 3, e1956.
- (62) Matson, J. B., Newcomb, C. J., Bitton, R., and Stupp, S. I. (2012) Nanostructure-templated control of drug release from peptide amphiphile nanofiber gels. *Soft Matter* 8, 3586–3595.
- (63) Webber, M. J., Matson, J. B., Tamboli, V. K., and Stupp, S. I. (2012) Controlled release of dexamethasone from peptide nanofiber gels to modulate inflammatory response. *Biomaterials* 33, 6823–6832.
- (64) Matson, J. B., Webber, M. J., Tamboli, V. K., Weber, B., and Stupp, S. I. (2012) A Peptide-Based Material for Therapeutic Carbon Monoxide Delivery. *Soft Matter* 8, 2689–2692.
- (65) Matson, J. B., and Stupp, S. I. (2011) Drug release from hydrazone-containing peptide amphiphiles. *Chem. Commun.* 47, 7962–7964.
- (66) Soukasene, S., Toft, D. J., Moyer, T. J., Lu, H., Lee, H.-K., Standley, S. M., Cryns, V. L., and Stupp, S. I. (2011) Antitumor activity of peptide amphiphile nanofiber-encapsulated camptothecin. *ACS Nano* 5, 9113–9121.
- (67) Bond, C. W., Angeloni, N. L., Harrington, D. A., Stupp, S. I., McKenna, K. E., and Podlasek, C. A. (2011) Peptide amphiphile nanofiber delivery of sonic hedgehog protein to reduce smooth muscle apoptosis in the penis after cavernous nerve resection. *J. Sex. Med.* 8, 78–89.

- (68) Castelletto, V., McKendrick, J. E., Hamley, I. W., Olsson, U., and Cenker, C. (2010) PEGylated amyloid peptide nanocontainer delivery and release system. *Langmuir* 26, 11624–11627.
- (69) Tzokova, N., Fernyhough, C. M., Butler, M. F., Armes, S. P., Ryan, A. J., Topham, P. D., and Adams, D. J. (2009) The effect of PEO length on the self-assembly of poly(ethylene oxide)-tetrapeptide conjugates prepared by “Click” chemistry. *Langmuir* 25, 11082–11089.
- (70) Castelletto, V., and Hamley, I. W. (2009) Self assembly of a model amphiphilic phenylalanine peptide/polyethylene glycol block copolymer in aqueous solution. *Biophys. Chem.* 141, 169–174.
- (71) Hamley, I. W., Cheng, G., and Castelletto, V. (2011) A thermoresponsive hydrogel based on telechelic PEG end-capped with hydrophobic dipeptides. *Macromol. Biosci.* 11, 1068–1078.
- (72) Eckhardt, D., Groenewolt, M., Krause, E., and Börner, H. G. (2005) Rational design of oligopeptide organizers for the formation of poly(ethylene oxide) nanofibers. *Chem. Commun. (Camb)*. 2814–2816.
- (73) De Graaf, A. J., Boere, K. W. M., Kemmink, J., Fokkink, R. G., van Nostrum, C. F., Rijkers, D. T. S., van der Gucht, J., Wienk, H., Baldus, M., Mastrobattista, E., Vermonden, T., and Hennink, W. E. (2011) Looped structure of flowerlike micelles revealed by 1H NMR relaxometry and light scattering. *Langmuir* 27, 9843–9848.
- (74) Hua, S.-H., Li, Y.-Y., Liu, Y., Xiao, W., Li, C., Huang, F.-W., Zhang, X.-Z., and Zhuo, R.-X. (2010) Self-Assembled Micelles Based on PEG-Polypeptide Hybrid Copolymers for Drug Delivery. *Macromol. Rapid Commun.* 31, 81–86.
- (75) Dong, H., Dube, N., Shu, J. Y., Seo, J. W., Mahakian, L. M., Ferrara, K. W., and Xu, T. (2012) Long-circulating 15 nm micelles based on amphiphilic 3-helix peptide-PEG conjugates. *ACS Nano* 6, 5320–5329.
- (76) Dube, N., Shu, J. Y., Dong, H., Seo, J. W., Ingham, E., Kheiriloom, A., Chen, P.-Y., Forsayeth, J., Bankiewicz, K., Ferrara, K. W., and Xu, T. (2013) Evaluation of doxorubicin-loaded 3-helix micelles as nanocarriers. *Biomacromolecules* 14, 3697–3705.
- (77) Jabbari, E., Yang, X., Moeinzadeh, S., and He, X. (2013) Drug release kinetics, cell uptake, and tumor toxicity of hybrid VVVVVVKK peptide-assembled polylactide nanoparticles. *Eur. J. Pharm. Biopharm.* 84, 49–62.
- (78) Rudra, J. S., Tian, Y. F., Jung, J. P., and Collier, J. H. (2010) A self-assembling peptide acting as an immune adjuvant. *Proc. Natl. Acad. Sci. U. S. A.* 107, 622–627.
- (79) De Temmerman, M.-L., Rejman, J., Demeester, J., Irvine, D. J., Gander, B., and De Smedt, S. C. (2011) Particulate vaccines: on the quest for optimal delivery and immune response. *Drug Discov. Today* 16, 569–582.

- (80) Rudra, J. S., Sun, T., Bird, K. C., Daniels, M. D., Gasiorowski, J. Z., Chong, A. S., and Collier, J. H. (2012) Modulating adaptive immune responses to peptide self-assemblies. *ACS Nano* 6, 1557–1564.
- (81) Chen, J., Pompano, R. R., Santiago, F. W., Maillat, L., Sciammas, R., Sun, T., Han, H., Topham, D. J., Chong, A. S., and Collier, J. H. (2013) The use of self-adjuvanting nanofiber vaccines to elicit high-affinity B cell responses to peptide antigens without inflammation. *Biomaterials* 34, 8776–8785.
- (82) Black, M., Trent, A., Tirrell, M., and Olive, C. (2010) Advances in the design and delivery of peptide subunit vaccines with a focus on toll-like receptor agonists. *Expert Rev. Vaccines* 9, 157–173.
- (83) Boato, F., Thomas, R. M., Ghasparian, A., Freund-Renard, A., Moehle, K., and Robinson, J. A. (2007) Synthetic virus-like particles from self-assembling coiled-coil lipopeptides and their use in antigen display to the immune system. *Angew. Chem. Int. Ed. Engl.* 46, 9015–9018.
- (84) Glover, D. J., Lipps, H. J., and Jans, D. A. (2005) Towards safe, non-viral therapeutic gene expression in humans. *Nat. Rev. Genet.* 6, 299–310.
- (85) Rudra, J. S., Tripathi, P. K., Hildeman, D. A., Jung, J. P., and Collier, J. H. (2010) Immune responses to coiled coil supramolecular biomaterials. *Biomaterials* 31, 8475–8483.
- (86) Rudra, J. S., Mishra, S., Chong, A. S., Mitchell, R. A., Nardin, E. H., Nussenzweig, V., and Collier, J. H. (2012) Self-assembled peptide nanofibers raising durable antibody responses against a malaria epitope. *Biomaterials* 33, 6476–6484.
- (87) Schwartz, J. J., and Zhang, S. (2000) Peptide-mediated cellular delivery. *Curr. Opin. Mol. Ther* 2, 162–167.
- (88) Sharma, R., Ghasparian, A., Robinson, J. A., and McCullough, K. C. (2012) Synthetic virus-like particles target dendritic cell lipid rafts for rapid endocytosis primarily but not exclusively by macropinocytosis. *PLoS One* 7, e43248.
- (89) Chesson, C. B., Huelsmann, E. J., Lacek, A. T., Kohlhapp, F. J., Webb, M. F., Nabatiyan, A., Zloza, A., and Rudra, J. S. (2014) Antigenic peptide nanofibers elicit adjuvant-free CD8⁺ T cell responses. *Vaccine* 32, 1174–1180.
- (90) Zhang, S., Holmes, T., Lockshin, C., and Rich, A. (1993) Spontaneous assembly of a self-complementary oligopeptide to form a stable macroscopic membrane. *Proc. Natl. Acad. Sci. U. S. A.* 90, 3334–3338.
- (91) Zhang, S., Holmes, T. C., DiPersio, C. M., Hynes, R. O., Su, X., and Rich, A. (1995) Self-complementary oligopeptide matrices support mammalian cell attachment. *Biomaterials* 16, 1385–1393.

- (92) Genové, E., Shen, C., Zhang, S., and Semino, C. E. (2005) The effect of functionalized self-assembling peptide scaffolds on human aortic endothelial cell function. *Biomaterials* 26, 3341–3351.
- (93) Miller, R. E., Grodzinsky, A. J., Vanderploeg, E. J., Lee, C., Ferris, D. J., Barrett, M. F., Kisiday, J. D., and Frisbie, D. D. (2010) Effect of self-assembling peptide, chondrogenic factors, and bone marrow-derived stromal cells on osteochondral repair. *Osteoarthritis Cartilage* 18, 1608–1619.
- (94) Kisiday, J., Jin, M., Kurz, B., Hung, H., Semino, C., Zhang, S., and Grodzinsky, A. J. (2002) Self-assembling peptide hydrogel fosters chondrocyte extracellular matrix production and cell division: implications for cartilage tissue repair. *Proc. Natl. Acad. Sci. U. S. A.* 99, 9996–10001.
- (95) Pochan, D. J., Schneider, J. P., Kretsinger, J., Ozbas, B., Rajagopal, K., and Haines, L. (2003) Thermally reversible hydrogels via intramolecular folding and consequent self-assembly of a *de novo* designed peptide. *J. Am. Chem. Soc.* 125, 11802–11803.
- (96) Haines-Butterick, L., Rajagopal, K., Branco, M., Salick, D., Rughani, R., Pilarz, M., Lamm, M. S., Pochan, D. J., and Schneider, J. P. (2007) Controlling hydrogelation kinetics by peptide design for three-dimensional encapsulation and injectable delivery of cells. *Proc. Natl. Acad. Sci. U. S. A.* 104, 7791–7796.
- (97) Sharp, T. H., Bruning, M., Mantell, J., Sessions, R. B., Thomson, A. R., Zaccai, N. R., Brady, R. L., Verkade, P., and Woolfson, D. N. (2012) Cryo-transmission electron microscopy structure of a gigadalton peptide fiber of *de novo* design. *Proc. Natl. Acad. Sci. U. S. A.* 109, 13266–13271.
- (98) Moutevelis, E., and Woolfson, D. N. (2009) A periodic table of coiled-coil protein structures. *J. Mol. Biol.* 385, 726–732.
- (99) Banwell, E. F., Abelardo, E. S., Adams, D. J., Birchall, M. A., Corrigan, A., Donald, A. M., Kirkland, M., Serpell, L. C., Butler, M. F., and Woolfson, D. N. (2009) Rational design and application of responsive alpha-helical peptide hydrogels. *Nat. Mater.* 8, 596–600.
- (100) Davies, R. P. W., Aggeli, A., Beevers, A. J., Boden, N., Carrick, L. M., Fishwick, C. W. G., Mcleish, T. C. B., Nyrkova, I., and Semenov, A. N. (2006) Self-assembling β -Sheet Tape Forming Peptides. *Supramol. Chem.* 18, 435–443.
- (101) Brunton, P. A., Davies, R. P. W., Burke, J. L., Smith, A., Aggeli, A., Brookes, S. J., and Kirkham, J. (2013) Treatment of early caries lesions using biomimetic self-assembling peptides—a clinical safety trial. *Br. Dent. J.* 215, E6.
- (102) Collier, J. H. (2008) Modular self-assembling biomaterials for directing cellular responses. *Soft Matter* 4, 2310–2315.
- (103) Mahler, A., Reches, M., Rechter, M., Cohen, S., and Gazit, E. (2006) Rigid, Self-Assembled Hydrogel Composed of a Modified Aromatic Dipeptide. *Adv. Mater.* 18, 1365–1370.

- (104) Jayawarna, V., Smith, A., Gough, J. E., and Ulijn, R. V. (2007) Three-dimensional cell culture of chondrocytes on modified di-phenylalanine scaffolds. *Biochem. Soc. Trans.* 35, 535–537.
- (105) Jayawarna, V., Ali, M., Jowitt, T. A., Miller, A. F., Saiani, A., Gough, J. E., and Ulijn, R. V. (2006) Nanostructured Hydrogels for Three-Dimensional Cell Culture Through Self-Assembly of Fluorenylmethoxycarbonyl-Dipeptides. *Adv. Mater.* 18, 611–614.
- (106) Zhou, M., Smith, A. M., Das, A. K., Hodson, N. W., Collins, R. F., Ulijn, R. V., and Gough, J. E. (2009) Self-assembled peptide-based hydrogels as scaffolds for anchorage-dependent cells. *Biomaterials* 30, 2523–2530.
- (107) Zhang, S., Greenfield, M. A., Mata, A., Palmer, L. C., Bitton, R., Mantei, J. R., Aparicio, C., de la Cruz, M. O., and Stupp, S. I. (2010) A self-assembly pathway to aligned monodomain gels. *Nat. Mater.* 9, 594–601.
- (108) Jung, J. P., Moyano, J. V., and Collier, J. H. (2011) Multifactorial optimization of endothelial cell growth using modular synthetic extracellular matrices. *Integr. Biol. (Camb)*. 3, 185–196.
- (109) Schneider, A., Garlick, J. A., and Egles, C. (2008) Self-assembling peptide nanofiber scaffolds accelerate wound healing. *PLoS One* 3, e1410.
- (110) Dubois, G., Segers, V. F. M., Bellamy, V., Sabbah, L., Peyrard, S., Bruneval, P., Hagège, A. A., Lee, R. T., and Menasché, P. (2008) Self-assembling peptide nanofibers and skeletal myoblast transplantation in infarcted myocardium. *J. Biomed. Mater. Res. B. Appl. Biomater.* 87, 222–228.
- (111) Gelain, F., Bottai, D., Vescovi, A., and Zhang, S. (2006) Designer self-assembling peptide nanofiber scaffolds for adult mouse neural stem cell 3-dimensional cultures. *PLoS One* 1, e119.
- (112) Wang, B., Sun, C., Shao, Z., Yang, S., Che, B., Wu, Q., and Liu, J. (2014) Designer self-assembling Peptide nanofiber scaffolds containing link protein N-terminal peptide induce chondrogenesis of rabbit bone marrow stem cells. *Biomed Res. Int.* Article ID: 421954.
- (113) Ellis-Behnke, R. G., Liang, Y.-X., You, S.-W., Tay, D. K. C., Zhang, S., So, K.-F., and Schneider, G. E. (2006) Nano neuro knitting: peptide nanofiber scaffold for brain repair and axon regeneration with functional return of vision. *Proc. Natl. Acad. Sci. U. S. A.* 103, 5054–5059.
- (114) Guo, J., Su, H., Zeng, Y., Liang, Y.-X., Wong, W. M., Ellis-Behnke, R. G., So, K.-F., and Wu, W. (2007) Reknitting the injured spinal cord by self-assembling peptide nanofiber scaffold. *Nanomedicine* 3, 311–321.
- (115) Berns, E. J., Sur, S., Pan, L., Goldberger, J. E., Suresh, S., Zhang, S., Kessler, J. A., and Stupp, S. I. (2014) Aligned neurite outgrowth and directed cell migration in self-assembled monodomain gels. *Biomaterials* 35, 185–195.
- (116) Kim, S. H., Hur, W., Kim, J. E., Min, H. J., Kim, S., Min, H. S., Kim, B. K., Kim, S. H., Choi, T. H., and Jung, Y. (2014) Self-Assembling Peptide Nanofibers Coupled with Neuropeptide Substance P for Bone Tissue Engineering. *Tissue Eng. Part A*. DOI: 10.1089/ten.tea.2014.0472.

- (117) Kirkham, J., Firth, A., Vernals, D., Boden, N., Robinson, C., Shore, R. C., Brookes, S. J., and Aggeli, A. (2007) Self-assembling Peptide Scaffolds Promote Enamel Remineralization. *J. Dent. Res.* 86, 426–430.
- (118) Guo, J., Leung, K. K. G., Su, H., Yuan, Q., Wang, L., Chu, T.-H., Zhang, W., Pu, J. K. S., Ng, G. K. P., Wong, W. M., Dai, X., and Wu, W. (2009) Self-assembling peptide nanofiber scaffold promotes the reconstruction of acutely injured brain. *Nanomedicine* 5, 345–351.
- (119) Ellis-Behnke, R. G., Liang, Y.-X., Tay, D. K. C., Kau, P. W. F., Schneider, G. E., Zhang, S., Wu, W., and So, K.-F. (2006) Nano hemostat solution: immediate hemostasis at the nanoscale. *Nanomedicine* 2, 207–215.
- (120) Song, H., Zhang, L., and Zhao, X. (2010) Hemostatic efficacy of biological self-assembling peptide nanofibers in a rat kidney model. *Macromol. Biosci.* 10, 33–39.
- (121) Davis, M. E., Motion, J. P. M., Narmoneva, D. A., Takahashi, T., Hakuno, D., Kamm, R. D., Zhang, S., and Lee, R. T. (2005) Injectable self-assembling peptide nanofibers create intramyocardial microenvironments for endothelial cells. *Circulation* 111, 442–450.
- (122) Meng, H., Chen, L., Ye, Z., Wang, S., and Zhao, X. (2009) The effect of a self-assembling peptide nanofiber scaffold (peptide) when used as a wound dressing for the treatment of deep second degree burns in rats. *J. Biomed. Mater. Res. B. Appl. Biomater.* 89, 379–391.
- (123) Lee, S. S., Huang, B. J., Kaltz, S. R., Sur, S., Newcomb, C. J., Stock, S. R., Shah, R. N., and Stupp, S. I. (2013) Bone regeneration with low dose BMP-2 amplified by biomimetic supramolecular nanofibers within collagen scaffolds. *Biomaterials* 34, 452–459.
- (124) Webber, M. J., Tongers, J., Newcomb, C. J., Marquardt, K.-T., Bauersachs, J., Losordo, D. W., and Stupp, S. I. (2011) Supramolecular nanostructures that mimic VEGF as a strategy for ischemic tissue repair. *Proc. Natl. Acad. Sci. U. S. A.* 108, 13438–13443.
- (125) Shah, R. N., Shah, N. A., Del Rosario Lim, M. M., Hsieh, C., Nuber, G., and Stupp, S. I. (2010) Supramolecular design of self-assembling nanofibers for cartilage regeneration. *Proc. Natl. Acad. Sci. U. S. A.* 107, 3293–3298.
- (126) Sargeant, T. D., Guler, M. O., Oppenheimer, S. M., Mata, A., Satcher, R. L., Dunand, D. C., and Stupp, S. I. (2008) Hybrid bone implants: self-assembly of peptide amphiphile nanofibers within porous titanium. *Biomaterials* 29, 161–171.
- (127) Westermark, P., Lundmark, K., and Westermark, G. T. (2009) Fibrils from designed non-amyloid-related synthetic peptides induce AA-amyloidosis during inflammation in an animal model. *PLoS One* 4, e6041.
- (128) Lee, O.-S., Cho, V., and Schatz, G. C. (2012) Modeling the self-assembly of peptide amphiphiles into fibers using coarse-grained molecular dynamics. *Nano Lett.* 12, 4907–4913.
- (129) Guo, C., Luo, Y., Zhou, R., and Wei, G. (2012) Probing the self-assembly mechanism of diphenylalanine-based peptide nanovesicles and nanotubes. *ACS Nano* 6, 3907–3918.
- (130) Riley, J. M., Aggeli, A., Koopmans, R. J., and McPherson, M. J. (2009) Bioproduction and characterization of a pH responsive self-assembling peptide. *Biotechnol. Bioeng.* 103, 241–251.

Chapter 3

Optimization of the recombinant production and purification of a self-assembling peptide in *Escherichia coli*

Mazda Rad-Malekshahi, Matthias Flement, Wim E. Hennink and Enrico Mastrobattista

Department of Pharmaceutics, Utrecht Institute for Pharmaceutical Sciences, Utrecht University,
Utrecht, The Netherlands

Published in *Microbial Cell Factories* 2014,13(1):987

Abstract

Amphiphilic peptides are important building blocks to generate nanostructured biomaterials for drug delivery and tissue engineering applications. We have shown that the self-assembling peptide SA2 (Ac-AAVVLLLWEE-COOH) can be recombinantly produced in *E. coli* when fused to the small ubiquitin-like modifier (SUMO) protein. Although this system yielded peptides of high purity with no residual amino acids after cleavage of the SUMO fusion protein, the yield after purification was generally low (~1 mg/L bacterial culture) as compared to other peptides and proteins produced with the same method and under the same conditions. The aim of this study is to understand the underlying mechanisms causing the low yield of this recombinant peptide in *E. coli* and to optimize both production and purification of recombinant SA2 peptides. It was demonstrated that by simply changing the medium to a well-balanced auto-induction medium the yield of recombinant production was augmented (~4 fold). Moreover, it was demonstrated that self-assembly of SUMO-SA2 fusion proteins caused the low peptide yields after purification. By replacing the second IMAC purification step with a selective precipitation step, peptide yields could be increased approx. 3 fold. With these optimizations in place the overall yield of purified SA2 peptide increased with 12-fold. Premature self-assembly of the SUMO-SA2 fusion construct interfered with proper purification of the SA2 peptide, resulting in low yields of purified peptide and this could be prevented by changing the mode of purification. These findings are important when setting up purification schemes for other self-assembling peptides with the use of a SUMO fusion construct.

1. Introduction

Amphiphilic peptides (Aps) represent a group of small peptides with sequestered hydrophobic and hydrophilic domains. Their amphiphilic nature allows them to self-assemble into supramolecular structures, such as micelles, nanotubes, belts or vesicles with interesting applications in drug delivery and tissue engineering¹⁻¹⁰.

Aps are produced by solid-phase peptide synthesis (SPPS)^{11,12} but also recombinantly in bacteria and yeast¹³⁻¹⁶. Production of Aps via SPPS has some limitations. The presence of large stretches of hydrophobic amino acids in Aps may cause collapse of the peptides on the solid support, which increases the risk of truncated peptides that even become more problematic in large scale synthesis¹⁷. Such truncated peptides which often differ in only one amino acid from the full length peptide, are difficult to remove during subsequent purification steps. It was shown that such impurities can have profound effects on the self-assembling behavior of these Aps¹⁷. Besides purity, high scale production of SPPS is costly^{18,19}.

Numerous attempts have been made for recombinant production of relatively small, self-assembling peptides. However, such methods have encountered several challenges: their amphiphilic nature and tendency to self-assemble can cause toxicity problems in the production cells or can lead to proteolytic degradation or sequestering in inclusion bodies²⁰. To prevent this, APs are often fused to a larger chaperone proteins²¹.

One such fusion construct that favors soluble production of small hydrophobic peptides is the small ubiquitin-like modifying protein (SUMO)²¹. It can protect the protein/peptide by using its chaperoning properties, enhance the solubility and increase production²⁰. This relatively small fusion protein (12.2 kD) can be specifically cleaved and separated from its fused partner by SUMO protease²². An important advantage of the SUMO fusion protein technology is that it generates peptides with a native N-terminus without residual amino acids after cleavage with SUMO protease^{22,23}. In previous studies, we have used the SUMO fusion technology for the recombinant production and purification of a 10 amino-acid amphiphilic peptide called SA2 (AAVVLLLWEE) in *E. coli*⁶. The fusion protein consisted of a 6 residue histidine tag at the N-terminus for purification, SUMO for stability and solubility and the SA2 peptide and the C-terminus. Cleavage of the fusion protein with SUMO protease enabled the release of SA2 without any residual amino acids (Figure 1). Since SA2 self-assembles into nanovesicles, the SUMO fusion technology was used to prevent premature self-assembly of the peptides into supramolecular structures and to keep the monomeric peptide soluble during recombinant

production. Although we succeeded to purify SA2 peptides following this approach, the yield was rather low, with approximately 1mg of purified SA2 peptide/L bacterial culture.

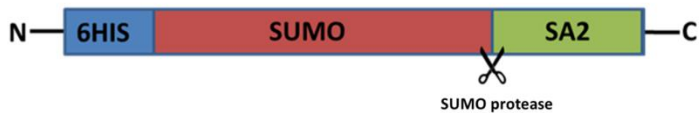


Figure 1 Schematic illustration of 6His-tagged SUMO-SA2. SUMO protease can specifically cut the recombinant construct and release the SA2 peptide.

In this study, the aim was therefore to determine and optimize the critical steps in the production and purification scheme of SA2 that limits the purified peptide yield and to maximize production yields of SA2 peptide.

2. Results and Discussion

2.1. Peptide biosynthesis

To increase the yield of purified, recombinant SA2 we first focused on the optimization of production of SUMO-SA2 in *E. coli*. Production of potentially toxic proteins generally does not benefit from the use of strong promoters to maximize transcription levels. Instead, tight control over the induction of expression is necessary to prevent premature expression and subsequent toxicity to the host. Strategies that enable induction of expression at high cell densities using auto-induction medium have been used to yield good levels of recombinant proteins²⁴. Moreover, auto-induction media have the added advantage of very low to no expression prior to the time of induction because of the catabolyte repression effect of glucose, which makes it particularly suitable for the expression of potentially toxic recombinant proteins²⁵. Here, we tested two different media for recombinant production of SA2: 1). Standard LB medium with IPTG as irreversible inducer of SUMO-SA2 expression under control of the *T7lac* promoter, and 2). ZYM medium, which leads to auto-induction of SUMO-SA2 expression based on glucose as preferable carbon source for *E. coli*. A restricted concentration of glucose not only is consumed preferentially during growth but also inhibits uptake of lactose. After consumption and depletion of glucose to reach a high cell density, lactose will be taken up and converted to the allolactose which is an inducer for T7 RNA polymerase expression under control of the *lacUV5* promoter and

unblocks the *T7lac* promoter, leading to high levels of expression²⁴. A 5 ml overnight culture of *E. coli* was diluted in 1000 ml of LB or ZYM medium. OD₆₀₀ was monitored for LB medium and IPTG was added when the OD₆₀₀ was ~0.4. Four hours after induction with IPTG (in case of LB medium) and 16 hrs after inoculation (in case of ZYM medium) the wet weight of the bacterial pellet was determined (Table 1). A higher biomass (~3.5 fold) was reached using the ZYM autoinduction medium in comparison with IPTG induction in LB medium²⁴.

Table 1. Yield of biomass, SUMO-SA2 and SA2 (mg) produced per liter of LB or ZYM medium

Medium	Wet Biomass (g)	SUMO-SA2 (mg)	Expected amount of SA2 (mg)	Amount of cleaved SA2(mg)	Amount of purified SA2(mg)
LB + 1 mM IPTG	2.18 ± 0.11	63 ± 2	5.04 ± 0.18	4.26 ± 0.15	3.20 ± 0.20
ZYM (Auto induction)	7.62 ± 0.03	243 ± 5	19.44 ± 0.45	16.21 ± 0.32	12.16 ± 0.43

These results show that compared to induction with IPTG, the auto induction medium significantly increased SUMO-SA2 production and subsequently the yield of purified SA2 peptides (>3.8 times).

2.2. SUMO-SA2 purification

After induction, *E.coli* cells were harvested and lysed. Cleared lysate was used for further purification of the SUMO-SA2 construct using Ni²⁺-NTA immobilized metal affinity chromatography. Eluted proteins were subjected to a buffer exchange with HEPES, pH 8.0 using a Hiprep 26/10 desalting column. Determination of total amount of SUMO-SA2 after desalting based on its extinction coefficient at 280 nm (6990 M⁻¹ cm⁻¹) indicated higher protein yield per volume (~3.8 time) using the ZYM autoinduction medium in comparison with IPTG induction in LB medium(Table 1).

SDS-PAGE analysis of SUMO-SA2 before and after desalting showed a major protein band with good purity at 16 kD and a smaller, less intense band at 14 kD.) (Figure 2). Further analysis of the

purified and desalted SUMO-SA2 with size exclusion chromatography revealed two peaks (Figure 3, dashed line), of which the first peak eluted in the void volume of the column with a retention volume of 7.5 ml. The second peak eluted at 11.2 ml, with the same retention volume of a 14 kD globular protein (ribonuclease A). This indicated that SUMO-SA2 was present in monomeric as well as aggregated form. This can be explained by the hydrophobic nature of SA2 peptide causing the formation of aggregates. We assumed that the attachment of SUMO would prevent premature self-assembly of SA2 in bacteria, allowing us to purify the soluble fusion protein directly from the cleared lysates in a two-step metal affinity chromatography purification^{6,20}.

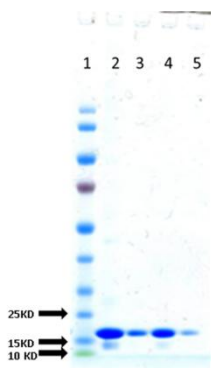
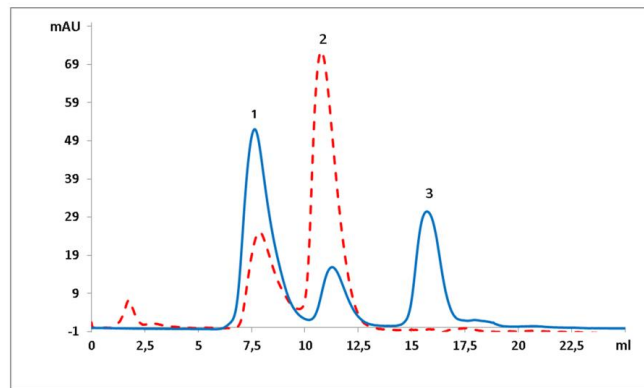


Figure 2. SDS-PAGE analysis of purified SUMO-SA2. Lane 1: 3 μ l PageRulerTM Prestained Protein Ladder (Fermentas, Vilnius, Lithuania). Lane 2: 25 μ l of purified SUMO-SA2 before desalting. Lane 3: same as lane 2, but 10x diluted in sample buffer. Lane 4: 25 μ l of purified SUMO-SA2 after desalting. Lane 5: same as lane 4 but 10x diluted in sample buffer.

Figure 3. Size exclusion chromatography of SUMO-SA2 before (dashed red line) and after (solid blue line) enzymatic cleavage with SUMO protease. Peak 1 corresponds to protein eluting in the void volume, peak 2 corresponds to SUMO-SA2 or cleaved SUMO and peak 3 corresponds to SA2 peptide.



Here we showed that the presence of the SUMO fusion protein, although beneficial for expression levels of the SA2 peptide, did not completely prevent premature self-assembly of the peptide-fusion construct.

2.3 SUMO-SA2 cleavage

Next, SUMO-SA2 was cleaved with SUMO protease to release the SA2 peptide from the SUMO protein. SUMO protease was added to the SUMO-SA2 solution at a mass ratio of 1:500, and the mixture was incubated at 30 °C for 6 hrs with gentle shaking. To monitor the enzymatic cleavage of SUMO-SA2, analytical size exclusion chromatography (SEC), was used (Figure 3, solid line). Before cleavage of SUMO-SA2, two peaks can be discerned, with the first peak eluting in the void volume of the SEC column and the second peak corresponding with monomeric SUMO-SA2. SDS-PAGE analysis confirmed that both peaks consisted of SUMO-SA2 only, suggesting that the first peak consists of a multimeric or aggregated form of SUMO-SA2. As expected, after cleavage a third peak at a retention volume of 15.9 ml appeared, which contained full length SA2 (as confirmed by mass spectrometry). Furthermore, after cleavage an increase in the area under the curve (AUC) of peak 1 and a decrease of AUC of peak 2 were observed, suggesting an increase in protein in the multimeric or aggregated form after cleavage.

To determine the composition of these aggregates, peak 1 was collected and again injected into the column. Interestingly, this fraction divided into three peaks, with the main part being monomeric SA2 peptide (Figure 4, dashed line). This demonstrated that the aggregate peak consisted of a mixture of SA2 and SUMO-SA2. In an attempt to dissolve the aggregates, we raised the pH of the sample and mobile phase to 11.5 prior to separation.

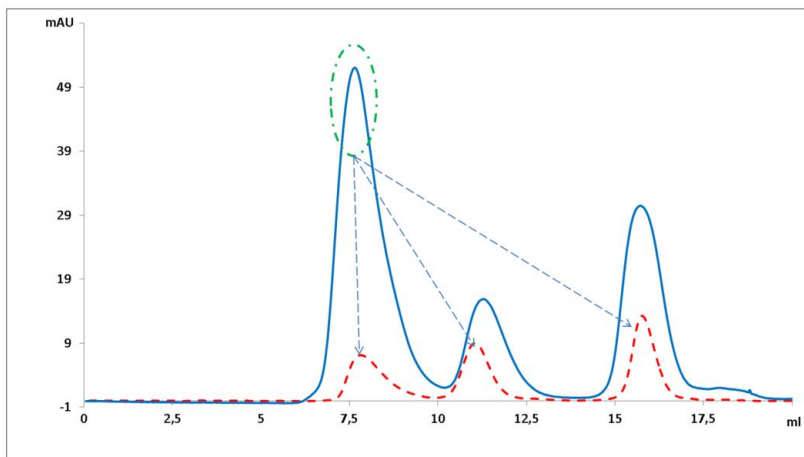


Figure 4. Size exclusion chromatography analysis of cleaved SUMO-SA2 in phosphate buffered saline (pH = 7.4). Chromatogram showed three main peaks (solid line). After collection and reinjection of the first peak the same three peaks appeared (dashed line). This indicates that the first peak contained complex aggregates of SUMO-SA2 and SA2.

As shown in Figure 5A, SEC analysis was performed with phosphate buffered saline (pH 11.5) as the mobile phase. Interestingly, the AUC for the SA2 peptide peak clearly increased, while the AUC of the first peak simultaneously reduced, which showed that increasing the pH could dissolve the major part of the aggregates. This finding revealed that at high pH, the portion of SA2 peptides in a soluble, monomeric state were higher and consequently purification could be done more easily.

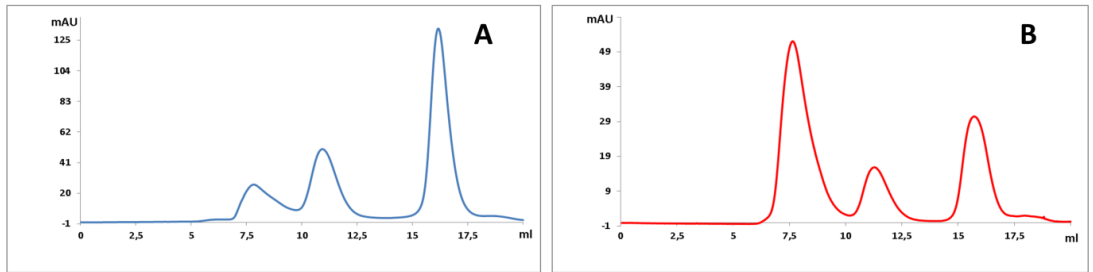


Figure 5. *The effect of alkaline medium on SA2 solubility. Size exclusion chromatograms of the SUMO-SA2 protein solution after treatment by SUMO protease. Phosphate buffered saline pH = 11.5 (A) or phosphate buffered saline pH = 7.4 (B) were used as the mobile phase*

2.4. Peptide purification

The original purification scheme for SUMO-SA2 entailed a two-step IMAC purification scheme in which the first step was the purification of SUMO-SA2 fusion protein from the cleared lysate. After cleavage of the purified SUMO-SA2 with SUMO protease, the His-tagged SUMO was separated from the released peptide by a second IMAC step. However, we observed that mixtures of uncleaved SUMO-SA2 and cleaved SA2 can form aggregates, which caused loss of the SA2 product during the second purification step (Figure 6). For that reason we adapted the purification scheme.

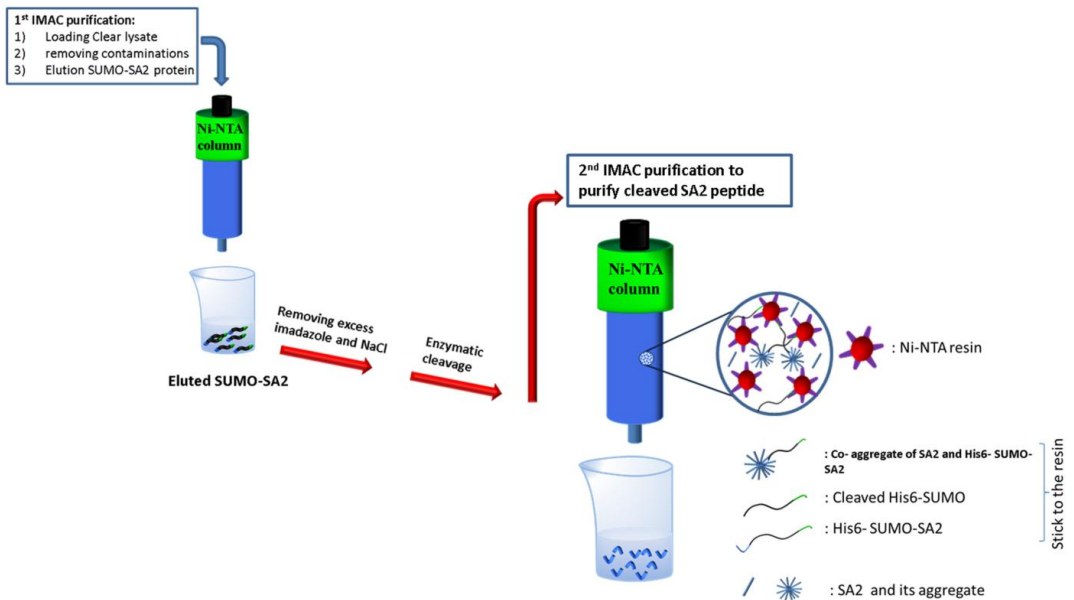


Figure 6. Schematic representation of IMAC purification and the peptide loss in 2nd IMAC purification after cleavage of SUMO-SA2 by SUMO protease. Released peptides are able to form aggregates with cleaved or uncleaved SUMO-SA2. Collected peptide in the flow through is low and most peptides stick to the column through the His tag of bigger proteins.

To separate the cleaved peptide from the SUMO protein, selective precipitation was applied. The pH of the protein solution after cleavage was adjusted to pH 11.5. SUMO, SUMO protease and uncleaved SUMO-SA2 were selectively precipitated by adding ethanol up to 50% (v/v) to the protein solution.

SEC analysis of the supernatant showed a major peak in the chromatogram, corresponding to the SA2 peptide which was confirmed by mass spectrometry (M.W. 1142.65 Da) (Figure 7A,C). To determine the yield of purification, the precipitate obtained after centrifugation was collected and resuspended in the same buffer and volume and analyzed by SEC. The chromatogram showed separation of most of the big proteins and aggregates and also some parts of SA2 (Figure 7B).

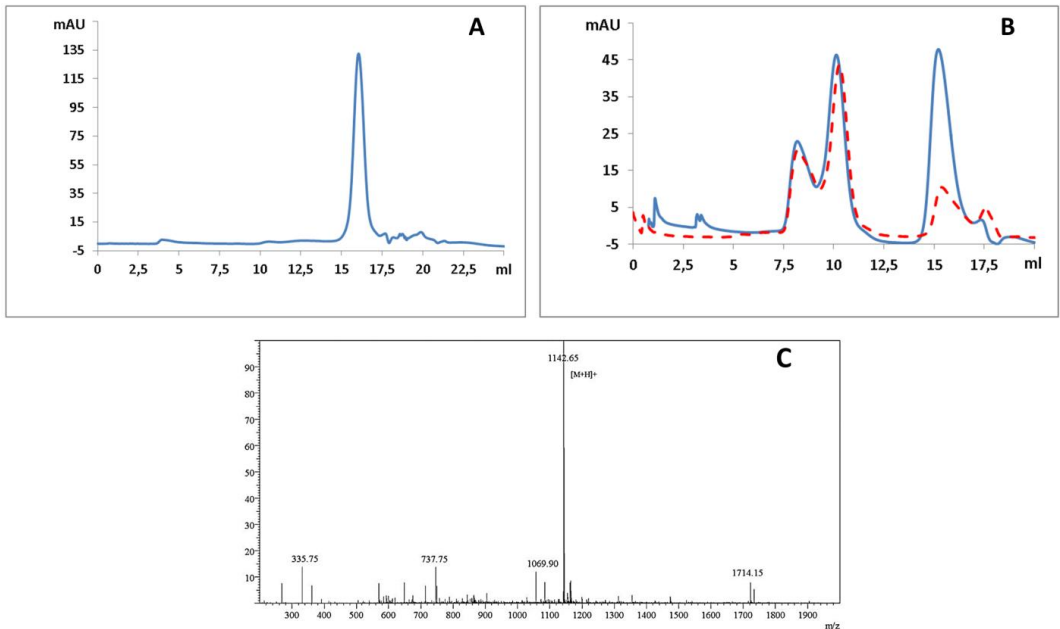


Figure 7. Peptide purification after enzymatic cleavage through selective precipitation. Selective precipitation was performed by adding ethanol up to 50% (v/v). A) Analysis of supernatant showed 1 major peak corresponding to SA2 B) SEC analysis of cleaved SUMO-SA2 before (solid line) and after (dashed line) selective precipitation. C) ESI-MS mass spectrum of the SA2 peptide in the supernatant after ethanol precipitation.

A comparison of the AUCs of the SA2 peptide peaks before and after ethanol precipitation revealed that 75% of the peptide was recovered in the supernatant (Table 1), and almost all other proteins were removed by ethanol precipitation.

3. Conclusion

In conclusion, the results of this study demonstrated that premature self-assembly of SUMO-SA2 interfered with the proper purification of SA2 peptides resulting in low yields of purified peptide. By refining the purification procedure and by altering the expression medium, we demonstrated a more than 12-fold increase in purified SA2 peptide from one liter of bacterial culture. Although these findings are specific for the purification of SA2 peptides, premature self-assembly during recombinant production may also take place with other amphiphilic peptides, which may to a certain extent explain the low yields reported for the recombinant production and purification of

such self-assembling peptides^{21,26,27}. A critical evaluation of the purification scheme of such peptides may therefore be advisable.

4. Materials and Methods

4.1 Materials

All chemicals and media were from Sigma-Aldrich (St.Louis, USA), unless indicated otherwise. Bicinchoninic acid (BCA) assay reagent was from Pierce (Rockford, IL, U.S.A.). DNase I was from Roche Diagnostics (Mannheim, Germany) and chicken egg white lysozyme was obtained from Fluka (Buchs, Switzerland; 84,468 U/mg). Hiprep 26/10 desalting and Superdex Peptide 10/300 columns were purchased from GE Healthcare, (Uppsala, Sweden). PageRuler™ Prestained Protein Ladder was from (Fermentas, Vilnius, Lithuania). Phosphate buffer saline (PBS) was obtained from Braun (Melsungen AG, Germany)

4.2. Bacterial strains and plasmids

Escherichia coli BL21(DE3) containing the T7 RNA polymerase under control of the *lacUV5* promoter was purchased from Invitrogen (Breda, The Netherlands). BL21 (DE3) was transformed with pET-SUMO-SA2⁶ and pSUPER-dtUD1 constructs (kindly donated by Prof. Patrick J. Loll)²⁸ separately according to the pET-SUMO supplier protocol (Invitrogen, Carlsbad, USA). Briefly, 6.5 ng of the plasmid DNA was added to 50 µl of chemically competent *E.coli* BL21(DE3) in a Eppendorf tube and shaken gently. The tube was put on ice for 30 min after which the cells were placed in a water bath of 42°C for 30 sec. Next, the tube was placed on ice. For recovery of cells, 250 µl of SOC medium was added to the tube. To make a stock for the transformed *E.coli* bacteria, 100 µl of the bacterial suspension was transferred into a LB plate containing 50 µg/ml of kanamycin and incubated at 37°C overnight. A single colony was selected and grown in 5 ml LB overnight. The overnight grown bacteria were cooled on ice and glycerol was added up to 30% of final volume before storage at -80 °C.

4.3. Peptide biosynthesis

4.3.1. Media Composition and protein expression

LB medium (peptone; 10 g/L, yeast extract; 5 g/L and 10 g/L of NaCl) was used for the pre-culture preparation and expression of SUMO-SA2 and SUMO protease (dtUD1). Auto induction medium (ZYM) was made according to the Studier method²⁴ and was used for SUMO-SA2 expression. In short, 1 L of ZYM medium that contained Tryptone (10 g/l), Yeast Extract(5 g/l), MgSO₄ (1 mM),

20 mL of 50x5052 solution (glycerol 250 g/l, glucose 25 g/l, alpha lactose 100g/l in RO water), kanamycin (100 mg/l) and 50 ml of 20xNPS solution ((NH₄)₂SO₄ (66 g/l), KH₂PO₄ (136 g/l), Na₂HPO₄ (142 g/l). One liter of autoclaved ZYM or LB media was inoculated with 5 ml of overnight seed culture of the transformed *E. coli* strain BL21 (DE3). LB medium was incubated in a shaking incubator (Innova 4335, New Brunswick Scientific, USA) at 37 °C/ 250 rpm and induced with 1 mM IPTG when the culture reached OD₆₀₀ =0.6-0.8. Next, bacteria were harvested after 4 hrs by centrifugation at 5,000xg for 30 min at 4 °C. Inoculated autoinduction medium was shaken at 37 °C/250 rpm and bacteria were collected after 16 hrs at 5,000xg for 30 min at 4 °C.

4.3.2. Purification of SUMO-SA2

For the isolation and purification of the SA2 peptide, bacterial pellets were suspended in the lysis buffer (3ml for each gram of biomass) (20 mM Na₂HPO₄, 150 mM NaCl, 20 mM imidazole, 5 mM MgCl₂ 1.5% N-lauroylsarcosine, pH 8) supplemented with DNase I 1µg/ml and chicken egg white lysozyme 300 µg/ml . The resulted suspension was incubated on ice for 30 min. Subsequently, urea was added to the suspension to achieve 4M final concentration. Lysis was accomplished using a Braun Labsonic tip-sonicator (Braun Biotech, Melsungen, Germany) for 5min with 30 second stop between each 30 second pulse and passing two times through high pressure homogenizer. Next, the cell lysate was centrifuged (30 minutes, 40.000 g, 20 °C) and supernatant was filtered through a 0.45 µm filter. SUMO-SA2 was purified by affinity chromatography using a 50 ml packed column of Ni-NTA Superflow (Qiagen, Chatsworth, CA) attached to an AKTA Purifier (GE Healthcare, Uppsala, Sweden). The column was washed with 5 column volumes of binding buffer (20 mM sodium phosphate, 0.5 M NaCl, 40 mM imidazole, pH 8) after which the cleared lysate was loaded onto a 50 ml packed Ni²⁺-NTA column at 0.5 ml/min at room temperature. After loading the cleared lysate, the column was washed with the binding buffer until the A₂₈₀ reached to the baseline. His-tagged proteins were eluted from the column with elution buffer (20 mM sodium phosphate, 0.5 M NaCl, 500 mM imidazole, pH 8).

To remove excess imidazole and NaCl, the elution buffer was exchanged with cleavage buffer (20 mM hepes, 150 mM NaCl, pH 8.0) by loading onto a Hiprep 26/10 desalting column.

As the molecular weight of SA2 peptide(1.142 kD) is 8 % of the molecular weight of the SUMO-SA2 (14295 kD), the highest expected amount of SA2 that can be released after enzymatic cleavage can be calculated.

4.3.3. Purification of SUMO Protease

The same protocol as described above was used for the purification of SUMO protease without addition of urea. Moreover, the elution buffer was replaced by the storage buffer (50 mM

NaH₂PO₄, 300 mM NaCl, 1mM DTT, pH 8.0) prior to protein quantification using the BCA assay which BSA used as a standard. Finally, 0.2mg/ml dilutions were made by adding glycerol 50% (v/v) and stored at -80°C until required.

4.3.4. Purification of SA2 peptide

SUMO protease was added at a 1:500 molar ratio to the purified SUMO-SA2 solution supplemented with 1 mM DTT and the mixture was incubated under gentle shaking for 6 hrs at 30°C to allow SUMO cleavage from the SA2 peptide.

To separate SA2 peptide from cleaved SUMO, SUMO protease and uncleaved SUMO-SA2, selective precipitation by ethanol was performed.

The pH of protein solution after cleavage was adjusted to 11.5 then ethanol was added up to 50% of the total volume to precipitate all proteins except SA2. After centrifugation at 5000xg at 4°C for 15 min, supernatant was collected and pH of supernatant was adjusted to 2 by adding 1M HCl to precipitate SA2. The precipitate was collected and suspended in 0.1 M HCl and centrifuged at 5000xg at 4°C. This procedure was repeated 3 times.

Subsequently, recovered peptide was confirmed by HPLC, and mass spectrometry. Finally the peptide pellet was lyophilized at -50 °C and at 0.5mbar in a Chris Alpha 1-2 freeze-drier (Osterode am Harz, Germany) for 12 hrs and stored at -20° C.

4.4. Characterization of produced peptide

4.4.1. Gel electrophoresis

The produced proteins were evaluated by SDS-PAGE. Samples were boiled in Laemmli sample buffer (Bio-Rad Laboratories, Hercules, CA, USA) for 5 min and loaded at 20 µl/well onto NuPAGE 10% Novex Bis-Tris gels (12 wells, 1.0-mm thickness; NuPAGE, Invitrogen, Carlsbad, CA, USA). Electrophoresis was performed at room temperature applying a constant voltage of 175 V for 50 min. The gel was stained with Page Blue™ Protein Staining Solution (Fermentas GMBH, St. Leon-Rot, Germany) and destained overnight by washing with RO water.

4.4.2. Size exclusion chromatography

Cleavage of SUMO-SA2 was followed by Size Exclusion Chromatography on a Superdex Peptide 10/300 GL column at a flow rate of 0.7 ml/min with phosphate buffered saline at pH=7.4 or pH=11.5 as the mobile phase. Prior to loading the samples a Gel Filtration LMW Calibration kit (GE Healthcare, Uppsala, Sweden) was used to validate column performance.

4.4.3. HPLC Analysis and Mass spectrometry

1 mg of Lyophilized SA2 peptide was dissolved in 1 ml of DMSO and 20 μ l of the peptide solution was diluted 5 times in RO water. 50 μ l of prepared sample was injected onto a Sunfire C18 column (waters Corporation, Milford, USA). A gradient was run at 1.0 ml/min flow rate from buffer A (5% acetonitrile, 0.1% trifluoroacetic acid, 95% water) in 30 minutes to buffer B (100% acetonitrile, 0.1% trifluoroacetic acid). UV absorption was monitored at 220 nm, 280 nm and also fluorescent emission at 350 nm of tryptophan residue upon excitation at 295 nm was recorded.

Furthermore, Electrospray ionization (ESI) mass spectrometry was carried out using a Shimadzu LCMS QP-8000 (Duisburg, Germany) single quadrupole bench top mass spectrometer (m/z range ,2000), coupled with a QP-8000 data system.

5. References

- (1) Vauthey, S., Santoso, S., Gong, H., Watson, N., and Zhang, S. (2002) Molecular self-assembly of surfactant-like peptides to form nanotubes and nanovesicles. *Proc. Natl. Acad. Sci. U. S. A.* 99, 5355–60.
- (2) Santoso, S., Hwang, W., Hartman, H., and Zhang, S. (2002) Self-assembly of Surfactant-like Peptides with Variable Glycine Tails to Form Nanotubes and Nanovesicles. *Nano Lett.* 2, 687–691.
- (3) Khoe, U., Yang, Y., and Zhang, S. (2008) Self-Assembly of Nanodonut Structure from a Cone-Shaped Designer Lipid-like Peptide Surfactant†. *Langmuir* 25, 4111–4114.
- (4) Khoe, U., Yang, Y., and Zhang, S. (2008) Synergistic effect and hierarchical nanostructure formation in mixing two designer lipid-like peptide surfactants Ac-A6D-OH and Ac-A6K-NH2. *Macromol. Biosci.* 8, 1060–7.
- (5) Chen, C., Pan, F., Zhang, S., Hu, J., Cao, M., Wang, J., Xu, H., Zhao, X., and Lu, J. R. (2010) Antibacterial activities of short designer peptides: a link between propensity for nanostructuring and capacity for membrane destabilization. *Biomacromolecules* 11, 402–11.
- (6) Van Hell, A. J., Costa, C. I. C. A., Flesch, F. M., Sutter, M., Jiskoot, W., Crommelin, D. J. A., Hennink, W. E., and Mastrobattista, E. (2007) Self-assembly of recombinant amphiphilic oligopeptides into vesicles. *Biomacromolecules* 8, 2753–61.
- (7) Schuster, T. B., de Bruyn Ouboter, D., Bordignon, E., Jeschke, G., and Meier, W. (2010) Reversible peptide particle formation using a mini amino acid sequence. *Soft Matter* 6, 5596.
- (8) Guo, X. D., Tandiono, F., Wiradharma, N., Khor, D., Tan, C. G., Khan, M., Qian, Y., and Yang, Y.-Y. (2008) Cationic micelles self-assembled from cholesterol-conjugated oligopeptides as an efficient gene delivery vector. *Biomaterials* 29, 4838–46.
- (9) Maham, A., Tang, Z., Wu, H., Wang, J., and Lin, Y. (2009) Protein-based nanomedicine platforms for drug delivery. *Small* 5, 1706–21.
- (10) Stupp, S. I., Zha, R. H., Palmer, L. C., Cui, H., and Bitton, R. (2013) Self-assembly of biomolecular soft matter. *Faraday Discuss.* 166, 9–30.
- (11) Corin, K., Baaske, P., Ravel, D. B., Song, J., Brown, E., Wang, X., Wienken, C. J., Jerabek-Willemsen, M., Duhr, S., Luo, Y., Braun, D., and Zhang, S. (2011) Designer lipid-like peptides: a class of detergents for studying functional olfactory receptors using commercial cell-free systems. *PLoS One* 6, e25067.
- (12) Gudlur, S., Sukthankar, P., Gao, J., Avila, L. A., Hiromasa, Y., Chen, J., Iwamoto, T., and Tomich, J. M. (2012) Peptide nanovesicles formed by the self-assembly of branched amphiphilic peptides. *PLoS One* 7, e45374.
- (13) Merrifield, R. B. (1963) Solid Phase Peptide Synthesis. I. The Synthesis of a Tetrapeptide. *J. Am. Chem. Soc.* 85, 2149–2154.
- (14) Muller, D., Bayer, K., and Mattanovich, D. (2006) Potentials and limitations of prokaryotic and eukaryotic expression systems for recombinant protein production - a comparative view. *Microb. Cell Fact.* 5, P61.
- (15) Trabbic-Carlson, K., Liu, L., Kim, B., and Chilkoti, A. (2004) Expression and purification of recombinant proteins from *Escherichia coli*: Comparison of an elastin-like polypeptide fusion with an oligohistidine fusion. *Protein Sci.* 13, 3274–3284.

- (16) Pasupuleti, M., Schmidtchen, A., and Malmsten, M. (2011) Antimicrobial peptides: key components of the innate immune system. *Crit. Rev. Biotechnol.* 32, 143–171.
- (17) Adams, D. J., Holtzmann, K., Schneider, C., and Butler, M. F. (2007) Self-assembly of surfactant-like peptides. *Langmuir* 23, 12729–36.
- (18) Singh, S. M., and Panda, A. K. (2005) Solubilization and refolding of bacterial inclusion body proteins. *J. Biosci. Bioeng.* 99, 303–10.
- (19) Hojo, K., Hara, A., Kitai, H., Onishi, M., Ichikawa, H., Fukumori, Y., and Kawasaki, K. (2011) Development of a method for environmentally friendly chemical peptide synthesis in water using water-dispersible amino acid nanoparticles. *Chem. Cent. J.* 5, 49.
- (20) Satakarni, M., and Curtis, R. (2011) Production of recombinant peptides as fusions with SUMO. *Protein Express Purif* 78, 113–119.
- (21) Prakash, A., Parsons, S. J., Kyle, S., and McPherson, M. J. (2012) Recombinant production of self-assembling β -structured peptides using SUMO as a fusion partner. *Microb. Cell Fact.* 11, 92.
- (22) Malakhov, M., Mattern, M., Malakhova, O., Drinker, M., Weeks, S., and Butt, T. (2004) SUMO fusions and SUMO-specific protease for efficient expression and purification of proteins. *J Struct Funct Genomics* 5, 75–86.
- (23) Butt, T. R., Edavettal, S. C., Hall, J. P., and Mattern, M. R. (2005) SUMO fusion technology for difficult-to-express proteins. *Protein Express Purif* 43, 1–9.
- (24) Studier, F. W. (2005) Protein production by auto-induction in high-density shaking cultures. *Protein Expr. Purif.* 41, 207–234.
- (25) Novy, R. (2013) Use of glucose to control basal expression in the pET System. *Innov.* 13 13–15.
- (26) Reed, D. C., Barnard, G. C., Anderson, E. B., Klein, L. T., and Gerngross, T. U. (2006) Production and purification of self-assembling peptides in *Ralstonia eutropha*. *Protein Expr. Purif.* 46, 179–188.
- (27) Hartmann, B. M., Kaar, W., Yoo, I. K., Lua, L. H., Falconer, R. J., and Middelberg, A. J. P. (2009) The chromatography-free release, isolation and purification of recombinant peptide for fibril self-assembly. *Biotechnol Bioeng* 104, 973–985.
- (28) Weeks, S. D., Drinker, M., and Loll, P. J. (2007) Ligation independent cloning vectors for expression of SUMO fusions. *Protein Expr. Purif.* 53, 40–50.

Chapter 4

The supramolecular organization of a peptide-based nanocarrier at high molecular detail

**Mazda Rad-Malekshahi ^a, Koen M. Visscher ^b, João P. G. L. M. Rodrigues ^b,
Renko de Vries ^c, Wim E. Hennink ^a, Marc Baldus ^b, Alexandre M. J. J.
Bonvin ^b, Enrico Mastrobattista ^a and Markus Weingarth ^b**

^a Department of Pharmaceutics, Utrecht Institute for Pharmaceutical Sciences, Utrecht University,
3584 CG Utrecht, The Netherlands

^b NMR Spectroscopy, Bijvoet Center for Biomolecular Research, Department of Chemistry,
Faculty of Science, Utrecht University, Padualaan 8, 3584 CH Utrecht, The Netherlands

^c Laboratory of Physical Chemistry and Colloid Science, Wageningen University, Dreijenplein 6,
6703 HB Wageningen, The Netherlands

**Accepted for publication in the Journal of the American Chemical Society (JACS) on June
11, 2015**

ABSTRACT

Nanovesicles self-assembled from amphiphilic peptides are promising candidates for applications in drug delivery. However, complete high-resolution data on the local and supramolecular organization of such materials has been elusive thus far, which is a substantial obstacle to their rational design. In the absence of precise information, nanovesicles built of amphiphilic ‘lipid-like’ peptides are generally assumed to resemble liposomes that are organized from bilayers of peptides with a tail-to-tail ordering. Using the nanocarrier formed by the amphiphilic SA2 peptide as an example, we derive the local and global organization of a multi-mega-Dalton peptide-based nanocarrier at high molecular detail and at close-to physiological conditions. By integrating a multitude of experimental techniques (solid-state NMR, AFM, SLS, DLS, FT-IR, CD) with large- and multi-scale MD simulations, we show that SA2 nanocarriers are built of interdigitated antiparallel β -sheets, which bear little resemblance to phospholipid liposomes. Our atomic level study allows analyzing the vesicle surface structure and dynamics as well as the intermolecular forces between peptides, providing a number of potential leads to improve and tune the biophysical properties of the nanocarrier. The herein presented approach may be of general utility to investigate peptide-based nanomaterials at high-resolution and at physiological conditions.

1. Introduction

Nanovesicles based on self-assembling amphiphilic peptides show great potential for controlled and safe drug delivery¹⁻⁸. Next to their inherent bio-degradability⁹⁻¹¹, the great appeal of peptides as building blocks for nanotechnology is their availability by solid-state synthesis and the ease with which their biophysical properties and functions can be tuned by changing the amino acids sequence or by conjugating chemical groups¹². Moreover, peptide-based nanoparticles can be equipped with bioactive epitopes that interact with cells or proteins¹³. Hence, peptide-based drug delivery systems could potentially be designed for many biomedical purposes, which requires control of their structural and functional aspects at a molecular level. However, since peptide-based nanovesicles are not amenable to high-resolution crystallography and too large (> MDa) for solution NMR, atomic-resolution data on the molecular and supramolecular organization of such nanomaterial is sparse and fragmentary, which represents a considerable obstacle to their efficient rational design. The use of high-resolution methods is further limited by the requirement of close-to physiological experimental conditions since the vesicle assembly process may be sensitive to the molecular environment².

Here we present an avenue to the high-resolution structural characterization of peptide-based nanovesicles and their assembly pathway based on the example of the nanocarrier formed by the SA2 peptide¹⁴. This amphiphilic decapeptide, Ac-AAVVLLWEE-COOH, spontaneously self-assembles into hollow spheres that bear potential as drug delivery systems¹⁵. The design of the SA2 peptide aimed at a conical shape, with a strongly negatively charged C-terminus, followed by a hydrophobic domain, which decreases in size towards the N-terminus. In the absence of sufficient high-resolution data, spherical assemblies of amphiphilic peptides are generally thought to adopt liposome-like structures composed of bilayers of parallel peptides with a tail-to-tail organization^{1,16,17}. By integrating an ensemble of experimental methods (solid-state NMR, AFM, SLS, DLS, FT-IR, CD) with large- and multi-scale molecular dynamics simulations, we describe the local and supramolecular organization of SA2 nanocarriers at the atomic-level. Notably, we demonstrate that SA2 peptides in mature nanovesicles adopt an antiparallel and interdigitated organization that strongly diverges from the common organization of phospholipids in liposomes. The herein presented approach allows studying peptide-based nanovesicles at physiological conditions and at high-resolution, an important advance towards the tailoring of such materials for medical applications.

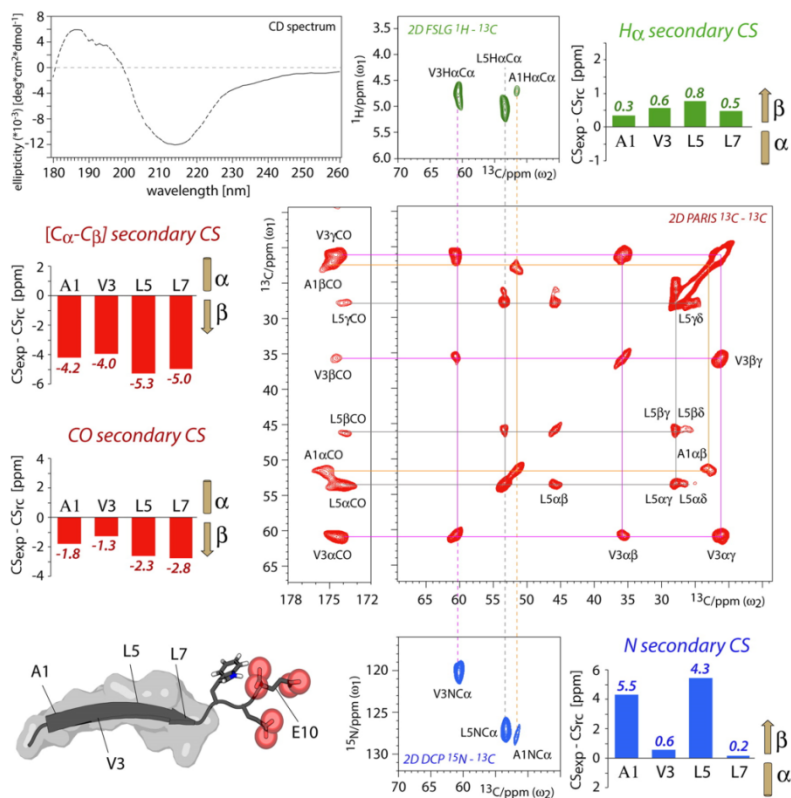


Figure 1. Solid-state NMR (ssNMR) experiments to determine SA2 nanovesicle secondary structure at high-resolution. 2D $^1\text{H} - ^{13}\text{C}$ FSLG¹⁸ (top right panel, colored in green), 2D $^{13}\text{C} - ^{13}\text{C}$ PARIS^{19,20} (middle right panel, red) and 2D $^{15}\text{N} - ^{13}\text{C}_\alpha$ SPECIFIC DCP²¹ (bottom right panel, blue) ssNMR experiments were applied to [$^{13}\text{C}, ^{15}\text{N}$]-A1, V3, L5 (construct A) and [$^{13}\text{C}, ^{15}\text{N}$]-A1, L7, E10 (construct B) site-specifically labeled SA2 nanocarriers. SSNMR spectra of construct B are shown in Figure S2. Analysis of secondary chemical shifts clearly indicated β -strand conformation for the hydrophobic residues. This was supported by a CD spectrum (top left panel). Residue E10 was invisible in dipolar-based experiments. A model of the SA2 secondary structure derived from ssNMR measurements is shown in the bottom left corner. All data (ssNMR and CD) were acquired at 10 mg/ml SA2 peptide concentration.

2. Results and Discussion

2.1. The high-resolution geometry of assembled SA2 peptides revealed by solid-state NMR experiments. Solid-state NMR (ssNMR) provides atomic-level structural information and is not curtailed by an intrinsic molecular size limit or sample heterogeneity, which renders the technique uniquely suited to characterize higher order aggregates such as peptide-based nanoparticles^{22–26}. In general, NMR chemical shifts are very sensitive to the local conformation. This offers a means to derive peptide secondary structure information at residue-level from the so-called ‘*secondary chemical shifts*’ that compare observed chemical shifts with random coil values and exhibit opposite arithmetic signs for α -helical and β -strand backbone conformations²⁷.

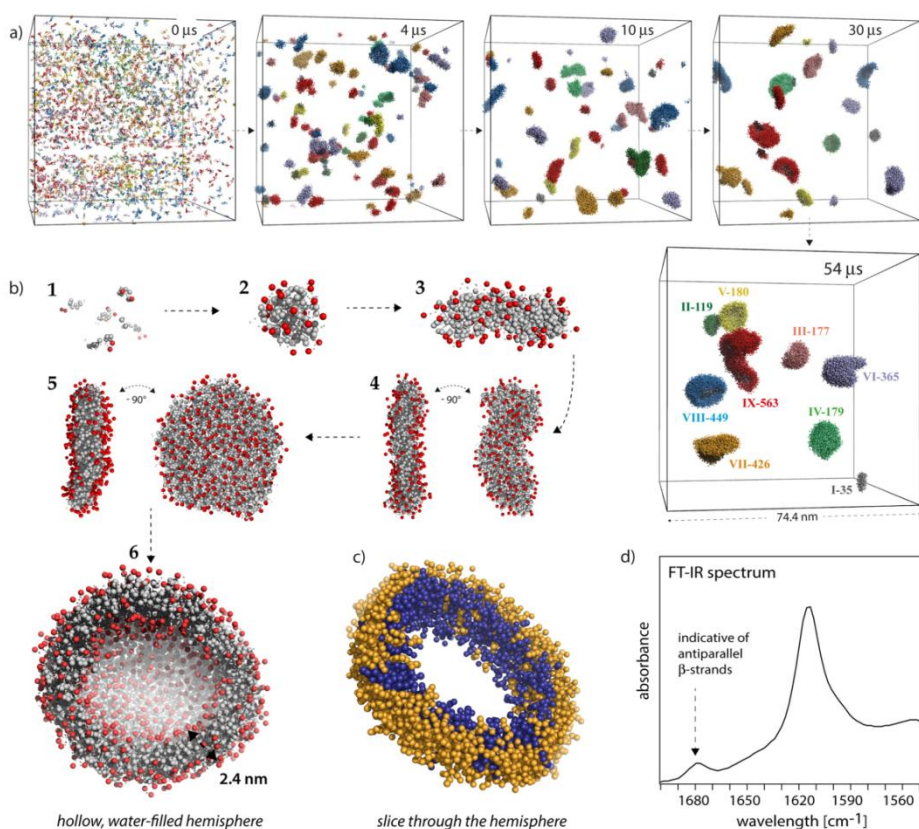


Figure 2. The assembly pathway and the supramolecular organization of SA2 nanocarriers. a) 2500 SA2 peptides were evolved over 54 μ s in a large cubic (74.4 nm side length) water-filled box using the MARTINI coarse-grained force field. Peptides that assembled in the same cluster after 54 μ s are depicted in the same color over the course of the trajectory. A small assembly of seven peptides was left out for clarity. b) The assembly pathway of SA2 peptides, derived from CGMD

simulations: Free peptides (1) assemble over micelle-like drops (2) to strings (3), followed by bilayer-like tiles (4), disks (5) and finally hemispheres (6). The hemisphere intermediate 6 shows Fragment VIII of Figure 2a. The negatively charged residues (E9 and E10) of the peptides' C-termini are colored in red. The 2.4 nm distance relates to the average separation between the backbone beads of residues E10 in opposing peptide layers. c) Peptides organize in antiparallel β -sheets in which the hydrophobic parts align, resulting in interdigitated peptide bilayers. Peptides with opposing C-termini are colored in orange and blue. d) The presence of a characteristic signal at 1680 cm^{-1} in FT-IR experiments confirms the antiparallel organization of peptides in SA2 nanocarriers.

Solid-state NMR experiments were performed with solid-phase synthesized SA2 peptides that were [^{13}C , ^{15}N]-isotope labeled at strategic positions. Two different labelling schemes (A1, V3 and L5 in *construct A*; A1, L7 and E10 in *construct B*) were used to provide secondary structure information for the entire peptide and to allow unambiguous assignments. Moreover, both constructs included one common label (A1) to assure the comparison of identical peptide conformations. The labeled peptides spontaneously assembled at a concentration of 10 mg/ml (8.5 mM) in phosphate buffered saline, which led to the formation of a colloidal suspension. In agreement with our previous studies, this sample preparation consisted of spherical SA2 nanovesicles, which was verified by atomic force microscopy (AFM) measurements (Figure S1). Several ssNMR experiments (2D ^{13}C - ^{13}C PARIS^{19,20}, 2D ^1H - ^{13}C FSLG¹⁸ and 2D ^{15}N - $^{13}\text{C}_\alpha$ SPECIFIC DCP²¹ experiments) were acquired to characterize the secondary structure in SA2 nanovesicles (Figures 1 and S2). All experiments yielded well-resolved spectra that allowed straightforward identification of the spin systems of the labeled hydrophobic residues (A1, V3, L5, L7) for which we could obtain extensive (CO, C_α , H_α , C_β , N) assignments (Table 1). Signals of residue E10 were invisible in dipolar-based experiments, which suggests that the negatively charged C-terminus exhibits fast dynamics (μs and faster). Indeed, signals of E10 could be detected at low sample temperature (235 K) with dipolar-based experiments and at higher temperature (278 K) by using direct ^{13}C excitation instead of dipolar cross-polarization transfer, demonstrating the high mobility of the peptide C-terminus (Figure S3) at physiological temperatures. Using published random coil average chemical shifts as reference²⁸, the calculation of secondary chemical shifts unanimously assigned β -strand conformation to residues A1, V3, L5 and L7 (Figure 1), strongly suggesting that residues A1 – L7 adopt a continuous β -strand. This result could be confirmed (Figure S4) by the CSI 2.0 program²⁹ that connects chemical shifts and sequence data to determine secondary structure with an accuracy (about 90 %) that is comparable

to structure-based methods such as DSSP³⁰. Moreover, a high content of β -strand secondary structure in SA2 nanocarriers is in agreement with circular dichroism (CD) measurements, which showed the typical profile of an extended secondary structure (Figure 1, top left panel).

The absence of peak doubling for residues V3 and L5 indicates that the hydrophobic core of the SA2 nanovesicles is relatively ordered (average C_{α} linewidth = 1.1 ± 0.1 ppm). Peak doubling was however observed for L7CO and all A1 carbon signals. Indeed, for A1, the C_{α} and CO signals showed at least two clearly distinguishable conformations, which could be detected in both constructs A and B, although with slightly different populations and chemical shifts. The A1 ^{13}C chemical shifts were also different for a second batch of *construct A* (Figure S5), which indicates that the conformation of the N-terminus is sensitive to subtle details of the sample preparation. The L7CO signals also showed two different peaks (174.5 and 173.2 ppm), while the L7 side chain exhibited both peak doubling and generally weak signal intensities. Note that all A1 and L7 conformations feature chemical shifts that are indicative of extended secondary structure. Hence, the ssNMR measurements reveal the local geometry in the assembled nanocarrier at atomic-level, demonstrating that the hydrophobic core A1 – L7 of peptides exhibits β -strand conformation, while the anionic C-terminus is mobile. Moreover, the experiments show that the local structure of SA2 nanovesicles is moderately disordered, with the heterogeneity increasing towards the N- and C-termini of the peptides.

Table 1. Solid-state NMR chemical shifts ^a

Residue	CO	C_{α}	H_{α}	C_{β}	N
A1	175.6	51.6	4.6	22.2	127.8
V3	174.5	60.6	4.7	35.4	120.2
L5	174.0	53.5	5.1	45.8	127.0
L7	173.9	53.7	4.8	45.7	121.7
E10	No inter-nuclear signals in dipolar experiments				

^a All values are in ppm and were measured at 500 MHz 1H -frequency and 9.1 kHz MAS. For A1 and L7CO, the indicated values represent an unweighted average of the observed conformations.

2.2. The supramolecular organization of SA2 nanocarriers. To get insights into the assembly pathway and the higher order architecture of SA2 nanovesicles, we integrated the ssNMR secondary structure information with molecular dynamics (MD) simulations. Based on light scattering measurements, which show an average molecular weight of > 5 MDa for SA2 nanocarrier (see also Supporting Information), a single spherical assembly should comprise several thousand peptides. The simulation of such large systems on the *a priori* unknown timescale of peptide self-assembly is very challenging. Moreover, the simulated system should be sufficiently dilute since the peptide concentration may modulate the assembly pathway^{2,31-33}. To meet these demanding requirements and yet to obtain high-resolution information on SA2 nanovesicles, we resorted to a sequential multi-scaling approach, in which a very large and very long (3.4 million beads, 54 μ s trajectory) coarse-grained (CG) simulation was connected in a series with a large and long (2.1 million atoms, 1 μ s trajectory) atomistic simulation. The computations were supplemented by various experimental measurements to assess and verify the supramolecular organisation and the morphology of the simulated assemblies.

The initial coarse-grained simulation step was carried out with the established MARTINI force field³⁴, which was recently successfully applied to study the self-assembly pathway of amphiphilic peptides into nanofibers and to investigate the assembly of diphenylalanine peptides^{31,35}. SSNMR experiments are an ideal complement to MARTINI since peptide secondary structure needs to be assigned at the beginning of the simulation and remains constant over the trajectory. Based on the ssNMR data, residues A2 – L7 were assigned as β -strand, similarly to W8 that links the hydrophobic and the hydrophilic peptide parts. To implicitly simulate the neutral acetylated N-terminus, which is not represented as an individual CG bead, we assigned A1 as a polar coil residue. Since the ssNMR experiments suggest that the anionic C-terminus is highly mobile, residues E9 and E10 were also assigned as coil. The glutamate side chains were deprotonated and charged, so as to simulate the peptides at neutral pH value. To set up the CG simulation system, 2500 SA2 peptides, randomly distributed, and 3.4 million CG water molecules were packed into a cubic box with a side length of 74.4 nm, corresponding to a peptide concentration of approximately 10 mM. This concentration is very close to the concentrations used in the ssNMR and AFM experiments. Na⁺ and Cl⁻ ions were added to neutralize the system and to mimic a 150 mM NaCl solution. The total system comprised 3.47 million CG beads and was simulated over 54 μ s at 300 K (Figure 2a and Supporting Movie 1). To best of our knowledge, this is the largest and longest reported simulation of a peptide-based nanoparticle to date. Over the course of total trajectory, the peptides assembled into nine large nanoparticles, many of which comprised several

hundred peptides. Depending on the progress of the simulation and the number of peptides involved, the particles adopted typical morphologies, from which we inferred the assembly pathway (Figure 2b), which in many aspects resembles the self-assembly pathway of liposomes³⁶. Within the first 2 μ s of the simulation, free SA2 peptides (Figure 2b, intermediate 1) quickly assembled to small (< 25 peptides) disordered micelles with a water-free core (intermediate 2), which grew further to elongated micelle-like strings (< 60 peptides, intermediate 3) within the first 5 μ s. These strings with an oil-like interior transformed, with increasing size of the assemblies and duration of the simulation, to tiles (< 200 peptides) reminiscent of lipid bilayers (intermediate 4). The tiles further evolved, without necessitating further particle-fusion events, towards circular disks with laterally even peptide distributions to minimize the peptide/water surface (intermediate 5). These disks finally merged into larger nanoparticles that exhibit a notable curvature, reminiscent of hollow hemispheres (intermediate 6), which presumably represent the onset of SA2 nanocarriers. Formation of closed nanocarriers was not observed at this timescale, but is anticipated to take milliseconds at the given MD settings and peptide concentration, something that would be computationally too expensive to demonstrate by CGMD. Note that the SA2 intermediates of Figure 2b were selected from the trajectory to enhance the clarity of the representation of the assembly pathway. The actual assembly pathway of particles can be followed in Supporting Movie 1.

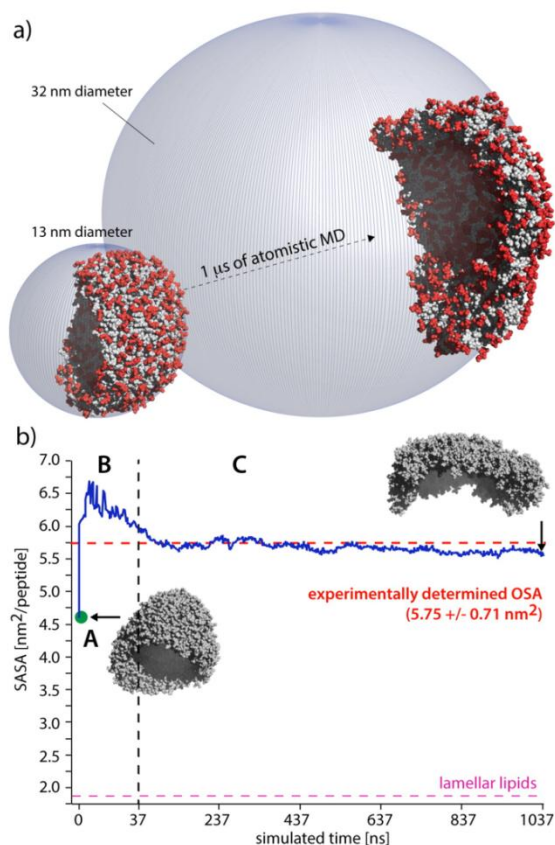


Figure 3. Remodeling of SA2 nanocarrier curvature. a) The curvature of hemispheric SA2 fragments (left) substantially decreases when subjected to atomistic simulations (right). This implies that CGMD simulations underestimate the size of SA2 nanocarriers. b) Comparison of the occupied surface area (OSA) measured by static light scattering (SLS) and the solvent accessible surface area (SASA) derived from MD simulations. Point A (in green) is the starting system of the atomistic simulation (comprising 2500 SA2 peptides), back-transformed from the CGMD simulation. This system was evolved for 37.5 ns, shown in passage B. In passage C, an assembly of 449 peptides was further evolved for 1 μ s.

In analogy to *liposomes* (lipid bilayers), amphiphilic peptide-based nanovesicles are assumed to form bilayer constructs^{1,16,17} often referred to as *peptosomes*, in which the hydrophobic peptide termini arrange tail-to-tail and the charged termini (the ‘headgroups’) are exposed to bulk water. As expected from this concept, the surface of simulated SA2 nanoparticles is rimmed with the C-terminal negatively charged glutamate residues (Figure 2b, in red). However, the wall (bilayer) thickness of CG SA2 nanoparticles amounts on average to a mere 24 Å (Figure 2b, intermediate

6). This speaks against a tail-to-tail arrangement of peptides, which would likely result in a thicker wall, given that the average C_α to $C_{\alpha+2}$ distance in straight β -strands is about 6 Å, implying that the β -strand A1 - L7 comprises already 18 Å. For comparison, Zhang *et al.* assumed a peptide length of 20 Å (and a bilayer thickness of 40 Å) for an eight-residue β -strand surfactant-like peptide¹. Indeed, further analysis on the organization of the CG SA2 nanoparticles revealed a notable degree of interdigitation, i.e., that the hydrophobic peptide tails of opposite peptide layers overlap and arrange as antiparallel β -strand (Figure 2c). This result could be reproduced in a well-equilibrated 100 μ s CGMD simulation of 120 SA2 peptides in a periodic bilayer slab (Figure S6). Interestingly, such an interdigitated arrangement of amphiphilic peptides was also proposed in a computational study of A₃K nanotubes³⁷.

We used fourier transform infrared spectroscopy (FT-IR) to validate this surprising finding. The experimental validation of the simulated peptide arrangement is especially important, given that β -sheet formation might not be very accurately modelled in MARTINI due to the missing hydrogen-bond directionality. The relative direction of β -strands can be assessed by FT-IR based on the analysis of the amid I band region (1700 – 1600 cm^{-1}), which, as demonstrated in several studies, exhibits an additional signal around 1695 - 1675 cm^{-1} in presence of antiparallel β -sheets^{22,38,39}. This additional band could be clearly detected in our measurements (Figure 2d), which strongly corroborates that SA2 nanocarriers are formed of interdigitated antiparallel β -strands. Hence, our study strongly indicates the build of SA2 nanocarriers substantially diverges from phospholipid liposomes.

2.3. The supramolecular structure of SA2 nanocarriers. While the CGMD simulations offered striking insights into the supramolecular organization of SA2 nanovesicles, a CG representation does in general not provide the precision or resolution of atomistic simulations. We especially worried that the large spatial dimensions of MARTINI water molecules and ions, which are ≥ 4 times larger than their atomistic equivalents, could distort the interaction of these molecules with the water-exposed anionic peptide C-termini. To simulate SA2 nanoparticles in a more accurate (and computationally more expensive) atomistic representation, we first compared several atomic force fields for their aptitude using a system of 60 randomly distributed SA2 peptides (Figure S7). In agreement with our ssNMR data, modern force fields (AMBER ff99SB-ILDN⁴⁰, GROMOS54a7⁴¹) consistently showed stable β -sheet formation, while older versions (AMBER ff99⁴²) yielded spurious α -helical peptides, which explains the outcome of previous computational studies⁴³. Accordingly, the GROMOS54a7 force field was used for all following atomistic simulations.

The 2500 peptides and the ions after 54 μ s of CGMD simulation were transformed to atomic coordinates using the BACKWARD tool⁴⁴, which was slightly modified to include an atomistic representation of the acetylated peptide N-terminus. The system, which comprised 41 million atoms after rehydration, was briefly equilibrated (see Material and Methods) and then freely evolved over 37.5 ns. From the endpoint of this simulation, a nanoparticle of 449 assembled peptides (fragment VIII in Figure 2a) was further simulated in a smaller box (2.1 million atoms in a cubic box of 28 nm side length) for 1 μ s. The peptide assemblies were stable in the atomistic representation, however, the curvature of hemispheric particles rapidly decreased, which implies an increase in the radius of the SA2 nanocarriers (see also Supporting Video 2). An estimated guess of the size of closed SA2 nanocarriers in CGMD simulations suggests a sphere-diameter of about 13 nm (Figure 3a). While it is complicated to infer the nanocarrier size from our atomistic MD simulations due to the difficulty to extrapolate from a fragment to the closed vesicle (and due to the lack of statistics), we estimate that the diameter of SA2 nanocarriers is at least 32 nm in the atomistic representation (i.e., 2.5 times larger than in the CG model). Remarkably, the larger spheres that we observe in the atomistic MD simulation are in agreement with the SA2 vesicle diameter of 20 – 60 nm that we observe by AFM (see Figure S1) and that was observed by cryo-TEM²⁶. The larger particle size is also in line with light scattering measurements, which show a hydrodynamic radius of 32 nm for SA2 nanovesicles (Table S1). The CGMD simulation however appears to underestimate the nanovesicle size, although it might be that the smaller diameter of the CG particles reflects surface tension effects and might increase to the experimental value if the system was given more time to equilibrate and form closed vesicles, which would however be very costly to simulate at the given peptide concentration. Moreover, considering the good agreement of the converted all-atom model with experimental data, we are confident that our model already gives a good approximation of the organization of SA2 nanocarriers.

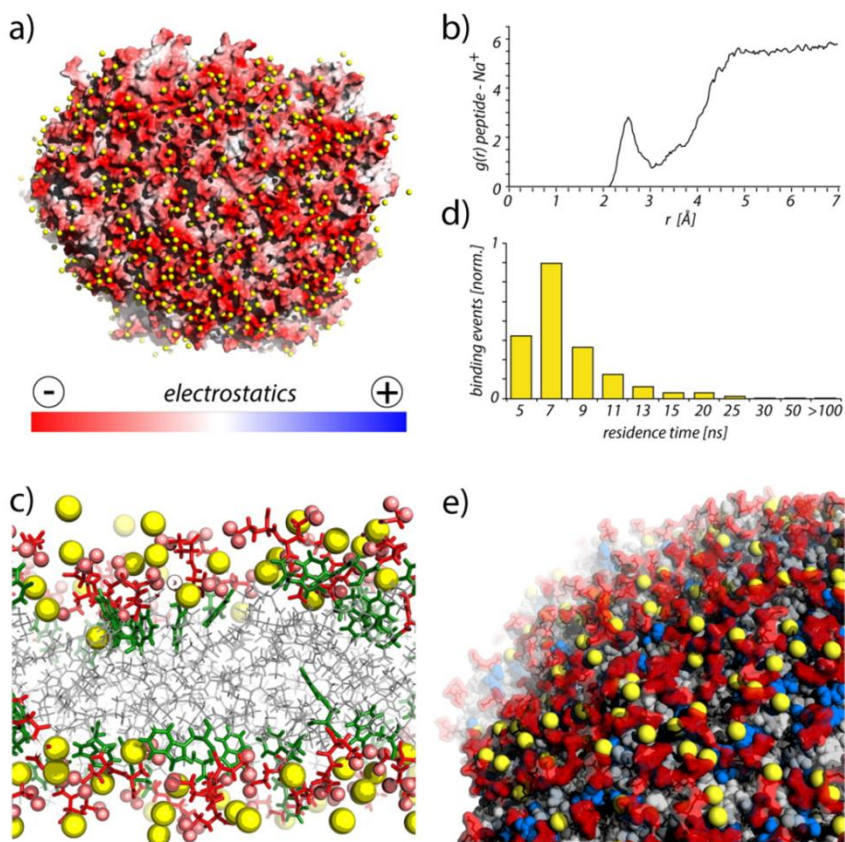


Figure 4. *The surface structure of SA2 nanovesicles. Data were derived from the 1 μs atomistic simulations with 449 peptides. a) The electrostatic surface of SA2 nanocarriers is strongly negatively charged and screened by Na^+ ions (in yellow). b) The radial distribution function between Na^+ ions and SA2 peptides shows a primary shell of direct peptide – ion coordination. c) Na^+ ions deeply intercalate between the C-terminal glutamate residues (red) and are bordered by tryptophan residues (green). d) Evaluation of the residence time of Na^+ ions of the primary shell at the nanocarrier surface. e) The vesicle surface exhibits a pattern of protruding glutamate spikes (red) and spacious cavities, in which Na^+ ions reside (yellow). Cavities are further widened by peptide N-termini (blue) that span the entire nanocarrier wall. These cavities explain the large OSA observed in experiments.*

On a molecular level, a change in particle curvature necessitates a rearrangement in the packing density of the peptides. To infer these changes and to validate the curvature flattening in atomistic simulations, we followed the solvent accessible surface area (SASA) of the simulated peptide assemblies over time and compared it to an experimentally determined occupied surface area

(OSA) (Figure 3b). OSA represents the average area projected onto the lateral plane of the peptide assembly and often will be slightly smaller than the SASA, due to out-of-plane fluctuations of the peptide molecules and surface convolution. Using static light scattering measurements, we calculated an OSA/peptide of $5.75 \pm 0.71 \text{ nm}^2$ (see Materials and Methods), which is astonishingly large in comparison to liposomes, for which the OSA/lipid is less than 1.0 nm^2 and the SASA/lipid amounts to less than 2.0 nm^2 ^{45,46}. In comparison to the experimental data, the SASA of the back-transformed SA2 particles (after 54 μs of CGMD simulation) is significantly lower with $4.6 \text{ nm}^2/\text{peptide}$ (point A in Figure 3b). However, within the first nanoseconds of the atomistic simulation, the SASA leaps to a peak of $6.7 \text{ nm}^2/\text{peptide}$ and then slowly decreases until it reaches a plateau at $5.6 \text{ nm}^2/\text{peptide}$ after 400 ns, which is stable for the remainder of the simulation. A second atomistic simulation over 1 μs with a nanoparticle of 179 peptides (fragment IV in Figure 2a) came to a comparable result of $5.9 \text{ nm}^2/\text{peptide}$. The slightly larger SASA of the smaller particle is accountable for by the larger contribution of edge effects to the surface. Hence, this analysis revealed an excellent match between computed (from the atomistic model) SASA and experimental OSA. This corroborates that our atomistic simulations capture a realistic representation of the molecular surface structure and the organization of SA2 nanocarriers.

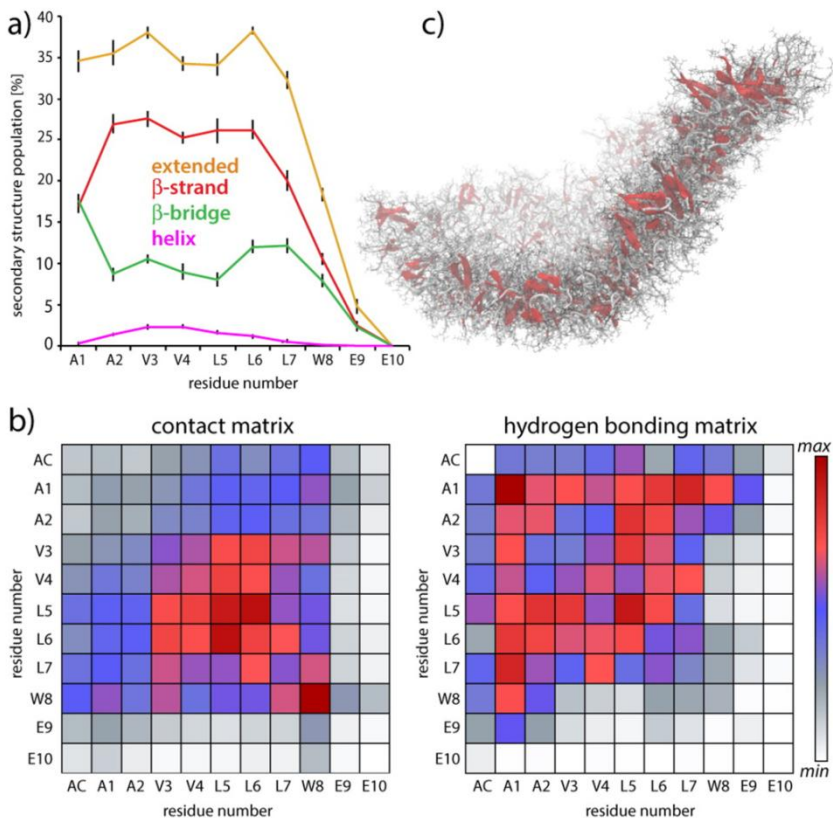


Figure 5. Interactions among SA2 peptides. Data were derived from the atomistic simulation of 449 peptides over 1 μ s. a) Residue-specific secondary structure propensity, averaged over the last 50 ns of the simulation. Black bars indicate the standard deviation. Extended secondary structure comprises β -strand and β -bridge, while helix comprises α -, 3_{10} - and π -helical elements. b) (Left) Intermolecular contact map using a distance cutoff of 4 \AA and (right) intermolecular hydrogen bonding map using a simple 4 \AA distance donor (backbone nitrogen) - acceptor (backbone oxygen) criterion. Both maps were averaged over the final 50 ns of the simulation. c) A snapshot of the nanoparticle after 1 μ s. Extended secondary structure elements are shown in red. See Figure S10 for other perspectives of the vesicle and a zoom into the nanocarrier wall.

The sudden leap of the SASA at the beginning of the atomistic simulation suggests a substantial reorganization of the nanocarrier surface. In both CGMD and atomistic simulations, the anionic surface is extensively screened by counterions (Figure 4a). However, while the large CG Na^+ beads remain on top of the surface, Na^+ ions intercalate between the anionic peptide C-termini. The radial distribution function $g(r)$ between SA2 peptides and Na^+ ions exhibits a primary ion

shell at short distance ($< 3 \text{ \AA}$) which indicates direct peptide – Na^+ interactions, (Figure 4b), as well as a secondary ion shell at longer distance which represents water-mediated interactions. Cations of the primary shell often penetrated deeply into the nanocarrier wall (Figure 4c), which accounts for the curvature flattening in atomistic simulations. Initially, after back-transformation, the anionic C-termini of peptides are too tightly packed and repel each other, resulting in the sudden SASA leap. This is followed by the intercalation of Na^+ ions, which increases the ‘headgroup’ area and thereby counterbalances the curvature induced by the conic hydrophobic N-termini. However, although Na^+ ions inserted deeply into the carrier wall, their residence times were relatively short ($< 10 \text{ ns}$ on average), which points to a dynamic vesicle surface (Figure 4d). The large SASA, in turn, results from the strong degree of peptide interdigitation in SA2 nanocarriers, leading to protruding anionic C-termini that stick out of the vesicle wall like spikes. These spikes electrostatically repel each other, resulting in spacious shallow cavities that are filled with weakly bound hydrated cations (Figure 4e) and account for the large SASA/peptide of SA2 nanocarriers. The cavities are further widened by the necessity to accommodate the bulky tryptophan residues that follow the glutamates in the peptide sequence and by N-termini of the opposite peptide layer which reach as far as the nanocarrier surface. Altogether, the SA2 surface structure is, if at all, only distantly related to common phospholipid liposomes.

The SA2 nanocarrier surface described by integrating ssNMR data with multi-scale simulations is in agreement with atomic-level (ssNMR) and global structural data (light scattering, FT-IR). Since the surface structure is a function of the interdigitated peptide arrangement, a well-described surface suggests a reasonable organization of the nanocarrier wall. Indeed, a quantitative analysis of secondary structure revealed a good consistency between the local geometry of the simulated vesicle wall and the ssNMR data (Figure 5a). The hydrophobic core A1 – L7 showed a pronounced (33 – 38 %) population of extended conformation, which then sharply decreased towards the C-terminus. The C-terminus E10 did not adopt any secondary structure and, in particular, exhibited strongly increased dynamics (Figure S8) in comparison to residues A1 – L7. This explains the absence of E10 in dipolar-based spectra. As a next step, we derived intermolecular interaction maps from the simulations (Figure 5b) to study which forces govern the nanocarrier interior. These matrices represent the absolute number of contacts (*contact matrix*) as well as polar contacts and hydrogen bonding (*hydrogen bonding matrix*). The contact matrix evidences that the nanovesicle core is dominated by hydrophobic clustering between residues V3 – L7 and that peptide-peptide interactions are largely restraint to residues A1 – W8. It is further visible that the N-terminal alanine residues feature most contacts with C-terminal residues, which

results from the antiparallel peptide arrangement. Moreover, tryptophan residues, organized in two belts (Figure 4c), heavily interact with each other, which is presumably favored by attractive electrostatics and packing effects between aromatic rings. As revealed by the hydrogen bonding matrix, the flipside of the interplay between bulky aromatic residues is their weak involvement in hydrogen bonding, which is a steric effect and only overcome by the slim alanine residues (of antiparallel peptides), which can squeeze into the aromatic belt. Generally, the alanine residues are active hydrogen bonding partners for parallel and antiparallel peptides. The simulations indeed indicate that interdigitated peptides form both antiparallel and parallel beta-sheets and it is tempting to suggest that these two conformations, together with lack of hydrogen bonds between bulky hydrophobic C-terminal residues, are responsible for the conformational heterogeneity observed in ssNMR experiments. Interestingly, while the hydrogen bonding maps showed hardly any backbone hydrogen bonds involving the glutamate residues, their carboxyl side chains extensively interacted with the W8 indole group (Figure S9), casting a kind of dynamical and loosely knit mesh at the vesicle surface.

A limitation of our analysis is the residual disorder in the system. A visual inspection (Figures 5c and S10) of the nanocarrier after 1 μ s of atomistic MD simulation showed large patches of up to 20 - 30 connected β -strands, but also regions without ordered secondary structure. Hence, although this heterogeneity is somewhat corroborated by our ssNMR data, peptide motion is considerable restricted within 1 μ s and much longer simulations might presumably result in a more homogeneous and potentially more accurate β -sheet vesicle core. The homogeneity of the system and may be improved by the incorporation of peptide – peptide ssNMR distance restraints. Such high-resolution data on the intermolecular peptide arrangement would presumably better define the molecular details of the peptide assembly and enhance our atomic-level understanding of the supramolecular organization of SA2 nanocarriers, which is in our study rather based on data of global character. Experiments to derive such restraints were however impeded due to extensive spectral overlap of residues L5 and L7 in constructs A and B and by the general challenge to obtain sensitive NMR spectra of peptide-based nanovesicles. For example, the $^{13}\text{C} - ^{13}\text{C}$ and $^{15}\text{N} - ^{13}\text{C}$ experiments to assign *construct B* (Figure S2) already required 896 and 10400 scans, respectively, corresponding to 2d 14h and 3d 17h of measurement time. In future studies, it may be advantageous to use isotope labelling schemes⁴⁷ that allow probing intermolecular contacts with more sensitive ^1H detected ssNMR experiments. Nevertheless, our study demonstrates that SA2 peptide nanocarriers are partially disordered and exhibit a highly dynamic surface. It is a particular strength of the combination of ssNMR and MD simulations to unravel and interpret such structural

heterogeneity, which is presumably an important factor to consider for the rational design of peptide-based nanoparticles.

The knowledge on the atomic-level geometry and dynamics of assembled peptides in relation to the supramolecular organization of the SA2 nanocarrier offers a number of starting points to tailor the biophysical properties of the vesicle such as its stability, surface texture or permeability. A promising lead could be the addition of a positive charge to the N-terminus, which is likely to modify the degree of interdigitation. Either the removal of the N-acetyl group (slim positive charge) or the replacement of the N-terminal alanine residue for an arginine/lysine residue (bulky and flexible positive charge) is likely to further enhance interdigitation with a further thinning of the nanocarrier wall. Another lead could be the substitution of the tryptophan residue by a less bulky aromatic residue such as phenylalanine or tyrosine. This could allow a better alignment of peptide backbones for hydrogen bonding (Figure 5b), enhance the hydrogen bonding activity of the C-terminal residues that precede the glutamates and thereby reduce structural heterogeneity and the high permeability of SA2 nanocarriers⁴⁸. Interestingly, while substitution to a tyrosine would allow for hydrogen bonds with the E9 and E10 carboxyl-groups, phenylalanine would break these bonds (Figure S8) and thus modulate the surface properties of the nanocarrier. The latter is particularly interesting since control over the surface dynamics and order is crucial for peptide-based nanomaterials that present epitopes or act as templates in material sciences².

3. Conclusions

Using an integration of several experimental techniques with large- and multi-scale MD simulations, we have presented for the first time an atomic level model of the supramolecular organization of the multi-mega-Dalton SA2 peptide-based nanocarrier, which suggests several potential leads for the rational design and tuning of such systems. In particular, we could show that the SA2 nanocarrier organization does not involve liposome-like tail-to-tail orientation of the amphiphilic molecules. To the best of our knowledge, this is the first description of such an arrangement in nanovesicles and speaks against the hitherto prevalent idea that ‘lipid-like’ amphiphilic peptides organize like lipids on the supramolecular level. Further high-resolution studies will be necessary to judge to what extent our findings can be generalized to other peptide-based nanocarriers.

The here introduced approach should be of broad utility for studies on peptide-based nanomaterials at atomic-level and at physiological conditions. Moreover, given that such nanomaterials are amenable to ssNMR, the level of detail could be readily expanded to peptide-water interactions⁴⁹

and to quantitative high-resolution dynamics of the assembled peptides⁵⁰, which would provide further valuable information for rational design of nanoscale drug delivery systems.

4. Materials and Methods

4.1. Sample preparation. Self-assembled peptide particles were prepared by dispersion of SA2 peptide powder (>95 % purity, acquired from Genscript, USA) in phosphate buffered saline (PBS = 140 mM NaCl, 13 mM Na₂HPO₄ and 2.5 mM NaH₂PO₄ [pH 7.4]) (Braun Melsungen AG, Germany) using bath sonication. SA2 peptide powder (according to the final concentration, e.g., 8.4 mg peptide powder for a 10 mM sample) was hydrated with 40 µl of 0.2 M NaOH. After each step, peptide dispersion was ultra-sonicated in a water bath for 5 min at 30°C. Before reaching final volume, the pH was adjusted to 7.4 by 0.2M HCl. The final dispersion was incubated overnight at 25°C to reach equilibrium. The peptide concentration in the solution was measured by UV-spectrophotometry using a tryptophan extinction coefficient of 5500 M⁻¹cm⁻¹. According to this procedure, samples with appropriate concentrations were prepared and applied for CD (10 mg/ml), AFM (2 mg/ml and 10 mg/ml), FT-IR (2mg/ml), DLS (0.6, 0.8, 1 and 2 mg/ml) and SLS analysis (0.6, 0.8, 1 mg/ml). For the ssNMR measurements, labeled peptides (construct A: ¹³C,¹⁵N-labeled at A1, V3, L5, purity> 90%, acquired from JPT Peptide Technologies GmbH, Germany ; construct B: ¹³C,¹⁵N-labeled at A1, L7, E10, purity> 95%, acquired from New England Peptide) were dispersed in PBS to a concentration of 10 mg/ml according the mentioned procedures.

4.2. Solid-state NMR spectroscopy. Experiments were carried out at a magnetic field of 11.7 T (500 MHz ¹H-frequency) at 9.1 kHz Magic Angle Spinning (MAS) frequency and 278 K sample temperature. ¹³C and ¹⁵N chemical shifts were calibrated using Adamantane and tri-peptide AGG as external references, respectively^{51,52}. The ¹H signal of Adamantane was used to reference ¹H chemical shifts. The 2D ¹³C - ¹³C PARIS¹⁹ experiments (N=0.5, i.e., phase inversion after 55 µs) were performed with 30 ms mixing time and a recoupling amplitude of 8 kHz. A short cross-polarization contact time of 125 µs was used in the 2D ¹H - ¹³C FSLG experiments¹⁸. A ¹H-¹H FSLG decoupling amplitude of 90 kHz was applied in the indirect dimension. FSLG measurements with ¹³C,¹⁵N Valine and additional ¹H-¹³C HECTOR experiments with SA2 peptides (at 13 kHz MAS, see Figure S11) were carried out to get the correct ¹H chemical shifts. A ¹⁵N - ¹³C contact time of 3.5 ms was used in the 2D SPECIFIC DCP²¹ experiments. Typical 90° pulse lengths for the experiments on the peptide constructs were 3.8 µs for ¹H, 3.4 µs for ¹³C and 8.5 µs for ¹⁵N. Further acquisition and processing parameters can be found in the Supporting Information (Table S2).

4.3. Molecular Dynamics simulations. *Coarse-grained (CG) molecular dynamics (MD) simulations* were carried out using the GROMACS simulations package version 4.5.4⁵³ and the MARTINI force field version 2.2³⁴ together with an integration step of 20 fs and the standard settings for non-bonded interactions in a NPT ensemble with period boundary conditions. Simulation times were multiplied by a factor 4 to account for the smoothness of the CG potentials. The system was coupled to a pressure bath at 1 bar ($\tau_p = 0.5$ ps) and coupled ($\tau_T = 1.0$ ps) to a heat bath of temperature 300 K. A fully extended SA2 peptide was used as starting structure, converted to CG representation using the martinize.py script and the secondary structure assigned from A1 to E10 as CEEEEEEEC (E= Extended, C=Coil). The A1 backbone bead was replaced by a polar P4 bead to mimic N-acetylation. To build the CG starting simulation system, 2500 peptides were randomly distributed in large, water-filled periodic and cubic box of 74.4 x 74.4 x 74.4 nm³ volume. 150 mM NaCl and counterions were added to electrostatically neutralize the system. The total system comprised 2500 peptides, 3405700 water beads, 10000 Na⁺ beads and 2500 Cl⁻ beads and was evolved for 54 μ s. The computation was, on average, run on 450 CPUs, which yielded about 0.6 μ s/day of simulation time.

Atomistic MD simulations were carried out using the GROMOS54a7 force field of the GROMACS package⁴¹. The CG system (except for water molecules) after 54 μ s of simulation time was transformed to atomic coordinates⁴⁴. This included addition of the N-terminal acetyl-group. The system (>41 million atoms) was rehydrated, equilibrated with position restraints and freely evolved for 37.5 ns at a temperature of 300 K (see Supporting Information for further details). Afterwards, two nanoparticles (particles IV and VIII in Figure 2a) were further evolved for 1 μ s (see Supporting Information for further details). On average, simulations were run on 550 CPUs, which yielded about 0.5 ns/day and 12 ns/day of simulations time for the full 41 million atoms system and the 449 peptides system, respectively. The STRIDE program was used to evaluate secondary structure⁵⁴. Protons were added to the peptides before calculations of peptide-peptide interactions matrixes. The peptide – Na⁺ radial distribution function and the peptide SASA were calculated with standard GROMACS scripts (g_rdf and g_sas). Na⁺ residence times were calculated using an in-house GROMACS analysis script (<http://zeffros.eu/confluence/display/ZS/Gromacs+Residence+Time+Tool>).

4.4. Circular dichroism spectroscopy. Experiments were measured in a double beam DSM 1000 CD spectrometer (Online Instrument Systems, Bogart, GA, USA) using a circular quartz cuvette of 0.5 mm path length (Hellma, Müllheim, Germany) and peptide dispersions in PBS (pH 7.4). Five measurements of 1.0 nm increment were scanned from 250 nm to 180 nm at room temperature. The average of five spectra was subtracted from the buffer spectrum as the background.

4.5. Light scattering techniques. Particle size of the self- assemblies was measured in PBS by Dynamic Light Scattering (DLS) at 90° on an ALV CGS-3 goniometer system (Malvern Instruments, Malvern, UK) equipped with a JDS Uniphase 22 mW He-Ne laser operating at 632.8 nm, an optical fiber-based detector, a digital LV/LSE-5003 correlator and a temperature controller (Julabo water bath) to set different temperatures. Autocorrelation curves were analyzed using DTS 4.0 particle analysis software (Malvern, UK). The reported hydrodynamic radius is the z-averaged hydrodynamic radius as reported by the DTS 4.0 software. To get insight into the shape of particles and determine the occupied surface area (OSA) per peptide in the assemblies, static light scattering (SLS) analysis was performed. The experiment was operated at different scattering angles (20° -140°) for three different peptide concentrations (600, 800 and 1000 µg/ml). A Zimm plot was constructed using ALVStat 4.31 software (ALV, Langen, Germany), and the molecular weight and the radius of gyration, using the dn/dc (~0.185 mL/g) of peptides in PBS, were obtained. See Supporting Information for further details.

4.6. Infrared spectroscopy. ATR-FT-IR measurements were performed at ambient temperature on a Perkin-Elmer 2000 Fourier transform spectrometer equipped with a DTGS detector. To avoid the H₂O absorption in the region 1600 - 1700 cm⁻¹, PBS was prepared with D₂O for peptide particle preparation. Spectra for a 2 mg/ml of SA2 peptide were recorded with an ATR accessory (PIKE) equipped with a diamond crystal as the reflecting element. The optical resolution was 4 cm⁻¹ and 30 scans were accumulated for one spectrum. Spectral interpretation was carried out after subtraction of the spectrum of PBS (D₂O) as background.

5. ASSOCIATED CONTENT

Supporting Information. AFM images of SA2 nanovesicles; ssNMR experiments of ¹³C, ¹⁵N-A1, L7, E10 SA2 peptide (construct B); comparison of atomic force fields; further analysis of the nanocarrier build; detailed description of DLS/SLS measurements; further details to the parameters of the atomistic simulation; details to the ssNMR acquisition and processing parameters; movies of the simulated nanocarrier assembly pathway. This material is available free of charge via the Internet at <http://pubs.acs.org>.

6. ABBREVIATIONS

SA2 peptide, self-assembling peptide 2; SASA, solvent accessible surface area; OSA, occupied surface area; ssNMR, solid-state nuclear magnetic resonance; CG, coarse-grained; MD, molecular dynamics; SLS, static light scattering; DLS, dynamic light scattering.

7. References

- (1) Vauthey, S., Santoso, S., Gong, H., Watson, N., and Zhang, S. (2002) Molecular self-assembly of surfactant-like peptides to form nanotubes and nanovesicles. *Proc. Natl. Acad. Sci. U. S. A.* 99, 5355–60.
- (2) Cui, H., Pashuck, E. T., Velichko, Y. S., Weigand, S. J., Cheetham, A. G., Newcomb, C. J., and Stupp, S. I. (2010) Spontaneous and x-ray-triggered crystallization at long range in self-assembling filament networks. *Science* 327, 555–559.
- (3) Zhao, X., Pan, F., Xu, H., Yaseen, M., Shan, H., Hauser, C. A. E., Zhang, S., and Lu, J. R. (2010) Molecular self-assembly and applications of designer peptide amphiphiles. *Chem. Soc. Rev.* 39, 3480–3498.
- (4) Bellomo, E. G., Wyrsta, M. D., Pakstis, L., Pochan, D. J., and Deming, T. J. (2004) Stimuli-responsive polypeptide vesicles by conformation-specific assembly. *Nat. Mater.* 3, 244–248.
- (5) Holowka, E. P., Pochan, D. J., and Deming, T. J. (2005) Charged polypeptide vesicles with controllable diameter. *J. Am. Chem. Soc.* 127, 12423–12428.
- (6) Xu, X., Li, Y., Li, H., Liu, R., Sheng, M., He, B., and Gu, Z. (2014) Smart Nanovehicles based on pH-triggered disassembly of supramolecular peptide-amphiphiles for efficient intracellular drug delivery. *Small* 10, 1133–1140.
- (7) Lin, B. F., Marullo, R. S., Robb, M. J., Krogstad, D. V, Antoni, P., Hawker, C. J., Campos, L. M., and Tirrell, M. V. (2011) *De novo* design of bioactive protein-resembling nanospheres via dendrimer-templated peptide amphiphile assembly. *Nano Lett.* 11, 3946–3950.
- (8) Gudlur, S., Sukthankar, P., Gao, J., Avila, L. A., Hiromasa, Y., Chen, J., Iwamoto, T., and Tomich, J. M. (2012) Peptide nanovesicles formed by the self-assembly of branched amphiphilic peptides. *PLoS One* 7, e45374.
- (9) Torchilin, V. P., Levchenko, T. S., Rammohan, R., Volodina, N., Papahadjopoulos-Sternberg, B., and D'Souza, G. G. M. (2003) Cell transfection *in vitro* and *in vivo* with nontoxic TAT peptide-liposome-DNA complexes. *Proc. Natl. Acad. Sci. U. S. A.* 100, 1972–1977.
- (10) Ellis-Behnke, R. G., Liang, Y.-X., You, S.-W., Tay, D. K. C., Zhang, S., So, K.-F., and Schneider, G. E. (2006) Nano neuro knitting: peptide nanofiber scaffold for brain repair and axon regeneration with functional return of vision. *Proc. Natl. Acad. Sci. U. S. A.* 103, 5054–5059.
- (11) Kisiday, J., Jin, M., Kurz, B., Hung, H., Semino, C., Zhang, S., and Grodzinsky, A. J. (2002) Self-assembling peptide hydrogel fosters chondrocyte extracellular matrix production and cell division: implications for cartilage tissue repair. *Proc. Natl. Acad. Sci. U. S. A.* 99, 9996–10001.
- (12) M., F. W. J., Scott, G. G., Abul-Haija, Y. M., Kalafatovic, D., Pappas, C. G., Javid, N., Hunt, N. T., Ulijn, R. V, and Tuttle, T. (2015) Exploring the sequence space for (tri-)peptide self-assembly to design and discover new hydrogels. *Nat. Chem.* 7, 30–37.

- (13) Silva, G. A., Czeisler, C., Niece, K. L., Beniash, E., Harrington, D. A., Kessler, J. A., and Stupp, S. I. (2004) Selective Differentiation of Neural Progenitor Cells by High-Epitope Density Nanofibers. *Science* (80-.). *303*, 1352–1355.
- (14) Van Hell, A. J., Costa, C. I. C. A., Flesch, F. M., Sutter, M., Jiskoot, W., Crommelin, D. J. A., Hennink, W. E., and Mastrobattista, E. (2007) Self-assembly of recombinant amphiphilic oligopeptides into vesicles. *Biomacromolecules* *8*, 2753–61.
- (15) Van Hell, A. J., Fretz, M. M., Crommelin, D. J. A., Hennink, W. E., and Mastrobattista, E. (2010) Peptide nanocarriers for intracellular delivery of photosensitizers. *J. Control. Release* *141*, 347–353.
- (16) Yang, S. J., and Zhang, S. (2006) Self-assembling behavior of designer lipid-like peptides. *Supramol. Chem.* *18*, 389–396.
- (17) Fatouros, D. G., Lamprou, D. A., Urquhart, A. J., Yannopoulos, S. N., Vizirianakis, I. S., Zhang, S., and Koutsopoulos, S. (2014) Lipid-like self-assembling peptide nanovesicles for drug delivery. *ACS Appl. Mater. Interfaces* *6*, 8184–8189.
- (18) Bielecki, A., Kolbert, A. C., and Levitt, M. H. (1989) Frequency-switched pulse sequences: Homonuclear decoupling and dilute spin NMR in solids. *Chem. Phys. Lett.* *155*, 341–346.
- (19) Weingarth, M., Bodenhausen, G., and Tekely, P. (2009) Broadband carbon-13 correlation spectra of microcrystalline proteins in very high magnetic fields. *J. Am. Chem. Soc.* *131*, 13937–13939.
- (20) Weingarth, M., Demco, D. E., Bodenhausen, G., and Tekely, P. (2009) Improved magnetization transfer in solid-state NMR with fast magic angle spinning. *Chem. Phys. Lett.* *469*, 342–348.
- (21) Baldus, M., Petkova, A. T., Herzfeld, J., and Griffin, R. G. (1998) Cross polarization in the tilted frame: Assignment and spectral simplification in heteronuclear spin systems. *Mol. Phys.* *95*, 1197–1207.
- (22) Cormier, A. R., Pang, X., Zimmerman, M. I., Zhou, H.-X., and Paravastu, A. K. (2013) Molecular structure of RADA16-I designer self-assembling peptide nanofibers. *ACS Nano* *7*, 7562–7572.
- (23) Takahashi, H., Viveerge, B., Lee, D., Rannou, P., and De Paëpe, G. (2013) Towards structure determination of self-assembled peptides using dynamic nuclear polarization enhanced solid-state NMR spectroscopy. *Angew. Chemie - Int. Ed.* *52*, 6979–6982.
- (24) Shaw, C. P., Middleton, D. A., Volk, M., and Lévy, R. (2012) Amyloid-derived peptide forms self-assembled monolayers on gold nanoparticle with a curvature-dependent β -sheet structure. *ACS Nano* *6*, 1416–1426.

- (25) Middleton, D. A., Madine, J., Castelletto, V., and Hamley, I. W. (2013) Insights into the molecular architecture of a peptide nanotube using FTIR and solid-state NMR spectroscopic measurements on an aligned sample. *Angew. Chemie - Int. Ed.* 52, 10537–10540.
- (26) Leonard, S. R., Cormier, A. R., Pang, X., Zimmerman, M. I., Zhou, H.-X., and Paravastu, A. K. (2013) Solid-state NMR evidence for β -hairpin structure within MAX8 designer peptide nanofibers. *Biophys. J.* 105, 222–230.
- (27) Wishart, D. S., Sykes, B. D., and Richards, F. M. (1992) The chemical shift index: A fast and simple method for the assignment of protein secondary structure through NMR spectroscopy. *Biochemistry* 31, 1647–1651.
- (28) Wang, Y., and Jardetzky, O. (2002) Probability-based protein secondary structure identification using combined NMR chemical-shift data. *Protein Sci.* 11, 852–861.
- (29) Hafsa, N. E., and Wishart, D. S. (2014) CSI 2.0: A significantly improved version of the Chemical Shift Index. *J. Biomol. NMR* 60, 131–146.
- (30) Kabsch, W., and Sander, C. (1983) Dictionary of protein secondary structure: pattern recognition of hydrogen-bonded and geometrical features. *Biopolym. - Pept. Sci. Sect.* 22, 2577–2637.
- (31) Guo, C., Luo, Y., Zhou, R., and Wei, G. (2012) Probing the self-assembly mechanism of diphenylalanine-based peptide nanovesicles and nanotubes. *ACS Nano* 6, 3907–3918.
- (32) Muñoz, A., Illescas, B. M., Sánchez-Navarro, M., Rojo, J., and Martín, N. (2011) Nanorods versus nanovesicles from amphiphilic dendrofullerenes. *J. Am. Chem. Soc.* 133, 16758–16761.
- (33) Korevaar, P. A., Newcomb, C. J., Meijer, E. W., and Stupp, S. I. (2014) Pathway selection in peptide amphiphile assembly. *J. Am. Chem. Soc.* 136, 8540–8543.
- (34) De Jong, D. H., Singh, G., Bennett, W. F. D., Arnarez, C., Wassenaar, T. A., Schäfer, L. V., Periolo, X., Tieleman, D. P., and Marrink, S. J. (2013) Improved parameters for the martini coarse-grained protein force field. *J. Chem. Theory Comput.* 9, 687–697.
- (35) Lee, O.-S., Cho, V., and Schatz, G. C. (2012) Modeling the self-assembly of peptide amphiphiles into fibers using coarse-grained molecular dynamics. *Nano Lett.* 12, 4907–4913.
- (36) Antonietti, M., and Förster, S. (2003) Vesicles and Liposomes: A Self-Assembly Principle Beyond Lipids. *Adv. Mater.* 15, 1323–1333.
- (37) Colherinhas, G., and Fileti, E. (2014) Molecular dynamics study of surfactant-like peptide based nanostructures. *J. Phys. Chem. B* 118, 12215–12222.
- (38) Cerf, E., Sarroukh, R., Tamamizu-Kato, S., Breydo, L., Derclayes, S., Dufrênes, Y. F., Narayanaswami, V., Goormaghtigh, E., Ruyschaert, J.-M., and Raussens, V. (2009) Antiparallel β -sheet: A signature structure of the oligomeric amyloid β -peptide. *Biochem. J.* 421, 415–423.

- (39) Bakota, E. L., Sensoy, O., Ozgur, B., Sayar, M., and Hartgerink, J. D. (2013) Self-assembling multidomain peptide fibers with aromatic cores. *Biomacromolecules* *14*, 1370–1378.
- (40) Lindorff-Larsen, K., Piana, S., Palmo, K., Maragakis, P., Klepeis, J. L., Dror, R. O., and Shaw, D. E. (2010) Improved side-chain torsion potentials for the Amber ff99SB protein force field. *Proteins Struct. Funct. Bioinforma.* *78*, 1950–1958.
- (41) Schmid, N., Eichenberger, A. P., Choutko, A., Riniker, S., Winger, M., Mark, A. E., and Van Gunsteren, W. F. (2011) Definition and testing of the GROMOS force-field versions 54A7 and 54B7. *Eur. Biophys. J.* *40*, 843–856.
- (42) Wang, J., Cieplak, P., and Kollman, P. A. (2000) How Well Does a Restrained Electrostatic Potential (RESP) Model Perform in Calculating Conformational Energies of Organic and Biological Molecules? *J. Comput. Chem.* *21*, 1049–1074.
- (43) Van Hell, A. J., Klymchenko, A., Burgers, P. P., Moret, E. E., Jiskoot, W., Hennink, W. E., Crommelin, D. J. A., and Mastrobattista, E. (2010) Conformation and intermolecular interactions of SA2 peptides self-assembled into vesicles. *J. Phys. Chem. B* *114*, 11046–11052.
- (44) Wassenaar, T. A., Pluhackova, K., Böckmann, R. A., Marrink, S. J., and Tieleman, D. P. (2014) Going backward: A flexible geometric approach to reverse transformation from coarse grained to atomistic models. *J. Chem. Theory Comput.* *10*, 676–690.
- (45) Tieleman, D. P., Van Der Spoel, D., and Berendsen, H. J. C. (2000) Molecular dynamics simulations of dodecylphosphocholine micelles at three different aggregate sizes: Micellar structure and chain relaxation. *J. Phys. Chem. B* *104*, 6380–6388.
- (46) Bond, P. J., and Sansom, M. S. P. (2003) Membrane protein dynamics versus environment: Simulations of OmpA in a micelle and in a bilayer. *J. Mol. Biol.* *329*, 1035–1053.
- (47) Sinnige, T., Daniëls, M., Baldus, M., and Weingarth, M. (2014) Proton clouds to measure long-range contacts between nonexchangeable side chain protons in solid-state NMR. *J. Am. Chem. Soc.* *136*, 4452–4455.
- (48) Van Hell, A. J., Crommelin, D. J. A., Hennink, W. E., and Mastrobattista, E. (2009) Stabilization of peptide vesicles by introducing inter-peptide disulfide bonds. *Pharm. Res.* *26*, 2186–2193.
- (49) Weingarth, M., Van Der Crujisen, E. A. W., Ostmeier, J., Lievestro, S., Roux, B., and Baldus, M. (2014) Quantitative analysis of the water occupancy around the selectivity filter of a K⁺ channel in different gating modes. *J. Am. Chem. Soc.* *136*, 2000–2007.
- (50) Lewandowski, J. R. (2013) Advances in solid-state relaxation methodology for probing site-specific protein dynamics. *Acc. Chem. Res.* *46*, 2018–2027.

- (51) Etzkorn, M., Martell, S., Andronesi, O. C., Seidel, K., Engelhard, M., and Baldus, M. (2007) Secondary structure, dynamics, and topology of a seven-helix receptor in native membranes, studied by solid-state NMR spectroscopy. *Angew. Chemie - Int. Ed.* 46, 459–462.
- (52) Luca, S., Filippov, D. V, Van Boom, J. H., Oschkinat, H., De Groot, H. J. M., and Baldus, M. (2001) Secondary chemical shifts in immobilized peptides and proteins: A qualitative basis for structure refinement under Magic Angle Spinning. *J. Biomol. NMR* 20, 325–331.
- (53) Hess, B., Kutzner, C., Van Der Spoel, D., and Lindahl, E. (2008) GRGMACS 4: Algorithms for highly efficient, load-balanced, and scalable molecular simulation. *J. Chem. Theory Comput.* 4, 435–447.
- (54) Heinig, M., and Frishman, D. (2004) STRIDE: A web server for secondary structure assignment from known atomic coordinates of proteins. *Nucleic Acids Res.* 32, W500–W502.

Supporting Information

The supramolecular organization of a peptide-based nanocarrier at high molecular detail

This Supporting Information contains:

Figures S1 – S13

Further details to the atomistic MD simulations, the SLS/DLS measurements and the ssNMR experiments

Descriptions of the Supporting Movies

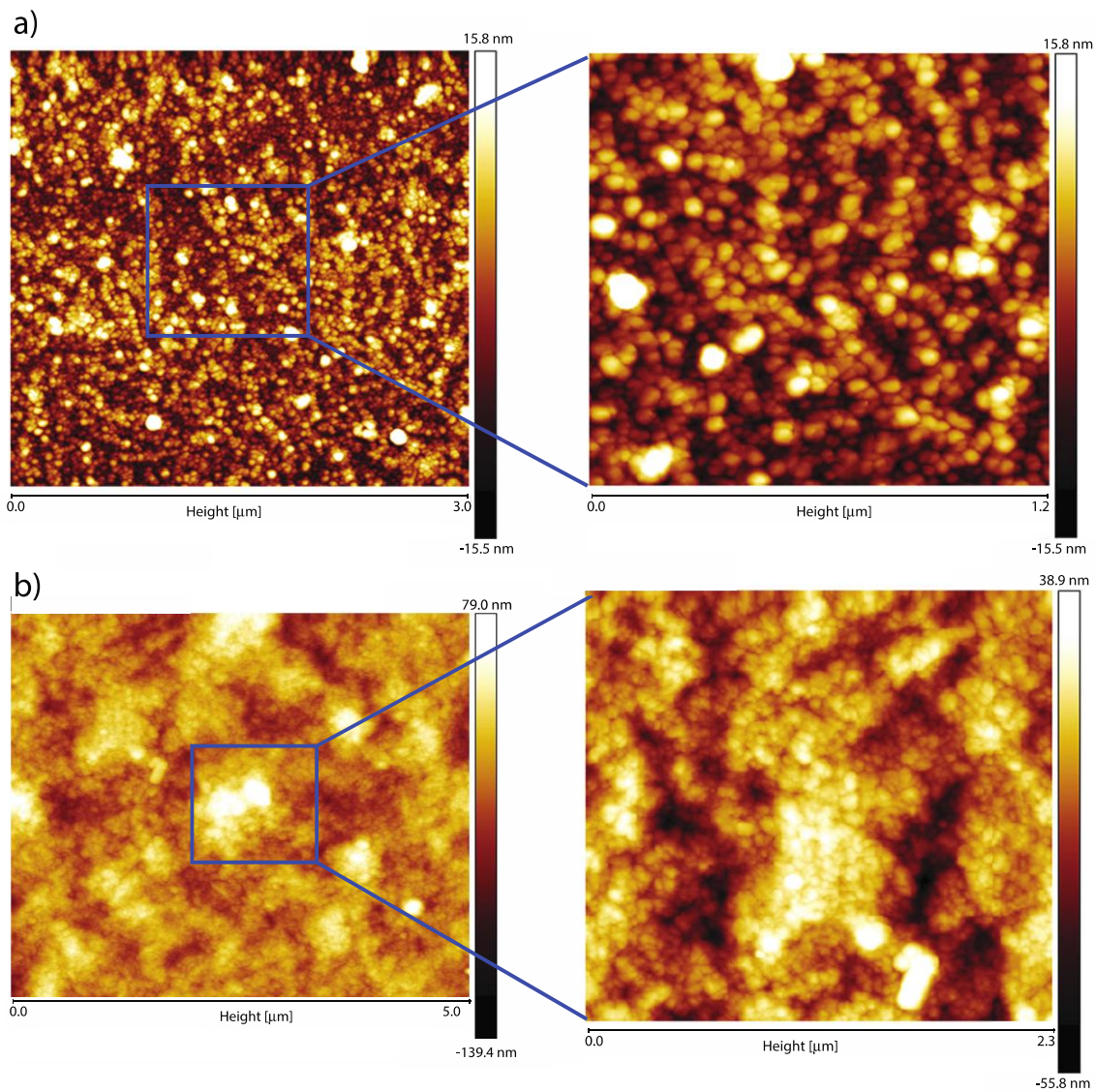


Figure S1. Atomic force microscopy (AFM). AFM measurements demonstrate that SA2 peptides self-assemble to spherical particles at peptide concentrations of 2 mg/ml and 10 mg/ml. a) AFM of 2 mg/ml of SA2 peptide assemblies immobilized on poly-L-lysine coated mica. Dispersed peptide in phosphate buffered saline (pH=7.4) formed spherical nanovesicles with a diameter between 20-60 nm. b) AFM images of 10 mg/ml of SA2 peptide assemblies. The peptides assembled to compactly packed spheres at this sample concentration.

Experimental details: Freshly cleaved mica wafer was incubated for 5 min with 5 times diluted poly-L-lysine solution (150-300 kDa, 0.1%, Sigma-Aldrich, St. Louis, MO) and subsequently washed three times with MQ water. A drop (50 μ L) of the prepared peptide dispersion was deposited on the coated mica and incubated for 5 minutes. The mica was washed three times with 500 μ L of dH₂O to remove salts, and dried under a stream of nitrogen. The dried sample was analyzed by a Nanoscope V in Scan Asyst imaging mode, using nonconductive silicon nitride probes (Veeco, NY, U.S.A.). Images were recorded and further processed with NanoScope Analysis 1.20 software (Veeco Instruments Inc. 2010, U.S.A.).

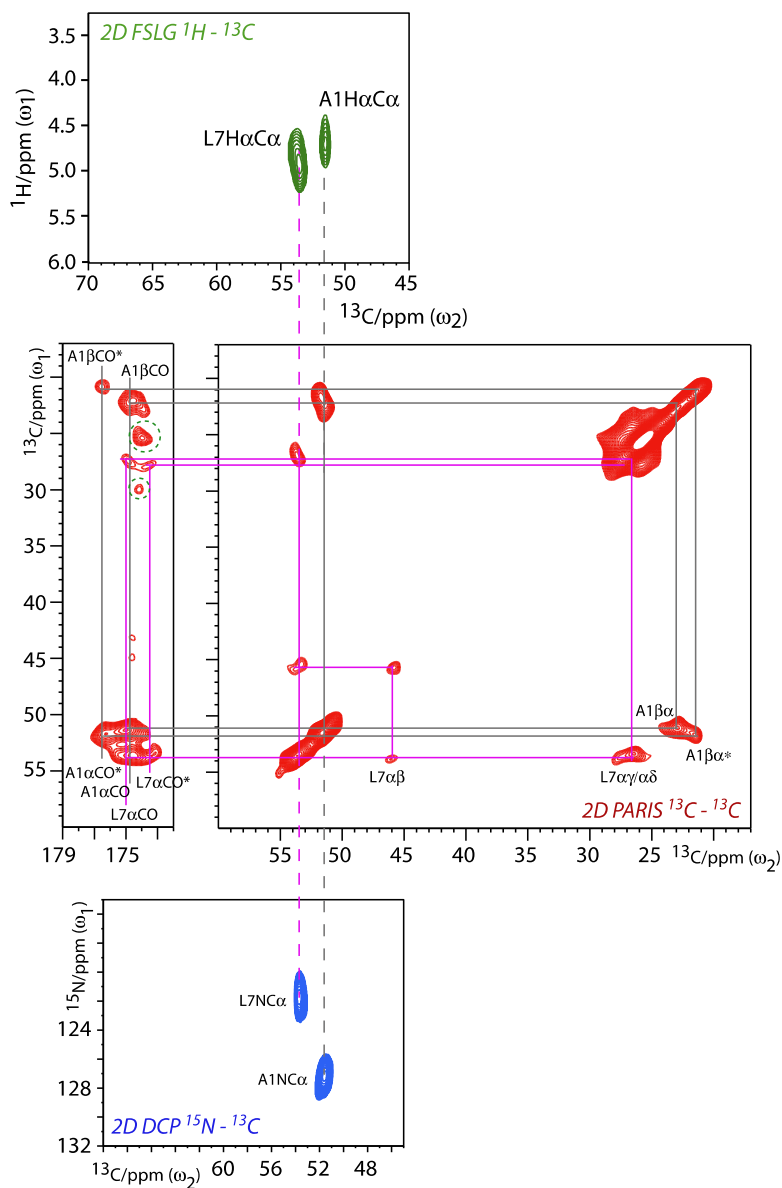


Figure S2. SSNMR experiments with SA2 construct B ($[^{13}\text{C}, ^{15}\text{N}]$ -labeled at A1, L7 and E10). All experiments were carried out at 500 MHz ^1H -frequency and 9.1 kHz MAS at a real temperature of 278 K. In blue: $2\text{D } ^1\text{H} - ^{13}\text{C}$ FSLG¹. In green: $2\text{D } ^{15}\text{N} - ^{13}\text{C}_\alpha$ SPECIFIC DCP². In red: $2\text{D } ^{13}\text{C} - ^{13}\text{C}$ PARIS³ experiment using a mixing time of 30 ms ($N = 0.5$). While the spin systems of A1 and L7 could be clearly identified, residue E10 showed no correlations. Moreover, peak doubling for L7CO, L7C_γ, and all signals of A1 is visible in the spectrum. L7 featured very weak correlations between the side chain carbons, which may point to residual mobility of the C-terminal hydrophobic residues next to conformational heterogeneity. Signals in green circles could not be identified with certainty.

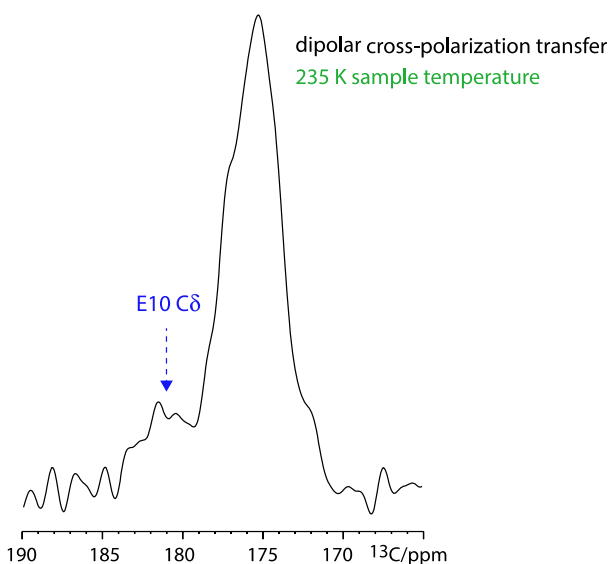
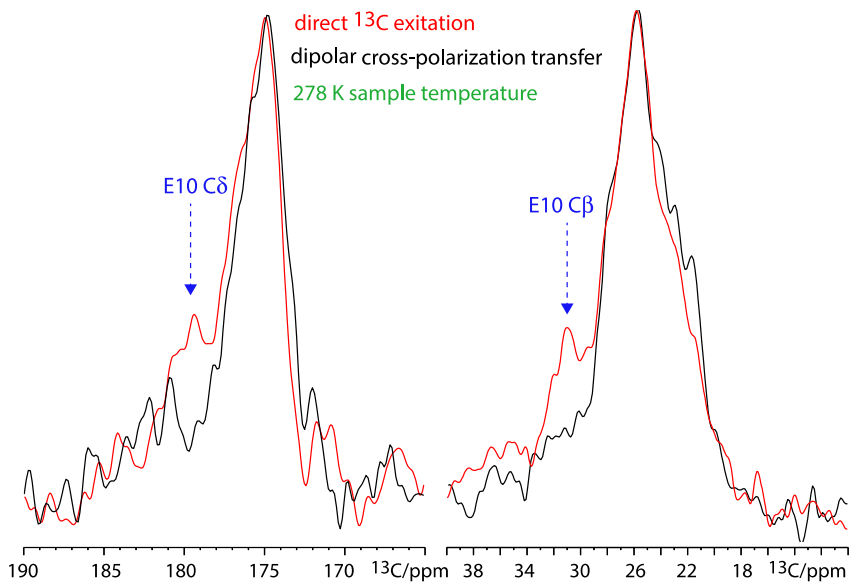


Figure S3. Detection of the C-terminal residue E10 in ^{13}C direct excitation experiments and at low temperature. At 278 K sample temperature, signals that were in good agreement with average chemical shifts of glutamate C δ and C β appeared in ^{13}C direct excitation experiments, while such signals were very weak or absent in experiments that used an initial dipolar ^1H - ^{13}C cross-polarization step. Moreover, at 235 K sample temperature, at which peptide mobility is reduced, a signal could be observed that matches well with the average chemical shift of glutamate C δ . This corroborates that residue E10 exhibits fast dynamics (μs or faster). Note that the E10C δ chemical shift is slightly different at lower temperatures.

1 AAVVLLLW 8

1 CBBBBBBC 8

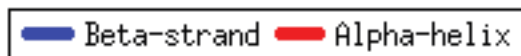


Figure S4. CSI.2.0 evaluation of chemical shift data. The recently developed CSI 2.0 program⁴ confirmed that the hydrophobic core of assembled SA2 peptides adopts β -strand secondary structure. The CSI 2.0 program uses machine learning techniques to combine chemical shift data and amino acid sequence data to analyze secondary structure with an accuracy comparable to structure based methods.

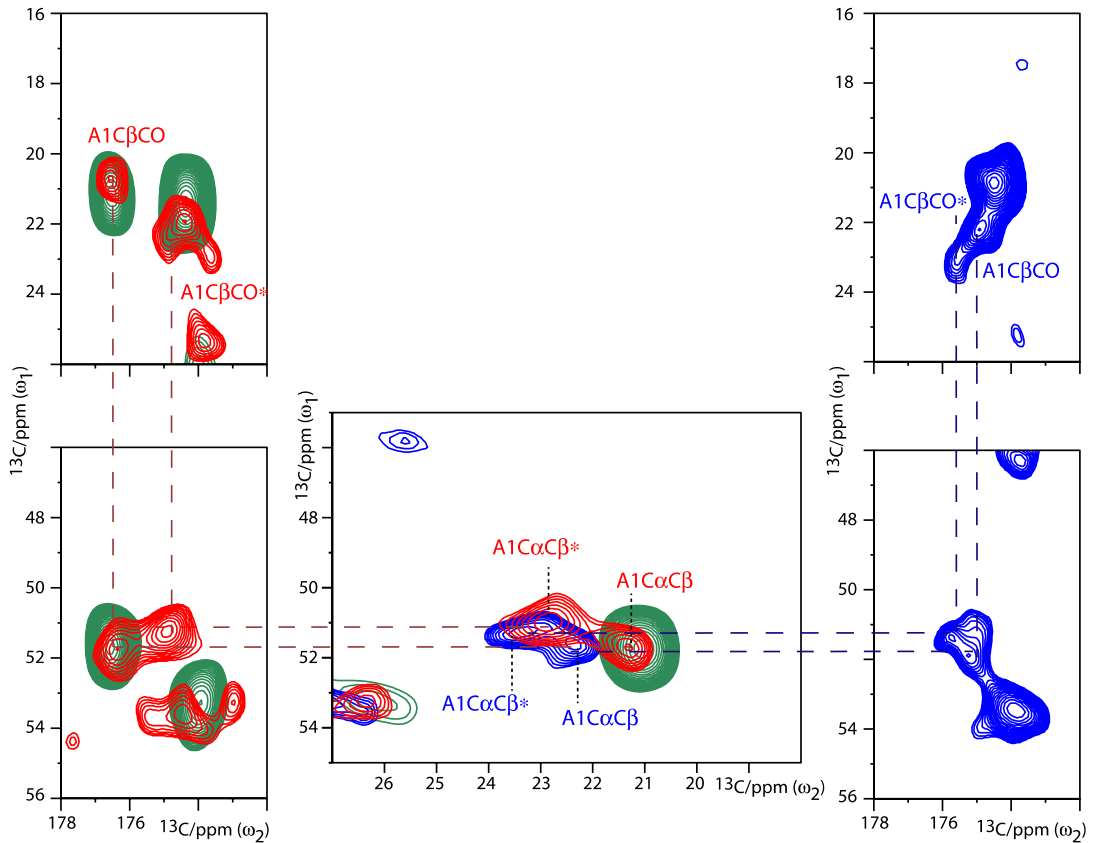


Figure S5. SSNMR experiments show that the local structure of SA2 nanovesicles is disordered around the N- and C-termini of peptides. 2D CC PARIS spectra showed two sets of conformations for all A1 carbons signals (marked as A1 and A1*). These two sets could be observed in both SA2 peptide labeling construct A (in blue) and B (in red), although the chemical shifts, especially of A1C β , slightly differed. Interestingly, we observed only one set A1 chemical shifts for a second batch of construct A (in green), which indicates that subtle differences in the sample preparation influence the conformation of the N-terminus. Note that all observed A1 conformations have chemical shifts consistent with β -strand secondary structure. Peak-doubling was also observed for L7 (see Figure S2).

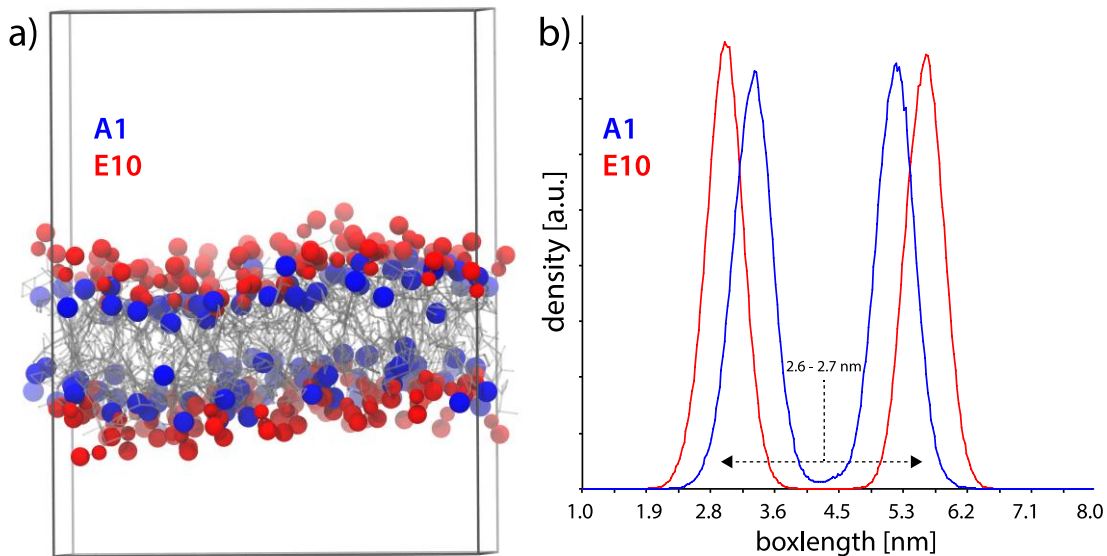


Figure S6. Simulation of a periodic slab of SA2 peptides. The peptide arrangement that we observe in the large CGMD simulation (Figure 2 of the main text) could potentially represent a non-equilibrated state. Therefore, we carried out a very long simulation of a much smaller SA2 peptide system to be certain to observe an equilibrated peptide arrangement. For this, 120 SA2 peptides, randomly distributed in a periodic box, were self-assembled and simulated for 100 μ s as a bilayer slab. a) Representative snapshot of this simulation. Residues A1 and E10 are shown in blue and red colors, respectively. The other residues are shown in gray. As it is readily visible in the snapshot and in b) the A1/E10 density profile, this simulation confirms the antiparallel and interdigitated arrangement of SA2 peptides which we had observed in the large CGMD simulation at close to experimental peptide concentrations (Figure 2 of the main text). Also the wall-thickness that we observe in the small system (2.6 - 2.7 nm) matches well with what we had observed in the large CGMD simulation (2.4 nm).

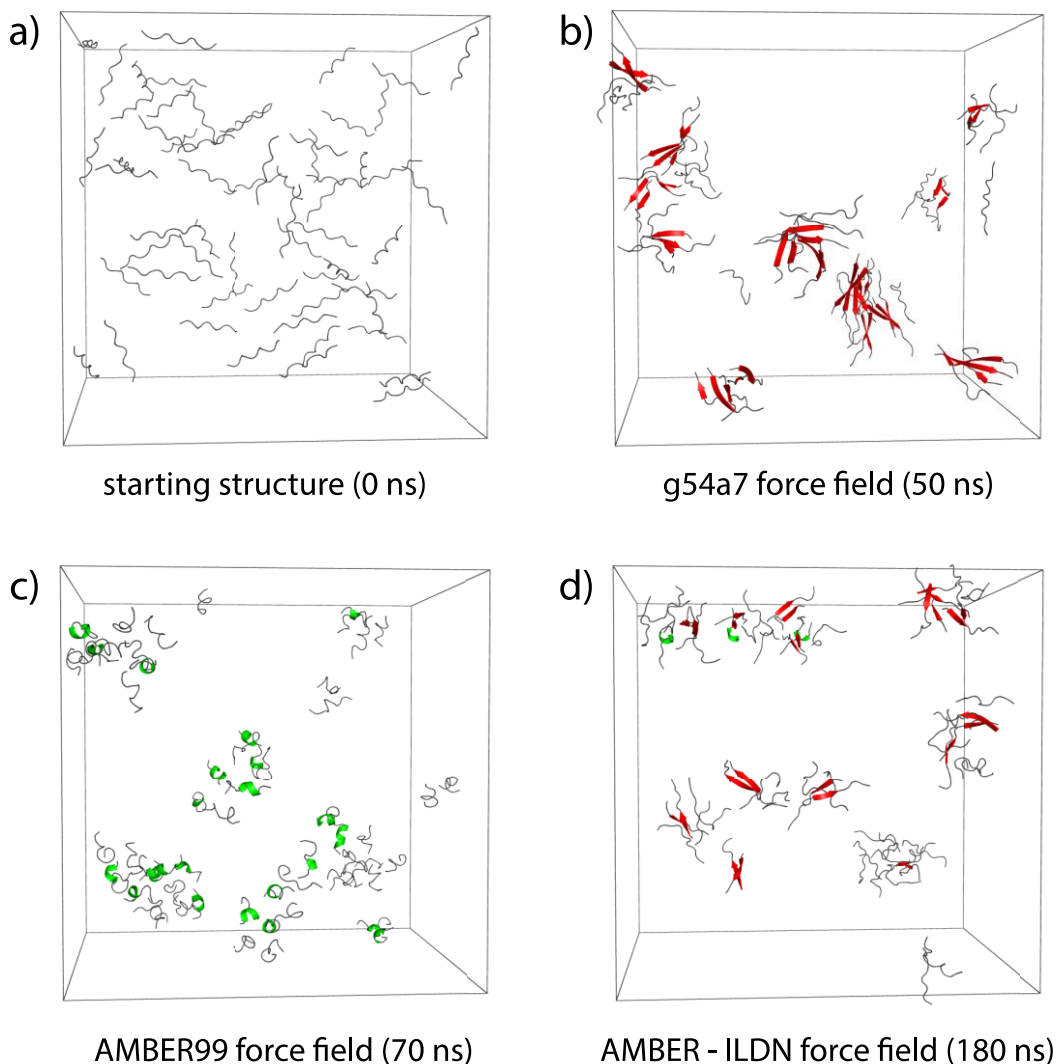


Figure S7. Comparison of atomic force fields for the simulation of SA2 peptides. a) 60 peptide monomers in extended conformation were simulated in a cubic periodic box of size $15 \times 15 \times 15 \text{ nm}^3$ at 300 K in an aqueous solution that contained 150 mM NaCl. Further simulation parameters correspond to parameters that were used for the atomistic simulations described in the main text and can be found in the Materials and Methods.

Modern force fields such as b) g54a7⁵ and d) AMBER ff99SB-ILDN⁶ reproduce the ssNMR results that assemblies of SA2 peptides adopt β -strand secondary structure. c) The AMBER ff99 force field⁷ however showed spurious assemblies of α -helices, which presumably explains the

outcome of previous computational studies⁸. All simulations were repeated with peptides in PPI helix torsion angles (φ , $\psi = -75, 160$), which led to the same results as described in b-d).

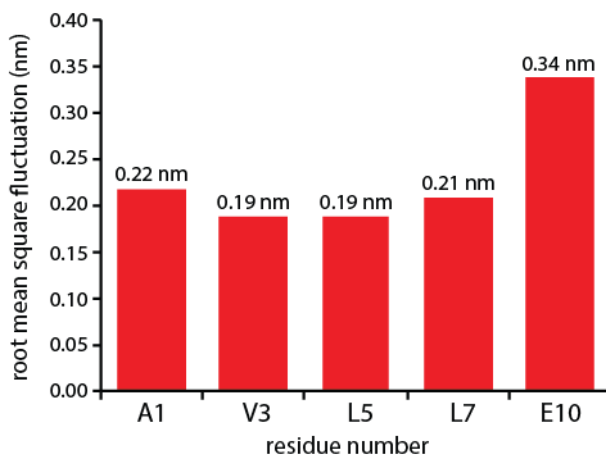


Figure S8. *The C-terminus showed increased dynamics in ssNMR experiments and MD simulations. The backbone root mean square fluctuation (rmsf) of peptide residues A1, V3, L5, L7 and E10 were averaged over 449 peptides and the last 200 ns of a 1 μ s atomistic simulation. The analysis showed that the C-terminal residue E10 was significantly more mobile than the hydrophobic core and the N-terminus, which is in excellent agreement with the ssNMR experiments.*

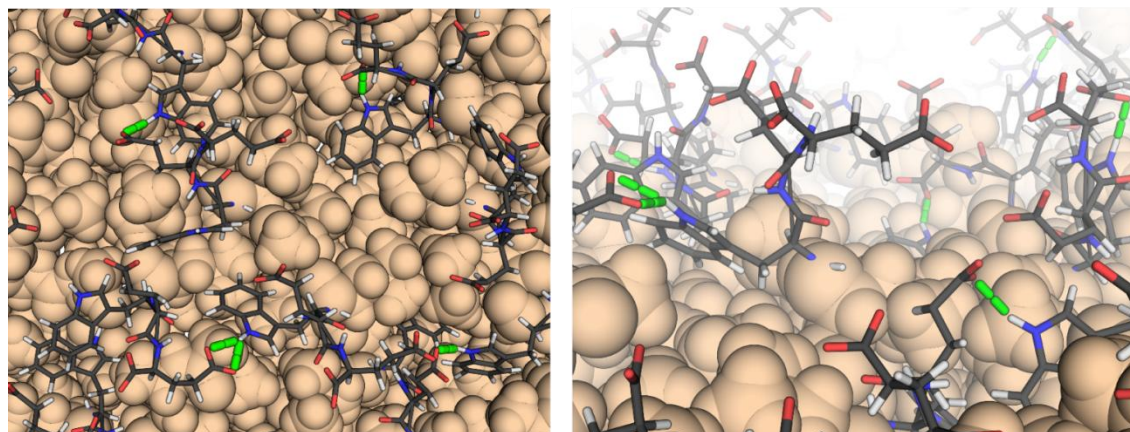


Figure S9. *Interactions between the W8 indole-ring and the E9/E10 carboxyl-groups at the nanocarrier surface. On average, approximately one out of three of the anionic C-termini form intra- and especially intermolecular hydrogen bonds (in green) with the indole-ring of residue W8.*

The Figure depicts a snapshot of the SA2 nanocarrier surface after 1 μ s of atomistic MD simulation. Left: top view; right: side view. Residues A1 – L7 are depicted as brown spheres.

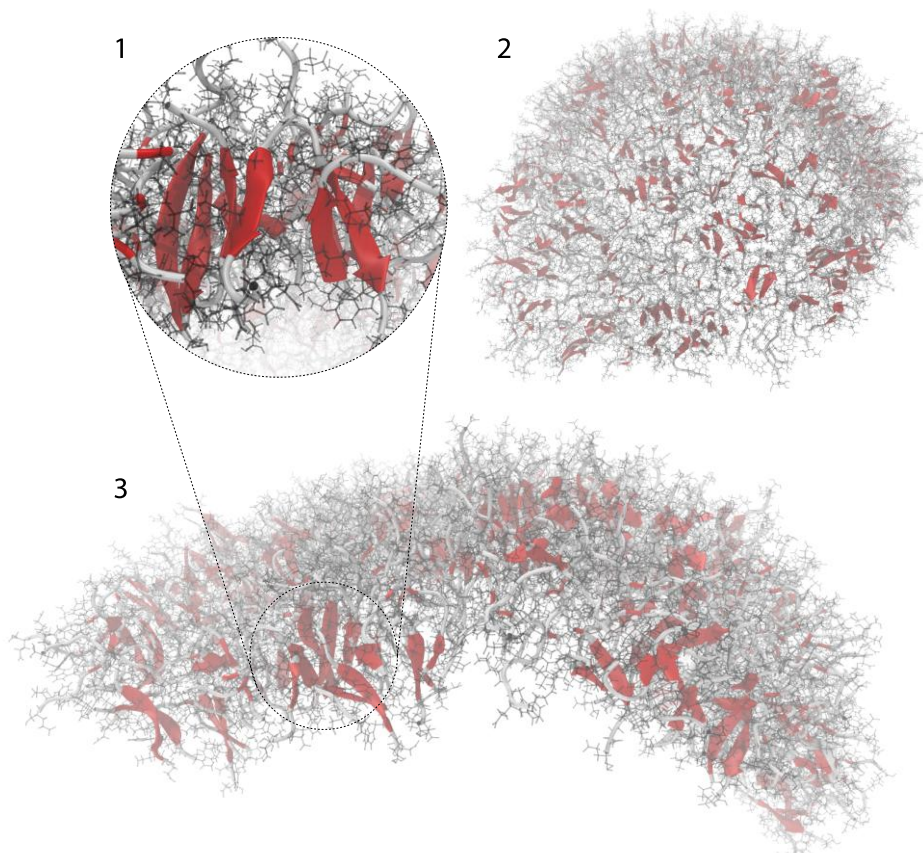


Figure S10. Further perspectives of the 449 peptides SA2 nanocarrier fragment after 1 μ s of atomistic simulation. Extended secondary structure elements are highlighted in red. Panel 1 shows a zoom.

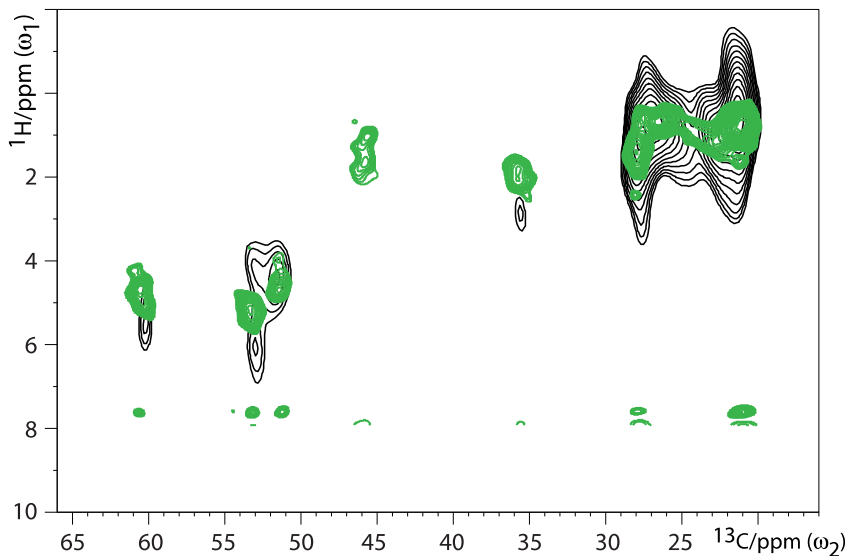


Figure S11. Comparison of 2D ^1H , ^{13}C correlation spectra measured with SA2 construct A in the presence (in green) and in the absence (in black) of ^1H - ^1H FSLG decoupling during the t_1 ^1H -evolution time.

Further details to the atomistic MD simulations and the SLS/DLS measurements

1. Atomistic MD simulations – parameter and further details to the analysis:

After 54 μs of CGMD simulation, the 2500 SA2 peptides (and ions) were transformed to atomistic representation using the BACKWARD tool⁹, which was slightly modified to include the N-terminal acetyl group. After rehydration, the final system consisted of 2500 SA2 peptides, 13579613 water molecules, 2500 chloride and 10000 sodium ions, i.e., a total of 41001339 atoms. Simulations were carried out in a cubic box of 74.4 x 74.4 x 74.4 nm^3 size with periodic boundary conditions. The system was minimized with Steepest Descent for 14000 steps. The system was further equilibrated in a NVT ensemble for 0.2 ns using positions restraints with force constants of 1000 $\text{kJ}/(\text{mol}\cdot\text{nm}^2)$ on all heavy atoms. Subsequently, the system was equilibrated in a NPT ensemble, using a Parinello Rahman barostat with isotropic pressure coupling of 1 bar, for 0.7 ns with positions restraints (100 $\text{kJ}/(\text{mol}\cdot\text{nm}^2)$) on all backbone heavy atoms and eventually freely

evolved for 37.5 ns using a time-step of 2 fs. The temperature in all simulations was kept constant at 300 K with a V-rescale thermostat¹⁰ using a coupling constant of 0.1 ps. Peptides as well as [water and ions] were separately coupled to the thermostat. Long-range electrostatic interactions were simulated with the PME method¹¹. The g54a7 force field⁵ and the GROMOS simulation package version 4.6.3¹² were used for all atomistic simulations.

After 37.5 ns of simulation, the nanoparticle corresponding to cluster VIII in Figure 2a of the main text was extracted from the system, rehydrated and sodium as well as chloride ions added. The final system consisted of 449 SA2 peptides, 699364 water molecules, 661 chloride and 2008 sodium ions, i.e., a total of 2145661 atoms and was simulated in cubic box of $28 \times 28 \times 28 \text{ nm}^3$ size with periodic boundary conditions (see Figure S12 below). The box dimensions were deliberately generous to allow for a potential stretching of the particle by a further decrease in particle curvature. The ion concentration in the system was slightly reduced in comparison to the 41 million atoms simulation to compensate for the reduced proportion of the aqueous phase. The system was minimized and further equilibrated as described above and then freely evolved for 1 μs . Analogously, the nanoparticle corresponding to cluster IV was extracted after 37.5 ns of simulation, equilibrated and then freely evolved for 1 μs .

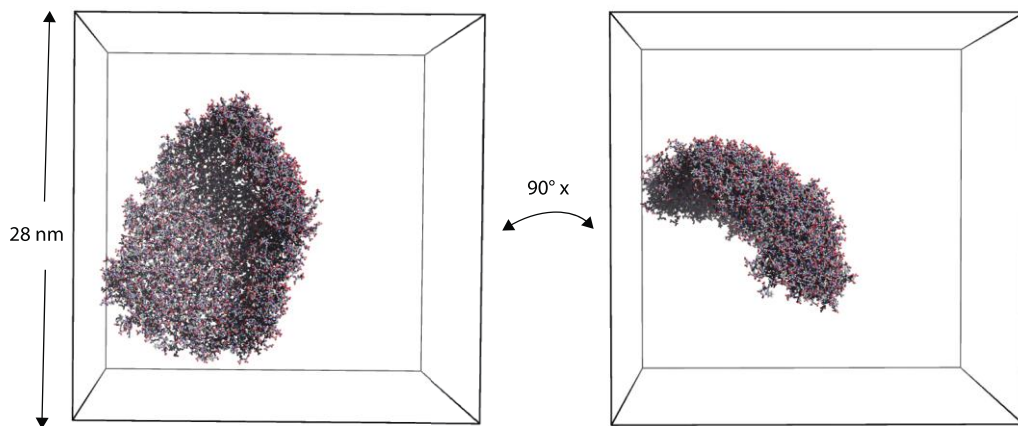


Figure S12. The final system comprised 449 SA2 peptides in aqueous solution and was simulated in periodic cubic box of $28 \times 28 \times 28 \text{ nm}^3$.

2. Light scattering techniques:

Particle size of the peptide nanocarriers was measured in PBS by dynamic light scattering (DLS) at 90° on an ALV CGS-3 goniometer system (Malvern Instruments, Malvern, UK) equipped with a JDS Uniphase 22 mW He-Ne laser operating at 632.8 nm, an optical fiber-based detector, a digital LV/LSE-5003 correlator and a temperature controller (Julabo water bath) to set different temperatures (Figure S13).

To determine the radius of gyration and weight-averaged molecular weight of peptide nanocarriers static light scattering (SLS) analysis was performed. The experiment was operated at different scattering angles (30° -150°) for three different peptide concentrations (600, 800 and 1000 µg/ml). By measuring the optical constant (K) and the excess Rayleigh ratio (ΔR_θ) in an infinite dilution, total weight-averaged molecular weight (Mw) and radius of gyration (Rg) can be determined by the extrapolation of $Kc/\Delta R_\theta$ to zero angle and zero concentration according to the following relation:

$$\frac{Kc}{\Delta R_\theta} = \frac{1}{M_w} \left[1 + \frac{16\pi^2 n^2}{3\lambda^2} R_g^2 \text{Sin}^2 \left(\frac{\theta}{2} \right) \right] + 2A_2c$$

Where K is the optical constant, which depends on the refractive index increment (dn/dc) of the peptide solution ($K = 4\pi^2 n^2 - (dn/dc)^2 / NA\lambda^4$, where NA is Avogadro's number, n is the refractive index of the liquid medium, and λ is the wavelength of the laser), and ΔR_θ is the excess Rayleigh ratio [$\Delta R_\theta = R_\theta$ (solution) - R_θ (solvent)], respectively. A Zimm plot was constructed using ALVStat 4.31 software (ALV, Langen, Germany), and the molecular weight and the radius of gyration, using the dn/dc (~0.185 mL/g) of peptides in PBS buffer, were obtained.

The shape factor ρ which equals R_g/R_h was calculated to be close to 1, which is indicative of a vesicular nature of the peptide assemblies (table 1). The number of peptides in one particle (N_{agg}) was calculated by dividing the weight-averaged Mw of particles estimated by SLS by the molecular weight of each peptide. The surface area occupied by each peptide (OSA) was derived from the sum of inner and outer surface areas of a vesicle divided by the aggregation number, using a peptide bilayer thickness of 2.4 nm as determined by MD:

$$OSA = (Surface\ Area_{outer} + Surface\ Area_{inner})/Number\ of\ aggregation = (4\pi R_g^2 + 4\pi(R_g - 2.4)^2)/N_{agg}$$

Where R_g is, radius of gyration and N_{agg} is the peptide aggregation number.

Table S1. Macromolecular properties of the peptide assemblies.

Peptide	R_g (nm)	R_h (nm)	ρ (R_g/R_h)	M_w (Da)	Aggregation number	Surface area/ peptide (nm^2)
SA2*	34±2	32±1	1.06±0.07	5.82 x 10 ⁶ ±3.14x10 ⁵	4911±264	5.75±0,71

* Three different peptide concentrations (600, 800 and 1000 $\mu g/ml$) were prepared in PBS (pH=7.4).

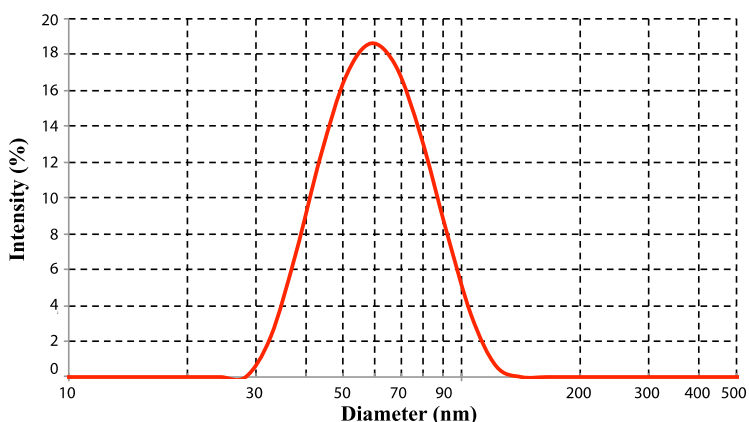


Figure S13. Particle size distribution of 2 mg/ml of SA2 peptide in phosphate buffered saline (pH=7.4) obtained from dynamic light scattering measurements. The z-average diameter is 62 nm and the peak position is at 57 nm with a PDI of 0.070.

3. SSNMR experiments:

Table S2. Details to the ssNMR acquisition and processing parameters

Peptide construct	Experiment	Number of scans	t_1 increments	Exp. time	Window funct.
A	^{13}C - ^{13}C PARIS	352	140	1d 2h	Qsin 3 / Qsin 3
A	^{15}N - ^{13}C DCP	1536	16	13h	Qsin 5 / Qsin 4
A	^1H - ^{13}C FSLG	672	190	3d	Qsin 4 / Qsin 4
B	^{13}C - ^{13}C PARIS	896	128	2d 14h	Qsin 3 / Qsin 3
B	^{15}N - ^{13}C DCP	10400	16	3d 17h	Qsin 5 / Qsin 4
B	^1H - ^{13}C FSLG	1024	116	2d 22h	Qsin 2 / Qsin 2

All experiments were carried out at 9.1 MAS frequency and 278 K sample temperature. The interscan delay was 1.85 – 2.1s for all experiments. Note that the higher number of repetitions with SA2 peptide construct B was due to the weak signal intensity of residue L7.

Descriptions of the Supporting Movies

Movie 1

Movie of the SA2 peptide self-assembly process described in Figure 2a of the main text. The movie shows the evolution of 2500 coarse-grained peptides over 54 μs of simulation. The time-resolution of the movie is 200 ns. Water and ions were left out for clarity (http://pubs.acs.org/doi/suppl/10.1021/jacs.5b02919/suppl_file/ja5b02919_si_002.avi).

Movie 2

Evolution of the 449 SA2 peptides nanoparticle (corresponding to cluster VIII in Figure 2a of the main text) over the initial 37.5 ns of the atomistic MD simulation after transformation from coarse-grained representation. The time-resolution of the movie is 1 ns (http://pubs.acs.org/doi/suppl/10.1021/jacs.5b02919/suppl_file/ja5b02919_si_003.avi).

References

- (1) Bielecki, A., Kolbert, A. C., and Levitt, M. H. (1989) Frequency-switched pulse sequences: Homonuclear decoupling and dilute spin NMR in solids. *Chem. Phys. Lett.* *155*, 341–346.
- (2) Baldus, M., Petkova, A. T., Herzfeld, J., and Griffin, R. G. (1998) Cross polarization in the tilted frame: Assignment and spectral simplification in heteronuclear spin systems. *Mol. Phys.* *95*, 1197–1207.
- (3) Weingarth, M., Bodenhausen, G., and Tekely, P. (2009) Broadband carbon-13 correlation spectra of microcrystalline proteins in very high magnetic fields. *J. Am. Chem. Soc.* *131*, 13937–13939.
- (4) Hafsa, N. E., and Wishart, D. S. (2014) CSI 2.0: A significantly improved version of the Chemical Shift Index. *J. Biomol. NMR* *60*, 131–146.
- (5) Schmid, N., Eichenberger, A. P., Choutko, A., Riniker, S., Winger, M., Mark, A. E., and Van Gunsteren, W. F. (2011) Definition and testing of the GROMOS force-field versions 54A7 and 54B7. *Eur. Biophys. J.* *40*, 843–856.
- (6) Lindorff-Larsen, K., Piana, S., Palmo, K., Maragakis, P., Klepeis, J. L., Dror, R. O., and Shaw, D. E. (2010) Improved side-chain torsion potentials for the Amber ff99SB protein force field. *Proteins Struct. Funct. Bioinforma.* *78*, 1950–1958.
- (7) Wang, J., Cieplak, P., and Kollman, P. A. (2000) How Well Does a Restrained Electrostatic Potential (RESP) Model Perform in Calculating Conformational Energies of Organic and Biological Molecules? *J. Comput. Chem.* *21*, 1049–1074.
- (8) Van Hell, A. J., Klymchenko, A., Burgers, P. P., Moret, E. E., Jiskoot, W., Hennink, W. E., Crommelin, D. J. A., and Mastrobattista, E. (2010) Conformation and intermolecular interactions of SA2 peptides self-assembled into vesicles. *J. Phys. Chem. B* *114*, 11046–11052.
- (9) Wassenaar, T. A., Pluhackova, K., Böckmann, R. A., Marrink, S. J., and Tieleman, D. P. (2014) Going backward: A flexible geometric approach to reverse transformation from coarse grained to atomistic models. *J. Chem. Theory Comput.* *10*, 676–690.
- (10) Bussi, G., Donadio, D., and Parrinello, M. (2007) Canonical sampling through velocity rescaling. *J. Chem. Phys.* *126*.
- (11) Essmann, U., Perera, L., Berkowitz, M. L., Darden, T., Lee, H., and Pedersen, L. G. (1995) A smooth particle mesh Ewald method. *J. Chem. Phys.* *103*, 8577–8593.
- (12) Hess, B., Kutzner, C., Van Der Spoel, D., and Lindahl, E. (2008) GRGMACS 4: Algorithms for highly efficient, load-balanced, and scalable molecular simulation. *J. Chem. Theory Comput.* *4*, 435–447.

Chapter 5

Synthesis and characterization of Self-Assembling Peptide Epitopes (SAPEs) for prophylactic and therapeutic cancer immunotherapy

**Mazda Rad-Malekshahi ^a, Marieke F. Fransen ^b, Meriem Bourajjaj ^a, Jian
Chen ^a, Ferry Ossendorp ^b, Wim E. Hennink ^a, Enrico Mastrobattista ^a,
Maryam Amidi ^a**

^a Department of Pharmaceutics, Utrecht Institute for Pharmaceutical Sciences, Utrecht University,
Utrecht, The Netherlands

^b Department of Immunohematology and Blood Transfusion, Leiden University Medical Center,
Leiden, The Netherlands

Manuscript in preparation

Abstract

We previously developed and characterized a particulate system based on a short self-assembling peptide (SA2: Ac-AAVVLLLWEE-COOH) that forms nanovesicular structures once dispersed in an aqueous solution. It was shown that the self-assembly was mainly dependent on the hydrophobic domain of the peptide (Ac-AAVVLLLW-COOH) with both hydrophobic clustering and intermolecular hydrogen bond formation as driving forces. In this study, peptide self-assembled epitopes (SAPEs) consisting of the hydrophobic domain of SA2 peptide elongated at its C-terminus with T cell epitopes derived from ovalbumin (OVA) were designed. The findings indicated that the SAPEs could form reproducible nanostructures at concentrations above the critical aggregation concentrations (CAC). The obtained SAPE nanostructures were characterized by atomic force microscopy (AFM), dynamic light scattering (DLS), circular dichroism (CD), and fluorescence spectroscopy. The SAPEs bearing the OVA CTL epitope (OSAP: Ac-AAVVLLLWSGLEQLESIINFEKL-COOH) formed 20-30 nm nanoparticles while SAPEs bearing the OVA T-helper epitope (OSAP-h: Ac-AAVVLLLWSAESLKISQAVHAAHAEINEAGR-COOH) formed a mixture of spherical nanoparticles and fibers. Notably, spherical nanoparticles were observed when OSAP and OSAP-h were mixed at a ratio of 8:3, respectively. It was also shown that the SAPEs adjuvanted with CpG were able to induce and expand specific CD8⁺ and CD4⁺ T cells in C57BL/6 mouse models. Furthermore, *in vivo* results indicated that the adjuvanted SAPEs delayed tumor growth and increased the survival proportion of mice both in a prophylactic as well as therapeutic tumor vaccination regimens. These interesting results warrant further testing of these tumor vaccines based on self-assembling peptide epitopes.

1. Introduction

Utilizing the patient's own immune system represents a powerful approach for eradication of cancer as a targeted treatment¹. Due to genetic instability, one of the hallmarks of cancer, changes in the antigenic repertoire of tumor cells can be frequently observed that may lead to immune recognition²⁻⁴. Cancer vaccines aim to evoke a strong adaptive immune response against these tumor antigens⁵⁻⁷. However, the way antigens are presented to the immune system determines to a great extent the quality and longevity of the induced immune response, in which antigen presenting cells (APCs) play a pivotal role. An example of professional antigen presenting cells are dendritic cells (DCs). DCs play a significant role in the induction of immune responses by continuously sampling the environment for foreign antigens and establishing the communication between the innate and adaptive immune system. Appropriate activated DCs can induce a robust cell-mediated immune response, which is required for effective eradication of established tumors^{8,9}. For this purpose, DCs are the key target cells for cancer vaccination.

There is an increasing interest in using minimal peptide antigenic epitopes to make well-defined vaccines which can elicit predictable and controllable immune responses. However, different studies demonstrated that these minimal peptide epitopes are poorly immunogenic¹⁰⁻¹². Administration of soluble peptides with adjuvants may not necessarily result in induction of efficient immune responses and may even induce tolerance and T cell anergy by direct binding to MHC molecules without being taken up and processed by DCs¹². Various studies have shown that peptide epitopes delivered with particulate systems such as polymeric particles or liposomes, increased peptide uptake by DCs and consequently increased vaccine efficacy¹³⁻¹⁷. Only few studies have utilized peptide self-assembly as a means to construct discrete nanoparticles for vaccine delivery^{18,19}.

In our laboratory, we have designed short amphiphilic peptides (SA2 and SA7) that form nanovesicular structures once dispersed in an aqueous solution^{20,21}. The self-assembly was mainly dependent on the hydrophobic stretch of the peptide with both hydrophobic clustering and intermolecular hydrogen bond formation as driving forces. Interestingly, extending the hydrophilic part of these self-assembling peptides from 2 to 7 glutamic acid residues had no effect on the self-assembling behaviour, with no change in vesicular shape and size. This suggests some degree of flexibility in exposing peptide epitopes on the surface of these peptide vesicles. The use of self-assembling peptides for the delivery of antigenic peptide epitopes offers several advantages over existing particulate vaccine delivery systems, such as polymeric and lipidic nanocarriers. They can be easily synthesized by standardized solid-phase peptide synthesis methods. Furthermore, they

are easy to formulate: simple dispersion of the self-assembling peptides in aqueous media results in the spontaneous formation of discrete and uniform particles, without the need for laborious processing as is often the case for other particulate systems. Finally, several functionalities such as self-assembly, antigenicity, adjuvanticity and receptor specificity can be combined in a single polypeptide which is a major advantage from a pharmaceutical point of view compared to more complex formulations consisting of multiple components. Another main advantage of self-assembling peptide particles is the high loading efficiency of antigens since almost all peptide chains contribute to particle formation. In comparison, other particulate systems such as liposomal or polymeric nanoparticles are often suffering from low encapsulation efficiencies, particularly for water soluble peptides. Moreover, multiple epitopes can be combined at will within these peptide assemblies with preservation of the high loading efficiency¹⁴⁻¹⁷.

The aim of this study was to apply peptide self-assembly as a means to obtain well-defined nanostructures which expose a high density of antigenic epitopes to be used as delivery systems in cancer immunotherapy. To this end, the C- terminus of the hydrophobic domain of SA2 (Ac-AAVLLLLW-COOH) was extended by the OVA250–264 peptide (covering a CTL epitope of ovalbumin: SIINFEKL) and the OVA316-339 peptide (covering a T-helper epitope of ovalbumin: ISQAVHAAHAEINEAGR) using standard solid phase peptide chemistry. The newly designed self-assembling peptide epitope (SAPE) vaccines were characterized for their particle size, morphology, zeta-potential, critical aggregation concentration (CAC) and secondary structure. Furthermore, the capacity of these vaccines to induce or expand OVA specific CD8⁺ T cell and CD4⁺ T-helper cells were tested in naïve mice and mice carrying OVA specific CD8⁺ (OT-I) and CD4⁺ (OT-II) T cells, respectively. Further, the capability of these vaccines to induce OVA-specific immune responses and to delay tumor growth were tested in mice bearing OVA-expressing B16 melanoma cells both in a prophylactic and therapeutic setting.

2. Materials and methods

2.1. Materials

OSAP (Ac-AAVLLLLWSGLEQLESIIINFEKL-COOH), containing SIINFEKL as a cytotoxic T lymphocyte (CTL) epitope of ovalbumin (OVA), and SA2 (Ac-AAVLLLLWEE-COOH) as a control peptide just containing self-assembling domain were synthesized by Genscript (New Jersey, USA). OSAP-h (Ac-AAVLLLLWSAESLKISQAVHAAHAEINEAGR-COOH), covering the T helper lymphocyte epitope of OVA, was synthesized by Selleck Chemicals (Houston, TX).

In addition, the following short peptides were purchased from Asynth Service BV (Roosendaal, Netherlands): OVA250–264: SGLEQLESIINFEKL (hereafter referred to as CTL peptide) and OVA316-339: SSAESLKISQAVHAAHAEINEAGR (hereafter referred to as Th peptide) as soluble epitopes covering CTL and Th epitopes, respectively. Purity of all ordered peptides was more than 95%. CpG ODN 1826 (CpG) was purchased from InvivoGen (Cayla, France). Nile red, poly-L-lysine ,hexafluoroisopropanol (HFIP) and 4-(2-hydroxyethyl) piperazine-1-ethanesulfonic acid (HEPES) were obtained from Sigma (Sigma-Aldrich, St. Louis, MO). Phosphate-buffered saline(PBS) containing 140 mM NaCl, 13 mM Na₂HPO₄ and 2.5 mM NaH₂PO₄ was obtained from B. Braun (Melsungen AG, Melsungen, Germany); sodium hydroxide and HCL were bought from Merck (Darmstadt, Germany). HEPA vent filters were obtained from Whatman (Kent, UK) All other chemicals were of analytical grade, and all aqueous solutions were prepared with Millipore Milli-Q deionized water (18.2 MΩ; Millipore Milli-Q system, Billerica, MA).

2.2. Preparation of self-assembling peptide epitopes (SAPEs)

To prepare SAPE formulations, for example, one milligram of peptide was dissolved in 200 µl of HFIP to give a clear solution. After solvent evaporation by flushing with nitrogen gas (HEPA filtered), the obtained peptide film was hydrated with 40 µl of 0.2 M NaOH solution. Subsequently, phosphate buffer saline (phosphate 10 mM, NaCl 150 mM, pH 7.4) was added in 200 µl portions up to 1ml. After each step, peptide dispersion was sonicated in a water bath sonicator (Fisher Scientific, Loughborough, UK) for 3 min at 30°C. Before reaching the final volume, the pH was adjusted to pH 7.4 by dropwise adding 0.2 M HCl. To prepare a formulation containing 2 peptides, separate stock solutions of each peptide were prepared in HFIP and the appropriate volumes of each stock solution were mixed to result in a homogenous solution of 2 peptides. Film preparation and hydration were similar as described above. After pH adjustment, some formulations were supplemented with CpG (20µg per injection; 10 µl of a 2 mg/ml of a stock solution of CpG in PBS) as adjuvant.

2.3. Characterization of self-assembling peptide epitopes

2.3.1. Critical Aggregation Concentration Determination

The critical aggregation concentration (CAC) was determined based on the Nile red assay as described by Zhang *et al*²². A series of peptide concentrations (0.1-500 µg/ml) in PBS (pH 7.4) was prepared. Next, 200 µl of each dilution was spiked with 0.2 µl of Nile red solution (1.25 mM in ethanol). After overnight incubation at room temperature in dark, fluorescence emission

(Ex550/Em635) was measured by a Horiba fluorolog fluorometer (Horiba Jobin Yvon, Longjumeau Cedex, France). The fluorescence intensity at 635 nm was plotted against the peptide concentration to determine the critical aggregation concentration (CAC). The point of intersection of two linear fits of the plot was considered as the CAC value.

2.3.2. Particle size and zeta potential measurement

Particle size of the self-assemblies was measured in PBS with Dynamic Light Scattering (DLS) on an ALV CGS-3 goniometer system (Malvern Instruments, Malvern, UK) equipped with a JDS Uniphase 22 mW He-Ne laser operating at 632.8 nm, an optical fiber-based detector, a digital LV/LSE-5003 correlator and a temperature controller (Julabo water bath) to set different temperatures. The results was analyzed by ALV Correlator 3.0 software (ALV, Langen, Germany).

The zeta potential of the peptide nanoparticles was measured in 10 mM HEPES pH=7.0 by a Malvern Zetasizer Nano-Z (Malvern Instruments, Malvern, UK) with universal ZEN 1002 ‘dip’ cells and DTS (Nano) software (version 4.20). DTS 1235 latex beads (Zeta Potential Transfer Standard, Malvern Instruments, Malvern, UK) were used as a test standard.

2.3.3. Atomic force microscopy

Fourty microlitres of a 0.02% (w/v) polylysine solution in water was placed on a freshly cleaved mica and after 5 min washed with filtered Milli-Q water followed by drying under N₂ flow. Then, 30 µl of sample was loaded on the treated mica and left for 1 min, followed by washing three times with 20 µl of filtrated Milli-Q water to discharge nonattached particles and salts. Finally, the prepared sample was dried by a N₂ flow.

ScanAsystTM image mode was used at room temperature with a Digital Instruments NanoScope V, equipped with silicon nitride cantilevers (Veeco, NY, USA). Images were analyzed by NanoScope Analysis 1.40 software. Several images were taken at different days of individually prepared samples to confirm the reproducibility of the obtained morphology.

2.3.4. Circular dichroism spectroscopic analysis

Circular dichroism spectra were recorded using a double beam DSM 1000 CD spectrometer (Online Instrument Systems, Bogart, GA, USA) using quartz cuvettes with different path lengths appropriate with the concentrations (Hellma, Müllheim, Germany). Samples were prepared in PBS

(pH 7.4). Five measurements at 25 °C using 1 nm intervals, 1 nm bandwidth at a wavelength range from 185–250 nm were performed. Next, averaged spectrum was subtracted from buffer as the background. To normalize the results for different concentration, the results are presented in terms of molar ellipticity.

2.4. Cell Line

B16OVA tumor cell line is a murine B16F10 melanoma cell line, engineered to stably express chicken ovalbumin (OVA). B16OVA cells were cultured in RPMI 1640 supplemented with 8% FBS and 400 µg/ml G418²³.

2.5. Mice

Inbred, 6–8-week-old female C57BL/6 mice were obtained from Charles River Laboratories (Maastricht, the Netherlands). Mice were maintained in the animal facility of the Utrecht University, in accordance with guidelines from the animal ethics committee of the Netherlands. Mice were immunized *s.c.* at the right flank with 200 µl of each formulation (see table 1). CD90.1 OT-1²⁴ and CD45.1 OT-2²⁵ mice are CD8⁺ T cell and CD4⁺ T cell TCR transgenic (Tg) mice expressing the TCR α-chain and β-chain recognizing OVA257–264 in H2-Kb and OVA323-339 in I-Ab, respectively and were bred at the Leiden University Medical Centre animal facility.

2.6. Immunization studies in mice

To evaluate the potency of SAPE vaccines in induction and expansion of OVA specific T cell response, *in vivo* antigen cross presentation and OVA-specific vaccination studies were performed in naïve mice. 6–8-week-old female C57BL/6 mice were immunized *s.c.* at the right flank with 200 µl of each formulation (see table 1).

2.6.1. *In vivo* antigen cross-presentation

To establish antigen presentation *in vivo* CD8⁺ and CD4⁺ T cells were isolated from spleen and lymph nodes from CD90.1 OT-I and CD45.1 OT-II mice, respectively. T cells were enriched using CD8⁺ and CD4⁺ enrichment kits according to manufacturers protocol (BD Bioscience) and 500.000 of each cell typewere injected intravenously into the tailvein of CD90.2, CD45.2 BL/6 mice (n=5/group). One day later, mice were vaccinated via subcutaneous injection with self-assembled or soluble peptide constructs containing OVA CTL epitopes (40 nmol/ injection), Th epitope (15 nmol) or mixed CTL/Th epitopes (Table 1). Peripheral blood mononuclear cells

(PBMCs) were collected at 3, 5, 7, and 10 days after T cell transfer to analyze the expansion of the transferred OVA-specific T cells caused by cross presentation of the OVA antigen (Figure 1). After lysis of red blood cells, T cells were stained with fluorescently labeled antibodies for CD8 α , CD4 and the OT-I congenic marker CD90.1 (Thy1.1), OT-II congenic marker CD45.1 and analyzed by flow cytometry. T cell expansion is expressed as the number of transferred (OT-I or OT-II) T cells, as percentage of total CD8 $^+$ or CD4 $^+$ T cells.

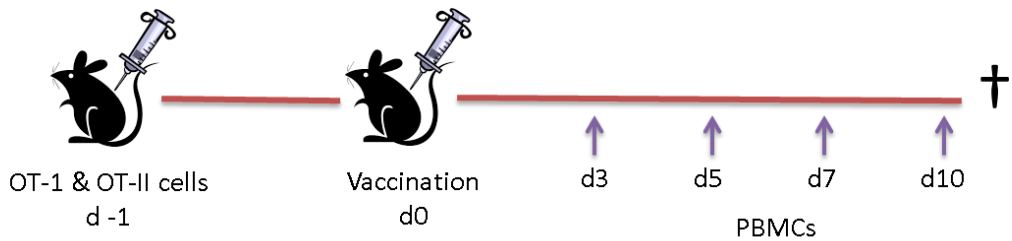


Figure 1: Schematic representation of the *in vivo* antigen cross presentation study

Table 1: List of peptides and self-assembling peptide vaccines used for immunization studies

<i>In vivo</i> experiment	Groups					
	1	2	3	4	5	6
<i>in vivo</i> antigen cross presentation	OSAP+OSAP-h with CpG	OSAP with CpG	OSAP-h with CpG	OSAP+OSAP-h	No treatment	-----
Vaccination in naïve mice induction of endogenous CD8 $^+$ T cells	OSAP+OSAP-h with CpG	No treatment	-----	-----	-----	----- -
Prophylactic tumor vaccination	OSAP+OSAP-h with CpG	OSAP with CpG	CTL peptide+ Th peptidewith CpG	CTL peptide with CpG	SA2 with CpG	No treatment
Therapeutic tumor vaccination	OSAP+OSAP-h with CpG	OSAP with CpG	CTL peptide+ Th peptidewith CpG	No treatment	-----	-----

- The dosage of OSAP and CTL peptide are 40 nmol/ injection (200 μ M), and the dosage of OSAP-h and Th peptide were 15 nmol/injection (75 μ M).

2.6.2. Endogenous CD8⁺ T cell activation

To evaluate the potency of OVA SAPE vaccines in induction of endogenous OVA specific CD8⁺ T cells, mice (n =5) were *s.c.* vaccinated in the right flank with the formulation of mixed particles of OSAP/OSAP-h with CpG at day 0 (table 1). After 14 days, the mice received the a booster injection (Figure 2). PBMCs were collected 10 days after prime vaccination and 5 and 7 days after the boost vaccination to quantify antigen-specific T cells stained by flow cytometry.

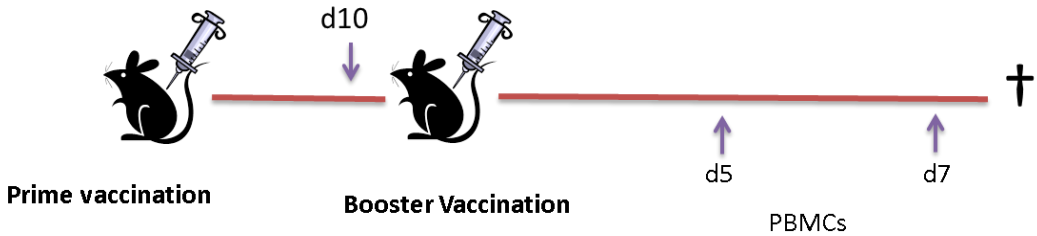


Figure 2: Schematic representation of the *in vivo* vaccination regime for endogenous CD8⁺ T cell activation.

2.7. Prophylactic tumor vaccination

For prophylactic vaccination, groups of mice (n = 10) received prime and two booster vaccinations with 2 weeks interval with the indicated vaccines in table 1. Seven days after the second booster vaccination, 200,000 B16/OVA melanoma tumor cells were *s.c.* injected into the right flank of mice. Tumor size was monitored manually every 2 days for 40 days using a caliper. Tumor volume was calculated by the formula: tumor volume [mm³] = (length [mm]) × (width [mm])² × 0.52²⁶. Mice were sacrificed once the tumor size reached 2000 mm³ in accordance with ethical guidelines (Figure 3). Before and after the first booster vaccination, blood samples were collected via submandibular bleeding (cheek puncture) in heparinized tubes for detection of OVA-specific CD8⁺ T cells by flow cytometry (Figure 3).

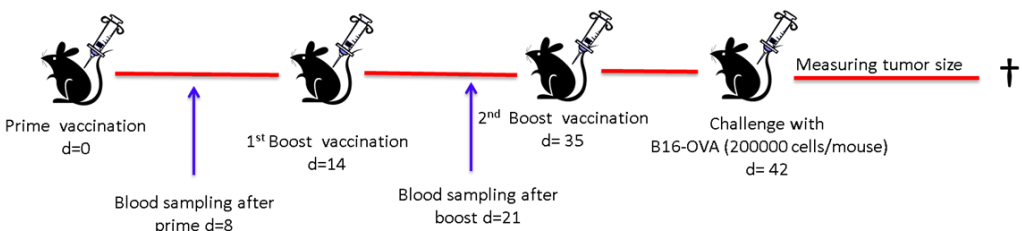


Figure 3: The prophylactic vaccination scheme in mice challenged with B16-OVA tumor cells.

2.8 Therapeutic vaccination in mice with established tumor

Groups of mice ($n = 10$) were challenged with 200,000 B16OVA melanoma tumor cells in the right flank. At day 7, when the tumors were palpable, mice were vaccinated with the vaccine formulation indicated in table 1. Ten days later, the mice received the same formulation as a booster injection (Figure 4). Tumor growth was monitored every 2-3 days for approximately 30 days and measured two-dimensionally with calipers to a maximum of 2000 mm³ after which the mice were sacrificed for ethical reasons. Before and after boost vaccination, blood samples were collected via submandibular bleeding (cheek puncture) in heparinized tubes for detecting of OVA-specific CD8⁺ T cells by flow cytometry.

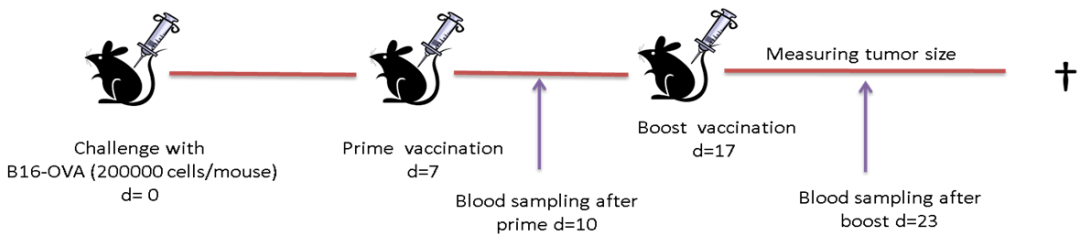


Figure 4: Schematic illustration of *in vivo* set up for therapeutic vaccination.

2.9 Detection of OVA specific CD8⁺ T cells in peripheral blood of tumor bearing mice by tetramer staining

Priming of endogenous OVA-specific CTL *in vivo* was analyzed by using SIINFEKL/Kb-tetramers labeled with allophycocyanin (APC)²⁷. To detect CD8⁺ cells bearing SIINFEKL antigen, red blood cells were removed using red blood cell lysis buffer (Roche, Almere, The Netherlands). The cells were washed with 2% BSA in PBS (FACS buffer) and stained for flow cytometry with FITC labeled α -CD8 α antibody (BD Biosciences, Breda, The Netherlands) and SIINFEKL/Kb-tetramers labeled with APC (Leiden University Medical Center (LUMC), Leiden, The Netherlands)²⁸. After staining, cells were washed 2 times with FACS buffer and resuspended in 200 μ l of FACS buffer before analysis by flow cytometry using a FACS Canto-II, with FACS Diva software (Becton Dickinson, San Jose, CA, USA)¹⁰.

2.10. Statistical analysis

Data were analyzed using GraphPad Prism 5.02 software. For tumor experiments Kaplan–Meier survival curves were applied, and the differences between survival curves were analyzed by log-rank test ($p < 0.05$ was considered statistically significant). Expansion of antigen-specific CD8⁺ T cells in the blood of tumor-bearing mice 5 or 7 days after the prime vaccination in mice treated with the vaccines was compared to untreated mice by student t-test.

3. Results

3.1. Peptide Design

OSAP (Ac-AAVVLLLVSGLEQLESIIINFEKL-COOH) and OSAP-h (Ac-AAVVLLLVSAESLKISQAVHAAHAEINEAGR-COOH) peptides were synthesized by standard solid phase synthesis, consisting of a self-assembly domain (underlined) fused to OVA₂₅₀₋₂₆₄ and OVA₃₁₆₋₃₃₉ epitopes, respectively. OVA₂₅₀₋₂₆₄ is an H2b restricted MHC class I peptide epitope, and OVA₃₁₆₋₃₃₉ (SSAESLKISQAVHAAHAEINEAGR) is an H-2b-restricted MHC class II peptide²⁹. Peptides were acetylated at the N-terminus to facilitate self-assembly by hydrophobic clustering and were purified by preparative C18 reversed-phase HPLC.

3.2. Characterization of self-assembling peptide epitopes

To characterize the peptide nanostructures, several complementary methods were applied (Table 2). Similar to the previously reported SA2 peptide, OSAP and OSAP-h peptides self-assemble into discrete nanostructures above a threshold concentration. The critical aggregation concentration (CAC) of OSAP and OSAP-h are in the same range as that of SA2 (Figure 5). Interestingly, the CAC of OSAP/OSAP-h mixture was in the same range of the other self-assembling peptides in this study. This is suggesting a cooperative assembly of these two peptides into nanoparticles.

Dynamic light scattering (DLS) measurements showed that the formed particles of OSAP had a smaller hydrodynamic diameter in comparison with OSAP-h particles. AFM revealed that OSAP particles had a spherical morphology with similar particle size as measured by DLS (Figure 6). According to the literature, the axial distance between adjacent residues is 3.6 Angstroms³⁰. Therefore, the considered length for OSAP peptide with 23 residues is 7.92 and the full length for two peptides that aligned tail to tail is 15.84 nm in extended state. Regarding this theoretical value (15.84 nm) and the obtained results from DLS and AFM, micellar structure can be assigned for the OSAP particles. However, OSAP-h particles showed a transition situation between spherical

micelles (~20 nm) and fibers which may explain the bigger particle size measured by DLS for these OSAP-h peptides. Interestingly, peptide particles prepared with 8:3 molar mixtures of OSAP(200 μ M) and OSAP-h: (75 μ M) only showed small, spherical structures. These findings strongly suggest that OSAP and OSAP-h mixtures resulted in the formation of mixed micelles rather than separate self-assembly of both peptides into distinct structures. As expected, a negative zeta potential was measured for both peptide particles at pH7.4 as the peptides have a net negative charge at this pH. Moreover, SA2 nanovesicles²¹ showed more negative zeta potential because of the localized 3 negative charges in 2 residues of its hydrophilic head (two glutamates). Circular dichroism (CD) of OSAP, OSAP-h, and their mixture showed spectra with its lowest point at 210-220 nm similar to SA2 which is characteristic for a β -sheet conformation^{14,21}.

Table 3: Characterization of self-assembling peptides with and without OVA CTL and helper epitopes.

Peptide(s)	M.W	CAC (μ M)	Size (nm)/ PDI	Zeta potential	Secondary structure
SA2 (Ac-AAVVLLWEE-COOH)	1185	17 \pm 2	66 \pm 2/0.12 \pm 0.02	-45 \pm 1	β -sheet
OSAP (Ac-AAVVLLWSGLEQL ESIINFEKL-COOH)	2628	15 \pm 1	24 \pm 3/0.29 \pm 0.16	-17 \pm 1	β -sheet
OSAP-H (Ac-AAVVLLWSAESLK ISQAVHAAHAEINE AGR-COOH)	3385	13 \pm 1	122 \pm 42/0.42 \pm 0.05	-12 \pm 1	β -sheet
OSAP/OSAP-h (ratio 8:3)	-	9 \pm 1 *	26 \pm 3/0.46 \pm 0.03	-14 \pm 1	β -sheet

* The presented CAC is based on the total OSAP and OSAP-h concentration regarding the 8:3 molar ratio.

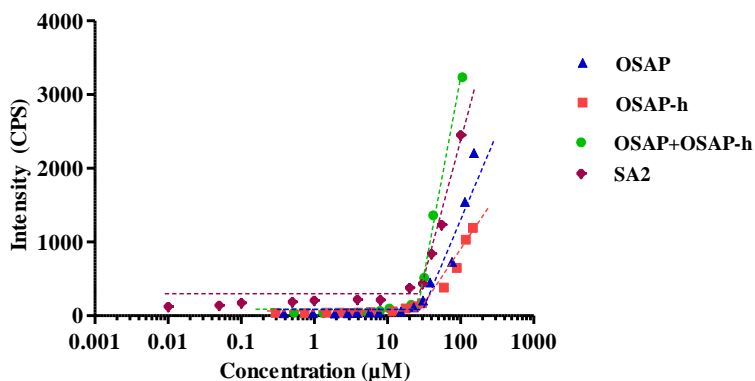


Figure 5: CAC determination of the self-assembling peptides. The fluorescence intensity of Nile red ($1.25 \mu\text{M}$) at 635 nm as a function of peptide concentration is plotted for the various self-assembling peptides.

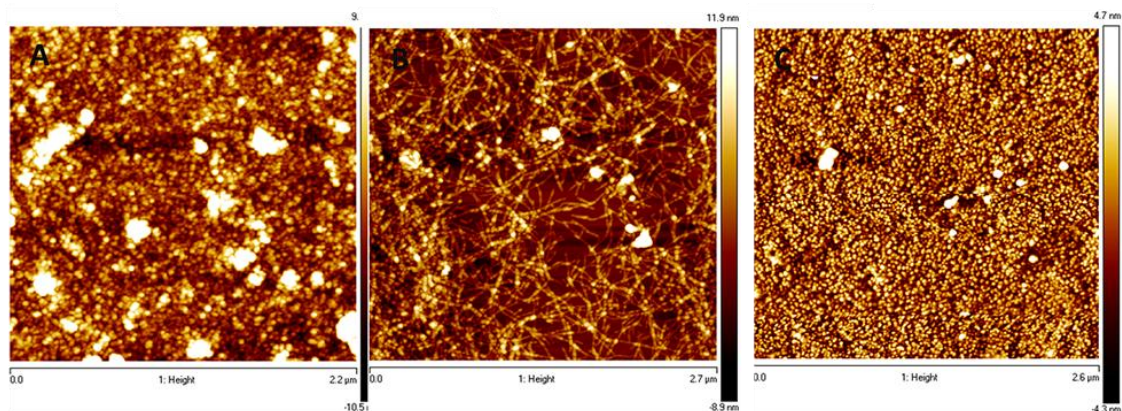


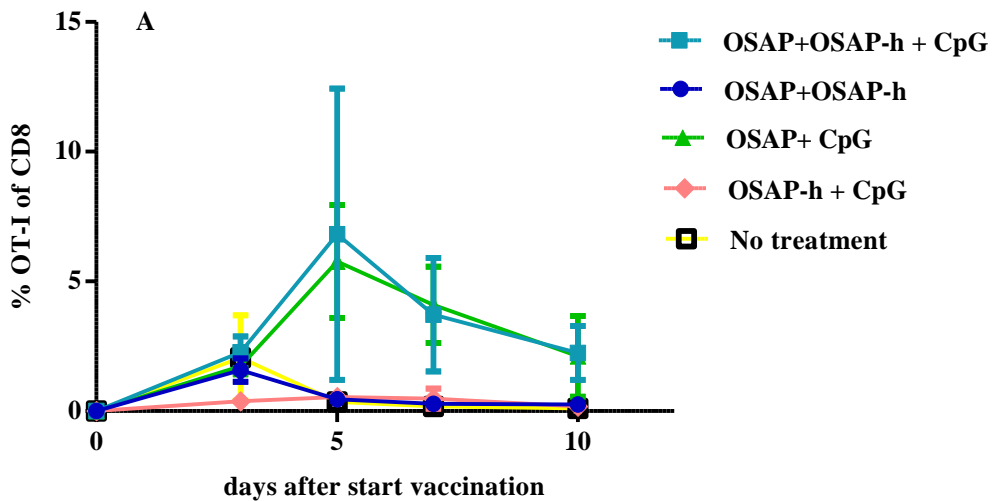
Figure 6: Atomic force microscopy of peptide assemblies immobilized on poly-L-lysine coated mica at the same concentration that applied for *in vivo* experiments: A) OSAP ($200 \mu\text{M}$), B) OSAP-h ($75 \mu\text{M}$) and C) mixed OSAP/OSAP-h ($200 \mu\text{M}:75 \mu\text{M}$).

3.3. *In vivo* antigen cross-presentation

To assess the capacity of the self-assembled peptide-epitopes (SAPes) to be internalized and processed by DCs and presented to CD8^+ T cells and CD4^+ T cells, OVA-specific CD8^+ and CD4^+ T cells (OT-I and OT-II, respectively) were injected into C57BL/6 mice one day before administration of SAPes. In this way, the precursor frequency of OVA-specific T cells was

artificially elevated to high levels, thereby facilitating the read out of *in vivo* antigen processing and presentation and enabling the detection of subtle differences between vaccine formulations in terms of (cross)-presentation of OVA antigens. The degree of OT-I and OT-II T cell expansion as a consequence of *in vivo* (cross)-presentation of the OVA antigens was determined by analyzing PBMCs by flow cytometry at various time points after vaccination.

High numbers of OT-I cells were observed in the blood samples peaking at day 5 after vaccination with OSAP micelles and mixed micelles of OSAP/OSAP-h adjuvanted with CpG, which proved far superior to the administration of the same formulations without CpG. As OSAP-h does not contain the SIINFEKL epitope, vaccination with the OSAP-h formulation with CpG did not result in OT-I cell expansion, and the level of OT-I cells in PBMCs was comparable with that measured in the control PBS group. Similarly, mixed micelles of OSAP/OSAP-h peptides and micelles of OSAP-h adjuvanted with CpG raised the number of OT-II cells in the blood of mice peaking at day 5 after vaccination. These results clearly show that peptide micelle formulations adjuvanted with CpG are efficiently processed *in vivo* leading to T cell activation (Figure 7). The presence of CpG adjuvant was necessary for eliciting an efficient immune response.



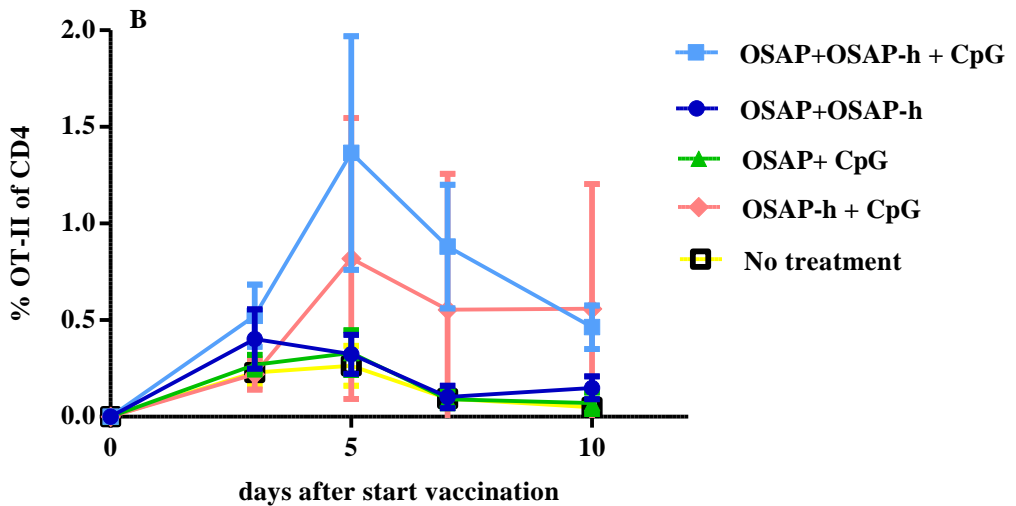


Figure 7: *In vivo* (cross)-presentation of OVA antigen to OVA-specific CD8⁺ (OT-I; panel A) and CD4⁺ (OT-II; panel B) T cells. Mice were vaccinated with 200 μ l of indicated peptide formulation. On day 3, 5, 7, 10 blood was collected, and PMBCs were isolated. The percentage of OT-I cells (panel A) and OT-II cells (panel B) relative to the total number of CD8⁺ or CD4⁺ T cells, respectively were determined by tetramer staining and subsequent flow cytometry.

3.4. Endogenous OVA specific CD8⁺ T cell activation

To assess the capability of these vaccines to prime endogenous OVA-specific CD8⁺ T cells, OSAP/OSAP-h mixed micelles with CpG were *s.c.* injection into naïve BL/6 mice on day one and ten as the prime and booster vaccination, respectively. The induction of OVA specific CD8⁺ T cells was analyzed at different time points post immunizations via tetramer staining. As shown in Figure 8, the mixed micelles were able to induce a detectable OVA specific CD8⁺ T cell response compared to background (No treatment mice) and the response further increased from day 5 to 7 after boost immunization. These results underscore the *in vivo* cross-presentation by the designed self-assembled peptide vaccines and also show the efficacy of these vaccines to induce high levels of OVA-specific endogenous CD8⁺ T cells needed for therapeutic vaccination.

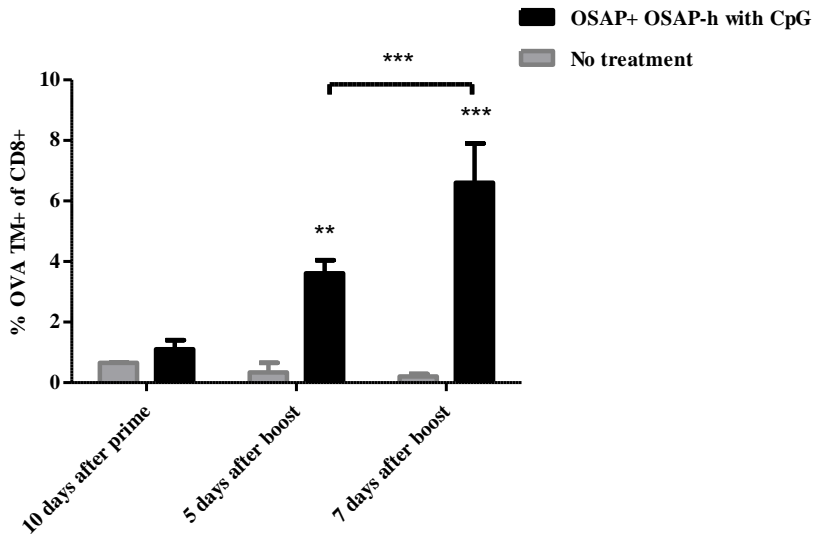


Figure 8: Relative amount of endogenous TM-OVA+ CD8+ T cells by FACS. Peripheral blood was stained and analyzed for the frequency of OVA-specific CD8+ T cells. Ten days after prime injection, five and seven days after boost vaccination. Statistical analysis (one way ANOVA) showed significant difference in TM-OVA+ CD8+ T cells in treatment group 5 days and 7 days after booster vaccination compared to 10 days after prime. Statistical analysis (unpaired T-test) were performed to compare treatment group versus no treatment group in each time point. The relative amount of endogenous TM-OVA+ CD8+ T cells showed significant increase after booster injection in treatment group versus no treatment group in each time points, however no significance difference in 10 days after prime (unpaired T-test). ** = $p < 0.01$, *** = $p < 0.001$. $N = 5$ mice per group.

3.5. Tumor vaccination

3.5.1. Prophylactic tumor vaccination

The prophylactic vaccine efficacy of SAPEs was investigated in a murine B16OVA tumor model. Both OSAP and OSAP/OSAP-h groups significantly delayed tumor growth with similar efficacy in prolonging mice survival compared to no treatment mice as the control group (Figure 9). In addition, these results show that this immunity was epitope dependent since SA2 formulation with adjuvant did not increase the animal survival compared to the control group. There was no significant difference between the survival rates of mice vaccinated with OSAP micelles as

compared to the OSAP/OSAP-h mixed micelle formulation. However, it should be noted that B16OVA cells aggressively develop tumors which can overshadow the differences between these two vaccine groups³¹.

Unexpectedly, the monomeric CTL peptide epitope and mixture of CTL peptide and Th peptide showed similar survival rates compared to the SAPE vaccines, suggesting that the formation of nanoparticles by self-assembly of the SAPE formulation did not result in a stronger anti-tumor immune response¹⁷. To explain this controversial result, these presumed soluble peptides were analyzed by DLS and AFM. Dynamic light scattering analysis revealed that the CTL peptide was able to form nanostructures with a diameter of 192 ± 2 nm (PDI: 0.10 ± 0.04), while no particles were detected for Th peptide. AFM analysis revealed the same (Figure 10). Moreover, CTL peptides mixed with Th peptides still formed nanoparticles (diameter: 200 ± 1 nm; PDI: 0.146 ± 0.025).

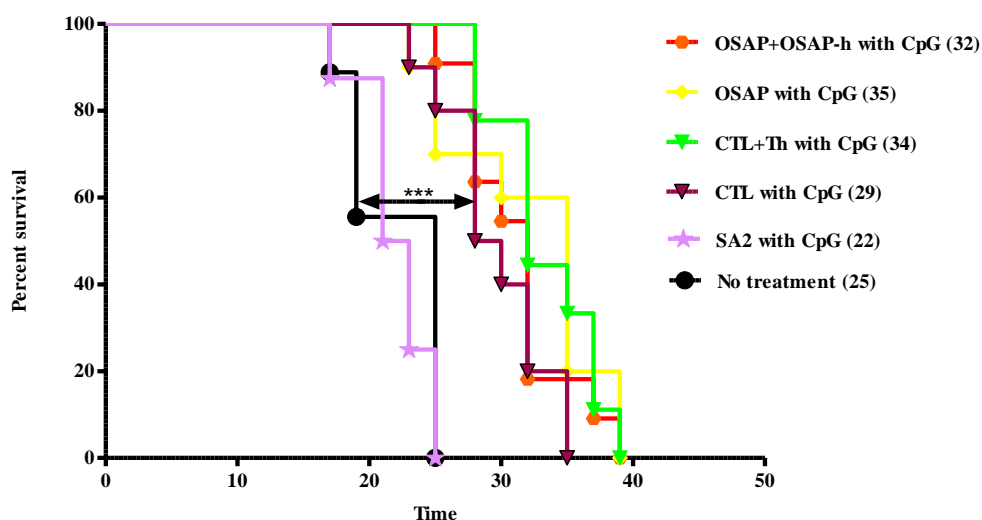


Figure 9: Efficacy of anti-tumor vaccines in prophylactic tumor model. The differences between the groups were calculated using log-rank (Mantel–Cox) test. The survival of mice vaccinated with all vaccines was significantly longer compared to the no treatment and SA2 with CpG groups ($p < 0.001$). However, there was no significant difference in survival between mice received vaccines containing either SAPEs, CTL or Th peptides. Numbers in the legends represent median survival in days.

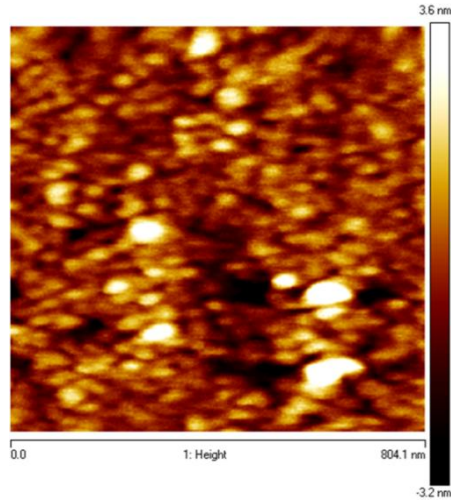


Figure 10: Atomic force microscopy of peptide assemblies of CTL peptide immobilized on mica at the same concentration as applied for in vivo experiments.

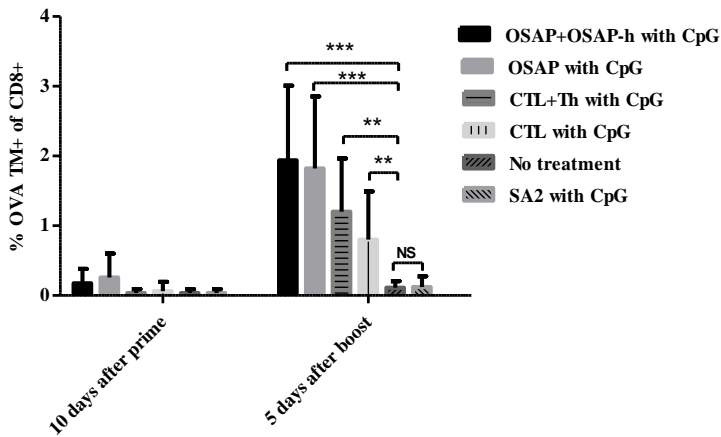


Figure 11: Expansion of OVA-specific $CD8^+$ T cells after prime and first boost vaccination in a prophylactic tumor model. The relative amount of OVA-specific $CD8^+$ T cells was significantly increased ($p < 0.05$) in mice that received the vaccine formulations containing antigenic peptides at 5 days after booster vaccination compared to 10 days after prime vaccination (paired T-test). Statistical analyses (unpaired T-test) in 5 days after booster injection indicated that all treated groups showed a significant difference ($p < 0.05$) compared to the no treatment group, except SA2 with CpG. NS = not significant, ** = $p < 0.01$, *** = $p < 0.001$. $N = 10$ mice per group.

The numbers of specific CD8⁺ T cells before and after the first boost injection were analyzed by tetramer staining, in order to examine the effects of different forms of vaccine peptides in the induction of OVA-specific CD8⁺ T cells. The percentage of OVA specific CD8⁺ T cells in peripheral blood sample is shown in Figure 11. Significant increase in the number of these specific cell population was observed after first boost injection for all vaccine forms. Overall, the FACS results are in agreement with the animal survival data.

3.5.2. Therapeutic tumor vaccination

Therapeutic efficacy of OSAP micelles and OSAP/OSAP-h mixed micelles was tested in B16OVA tumor bearing mice. Vaccinated animals displayed statistically higher survival percentage compared to non-treated ($p < 0.05$) (Figure 12). FACS analysis showed an increase in OVA-specific CD8⁺ T cells after booster vaccination (Figure 13). This increase of primed CD8⁺ T cells showed the importance of boost injection in immunization^{32,33}.

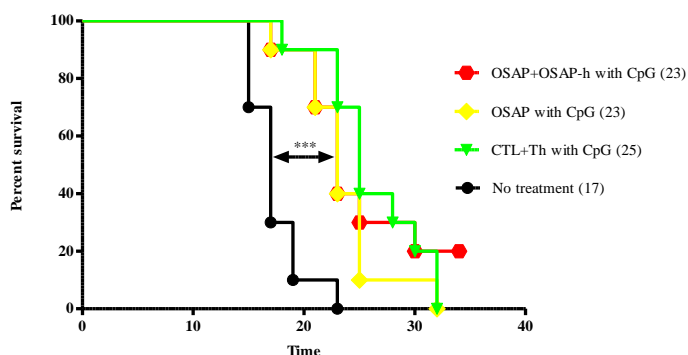


Figure 12: Efficacy of anti-tumor vaccines in a therapeutic tumor model. The differences between the groups were calculated using log-rank (Mantel–Cox) test. The survival of mice vaccinated with all vaccines was significantly longer compared to the no treatment group ($p < 0.001$). However, there was no significant difference in survival between mice received vaccines containing either SAPEs, CTL+Th peptides. Numbers in the legends represent median survival in days.

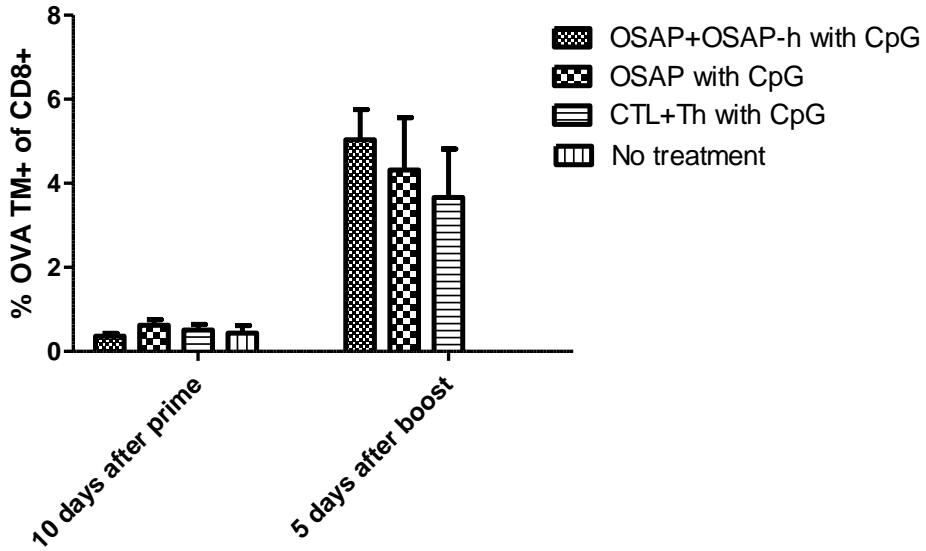


Figure 13: Expansion of OVA-specific $CD8^+$ T cells in blood of tumor-bearing mice, 10 days after prime and 5 days after booster vaccination. The differences within the groups were analyzed using the paired *t* test. The relative amount of OVA-specific $CD8^+$ T cells was significantly increased ($p < 0.05$) in all mice that received the vaccine formulations at 5 days after booster vaccination compared to 10 days after prime vaccination. There was no significant differences between groups in 5 days after booster vaccination. (one way ANOVA). $N = 10$ mice per group. All mice in the no-treatment group reached the humane endpoint before T cells could be analyzed 5 days after boost.

Again, the particulate form of CTL peptides can be the reason for the same efficacy as the self-assembled peptide formulations.

4. Discussion

Peptide vaccines offer a promising approach to raising specific humoral or cellular immune responses against cancer cells³⁴. Various studies propose to deliver the peptide vaccines in a particulate form which favors innate immune recognition and activation^{17,35}. Only a few studies explored peptide self-assembly as a means to present peptide epitopes in a particulate form to the immune system. For example, Collier and coworkers produced a nanofiber vaccine by incorporation a fibrilizing self-assembling peptide into the structure of a peptide antigen¹³. They showed that the self-assembling peptide epitope triggered the formation of high-levels of IgG1, IgG2a and IgG3 antibodies against the attached antigen epitope¹³. Most other studies used long

stretches of amino acids to drive peptide-self-assembly, which is prohibitive for solid phase peptide synthesis^{18,36–38}. In addition, it also increases the risk of immunogenicity against the carrier part³⁹.

In this study, we demonstrated that by attaching an 8 amino acid peptide sequence to antigenic peptide epitopes with different length and residue composition, discrete nanostructures could be generated in a reproducible fashion. This strategy can overcome some shortages of other particulate systems. Besides the ease of production and well-defined formulation, several studies indicated the correlation between epitope density and immune responses^{40–42}. Since, in the designed SAPEs, the self-assembly domain has a lower weight ratio compared to the antigen domain, the generated particles comprise a high density of antigenic epitopes displayed on the surface of micelles. For example, in OSAP particles, 65 % of particle mass consists of antigenic epitopes while in several studied polymeric nanoparticles the reported peptide loading was on average less than 5%^{43,44}. Moreover, as demonstrated in the present study, different peptide epitopes can be mixed at will to form peptide vesicles with multiple epitopes. These features enable us to target the immune system with controlled dosage of various antigen epitopes.

It is generally accepted that for efficient antigen presentation, antigens should reach lymph nodes where there are high concentrations of DCs and T cells⁴⁵. Apart from traveling DCs with captured antigens, soluble antigens can also drain spontaneously into lymph capillaries and travel to lymph nodes¹⁷. However, there is a size limitation for nanoparticles. In general, nanoparticles smaller than 100 nm can travel through interstitial matrix and reach lymph nodes via lymphatic vessels⁴⁶. Here, we show that the designed vaccines are able to form micelles with average size less than 30 nm in diameter which is more favorable for spontaneous draining into the lymph nodes, resulting in an efficient adaptive immunity. Further research is needed to proof that such peptide vesicles can indeed reach peripheral lymph nodes from the injection site.

A strong expansion of OT-I cells indicated the capacity of these designed vaccines for cross presentation which is necessary for effective induction of cellular immunity⁴⁷. The results also demonstrate that CpG adjuvant was needed for the SAPE vaccine to work and mount efficient cellular immune responses, which is in line with previous reported work⁴⁸. Therefore, future work should focus on integrating strong adjuvants, such as toll-like receptor ligands with the SAPEs to improve the efficiency of such systems. Several peptide-based ligands exist, such as (RS01: Gln-Glu-Ile-Asn-Ser-Ser-Tyr and RS09: Ala-Pro-Pro-His-Ala-Leu-Ser) that might be used for this purpose⁴⁹.

The *in vivo* experiments in mice show that the designed self-assembling peptide-epitopes delayed tumor growth and increased the survival proportion of subjected animals in prophylactic and therapeutic tumor models. Further analysis revealed that this was an antigen-specific response and not merely caused by a direct toxic or adjuvant effect of the particulate delivery systems. Comparison of our results with other particulate vaccine delivery studies is not feasible due to differences in experimental setup with many variables such as form of antigen (whole protein, synthetic long peptide or minimal epitope), antigen dosage, type and dosage of adjuvant, adjuvant in soluble form or co-encapsulated, charge and size of particles. However, even in successful tumor vaccinations complete tumor regression is rare in this tumor model and mostly caused significant delay in tumor growth and survival proportion⁵⁰. In the present study also, no evidence of tumor regression was observed. It can be related to the aggressive nature of B16 OVA tumor and also the inhibitory mechanisms that can suppress immune responses such as downregulation or loss of MHC class I, perturbation of antigen processing or expression of immune checkpoint receptors^{51,52}. In addition, it is known that tumors can restrict the immune response by induction and/or production of some factors such as TGF-beta⁵³, IL-10⁵⁴⁻⁵⁶, VEGF⁵⁷ and also Tregs activation⁵⁸.

Unexpectedly, mice vaccinated with peptide epitopes without self-assembling domain, led to efficient immunization and an increase in survival similar to those mice vaccinated with SAPEs. This effect was linked to the ability of the CTL peptides to form nano-sized structures. Due to the particle formation, this CTL peptide was not a proper control to demonstrate the added benefit of peptide self-assembly on antigen processing and immune activation. These findings show the importance of peptide aggregation analysis in proper vaccine design as some of apparently soluble peptides can form nonvisible and nano-sized structures. Nevertheless, this study shows that peptide nanoparticles when adjuvanted with CpG can induce some degree of protection against an aggressively growing tumor by inducing tumor-specific T cell responses and is an attractive and simple alternative for other particulate vaccine delivery systems to improve tumor-specific T cell response for cancer treatment.

5. References

- (1) Arens, R., van Hall, T., van der Burg, S. H., Ossendorp, F., and Melief, C. J. M. (2013) Prospects of combinatorial synthetic peptide vaccine-based immunotherapy against cancer. *Semin. Immunol.* 25, 182–190.
- (2) Reuschenbach, M., von Knebel Doeberitz, M., and Wentzensen, N. (2009) A systematic review of humoral immune responses against tumor antigens. *Cancer Immunol. Immunother.* 58, 1535–1544.
- (3) Khodadoust, M. S., and Alizadeh, A. A. (2014) Tumor antigen discovery through translation of the cancer genome. *Immunol. Res.* 58, 292–299.
- (4) Protti, M. P., Monte, L. D., and Lullo, G. D. (2014) Tumor antigen-specific CD4+ T cells in cancer immunity: From antigen identification to tumor prognosis and development of therapeutic strategies. *Tissue Antigens* 83, 237–246.
- (5) Itoh, K., Yamada, A., Mine, T., and Noguchi, M. (2009) Recent advances in cancer vaccines: An overview. *Jpn. J. Clin. Oncol.* 39, 73–80.
- (6) Cuppens, K., and Vansteenkiste, J. (2014) Vaccination therapy for non-small-cell lung cancer. *Curr. Opin. Oncol.* 26, 165–170.
- (7) Melero, I., Gaudernack, G., Gerritsen, W., Huber, C., Parmiani, G., Scholl, S., Thatcher, N., Wagstaff, J., Zielinski, C., Faulkner, I., and Mellstedt, H. (2014) Therapeutic vaccines for cancer: an overview of clinical trials. *Nat. Rev. Clin. Oncol.* 11, 509–524.
- (8) Radford, K. J., Tullett, K. M., and Lahoud, M. H. (2014) Dendritic cells and cancer immunotherapy. *Curr. Opin. Immunol.* 27, 26–32.
- (9) Anguille, S., Smits, E. L., Lion, E., van Tendeloo, V. F., and Berneman, Z. N. (2014) Clinical use of dendritic cells for cancer therapy. *Lancet Oncol.* 15, e257–267.
- (10) Welters, M. J. P., Bijker, M. S., van den Eeden, S. J. F., Franken, K. L. M. C., Melief, C. J. M., Offringa, R., and van der Burg, S. H. (2007) Multiple CD4 and CD8 T-cell activation parameters predict vaccine efficacy in vivo mediated by individual DC-activating agonists. *Vaccine* 25, 1379–1389.
- (11) Bijker, M. S., Van Den Eeden, S. J. F., Franken, K. L., Melief, C. J. M., Offringa, R., and Van Der Burg, S. H. (2007) CD8+ CTL priming by exact peptide epitopes in incomplete Freund's adjuvant induces a vanishing CTL response, whereas long peptides induce sustained CTL reactivity. *J. Immunol.* 179, 5033–5040.
- (12) Bijker, M. S., Melief, C. J. M., Offringa, R., and van der Burg, S. H. (2007) Design and development of synthetic peptide vaccines: past, present and future. *Expert Rev. Vaccines* 6, 591–603.

- (13) Rudra, J. S., Tian, Y. F., Jung, J. P., and Collier, J. H. (2010) A self-assembling peptide acting as an immune adjuvant. *Proc. Natl. Acad. Sci. U. S. A.* 107, 622–627.
- (14) Rudra, J. S., Sun, T., Bird, K. C., Daniels, M. D., Gasiorowski, J. Z., Chong, A. S., and Collier, J. H. (2012) Modulating adaptive immune responses to peptide self-assemblies. *ACS Nano* 6, 1557–1564.
- (15) Chen, J., Pompano, R. R., Santiago, F. W., Maillat, L., Sciammas, R., Sun, T., Han, H., Topham, D. J., Chong, A. S., and Collier, J. H. (2013) The use of self-adjuvanting nanofiber vaccines to elicit high-affinity B cell responses to peptide antigens without inflammation. *Biomaterials* 34, 8776–8785.
- (16) Black, M., Trent, A., Tirrell, M., and Olive, C. (2010) NIH Public Access 9, 157–173.
- (17) De Temmerman, M.-L., Rejman, J., Demeester, J., Irvine, D. J., Gander, B., and De Smedt, S. C. (2011) Particulate vaccines: on the quest for optimal delivery and immune response. *Drug Discov. Today* 16, 569–582.
- (18) Boato, F., Thomas, R. M., Ghasparian, A., Freund-Renard, A., Moehle, K., and Robinson, J. A. (2007) Synthetic virus-like particles from self-assembling coiled-coil lipopeptides and their use in antigen display to the immune system. *Angew. Chem. Int. Ed. Engl.* 46, 9015–9018.
- (19) Sharma, R., Ghasparian, A., Robinson, J. A., and McCullough, K. C. (2012) Synthetic virus-like particles target dendritic cell lipid rafts for rapid endocytosis primarily but not exclusively by macropinocytosis. *PLoS One* 7, e43248.
- (20) Van Hell, A. J., Costa, C., Flesch, F. M., Sutter, M., Jiskoot, W., Crommelin, D. J. A., Hennink, W. E., and Mastrobattista, E. (2007) Self-assembly of recombinant amphiphilic oligopeptides into vesicles. *Biomacromolecules* 8, 2753–2761.
- (21) Rad-Malekshahi, M., Visscher, K. M., Rodrigues, J. P. G. L. M., De Vries, R., Hennink, W. E., Baldus, M., Bonvin, A. M. J. J., Mastrobattista, E., and Weingarth, M. (2015) The supramolecular organization of a peptide-based nanocarrier at high molecular detail. *J. Am. Chem. Soc.* Accepted for publication, chapter 4 of this thesis.
- (22) Zhang, A., Zhang, Z., Shi, F., Ding, J., Xiao, C., Zhuang, X., He, C., Chen, L., and Chen, X. (2013) Disulfide crosslinked PEGylated starch micelles as efficient intracellular drug delivery platforms. *Soft Matter* 9, 2224–2233.
- (23) Redondo, P., Del Olmo, J., López-Díaz De Cerio, A., Inoges, S., Marquina, M., Melero, I., and Bendandi, M. (2007) Imiquimod enhances the systemic immunity attained by local cryosurgery destruction of melanoma lesions. *J. Invest. Dermatol.* 127, 1673–1680.
- (24) Hogquist, K. A., Jameson, S. C., Heath, W. R., Howard, J. L., Bevan, M. J., and Carbone, F. R. (1994) T cell receptor antagonist peptides induce positive selection. *Cell* 76, 17–27.

- (25) Barnden, M. J., Allison, J., Heath, W. R., and Carbone, F. R. (1998) Defective TCR expression in transgenic mice constructed using cDNA-based alpha- and beta-chain genes under the control of heterologous regulatory elements. *Immunol. Cell Biol.* 76, 34–40.
- (26) Li, M., Zhang, Y., Liu, Z., Bharadwaj, U., Wang, H., Wang, X., Zhang, S., Liuzzi, J. P., Chang, S.-M., Cousins, R. J., Fisher, W. E., Brunnicardi, F. C., Logsdon, C. D., Chen, C., and Yao, Q. (2007) Aberrant expression of zinc transporter ZIP4 (SLC39A4) significantly contributes to human pancreatic cancer pathogenesis and progression. *Proc. Natl. Acad. Sci. U. S. A.* 104, 18636–18641.
- (27) Schuurhuis, D. H., Laban, S., Toes, R. E., Ricciardi-Castagnoli, P., Kleijmeer, M. J., van der Voort, E. I., Rea, D., Offringa, R., Geuze, H. J., Melief, C. J., and Ossendorp, F. (2000) Immature dendritic cells acquire CD8(+) cytotoxic T lymphocyte priming capacity upon activation by T helper cell-independent or -dependent stimuli. *J. Exp. Med.* 192, 145–150.
- (28) Den Boer, A. T., Van Mierlo, G. J. D., Franssen, M. F., Melief, C. J. M., Offringa, R., and Toes, R. E. M. (2005) CD4+ T cells are able to promote tumor growth through inhibition of tumor-specific CD8+ T-cell responses in tumor-bearing hosts. *Cancer Res.* 65, 6984–6989.
- (29) Yang, M., and Mine, Y. (2009) Novel T-cell epitopes of ovalbumin in BALB/c mouse: Potential for peptide-immunotherapy. *Biochem. Biophys. Res. Commun.* 378, 203–208.
- (30) PAULING, L., and COREY, R. B. (1951) The pleated sheet, a new layer configuration of polypeptide chains. *Proc. Natl. Acad. Sci. U. S. A.* 37, 251–256.
- (31) Ronchetti, A., Iezzi, G., Crosti, M. C., Garancini, M. P., Protti, M. P., and Bellone, M. (1999) Role of antigen-presenting cells in cross-priming of cytotoxic T lymphocytes by apoptotic cells. *J. Leukoc. Biol.* 66, 247–251.
- (32) Eskander, R. N., and Tewari, K. S. (2015) Immunotherapy: An Evolving Paradigm in the Treatment of Advanced Cervical Cancer. *Clin. Ther.* 37, 20–38.
- (33) Rosalia, R. A., Cruz, L. J., van Duikeren, S., Tromp, A. T., Silva, A. L., Jiskoot, W., de Gruijl, T., Löwik, C., Oostendorp, J., van der Burg, S. H., and Ossendorp, F. (2015) CD40-targeted dendritic cell delivery of PLGA-nanoparticle vaccines induce potent anti-tumor responses. *Biomaterials* 40, 88–97.
- (34) Slingluff, C. L. (2011) The present and future of peptide vaccines for cancer. *Cancer J.* 17, 343–350.
- (35) Storni, T., Kündig, T. M., Senti, G., and Johansen, P. (2005) Immunity in response to particulate antigen-delivery systems. *Adv. Drug Deliv. Rev.* 57, 333–355.
- (36) Miller, K. D., Roque, R., and Clegg, C. H. (2014) Novel anti-nicotine vaccine using a trimeric coiled-coil hapten carrier. *PLoS One* 9, e114366.

- (37) Kaba, S. A., Brando, C., Guo, Q., Mittelholzer, C., Raman, S., Tropel, D., Aebi, U., Burkhard, P., and Lanar, D. E. (2009) A nonadjuvanted polypeptide nanoparticle vaccine confers long-lasting protection against rodent malaria. *J. Immunol.* *183*, 7268–7277.
- (38) Al-Warhi, T. I., Al-Hazimi, H. M. A., and El-Faham, A. (2012) Recent development in peptide coupling reagents. *J. Saudi Chem. Soc.* *16*, 97–116.
- (39) Schlossman, S. F., Yaron, A., Ben-Efraim, S., and Sober, H. A. (1965) Immunogenicity of a series of α ,N-DNP-L-lysines. *Biochemistry* *4*, 1638–1645.
- (40) Liu, W., and Chen, Y.-H. (2005) High epitope density in a single protein molecule significantly enhances antigenicity as well as immunogenicity: A novel strategy for modern vaccine development and a preliminary investigation about B cell discrimination of monomeric proteins. *Eur. J. Immunol.* *35*, 505–514.
- (41) Kersten, G. F. A., and Crommelin, D. J. A. (1995) Liposomes and ISCOMS as vaccine formulations. *BBA - Rev. Biomembr.* *1241*, 117–138.
- (42) Reche, P. A., Fernandez-Caldas, E., Flower, D. R., Fridkis-Hareli, M., and Hoshino, Y. (2014) Peptide-based immunotherapeutics and vaccines. *J. Immunol. Res.* *2014*, 256784.
- (43) Rosalia, R. A., Cruz, L. J., van Duikeren, S., Tromp, A. T., Silva, A. L., Jiskoot, W., de Gruijl, T., Löwik, C., Oostendorp, J., van der Burg, S. H., and Ossendorp, F. (2015) CD40-targeted dendritic cell delivery of PLGA-nanoparticle vaccines induce potent anti-tumor responses. *Biomaterials* *40*, 88–97.
- (44) Rahimian, S., Kleinovink, J. W., Fransen, M. F., Mezzanotte, L., Gold, H., Wisse, P., Overkleeft, H., Amidi, M., Jiskoot, W., Löwik, C. W., Ossendorp, F., and Hennink, W. E. (2014) Near-infrared labeled, ovalbumin loaded polymeric nanoparticles based on a hydrophilic polyester as model vaccine: In vivo tracking and evaluation of antigen-specific CD8(+) T cell immune response. *Biomaterials* *37*, 469–477.
- (45) Zinkernagel, R. M., Ehl, S., Aichele, P., Oehen, S., Kündig, T., and Hengartner, H. (1997) Antigen localisation regulates immune responses in a dose- and time-dependent fashion: A geographical view of immune reactivity. *Immunol. Rev.* *156*, 199–209.
- (46) Reddy, S. T., Rehor, A., Schmoekel, H. G., Hubbell, J. A., and Swartz, M. A. (2006) In vivo targeting of dendritic cells in lymph nodes with poly(propylene sulfide) nanoparticles. *J. Control. Release* *112*, 26–34.
- (47) Ackerman, A. L., and Cresswell, P. (2004) Cellular mechanisms governing cross-presentation of exogenous antigens. *Nat. Immunol.* *5*, 678–684.
- (48) Ilyinskii, P. O., Roy, C. J., O’Neil, C. P., Browning, E. A., Pittet, L. A., Altreuter, D. H., Alexis, F., Tonti, E., Shi, J., Basto, P. A., Iannaccone, M., Radovic-Moreno, A. F., Langer, R. S.,

- Farokhzad, O. C., von Andrian, U. H., Johnston, L. P. M., and Kishimoto, T. K. (2014) Adjuvant-carrying synthetic vaccine particles augment the immune response to encapsulated antigen and exhibit strong local immune activation without inducing systemic cytokine release. *Vaccine* 32, 2882–2895.
- (49) Shanmugam, A., Rajoria, S., George, A. L., Mittelman, A., Suriano, R., and Tiwari, R. K. (2012) Synthetic toll like receptor-4 (TLR-4) agonist peptides as a novel class of adjuvants. *PLoS One* 7, e30839.
- (50) De Titta, A., Ballester, M., Julier, Z., Nembrini, C., Jeanbart, L., Van Der Vlies, A. J., Swartz, M. A., and Hubbell, J. A. (2013) Nanoparticle conjugation of CpG enhances adjuvancy for cellular immunity and memory recall at low dose. *Proc. Natl. Acad. Sci. U. S. A.* 110, 19902–19907.
- (51) Melero, I., Gaudernack, G., Gerritsen, W., Huber, C., Parmiani, G., Scholl, S., Thatcher, N., Wagstaff, J., Zielinski, C., Faulkner, I., and Mellstedt, H. (2014) Therapeutic vaccines for cancer: An overview of clinical trials. *Nat. Rev. Clin. Oncol.* 11, 509–524.
- (52) Tabi, Z., and Man, S. (2006) Challenges for cancer vaccine development. *Adv. Drug Deliv. Rev.* 58, 902–915.
- (53) Gajewski, T. F., Meng, Y., and Harlin, H. (2006) Immune suppression in the tumor microenvironment. *J. Immunother.* 29, 233–240.
- (54) Yang, A. S., and Lattime, E. C. (2003) Tumor-induced interleukin 10 suppresses the ability of splenic Dendritic Cells to stimulate CD4 and CD8 T-cell responses. *Cancer Res.* 63, 2150–2157.
- (55) Sato, T., McCue, P., Masuoka, K., Salwen, S., Lattime, E. C., Mastrangelo, M. J., and Berd, D. (1996) Interleukin 10 production by human melanoma. *Clin. Cancer Res.* 2, 1383–1390.
- (56) Halak, B. K., Maguire Jr., H. C., and Lattime, E. C. (1999) Tumor-induced interleukin-10 inhibits type 1 immune responses directed at a tumor antigen as well as a non-tumor antigen present at the tumor site. *Cancer Res.* 59, 911–917.
- (57) Gabrilovich, D. I., Chen, H. L., Girgis, K. R., Cunningham, H. T., Meny, G. M., Nadaf, S., Kavanaugh, D., and Carbone, D. P. (1996) Production of vascular endothelial growth factor by human tumors inhibits the functional maturation of dendritic cells. *Nat. Med.* 2, 1096–1103.
- (58) Liu, V. C., Wong, L. Y., Jang, T., Shah, A. H., Park, I., Yang, X., Zhang, Q., Lonning, S., Teicher, B. A., and Lee, C. (2007) Tumor evasion of the immune system by converting CD4+CD25- T cells into CD4+CD25+ T regulatory cells: Role of tumor-derived TGF- β . *J. Immunol.* 178, 2883–2892.

Chapter 6

Synthesis and characterization of a Self-Assembling Peptide Epitope (SAPE) for therapeutic cancer immunotherapy in TC-1 tumor-bearing mice

Mazda Rad-Malekshahi ^a, Marieke F. Fransen ^b, Ferry Ossendorp ^b, Wim E. Hennink ^a, Enrico Mastrobattista ^a, Maryam Amidi ^a

^a Department of Pharmaceutics, Utrecht Institute for Pharmaceutical Sciences, Utrecht University, Utrecht, The Netherlands

^b Department of Immunohematology and Blood Transfusion, Leiden University Medical Center, Leiden, The Netherlands

Manuscript in preparation

Abstract

Capitalizing on our previous work on self-assembling peptides for vaccination, we designed a self-assembling peptide epitope (SAPE) bearing human papillomavirus antigens covering both CD8⁺ and CD4⁺ epitopes of the HPV16 E7 protein. Self-assembly behavior of the designed SAPE (HPV-SA) was evaluated with atomic force microscopy (AFM), dynamic light scattering (DLS), and circular dichroism (CD) and fluorescence spectroscopy. It was demonstrated that HPV-SA peptide formed nanostructures of 80-100 nm in diameter above a critical concentration (> 15 μM). Endogenous induction of antigen-specific CD8⁺ T cells by a prime-boost vaccination with CpG-adjuvanted HPV-SA in C57BL/6 mouse model indicated the ability of these particles to deliver tumor antigen into the MHC-class I pathway. Moreover, *in vivo* results indicated that the adjuvanted HPV-SA vaccine delayed tumor growth and increased the survival proportion of mice in a therapeutic tumor vaccination regimen compared to the adjuvanted soluble form of tumor antigen. These results demonstrate the added benefit of peptide self-assembly as a means to obtain more effective antigen processing and presentation and subsequently a better anti-tumor efficacy.

1. Introduction

Human papillomavirus (HPV) infection is known as the primary cause of several gynecological cancers, in particular, cervical intraepithelial neoplasia and cervical carcinoma¹. Infection with high-risk HPVs (hrHPVs), consisting of HPV types 16 and 18 is the most common cause of HPV-related cancer². These hrHPVs are regularly transmitted by sexual contact and primary target the undifferentiated keratinocytes of the squamous epithelia³. HPV16 expresses two tumor-specific oncoproteins E6 and E7 that contribute to cancer progression. As with most virus-induced malignancies, HPV-induced cancers are potentially good targets for immunotherapy because these tumors often express viral immunogenic oncoproteins that are not found in healthy cells.

Immunotherapy aims to provide tools to boost the humoral and/or cellular immune system to prevent or cure cancer⁴. The immune system is well equipped to identify and eliminate malignant cells. However, in some cases tumor cells can escape from immune surveillance which leads to the development of life-threatening tumors with potential to metastasize⁵. Cancer vaccines based on synthetic peptide epitopes represent a versatile generation of vaccines that can trigger the immune system in a highly targeted manner⁶. However, poor immunogenicity even in combination with adjuvants is one of their drawbacks. An important reason for this is poor antigen uptake by antigen-presenting cells, including dendritic cells (DCs) and, therefore, lack of proper activation of these cells⁷. Moreover, minimal epitopes can also bind directly to MHC molecules which may lead to T cell tolerance^{8,9}. Synthetic long peptides (SLPs) were introduced as a simple solution for many shortages of minimal epitopes. Elongation of minimal epitopes by (non)-natural amino acids prevents direct binding to the MHC-I or II molecules. Thus, SLPs have to be taken up and processed in order to elicit proper immune response⁸. However, SLPs are prone to enzymatic degradation by proteases present in blood and also by endopeptidases and exopeptidases present on the surface of DCs. Moreover, since peptides are small they rapidly distribute after injection and as a consequence their uptake by DCs is limited⁹.

Several studies demonstrated that better uptake by DCs can be achieved when peptide epitopes are delivered with particulate carriers as compared to non-formulated, soluble peptide epitopes^{7,10-13}.

Nanoparticulate carrier systems for antigenic peptides can be obtained in various ways, including electrostatic complexation or adsorption to preformed nanostructures or entrapment into solid nanospheres^{14,15}. A particular attractive approach is the use of self-assembling peptides. With the current knowledge of how peptides fold and assemble it has become possible to engineer small peptides whose self-assembling behavior can be well-predicted. When such engineered peptides are equipped with antigenic epitopes, highly immunogenic peptide particles can be obtained^{10,11,16}.

These particulate peptide vaccines do not only improve antigen uptake by antigen presenting cells but also decrease the extracellular enzymatic degradation in comparison with their SLPs counterparts. Moreover, peptide self-assembly enables to reach a very high antigen density at the particle surface something which is difficult to achieve with encapsulated systems for antigen delivery, including liposomes or polymeric particles. Moreover, as peptide nanoparticles can be readily constructed from a single peptide and do not require cumbersome processing in order to obtain discrete and monodisperse particles, these systems are from a pharmaceutical point of view very attractive.

In the previous chapter of this thesis, we showed the ability of two designed self-assembling peptide epitopes (SAPEs) containing ovalbumin CTL and T-helper epitopes, to form nanoparticles. Mice vaccinated with these SAPEs developed antigen-specific T cell responses that gave a moderate protection against the outgrowth of OVA-expressing tumors as compared to non-vaccinated mice. However, there was not a significant difference in efficacy between vaccinations with the supposedly soluble CTL peptide epitope vs. the SAPE formulations. Analysis afterward revealed that the supposedly “soluble” CTL peptide formed nanoparticles and as such was a poor control for determining the effect of self-assembly and particulate form on vaccine efficacy.

In this study, we have tested the capacity of peptide self-assembly as a platform for delivery of T cell epitopes for tumor vaccination in a more relevant tumor model based on murine TC-1 primary lung epithelial cells co-transformed with HPV-16 E6 and E7 and c-Ha-ras oncogenes¹⁷. We designed another SAPE bearing human papillomavirus antigens (HPV 16 E7₄₄₋₅₇) of which each peptide chain contains both a CD8⁺ epitope (RAHYNIVTF) and a CD4⁺ epitope (DRAHYNI) of the HPV16 E7 protein for BL/6 mice.

Self-assembly behavior of the designed peptide was evaluated by different analytical methods such as DLS, AFM, and CD. Moreover, the immune activating potential of such self-assembling peptide epitope was studied in mice. Finally, *in vivo* studies were conducted to evaluate the efficacy of this self-assembled vaccine as a therapeutic vaccine in tumor-bearing animals.

2. Materials and methods

2.1. Materials

Nile red, poly-L-lysine and 4-(2-hydroxyethyl) piperazine-1-ethanesulfonic acid (HEPES) were purchased from Sigma (Sigma-Aldrich, St. Louis, MO). Sterile phosphate-buffered saline (PBS)

was obtained from B. Braun (Melsungen AG, Melsungen, Germany), sodium hydroxide and hydrochloric acid (HCl) were bought from Merck (Darmstadt, Germany). CpG ODN 1826 (CpG) was purchased from InvivoGen (Cayla, France).

Self-assembling peptide epitope containing both CD8⁺ and CD4⁺ epitope of the HPV16 E7 protein (Ac- AAVVLLLWGQAEPDRAHYNIVTF-COOH with purity >95%; hereafter referred to as HPV-SA) was obtained from Selleck Chemicals (Houston, TX, USA). HPV 16 E7₄₉₋₅₇ with purity >95% (GQAEPDRAHYNIVTF; hereafter referred to as HPV peptide) was purchased from Ansynth Service BV (Roosendaal, The Netherlands).

2.2. Peptide self-assembly

HPV-SA peptide particles were prepared by a direct dispersion procedure. Briefly, 1 mg of peptide powder was hydrated with 40 µl of 0.2 M NaOH solution. Next, phosphate buffered saline (phosphate 10 mM, NaCl 150 mM, pH 7.4) was added in 200 µl portions up to 1 ml. After each step, the peptide dispersion was sonicated (Fisher Scientific, Loughborough, UK) for 3 min at 30 °C. Before reaching the final volume, the pH was adjusted to pH 7.4 by dropwise adding 0.2 M HCl. The concentration of the peptide in solution was measured by UV-spectrophotometry using an extinction coefficient for HPV-SA of 6990 M⁻¹cm⁻¹ (provide a reference). The HPV peptide formulation was prepared as described above. Where indicated, peptide formulations were supplemented with CpG (20 µg/injection; 10 µl of a 2 mg/ml from a stock solution of CpG in PBS).

2.3. Critical Aggregation Concentration Determination

Nile red assay was used to determine the critical aggregation concentration (CAC) of HPV-SA¹⁸. Serial dilutions of the HPV-SA peptide (0.1-200 µg/ml) in PBS (pH 7.4) with a fixed Nile red concentration of 1.25 µM were prepared. After overnight incubation at room temperature and in the dark, fluorescence emission (Ex550/Em635 nm) was measured by a Horiba fluorolog fluorometer (Horiba Jobin Yvon, Longjumeau Cedex, France). Fluorescence emission of Nile red at 635 nm was recorded as a function of increasing peptide concentration through serial dilutions at room temperature. The point of intersection of two linear fits of the plot was considered as the CAC value.

2.4. Particle size and zeta potential measurements

Prepared peptide particles in PBS (pH7.4) were sized using an ALV CGS-3 goniometer system (Malvern Instruments, Malvern, UK) equipped with a JDS Uniphase 22 mW He-Ne laser operating at 632.8 nm, an optical fiber-based detector, a digital LV/LSE-5003 correlator and a temperature controller (Julabo water bath) to set different temperatures. The DLS time correlation was analyzed by ALV Correlator 3.0 software (ALV, Langen, Germany). Zeta potential measurement of the peptide particles was performed in 10 mM HEPES pH 7.0 at 25 °C using a Malvern Zetasizer Nano-Z (Malvern Instruments, Malvern, UK) with universal ZEN 1002 ‘dip’ cells and DTS (Nano) software (version 4.20). DTS 1235 latex beads (Zeta Potential Transfer Standard, Malvern Instruments, Malvern, UK) were used as a test standard.

2.5. Atomic force microscopy

Freshly peeled mica was treated for 5 min with 40 µl of a 0.02% (w/v) polylysine solution in water, rinsed with filtered Milli-Q water, and dried by a N₂ flow for 2 min. Next, 30 µl of 300 µM of HPV-SA in PBS was deposited on the treated mica and left for 1 min, rinsed three times with 20 µl of filtrated Milli-Q water to remove excess particles and salts, and dried by a N₂ flow. ScanAsyst™ image mode was used at room temperature with a Digital Instruments NanoScope V, equipped with silicon nitride cantilevers (Veeco, NY, USA). Images were analyzed by NanoScope Analysis 1.40 software. To ensure the reproducibility of obtained morphology, several images were taken at different days from independently prepared samples.

2.6. Circular dichroism spectroscopic analysis

CD spectra of 300 µM of HPV-SA in PBS were recorded with a double beam DSM 1000 CD spectrometer (Online Instrument Systems, Bogart, GA, USA) using quartz cuvettes with 1 mm path length (Hellma, Müllheim, Germany). Spectra were acquired for five measurements at 25 °C using 1 nm intervals, 1 nm bandwidth at a wavelength range from 185–250 nm. Next, the averaged spectrum was subtracted from the buffer as the background.

2.7. Animals and cells

Inbred, female C57BL/6 mice (age 8–10 weeks) were purchased from Charles River Laboratories (Maastricht, the Netherlands). All animal experiments were performed in accordance with guidelines from the animal ethics committee of Utrecht University. TC-1 cells are derived from primary lung epithelial cells of C57BL/6 mice co-transformed with HPV-16 E6 and E7 and c-Ha-

ras oncogenes¹⁷. These cells were cultured at 37 °C with 5% CO₂ in IMDM, supplemented with 8% fetal calf serum (FCS) (Greiner), 400 µg/ml of geneticin (G418) (Life Technology), 2 mM L-glutamine, 1 mM sodium pyruvate, 2 mM non-essential amino acids and 100 IU/ml penicillin¹⁹.

2.8. Endogenous CD8⁺ T cell activation

Mice (n =5) were vaccinated at day 0 with 60 nmoles of the vaccine in the right flank to evaluate the capability of the HPV-SA vaccine to activate endogenous HPV 16 E7₄₉₋₅₇-specific CD8⁺ T cells. After 14 days, the animals received the same formulation as a booster injection. The percentage of HPV16 E7-specific CD8⁺ T cells in peripheral blood of tumor-bearing mice was measured by tetramer staining 10 days after the prime immunization, and 5 and 7 days after the booster injection (Figure 1)¹⁹.

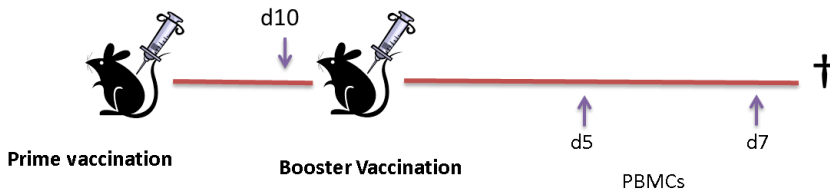


Figure 1. Schematic representation of the *in vivo* experimental setup for endogenous CD8⁺ T cell activation.

2.9. Therapeutic vaccination

TC-1 tumor cells (1×10^5) dispersed in 200 µL of PBS were injected subcutaneously into the right flank of mice (n=10). At day 7, when the tumors were palpable, mice were vaccinated with the indicated vaccines of Table 1 as a prime vaccination, and two weeks later the booster dose was injected (Figure 2). Tumor size was measured two-dimensionally with calipers 2-3 times per week for 70 days. Tumor volumes were calculated using the formula:

$$\text{tumor volume [mm}^3\text{]} = (\text{length [mm]}) \times (\text{width [mm]})^2 \times 0.52^{20}.$$

Mice were sacrificed when the tumor volume reached 2000 mm³ or became ulcerated.

Table 1: List of peptides and formulations investigated in this study.

<i>In vivo</i> experiment	Groups			
	1	2	3	4
<i>In vivo</i> antigen cross presentation	HPV-SA ^a with CpG	No treatment	-----	-----
Therapeutic tumor vaccination	HPV-SA with CpG	HPV-SA	HPV-peptide ^b with CpG	No treatment

a) HPV-SA: Ac- AAVLLLLWGQAEPDRAHYNIVTF-COOH

b) HPV- peptide: GQAEPDRAHYNIVTF



Figure 2. Therapeutic vaccination time schedule. On day 0, mice were injected with 1×10^5 of TC-1 cells in the right flank. After 1 week, mice received 200 μ l of peptide vaccine in the same flank and again two weeks after prime. Tumor size was monitored every other day starting on day 7.

2.10. Detection of HPV16 E7-specific CD8⁺ T cells in peripheral blood of tumor-bearing mice

To detect CD8⁺ T cells recognizing MHC-Class I/RAHYNIVTF antigen complexes, peripheral blood was collected via the tail vein (20 μ l). After removing erythrocytes using red blood cell lysis buffer (Roche, Almere, The Netherlands) the cells were washed with FCS 2% (w/v) in PBS and stained for cell surface markers CD8 α and the allophycocyanine (APC)-conjugated H-2Db E749APC tetramer which binds to the T cell receptor recognizing RAHYNIVTF epitope and were analyzed using a FACS Canto-II, with FACS Diva software (Becton Dickinson, San Jose, CA, USA)¹⁹.

2.11. Statistical analysis

Data were analyzed using GraphPad Prism 5.02 software. For tumor experiments Kaplan–Meier survival curves were applied, and the differences between survival curves were analyzed by log-rank test ($p < 0.05$ was considered statistically significant). Expansion of HPV-specific CD8⁺ T

cells in the blood of mice 5 or 7 days after the prime vaccination in mice treated with HPV vaccine and CpG formulation was compared to untreated mice by student t-test.

3. Result and Discussion

3.1. Peptide Design

Capitalizing on our previous work with SAPEs based on OVA-specific epitopes (Chapter 5 of this thesis), we designed HPV-SA (Ac-AVLLLLWGQAEPDRAHYNIVTF) as a new self-assembling peptide epitope, containing the E7₄₃₋₅₇ peptide of HPV 16 to explore the capability of particle formation of the designed self-assembling peptide tag. E7₄₃₋₅₇ (GQAEPDRAHYNIVTF) covers an H-2b-restricted cytotoxic T cell (CTL) epitope (RAHYNIVTF: bold) and a T helper (Th) epitope (DRAHYNI: underlined) of E7 protein of human papillomavirus type 16 (HPV16) (Table 1).

3.2. Self-assembling peptide epitope (SAPE) characterization

Using a Nile red partitioning assay, we determined the critical concentration at which the HPV-SA peptide started to form nanostructures in an aqueous medium. Interestingly, the obtained critical aggregation concentration (CAC) (15 μM) based on the Nile red assay is comparable with the CAC of previously designed OSAP and OSAP-h assemblies (Chapter 5). The obtained HPV-SA nanoparticles were analyzed at concentrations relevant for *in vivo* use (300 μM) which showed consistent characteristics regarding size and morphology. Dynamic light scattering for the HPV-SA peptide revealed that this peptide formed nanostructures with a mean hydrodynamic diameter of 85 nm in size and a PDI of 0.37 (Table 2). AFM analysis of immobilized nanostructure on polylysine coated mica revealed toroidal structures with a diameter of ~ 100 nm, in accordance with the size obtained by DLS (Figure 3). The observed concave structures may suggest a hollow, vesicular nature of these nanostructures, similar to the vesicular structures formed by the previously reported SA2 peptide (Chapter 4). Although the CAC for the different SA based peptides were dictated by the SA tag, the morphology of the nanoparticles, however, was affected by the appended peptide epitope sequences. The presence of amino acids with negatively charged side chains at physiological pH (Glu and Asp) and a carboxylic acid at the C-terminus resulted in a net negative charge for this peptide at pH 7 (negative zeta potential was -20 mV). The CD spectrum of the HPV-SA nanoparticles showed a negative peak between 210-220 nm, which is typical for peptides forming β -sheets¹¹. This result is in accordance with the obtained secondary structure of previously studied self-assembling peptides (Chapter 3 and 4).

Table 2. Characterization of the self-assembling peptide epitope HPV-SA.

Peptide	MW ^a	Net charge at pH=7 ^a	CAC (μM)	Size (nm) / PDI ^b	Zeta potential ^b	Secondary structure ^b
HPV-SA Ac- AAVLLLVWGQAEPDRAHY NIVTF-COOH	2626	-1.9	15 \pm 1	86 \pm 7/ 0.37 \pm 0.03	-20 \pm 2	β -sheet

a. Obtained using the Innovagen peptide property calculator²¹.

b. Measured at the applied concentration for *in vivo* experiments (300 μM).

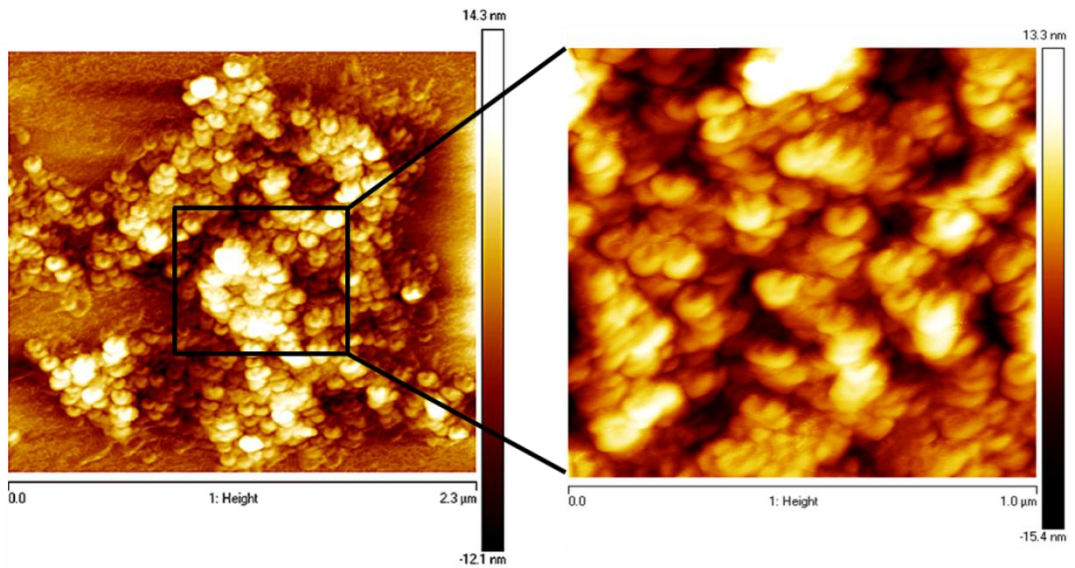


Figure 3. AFM image of 300 μM of HPV-SA peptides self-assemblies immobilized on poly-L-lysine coated mica.

3.3. Endogenous CD8⁺ T cell activation

To evaluate the immunostimulatory potential of the HPV-SA, the induction of an endogenous T cell response was investigated in naïve C57BL/6 mice after *s.c.* injection of HPV-SA in a prime-boost regimen (Figure 4). Ten days after prime injection and at 5 and 7 days after boost injection, the induction of HPV-specific CD8⁺ T cells was analyzed in the collected blood samples using tetramer staining and flow cytometry. As shown in Fig 4, the level of the induced RAHYNIVTF specific CD8⁺ T cell response was significantly increased after prime and particularly after boost injection ($P < 0.05$). These results clearly shows the *in vivo* cross-presentation by HPV-SA.

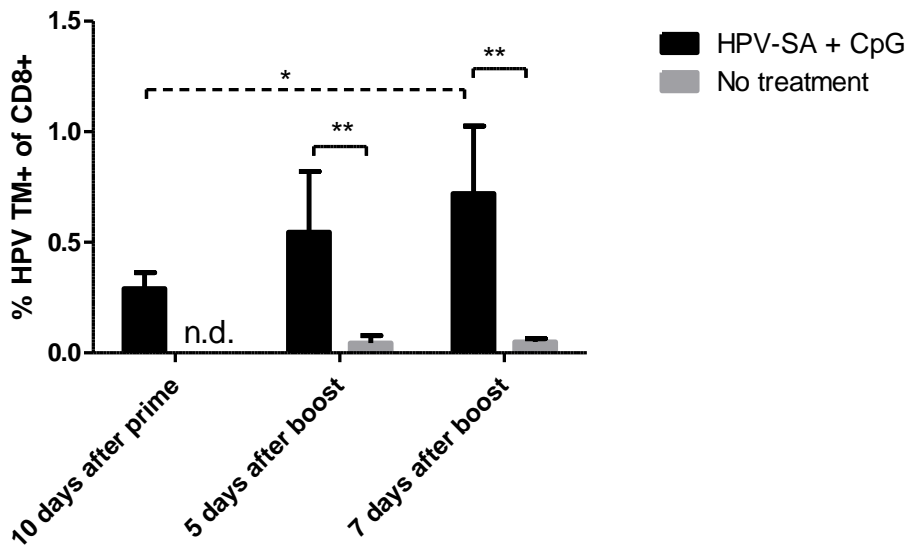


Figure 4. Relative amount of endogenous HPV 16 E7 49-57-specific CD8⁺ T cells in peripheral blood by FACS. Vaccinations with HPV-SA assemblies induced endogenous HPV-specific CD8⁺ T cells in naïve mice particularly after boost injection. Statistical analysis (one way ANOVA) showed significant difference in TM-HPV⁺ CD8⁺ T cells in treatment group in 7 days after booster vaccination compared to 10 days after prime. TM-HPV⁺ CD8⁺ T cells showed significant increase after booster injection in treatment group versus no treatment group in each time points, however no significance difference in 10 days after prime (unpaired T-test). * = $p < 0.05$, ** = $p < 0.01$. $N = 5$ mice per group.

3.4. Therapeutic vaccination with HPV-SA Vaccine:

To investigate the potential anti-tumor efficacy of the HPV-SA nanoparticles naïve mice were challenged *s.c.* with 1×10^5 of TC-1 cells expressing HPV16 oncogenes E6 and E7. Seven days after tumor inoculation, when the tumors were palpable, the treatment group received HPV-SA adjuvanted with CpG in a prime-boost regimen. In addition, one group of mice was vaccinated with non-adjuvanted HPV-SA to assess the intrinsic protective effect of peptide nanoparticles bearing HPV antigens. Moreover, to compare the effectiveness of the designed vaccine with non self-assembled epitope, one group was vaccinated with the HPV peptide with CpG as the soluble form of peptide vaccine. As a control, one group did not receive any formulation. Tumor size was

monitored over time, and the proportions of mice with a tumor size not exceeding the humane endpoint (tumor size of 2000 mm³) are presented in a Kaplan-Meier plot (Figure 5). HPV-SA nanoparticles adjuvanted with CpG strongly delayed the tumor growth and significantly prolonged the overall survival of mice compared with untreated mice. In contrast, development of HPV-associated tumors was not delayed by injection of HPV-SA formulation without CpG, indicating that the presence of an adjuvant was necessary for effective anti-tumor responses by the peptide vaccine. Moreover, in the group of mice that received short HPV peptide adjuvanted with CpG, no tumor regression was observed.

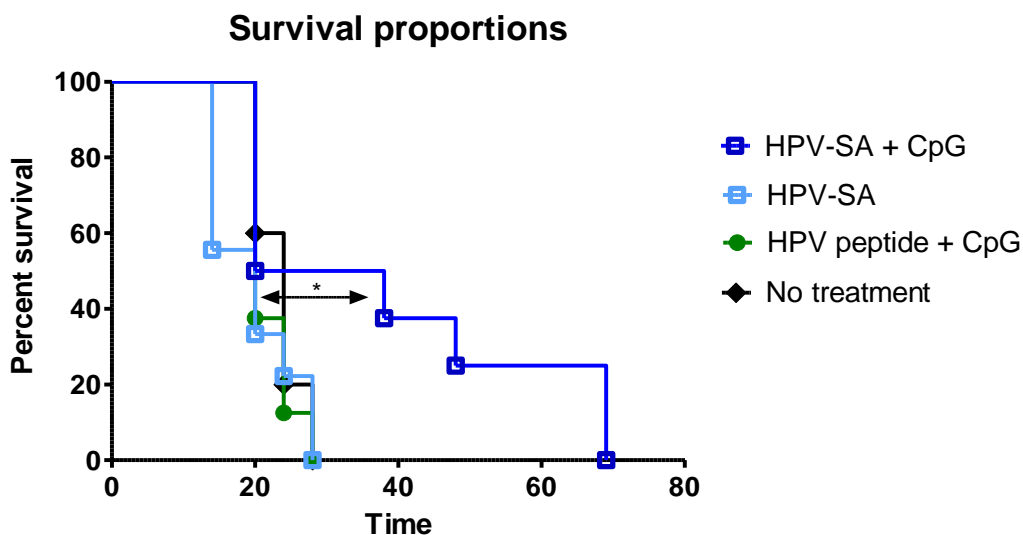


Figure 5. Efficacy of anti-tumor vaccines in a therapeutic tumor model. The survival of mice vaccinated with HPV-SA nanoparticles without CpG and HPV peptide with CpG showed no significance differences compared to no treatment group. Adjuvanted HPV-SA with CpG significantly prolonged the survival of mice compared to the HPV-SA without CpG. (* = $p < 0.05$).

4. Discussion & conclusion

In this study, it is demonstrated that SAPE nanoparticles comprising a self-assembling domain and an antigenic peptide derived from HPV E7 oncoprotein and adjuvanted with CpG substantially prolonged the survival of mice in a therapeutic tumor model. To the best of our knowledge, this study is the first to demonstrate the use of a short self-assembly domain to form nanostructures for therapeutic vaccination *in vivo*. The use of nanocarriers for the delivery of peptide epitopes for

vaccination is not novel and in fact a plenitude of different carriers have been tested for this purpose (for review see De Temmerman *et al.*⁷). For example, Rahimian *et al.* evaluated the anti-tumor efficacy of a synthetic long peptide (SLP) covering HPV peptide encapsulated in PLGA nanoparticles (NPs) in a therapeutic tumor model²². Similar to our results, they showed that the peptide vaccine in the particulate form without adjuvant (Poly I:C) did not significantly delay tumor growth and prolong the survival of mice in comparison with untreated mice. Interestingly, SLP loaded nanoparticles with poly I:C (encapsulated or soluble) significantly prolonged the survival of mice compared to untreated group. Although there were differences between our and their studies in the experiment settings, such as the nature of particulate carrier, type and dosage of the adjuvants and length of HPV peptide vaccines, however, similar trends were observed. Such bipartite or multipartite systems are often difficult to formulate, and it is difficult to obtain optimal loading of the peptide in the nanocarrier and consistent particle sizes. A monopartite system, consisting of a single peptide unit is from a pharmaceutical point of view desired. Surprisingly, only a few groups have investigated the utilization of peptide-self-assembly as a means to obtain peptidic nanocarriers for enhanced uptake and processing of peptide epitopes by professional APCs²³.

In general, research into therapeutic cancer vaccines aims to raise the number of antigen-specific CD8⁺ cytotoxic T lymphocyte cells²⁴. Induction of endogenous antigen-specific CD8⁺ T cells by vaccination with adjuvanted HPV-SA indicated the ability of these particles for cross presentation. At present, the mechanisms by which the SAPE vaccine can deliver epitopes into the MHC-class I pathway is unclear and requires further mechanistic studies. A proposed working mechanism could be that the particulate nature of the SAPEs prevents or delays enzymatic degradation of the peptide epitopes in addition to rapid distribution from the site of injection as compared to soluble epitopes. Moreover, the particulate nature favors DC uptake in comparison with the short soluble peptide. These aspects may all have contributed to an increased antigen loading of DCs. The presence of CpG seems to be crucial for the SAPE vaccine to be effective. It has been shown in other studies that CpG enhanced antigen cross-presentation and improved CTL responses^{25,26}. The effect of ODNs containing unmethylated cytosine-guanine (CpG) motifs as a toll-like receptor 9 (TLR-9) agonist on cellular immunity has been attributed to its ability to induce and expand the number of activated DCs. In addition, it can elevate the expansion of antigen-stimulated T cells by inhibiting activation-induced cell death^{27,28}.

Vaccination with adjuvanted HPV-SA as a particulate form of peptide vaccine significantly improved the survival of mice and delayed tumor growth compared to HPV-SA without CpG as

well as HPV peptide with CpG. These results emphasize the complementary effect of the adjuvant and particulate form for an effective vaccination²⁹. Moreover, we have to take into account that in the latter group 50% of mice had to be sacrificed before receiving the booster vaccination due to the progressive growth of the TC-1 tumor cells. Although the comparison of this study with other similar studies due to different variables is difficult, however, in effective vaccines increasing the survival of animals was observed while complete tumor eradication is rare²².

Melief *et al.* obtained promising results with vaccination by an elongated version of HPV16 E7₄₃₋₆₉ (SLP-HPV: a 27-mer peptide) in human clinical trials after successful preclinical data. Interestingly, as it has been reported in several previous studies, this peptide does not have good solubility in aqueous media^{8,30}. Based on our findings about the ability of peptides to form nanostructures either by intentionally insertion of a self-assembling domain or based on the peptide nature (Chapter 5), it may well be possible that the effectiveness of SLP-HPV can be related to its ability to form nanostructures which consequently facilitate uptake and cross presentation by DCs. Although we obtained some promising results with the SAPE vaccine in this study, it remains necessary to explore different aspects of this particle formation approach to improve the therapeutic effectiveness. Questions that remains to be answered are: 1) What is/are the determining factor(s) that drive SAPEs to different shapes such as micelles or vesicles? 2) For how long do the particles remain stable after *s.c* injection? 3) Are particles able to travel and reach lymph nodes independent of DCs? 4) How does particle size affect the generated immune response for these kind of particles? The CAC results for at least these 3 SAPEs (OSAP, OSAP-h, and HPV-SA) indicated that the peptide epitope sequences appended to the C-terminus of the self-assembling SA domain only had a marginal effect on the CAC. However, these similar CACs may be a result of limitations in the Nile red assay (unpublished results). It is therefore important for future work to include probe-independent techniques to determine the true CAC of these peptides, such as surface tension and/or fluorescence anisotropy measurements. Applying more instrumental and computational techniques can help to address these and other questions to improve and establish this novel strategy as a robust platform for other peptide vaccines.

In conclusion, in line with our previous findings, we provide more evidence that SAPEs can be used as a versatile platform for the development of particulate peptide-based vaccines.

5. References

- (1) Van Poelgeest, M. I. E., Welters, M. J. P., van Esch, E. M. G., Stynenbosch, L. F. M., Kerpershoek, G., van Persijn van Meerten, E. L., van den Hende, M., Löwik, M. J. G., Berends-van der Meer, D. M. a, Fathers, L. M., Valentijn, a R. P. M., Oostendorp, J., Fleuren, G. J., Melief, C. J. M., Kenter, G. G., and van der Burg, S. H. (2013) HPV16 synthetic long peptide (HPV16-SLP) vaccination therapy of patients with advanced or recurrent HPV16-induced gynecological carcinoma, a phase II trial. *J. Transl. Med.* 11, 88.
- (2) Karim, R., Tummers, B., Meyers, C., Biryukov, J. L., Alam, S., Backendorf, C., Jha, V., Offringa, R., van Ommen, G.-J. B., Melief, C. J. M., Guardavaccaro, D., Boer, J. M., and van der Burg, S. H. (2013) Human papillomavirus (HPV) upregulates the cellular deubiquitinase UCHL1 to suppress the keratinocyte's innate immune response. *PLoS Pathog.* 9, e1003384.
- (3) Doorbar, J. (2006) Molecular biology of human papillomavirus infection and cervical cancer. *Clin. Sci. (Lond).* 110, 525–541.
- (4) Amoozgar, Z., and Goldberg, M. S. (2014) Targeting myeloid cells using nanoparticles to improve cancer immunotherapy. *Adv. Drug Deliv. Rev.* Article in press.
- (5) Van Mierlo, G. J. D., den Boer, A. T., Medema, J. P., van der Voort, E. I. H., Fransen, M. F., Offringa, R., Melief, C. J. M., and Toes, R. E. M. (2002) CD40 stimulation leads to effective therapy of CD40(-) tumors through induction of strong systemic cytotoxic T lymphocyte immunity. *Proc. Natl. Acad. Sci. U. S. A.* 99, 5561–5566.
- (6) Yang, J., Zhang, Q., Li, K., Yin, H., and Zheng, J.-N. (2015) Composite peptide-based vaccines for cancer immunotherapy (Review). *Int. J. Mol. Med.* 35, 17–23.
- (7) De Temmerman, M. L., Rejman, J., Demeester, J., Irvine, D. J., Gander, B., and De Smedt, S. C. (2011) Particulate vaccines: On the quest for optimal delivery and immune response. *Drug Discov. Today* 16, 569–582.
- (8) Melief, C. J. M., and Van Der Burg, S. H. (2008) Immunotherapy of established (pre)malignant disease by synthetic long peptide vaccines. *Nat. Rev. Cancer* 8, 351–360.
- (9) Bijker, M. S., Melief, C. J. M., Offringa, R., and van der Burg, S. H. (2007) Design and development of synthetic peptide vaccines: past, present and future. *Expert Rev. Vaccines* 6, 591–603.
- (10) Rudra, J. S., Tian, Y. F., Jung, J. P., and Collier, J. H. (2010) A self-assembling peptide acting as an immune adjuvant. *Proc. Natl. Acad. Sci. U. S. A.* 107, 622–627.
- (11) Rudra, J. S., Sun, T., Bird, K. C., Daniels, M. D., Gasiorowski, J. Z., Chong, A. S., and Collier, J. H. (2012) Modulating adaptive immune responses to peptide self-assemblies. *ACS Nano* 6, 1557–1564.

- (12) Chen, J., Pompano, R. R., Santiago, F. W., Maillat, L., Sciammas, R., Sun, T., Han, H., Topham, D. J., Chong, A. S., and Collier, J. H. (2013) The use of self-adjuvanting nanofiber vaccines to elicit high-affinity B cell responses to peptide antigens without inflammation. *Biomaterials* 34, 8776–8785.
- (13) Black, M., Trent, A., Tirrell, M., and Olive, C. (2010) Advances in the design and delivery of peptide subunit vaccines with a focus on toll-like receptor agonists. *Expert Rev. Vaccines* 9, 157–173.
- (14) Zhao, L., Seth, A., Wibowo, N., Zhao, C.-X., Mitter, N., Yu, C., and Middelberg, A. P. J. (2014) Nanoparticle vaccines. *Vaccine* 32, 327–37.
- (15) De Temmerman, M.-L., Rejman, J., Demeester, J., Irvine, D. J., Gander, B., and De Smedt, S. C. (2011) Particulate vaccines: on the quest for optimal delivery and immune response. *Drug Discov. Today* 16, 569–582.
- (16) Rudra, J. S., Mishra, S., Chong, A. S., Mitchell, R. A., Nardin, E. H., Nussenzweig, V., and Collier, J. H. (2012) Self-assembled peptide nanofibers raising durable antibody responses against a malaria epitope. *Biomaterials* 33, 6476–6484.
- (17) Lin, K. Y., Guarnieri, F. G., Staveley-O'Carroll, K. F., Levitsky, H. I., August, J. T., Pardoll, D. M., and Wu, T. C. (1996) Treatment of established tumors with a novel vaccine that enhances major histocompatibility class II presentation of tumor antigen. *Cancer Res.* 56, 21–26.
- (18) Zhang, A., Zhang, Z., Shi, F., Ding, J., Xiao, C., Zhuang, X., He, C., Chen, L., and Chen, X. (2013) Disulfide crosslinked PEGylated starch micelles as efficient intracellular drug delivery platforms. *Soft Matter* 9, 2224–2233.
- (19) Van Duikeren, S., Fransen, M. F., Redeker, A., Wieles, B., Platenburg, G., Krebber, W.-J., Ossendorp, F., Melief, C. J. M., and Arens, R. (2012) Vaccine-induced effector-memory CD8+ T cell responses predict therapeutic efficacy against tumors. *J. Immunol.* 189, 3397–3403.
- (20) Li, M., Zhang, Y., Liu, Z., Bharadwaj, U., Wang, H., Wang, X., Zhang, S., Liuzzi, J. P., Chang, S.-M., Cousins, R. J., Fisher, W. E., Brunicaardi, F. C., Logsdon, C. D., Chen, C., and Yao, Q. (2007) Aberrant expression of zinc transporter ZIP4 (SLC39A4) significantly contributes to human pancreatic cancer pathogenesis and progression. *Proc. Natl. Acad. Sci. U. S. A.* 104, 18636–18641.
- (21) Innovagen peptide property calculator. <http://www.innovagen.se/custom-peptide-synthesis/peptide-property-calculator/peptide-property-calculator.asp>.
- (22) Rahimian, S., Fransen, M. F., Kleinovink, J. W., Christensen, J. R., Amidi, M., Hennink, W. E., and Ossendorp, F. (2015) Polymeric nanoparticles for co-delivery of synthetic long peptide antigen and poly IC as therapeutic cancer vaccine formulation. *J. Control. Release* 203, 16–22.

- (23) Khallouf, H., Grabowska, A. K., and Riemer, A. B. (2014) Therapeutic vaccine strategies against Human Papillomavirus. *Vaccines* 2, 422–462.
- (24) Rosenberg, S. A., Yang, J. C., and Restifo, N. P. (2004) Cancer immunotherapy: Moving beyond current vaccines. *Nat. Med.* 10, 909–915.
- (25) Lahiri, A., Lahiri, A., Das, P., Vani, J., Shaila, M. S., and Chakravorty, D. (2010) TLR 9 activation in dendritic cells enhances salmonella killing and antigen presentation via involvement of the reactive oxygen species. *PLoS One* 5.
- (26) Najjar, H. M., and Dutz, J. P. (2008) Topical CpG enhances the response of murine malignant melanoma to dacarbazine. *J. Invest. Dermatol.* 128, 2204–2210.
- (27) Davila, E., Kennedy, R., and Cells, E. (2003) Generation of antitumor immunity by cytotoxic T lymphocyte epitope peptide vaccination, CpG-oligodeoxynucleotide adjuvant, and CTLA-4 blockade. *Cancer Res.* 63, 3281–3288.
- (28) Grossmann, M. E., Davila, E., and Celis, E. (2001) Avoiding tolerance against prostatic antigens with subdominant peptide epitopes. *J. Immunother.* 24, 237–241.
- (29) Ilyinskii, P. O., Roy, C. J., O’Neil, C. P., Browning, E. A., Pittet, L. A., Altreuter, D. H., Alexis, F., Tonti, E., Shi, J., Basto, P. A., Iannaccone, M., Radovic-Moreno, A. F., Langer, R. S., Farokhzad, O. C., von Andrian, U. H., Johnston, L. P. M., and Kishimoto, T. K. (2014) Adjuvant-carrying synthetic vaccine particles augment the immune response to encapsulated antigen and exhibit strong local immune activation without inducing systemic cytokine release. *Vaccine* 32, 2882–2895.
- (30) Kenter, G. G., Welters, M. J. P., Valentijn, A. R. P. M., Lowik, M. J. G., Berends-van Der Meer, D. M. A., Vloon, A. P. G., Essahsah, F., Fathers, L. M., Offringa, R., Drijfhout, J. W., Wafelman, A. R., Oostendorp, J., Fleuren, G. J., Van Der Burg, S. H., and Melief, C. J. M. (2009) Vaccination against HPV-16 oncoproteins for vulvar intraepithelial neoplasia. *N. Engl. J. Med.* 361, 1838–1847.

Chapter 7

Summarizing Discussion and Future Perspectives

1. Summarizing Discussion

In this thesis, the use of short, self-assembling peptides to construct nanoparticles for cancer vaccination was investigated. Self-assembling peptides have gained increasing attention as a way to construct biocompatible scaffolds for tissue engineering or nanomaterials for drug and vaccine delivery. An overview of the recent literature covering these applications can be found in **chapter 2**. In this chapter, special emphasis is given to self-assembling peptides that can form discrete nanostructures such as micelles, spheres or vesicles, as these might be particularly attractive as drug and vaccine delivery systems. Previous work in our laboratory had shown that a 10 amino acid amphiphilic peptide (SA2:Ac-AAVLLLLWEE-COOH) is capable of forming spherical nanostructures^{1,2}. These SA2 peptides were produced recombinantly in *E. coli* as this would enable cost-effective scaling up of the production of these peptides. However, the problem with recombinant production of such short amphiphilic peptides is low yields due to peptide degradation or host toxicity. Fusing the amphiphilic peptide to a larger, well-folded protein can help in preventing degradation and toxicity. However, despite the fact that SA2 was expressed in tandem with the small ubiquitin modifier (SUMO), low yields of the SA2 peptides were generally obtained. In **chapter 3** of this thesis, it is demonstrated that premature self-assembly of SA2 and SUMO-SA2 was the main cause of this low yield after production and purification. We showed here that by increasing the pH (>10.5) during purification we could prevent to a great extent the premature self-assembly, which leads to material loss during purification. Furthermore, by applying a selective precipitation technique instead of the second IMAC purification step we could increase the SA2 peptide yield after purification approximately 3 fold. In addition, it was shown that by simply changing the medium to a well-balanced auto-induction medium that the yield of recombinant production was augmented (~4 fold). With these optimizations in place the overall yield of purified SA2 peptide increased with 12-fold.

The work of van Hell *et al.* also showed that SA2 formed spherical structures above a critical concentration and at neutral pH. Static light scattering analysis hinted at the existence of nanovesicles although the co-existence of micelles and vesicles could not be excluded at that time. Here, a more in-depth analysis of the supramolecular architecture of these peptide vesicles formed by SA2 was performed, making use of sophisticated analytical techniques such as ssNMR, AFM and FTIR and supported by coarse-grained and atomistic molecular dynamics simulations (**chapter 4**). We could demonstrate that self-assembly of SA2 peptides in solution indeed resulted in the formation of nanovesicles. Moreover, it was demonstrated that the hydrophobic domain of the SA2 peptides when self-assembled in nanovesicles adopted an antiparallel beta-sheet

configuration and interdigitated organization that strongly diverged from the common organization of phospholipids in liposomes. This study underscored the importance of computational analyses as a robust technique for rational design of self-assembling peptides and investigation on the impact of the modifications on the self-assembly behavior.

Previous work also demonstrated that extending the hydrophilic part of SA2 peptide from 2 to 7 glutamic acid residues had no effect on the self-assembling behavior, with no change in vesicular shape and size¹. Inspired by these interesting results we aimed to develop cancer vaccines based on peptide self-assembly. In **chapter 5**, we demonstrated that discrete nanostructures could be generated in a reproducible manner by extending the hydrophobic domain of SA2 (Ac-AAVLLLLW-COOH) with a CTL epitope and T helper epitope of ovalbumin. The self-assembling peptide epitope (SAPE) extended with the CTL epitope (OSAP) generated spherical micelles (20-30 nm) whereas the SAPE covering T helper epitope (OSAP-h) generated a mixture of spherical micelles and fibers as determined by atomic force microscopy. Notably, spherical nanoparticles were observed when OSAP and OSAP-h were mixed at a ratio of 8:3, respectively. We also showed that the SAPEs adjuvanted with CpG were able to induce and expand specific CD8⁺ and CD4⁺ T cells in C57BL/6 mouse models. Furthermore, *in vivo* results indicated that the adjuvanted SAPEs delayed tumor growth and increased the survival proportion of mice both in a prophylactic as well as therapeutic tumor vaccination regimens. Unexpectedly, mice vaccinated with peptide epitopes without a self-assembling domain also led to efficient immunization and an increase in survival similar to those mice vaccinated with SAPEs. This effect was linked to the ability of the CTL peptides to form nano-sized structures. Due to the particle formation, this CTL peptide was not a proper control to demonstrate the added benefit of peptide self-assembly on antigen processing and immune activation. Thus to demonstrate the flexibility of the self-assembling domain to create a nanoparticles when extended with different peptide epitopes and show the added benefit of SAPEs compared to soluble peptide vaccine, in **chapter 6** we designed another self-assembling peptide epitope (SAPE) bearing human papillomavirus antigens covering both CD8⁺ and CD4⁺ epitopes of the HPV16 E7 protein. We showed that this SAPE (HPV-SA) formed nanostructures of 80-100 nm in diameter above a critical concentration (> 15 μ M). Interestingly, the HPV-SA nanostructures as observed by AFM resembled nanovesicles whereas OSAP and OSAP-h formed much smaller spherical structures, presumably micelles. Endogenous induction of antigen-specific CD8⁺ T cells by a prime-boost vaccination with adjuvanted HPV-SA in C57BL/6 mouse model indicated the ability of this nanoparticles for cross-presentation. Moreover, vaccination of tumor-bearing mice indicated that the adjuvanted HPV-SA delayed

tumor growth and increased the survival proportion of mice in a therapeutic tumor vaccination regimen compared to the adjuvanted soluble form of tumor antigen.

2. Future Perspectives

In this thesis the recombinant production, characterization and clinical application of peptide self-assemblies derived from SA2 peptide were discussed. Despite the promising results obtained there are still some technical and scientific hurdles that need to be taken before self-assembling peptides can be used for vaccination in patients. Some questions that remain are:

7.2.1 How can we get a higher yield of recombinant production of self-assembling peptides?

7.2.2-7.2.5 How can we improve the immunostimulatory potential of the self-assembling vaccines?

7.2.6 What other applications can these self-assembling peptides be used?

2.1 Recombinant production

In **chapter 3** we described the challenges for the recombinant production of SA2 peptide. By applying an auto-induction medium and refinement of purification method, we could increase the production yield of SA2 12 fold compared to the initial production and purification method. However, the amount of produced SA2 in comparison with the capacity of recombinant production is still low (e.g., Kyle *et al.* reported 203 mg/L for an 11-residue peptide³). Besides toxicity to the host cell, another explanation for the low yield is the low weight ratio of SA2 peptide compared to the SUMO fusion protein which corresponds to only 9 % of the entire recombinant protein (6xHis-SUMO-SA2; 14 kD). The suggestive solution for this challenge could be a recombinant expression of tandem SA2 peptide repeats then releasing peptide by site-specific cleavage reaction³. There are several enzymes and chemicals that can specifically cleave peptide bounds (Figure 1). However, it should be considered that some of cleaving agents and endopeptidase may leave unwanted residues at the site of cleavage. Thus, considering the impact of these residues on peptide self-assembly behavior is crucial.

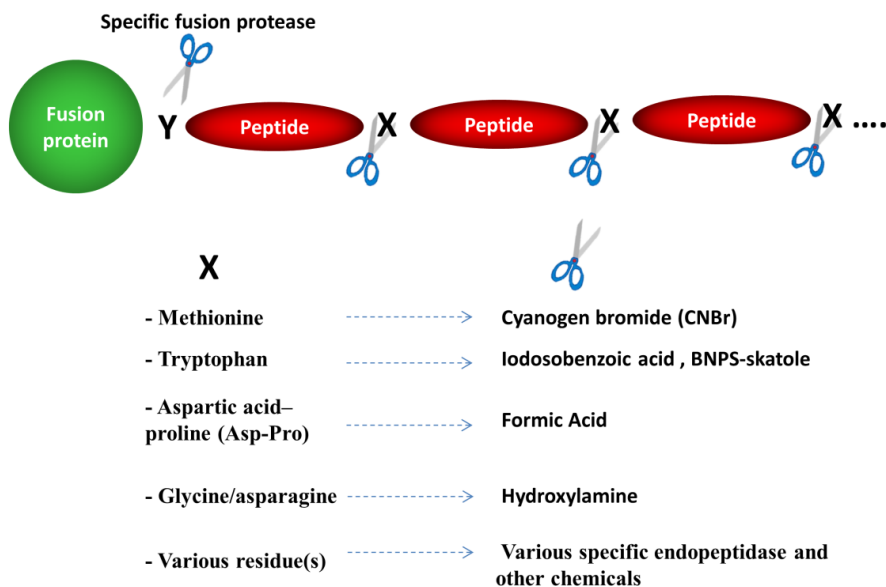


Figure 1. Schematic representation of recombinant expression of tandem peptide repeats. Scissors indicate chemical (X) or enzymatic (X and Y) cleavage sites to release monomeric peptides.

2.2. Particle morphology

It is well documented that delivery of antigen to lymph nodes through direct drainage or by migration of matured DCs that have taken up antigen from the site of injection is important for induction of an effective immune response⁴. Migration of nanoparticles to the lymph nodes is mainly affected by size⁵. In general, nanoparticles with a size range of 10-100 nm can travel through interstitial matrix and reach lymph nodes via lymphatic vessels⁶. In this thesis, several self-assembling peptides were designed based on SA2 peptide and their morphology was studied. Although the peptides showed similar CAC values once dispersed in the same buffer, different nanostructures in shape and size were obtained. For example the self-assembling peptides SA2 (60 nm) formed vesicles and HPV-SA formed spherical structures (85 nm) that appeared similar to SA2 vesicles on AFM, OSAP generated micellar structures (20-30 nm) and OSAP-h formed mixture of spherical micelles (20-30 nm) and nanofibers (micrometers in length). The structural variables that determine the shape and size remains unclear. However, it can be hypothesized that the studied self-assembling peptides in this thesis have a tendency to form vesicular structures through an anti-parallel beta sheet conformation as showed in chapter 4 for SA2 peptide. However, due to the extension of the hydrophilic head of OSAP and OSAP-h self-assembling peptides the

inner compartment of these vesicles cannot embed the long chain of peptides properly so self-assemblies transform to micellar structures in some cases. To understand the exact mechanism, it is necessary to develop robust techniques that enable to rational design of peptide nanostructures. In **chapter 4**, we highlighted the central role of coarse-grained and atomistic simulations that assisted us to get an insight into the sub-molecular levels of assemblies. Molecular dynamic simulations can be used as a robust technique for prediction of size and shape of self-assembly before more instrumental experiments.

2.3. *In vivo* fate of self-assembling peptides

In vivo fate of the self-assembling peptide nanoparticles was not addressed in this thesis, but it is an important aspect for future studies. Future studies should address questions about the stability of the nanoparticles after injection, interaction of self-assembling particles/ peptides with cell membrane and interstitial proteins and interestingly the cross-presentation mechanism by which these self-assembling peptide epitopes end up in the MHC class I molecules. To assess the stability of nanoparticles in physiological fluids, labeling of particles with fluorophores can be applicable. Labelled particles will be dispersed *ex vivo* or *in vivo* in desired physiological fluids such as blood or interstitial fluids and analysis the fluorescence intensity of particles at different time points by for example fluorescence correlation spectroscopy (FCS)⁷. Moreover, labeling peptide particles by near-infrared (NIR) fluorescent dyes followed by *in vivo* tracking can determine the fate of nanoparticle vaccines⁸.

Interestingly, intracellular immunofluorescence enables us to track labeled nanoparticles inside DCs either cultured or collected from tissue which could provide valuable information regarding the antigen presentation pathway^{9,10}.

2.4. Adjuvant delivery

Different studies have shown that augmentation of immunogenicity can be achieved by co-delivery of an antigen and an adjuvant with particulate delivery systems¹¹⁻¹³. Self-assembling peptide epitopes also have the capacity to carry antigens and adjuvants simultaneously to individual DCs. Moreover, several peptides have been identified as toll-like receptor ligands¹⁴. It can be an interesting approach to attach these adjuvant peptides either to the hydrophobic domain of SA2 (to construct self-assembling peptide adjuvants (SAPAs) or to the SAPE molecules individually. In addition, synthetic toll-like receptor ligands can be conjugated to the SAPE molecules. Particularly suitable are the small TLR ligands, such as the adenine derivatives^{15,16} which are expected to have little effect on the self-assembly behavior of the final SAPE molecules.

2.5. Immune checkpoint inhibitors

In **chapter 5 and 6** we showed the potency of SAPEs to elevate antigen-specific CD8+ and CD4+ T-cells and delay tumor growth thereby resulting in an increase in survival of mice. However, we did not observe complete tumor regression with this particular tumor model, which is in line with what other studies have reported^{17,18}.

It is well established that tumors can dampen the immune response by induction and/or production of some factors such as TGF-beta¹⁹, IL-10²⁰⁻²², VEGF²³ and also by induction of Tregs²⁴.

Several immune checkpoint inhibitors have recently entered the market such as anti-CTLA-4 (e.g. ipilimumab), anti-PD1 (e.g. nivolumab) or are in the last phases of clinical trials (e.g. MPDL3280A as an anti-PDL1). Clinical administration of these mAbs indicated long-lasting clinical benefits in end-stage cancer patients. For example, in two large phase III trials, ipilimumab significantly prolonged overall survival in patients with advanced melanoma²⁵.

A combination of tumor vaccination to increase effector T cells and administration of immune checkpoint inhibitor mAbs will most likely lead to synergistic clinical effects in patients.

2.6. Other application of self-assembling peptides

2.6.1. Drug delivery

In previous work by van Hell *et al.* the feasibility of SA2 peptide vesicles as a drug carrier was investigated. Their results indicated that although SA2 vesicles could entrap small fluorescent dyes, the encapsulation efficiency was rather low as compared to liposomes at the same vesicle concentration²⁶. The low encapsulation efficiency was linked to the high permeability of vesicle membranes for the molecules. One strategy to increase the encapsulation efficiency is the conjugation of drug molecules using cleavable linkers to the peptide such as disulfide or hydrazone bonds²⁷. In addition, based on the successful approach of C-terminal extension of SA2 peptide with antigenic epitopes, this strategy can also be applied to therapeutic peptides. Direct extension of the self-assembling domain of SA2 with therapeutic peptide sequences such as anti-cancer peptides²⁸ can potentiate therapeutic peptides for particle formation. Another interesting feature for self-assembling peptide particle is tumor targeting. By extension of the self-assembling domain with selective ligands such as RGD peptides which bind to integrins on tumor vasculature or conjugation of small molecule ligands such as folic acid, we can equip nanoparticles for tumor targeting. In conclusion, self-assembling peptide particles can readily be functionalized with several agents to achieve selectivity for particular cells or tissues.

2.6.2. Tissue regeneration

In **chapter 2**, a literature review on application of peptide self-assembly showed that fibrous scaffolds formed by peptide self-assembly can mimic the extracellular matrix (ECM) and promote cell growth. Since many different functionalities can be integrated into the self-assembling peptide sequence, including cell-attachment or signaling domains, multifunctional scaffolds can be generated from a single molecular entity^{29–32}. Interestingly in **chapter 5** we observed that OSAP-h peptide at a concentration of 75 μM generated a mixture of spherical micelles and elongated fibers. By increasing the concentration to 3 mM (1% w/v), it formed a translucent hydrogel (data not published). This observation shows that SA2 can be engineered to form macroscopic hydrogels and opens up a new avenue for these peptides to be used in tissue engineering.

3. Final conclusion

To conclude, this thesis illustrates the potential of peptide self-assembly to produce clean and well-defined tumor vaccines. Moreover, practical approaches for recombinant production and characterization of self-assembling peptides with high resolution were presented. Together, the results in this thesis form a solid foundation for further research on these intriguing self-assembling peptides.

4. References

- (1) Van Hell, A. J., Costa, C., Flesch, F. M., Sutter, M., Jiskoot, W., Crommelin, D. J. A., Hennink, W. E., and Mastrobattista, E. (2007) Self-assembly of recombinant amphiphilic oligopeptides into vesicles. *Biomacromolecules* 8, 2753–2761.
- (2) Van Hell, A. J. (2009) Structural and functional characterization of self-assembling amphiphilic oligopeptides. Thesis Utrecht University. ISBN: 978-90-393-4986-1.
- (3) Kyle, S., Aggeli, A., Ingham, E., and McPherson, M. J. (2010) Recombinant self-assembling peptides as biomaterials for tissue engineering. *Biomaterials* 31, 9395–9405.
- (4) Zhao, L., Seth, A., Wibowo, N., Zhao, C.-X., Mitter, N., Yu, C., and Middelberg, A. P. J. (2014) Nanoparticle vaccines. *Vaccine* 32, 327–337.
- (5) De Temmerman, M.-L., Rejman, J., Demeester, J., Irvine, D. J., Gander, B., and De Smedt, S. C. (2011) Particulate vaccines: on the quest for optimal delivery and immune response. *Drug Discov. Today* 16, 569–582.

- (6) Reddy, S. T., Rehor, A., Schmoekel, H. G., Hubbell, J. A., and Swartz, M. A. (2006) *In vivo* targeting of dendritic cells in lymph nodes with poly(propylene sulfide) nanoparticles. *J. Control. Release* 112, 26–34.
- (7) Dakwar, G. R., Zagato, E., Delanghe, J., Hobel, S., Aigner, A., Denys, H., Braeckmans, K., Ceelen, W., De Smedt, S. C., and Remaut, K. (2014) Colloidal stability of nano-sized particles in the peritoneal fluid: Towards optimizing drug delivery systems for intraperitoneal therapy. *Acta Biomater.* 10, 2965–2975.
- (8) Rahimian, S., Kleinovink, J. W., Fransen, M. F., Mezzanotte, L., Gold, H., Wisse, P., Overkleeft, H., Amidi, M., Jiskoot, W., Löwik, C. W., Ossendorp, F., and Hennink, W. E. (2014) Near-infrared labeled, ovalbumin loaded polymeric nanoparticles based on a hydrophilic polyester as model vaccine: *In vivo* tracking and evaluation of antigen-specific CD8(+) T cell immune response. *Biomaterials* 37C, 469–477.
- (9) Morón, V. G., Rueda, P., Sedlik, C., and Leclerc, C. (2003) *In vivo*, dendritic cells can cross-present virus-like particles using an endosome-to-cytosol pathway. *J. Immunol.* 171, 2242–2250.
- (10) Matheoud, D., Perié, L., Hoeffel, G., Vimeux, L., Parent, I., Marañón, C., Bourdoncle, P., Renia, L., Prevost-Blondel, A., Lucas, B., Feuillet, V., and Hosmalin, A. (2010) Cross-presentation by dendritic cells from live cells induces protective immune responses *in vivo*. *Blood* 115, 4412–4420.
- (11) Ilyinskii, P. O., Roy, C. J., O’Neil, C. P., Browning, E. A., Pittet, L. A., Altreuter, D. H., Alexis, F., Tonti, E., Shi, J., Basto, P. A., Iannaccone, M., Radovic-Moreno, A. F., Langer, R. S., Farokhzad, O. C., von Andrian, U. H., Johnston, L. P. M., and Kishimoto, T. K. (2014) Adjuvant-carrying synthetic vaccine particles augment the immune response to encapsulated antigen and exhibit strong local immune activation without inducing systemic cytokine release. *Vaccine* 32, 2882–2895.
- (12) Hamdy, S., Molavi, O., Ma, Z., Haddadi, A., Alshamsan, A., Gobti, Z., Elhasi, S., Samuel, J., and Lavasanifar, A. (2008) Co-delivery of cancer-associated antigen and Toll-like receptor 4 ligand in PLGA nanoparticles induces potent CD8+ T cell-mediated anti-tumor immunity. *Vaccine* 26, 5046–5057.
- (13) Schlosser, E., Mueller, M., Fischer, S., Basta, S., Busch, D. H., Gander, B., and Groettrup, M. (2008) TLR ligands and antigen need to be coencapsulated into the same biodegradable microsphere for the generation of potent cytotoxic T lymphocyte responses. *Vaccine* 26, 1626–1637.

- (14) Shanmugam, A., Rajoria, S., George, A. L., Mittelman, A., Suriano, R., and Tiwari, R. K. (2012) Synthetic toll like receptor-4 (TLR-4) agonist peptides as a novel class of adjuvants. *PLoS One* 7, e30839.
- (15) Weterings, J. J., Khan, S., van der Heden van Noort, G. J., Melief, C. J. M., Overkleeft, H. S., van der Burg, S. H., Ossendorp, F., van der Marel, G. A., and Filippov, D. V. (2009) 2-Azidoalkoxy-7-hydro-8-oxoadenine derivatives as TLR7 agonists inducing dendritic cell maturation. *Bioorganic Med. Chem. Lett.* 19, 2249–2251.
- (16) Nakamura, T., Wada, H., Kurebayashi, H., McNally, T., Bonnert, R., and Isobe, Y. (2013) Synthesis and evaluation of 8-oxoadenine derivatives as potent Toll-like receptor 7 agonists with high water solubility. *Bioorganic Med. Chem. Lett.* 23, 669–672.
- (17) De Titta, A., Ballester, M., Julier, Z., Nembrini, C., Jeanbart, L., Van Der Vlies, A. J., Swartz, M. A., and Hubbell, J. A. (2013) Nanoparticle conjugation of CpG enhances adjuvancy for cellular immunity and memory recall at low dose. *Proc. Natl. Acad. Sci. U. S. A.* 110, 19902–19907.
- (18) Rahimian, S., Fransen, M. F., Kleinovink, J. W., Christensen, J. R., Amidi, M., Hennink, W. E., and Ossendorp, F. (2015) Polymeric nanoparticles for co-delivery of synthetic long peptide antigen and poly IC as therapeutic cancer vaccine formulation. *J. Control. Release* 203, 16–22.
- (19) Gajewski, T. F., Meng, Y., and Harlin, H. (2006) Immune suppression in the tumor microenvironment. *J. Immunother.* 29, 233–240.
- (20) Yang, A. S., and Lattime, E. C. (2003) Tumor-induced interleukin 10 suppresses the ability of splenic Dendritic Cells to stimulate CD4 and CD8 T-cell responses. *Cancer Res.* 63, 2150–2157.
- (21) Sato, T., McCue, P., Masuoka, K., Salwen, S., Lattime, E. C., Mastrangelo, M. J., and Berd, D. (1996) Interleukin 10 production by human melanoma. *Clin. Cancer Res.* 2, 1383–1390.
- (22) Halak, B. K., Maguire Jr., H. C., and Lattime, E. C. (1999) Tumor-induced interleukin-10 inhibits type 1 immune responses directed at a tumor antigen as well as a non-tumor antigen present at the tumor site. *Cancer Res.* 59, 911–917.
- (23) Gabrilovich, D. I., Chen, H. L., Girgis, K. R., Cunningham, H. T., Meny, G. M., Nadaf, S., Kavanaugh, D., and Carbone, D. P. (1996) Production of vascular endothelial growth factor by human tumors inhibits the functional maturation of dendritic cells. *Nat. Med.* 2, 1096–1103.
- (24) Liu, V. C., Wong, L. Y., Jang, T., Shah, A. H., Park, I., Yang, X., Zhang, Q., Lonning, S., Teicher, B. A., and Lee, C. (2007) Tumor evasion of the immune system by converting CD4+CD25 - T cells into CD4+CD25+ T regulatory cells: Role of tumor-derived TGF- β . *J. Immunol.* 178, 2883–2892.
- (25) Fellne, C. (2012) Ipilimumab (Yervoy) prolongs survival in advanced melanoma: Serious side effects and a hefty price tag may limit its use. *P T* 37, 503–511.

- (26) Van Hell, A. J., Fretz, M. M., Crommelin, D. J. A., Hennink, W. E., and Mastrobattista, E. (2010) Peptide nanocarriers for intracellular delivery of photosensitizers. *J. Control. Release* 141, 347–353.
- (27) Webber, M. J., Matson, J. B., Tamboli, V. K., and Stupp, S. I. (2012) Controlled release of dexamethasone from peptide nanofiber gels to modulate inflammatory response. *Biomaterials* 33, 6823–6832.
- (28) Thundimadathil, J. (2012) Cancer treatment using peptides: current therapies and future prospects. *J. Amino Acids* 2012, 967347.
- (29) Miller, R. E., Grodzinsky, A. J., Vanderploeg, E. J., Lee, C., Ferris, D. J., Barrett, M. F., Kisiday, J. D., and Frisbie, D. D. (2010) Effect of self-assembling peptide, chondrogenic factors, and bone marrow-derived stromal cells on osteochondral repair. *Osteoarthritis Cartilage* 18, 1608–1619.
- (30) Dubois, G., Segers, V. F. M., Bellamy, V., Sabbah, L., Peyrard, S., Bruneval, P., Hagège, A. A., Lee, R. T., and Menasché, P. (2008) Self-assembling peptide nanofibers and skeletal myoblast transplantation in infarcted myocardium. *J. Biomed. Mater. Res. B. Appl. Biomater.* 87, 222–228.
- (31) Berns, E. J., Sur, S., Pan, L., Goldberger, J. E., Suresh, S., Zhang, S., Kessler, J. A., and Stupp, S. I. (2014) Aligned neurite outgrowth and directed cell migration in self-assembled monodomain gels. *Biomaterials* 35, 185–195.
- (32) Lee, S. S., Huang, B. J., Kaltz, S. R., Sur, S., Newcomb, C. J., Stock, S. R., Shah, R. N., and Stupp, S. I. (2013) Bone regeneration with low dose BMP-2 amplified by biomimetic supramolecular nanofibers within collagen scaffolds. *Biomaterials* 34, 452–459.

Appendices

Nederlandse samenvatting

Acknowledgments

Curriculum Vitae

List of Publications

Nederlandse Samenvatting

Kanker is de algemene term voor uiteenlopende neoplastische ziekten, die worden gekenmerkt door ongecontroleerde en invasieve groei en soms ook verspreiding van kwaadaardige cellen over het lichaam. Bij kankerpatiënten met een vergevorderd ziektebeeld hebben de huidige kankertherapieën, zoals chirurgie, chemotherapie en radiotherapie niet altijd het gewenste curatieve effect. Veel vormen van kanker die niet effectief verwijderd kunnen worden door de conventionele behandelingsmethoden hebben een hoge mortaliteit. Daarom zijn nieuwe, doeltreffende behandelingen nodig om kanker adequaat te behandelen. Immunotherapie van kanker, waarbij gebruik wordt gemaakt van het immuunsysteem van de patient om tumorcellen te doden, heeft in experimentele (pre-)klinische studies tot veelbelovende resultaten geleid met in sommige gevallen complete regressie van tumoren.

Kankervaccinatie is een vorm van immunotherapie waarbij een antigeenpreparaat wordt toegediend die het immuunsysteem van de patiënt moet stimuleren om tumorcellen specifiek te herkennen en te doden. Net als conventionele vaccins ter voorkoming van infectieziekten kan een kankervaccin ingezet worden ter voorkoming van bepaalde vormen van kanker, maar de meest interessante toepassing is het inzetten van kankervaccins als therapie bij bestaande tumoren. Voor deze toepassing moet het kankervaccin in staat zijn een bestaande tumormassa die meestal niet erg immunogeen is en tevens mechanismen heeft ontwikkeld om het immuunsysteem om de tuin te leiden, te herkennen en te elimineren.

Subunit vaccins gebaseerd op synthetische peptiden zijn van groot belang in de moderne immunotherapie omdat deze goed gedefinieerde en makkelijk te produceren constructen in staat zijn om specifieke humorale en cellulaire immunoreacties tegen kankercellen op te wekken. Een nadeel is echter dat peptide-antigenen relatief zwak immunogeen zijn, zelfs in combinatie met sterke adjuvantia. Het formuleren van deze peptiden in nanodeeltjes heeft aangetoond te leiden tot een verbeterde immunogeniciteit door verbeterde opname door en activatie van antigeenpresenterende cellen. Het toepassen van peptiden die uit zichzelf nanodeeltjes vormen kan gebruikt worden om peptidevaccins meer immunogeen te maken.

In ons laboratorium zijn korte amfifiele peptiden ontworpen met de aminozuursequentie Ac-AAVLLLLWEE-COOH. Deze SA2 peptiden vormen spontaan vesiculaire nanostructuren wanneer deze gedispergeerd worden in een waterige oplossing. Deze zelfassemblage is voornamelijk afhankelijk van het hydrofobe gedeelte van het peptide met zowel hydrofobe aggregatie en intermoleculaire waterstofbinding als drijvende krachten. Onderzoek heeft aangetoond dat de sequentie en lengte van het hydrofiele gedeelte van dit amfifiele peptide minder bepalend is voor de manier waarop dit peptide goed gedefinieerde nanostructuren vormt. Deze

flexibiliteit in de keuze van het hydrofiele stuk maakt het in principe mogelijk peptide nanodeeltjes te vormen waarbij de buitenkant van de nanodeeltjes bestaat uit repeterende eenheden van tumor-specifieke T cell epitopen als nieuw vaccin tegen kanker.

Dit proefschrift beschrijft de ontwikkeling van zelfassemblerende peptiden als vaccin tegen kanker. In **hoofdstuk 2** geven we een algemeen overzicht van zelfassemblerende peptiden. De invloed van de primaire en secundaire peptide structuur op peptide assemblage en de verschillende categorieën van goed gedefinieerde supramoleculaire structuren, zoals micellen, fibrillen, nanobuisjes en vesiculaire structuren worden beschreven. Het tweede deel geeft een overzicht van de recente literatuur over studies betreffende peptide zelfassemblage voor toepassing in medicijnafgifte, vaccinatie, en weefselregeneratie.

Eerder onderzoek in ons laboratorium heeft uitgewezen dat SA2 peptiden recombinant geproduceerd kunnen worden in *E. coli* wat grootschalige en kosteneffectieve productie van deze peptiden mogelijk maakt. De opbrengst van dit recombinante peptide in vergelijking met andere peptiden die op dezelfde manier geproduceerd werden viel echter tegen (~ 1 mg/L bacteriecultuur). Vandaar dat in **hoofdstuk 3** van dit proefschrift gekeken is naar het verbeteren van de recombinante productie en zuivering van dit peptide. Door het wisselen van het groeimedium voor een goed uitgebalanceerd auto-inductie medium kon de opbrengst van het SA2 peptide met een factor 4 worden verhoogd. Bovendien werd aangetoond dat door het tegengaan van voortijdige zelfassemblage van het peptide tijdens de zuivering en het invoeren van een selectieve precipitatiestap de opbrengst na zuivering verder kon worden verhoogd. Met deze wijzigingen in productie- en zuiveringmethodes kon de opbrengst van SA2 met een factor 12 worden verhoogd zonder dat de kosten van de productie toenamen.

Hoewel eerder onderzoek heeft aangetoond dat SA2 peptiden nanovesiculaire structuren vormen van gemiddeld 70 nm in diameter was het onduidelijk welke moleculaire mechanismen ten grondslag lagen aan deze supramoleculaire assemblage. Bovendien was onduidelijk wat de exacte oriëntatie van de peptiden in de gevormde nanostructuren was, iets wat essentieel is voor een rationeel ontwerp van dit soort peptidestructuren. In **hoofdstuk 4** is daarom een diepgaande analyse uitgevoerd naar de supramoleculaire architectuur van de nanovesiculaire structuren gevormd door zelfassemblage van het SA2 peptide. Hiervoor is gebruik gemaakt van moleculaire dynamica (MD) computersimulaties ondersteund door geavanceerde analytische technieken zoals ssNMR, AFM en FTIR. Met deze technieken kon aangetoond worden dat de SA2 peptiden een antiparallele beta-sheet conformatie aannemen die de “bilaag” van het peptideblaasje vormen. Deze oriëntatie wijkt sterk af van wat hiervoor werd aangenomen, namelijk dat de peptiden net

zoals lipiden in een membraan een bilaag zouden vormen waarbij de hydrofobe domeinen van de beide monolagen naar elkaar zijn toegekeerd zonder te overlappen. Dit onderzoek bevestigt het belang van geavanceerde MD computersimulaties als een robuuste techniek voor het kunnen voorspellen van de manier waarop amfifiele peptiden supramoleculaire structuren vormen.

In **hoofdstuk 5 en 6** werd de mogelijkheid onderzocht om zelfassemblerende peptiden als afgiftesysteem voor T cel epitopen in tumor vaccinatiestudies te gebruiken. Er werd aangetoond dat verlenging van de SA2 aminozuursequentie met sequenties coderend voor T cel epitopen afgeleid van ovalbumine of humaan papillomavirus E7 eiwit mogelijk is zonder dat dit de zelfassemblage van het peptide negatief beïnvloedde. De verwachting was dat deze peptide nanostructuren een betere antigeenpresentatie en activatie van het immuunsysteem zouden geven in vergelijking met monomere peptide-epitopen wat vervolgens zou moeten leiden tot een betere bescherming tegen uitgroei van tumoren waartegen werd gevaccineerd. In beide dierstudies werd inderdaad aangetoond dat zelfassemblage een positief effect had op activering van een tumor-specifieke immuunreactie zolang CpG als adjuvant werd gebruikt. In de studie waarin muizen werden gevaccineerd die een tumor droegen die het HPV E7 antigeen tot expressie brachten, kon worden aangetoond dat vaccinatie met zelfassemblerende peptide epitopen in tegenstelling tot dezelfde peptide epitopen in monomere vorm bescherming gaven tegen de uitgroei van tumoren. Deze resultaten geven aan dat zelfassemblerende peptideepitopen een mogelijke toepassing hebben als tumor-specifieke vaccins.

Acknowledgments

The completion of this thesis would not have been possible without the generous support and the precious contribution of many people to whom I am very grateful.

First, I would like to express my sincerest gratitude to my inspiring promoter Professor Wim Hennink. I especially thank him for insightful scientific discussions and valuable advice. I greatly appreciate his guidance and fruitful input throughout my PhD study. Dear Wim, it was an honor to accomplish my PhD under your supervision. You taught me we should love science and more importantly we have to take care of it.

I would like to extend my deepest gratitude to my copromotor Dr. Enrico Mastrobattista for everything he has taught me, for all his support from both professional and personal points of view. Dear Enrico, thank you for constantly encouraging and inspiring me. Our meetings were always important occasions to receive wise suggestions and useful feedbacks from a super clever gentleman.

I have a great opportunity to work with Dr. Mayam Amidi as the second copromotor, whose knowledge of immunology has made my research much more successful and helped me to achieve our targets much faster. Dear Maryam, your brilliant idea regarding vaccination pushed me in an interesting area of science that definitely assists me in my future carrier. Thanks for everything.

Also, I would like to thank Mies van Steenberg, our joyful and skilled technician who loves science. Dear Mies, thank you for the excellent technical supports in all the frustrating experiments.

I want to thank Georgi Nadibaidze, Joep van den Dikkenberg, Ebel Pieters and Louis van Bloois who were always very helpful in my research. Dear Georgi, I never forget your calm and helpful manner which put me at ease in my experiments. Dear Joep many thanks for wearing different T-shirts, right now, I know about different music bands and Schrodinger cat!

I would like to show my gratitude to Barbara de Jong-van Amstel for generously making living and working in the Netherlands very easy for me and other research visitors.

It was impossible to assemble this book without collaboration. I am very thankful to Prof. Ferry Ossendorp, Dr. Marieke Herbert-Fransen, Prof. Alexandre Bonvin, Dr. Markus Weingarh and Dr. Renko de Vries who shared their professional experiences in this book and elevated my knowledge by their guidance. Dear Markus, you are definitely one of the most important collaborators that I have ever had. We have had a fruitful collaboration which led to a worthwhile publication. I hope we can continue our collaboration in future.

A special thanks to Meriem Bourajjij. Dear Meriem, if I know something about animal studies and in vivo experiments all are just because of your kind and professional help. You gave me useful comments for research and personal life. I wish the bests for you.

I would also like to express my gratitude to Prof. dr. Dinarvand and Prof. dr. Atyabi for their encouragement and constant help in these years..

Dear Dr. Rene van Nostrum ,Dr. Robert Jan, Tina Vermonden, Dr. Herre Talsma, I would like to thank you for the constructive discussions, comments and suggestions.

I would like to acknowledge my students that helped me to shape this thesis. Dear Mathias, Antonio, Michael, Ali and ludwijn thank you for your efforts and continually challenging me that pushed me to learn more. I wish the bests for you all.

I would like to thank all my Iranian friends in Utrecht, who made my life joyful far away from my family. Ali,Mehrnoush, Artina, Abtin; Amir, Fariba, Yasamin, Aryana; Hamid, Soulmaz; Mojtaba, Mahyar; Ali, Mohadeseh, Mohammad Reza and Sadra; I will never forget your kindness and hospitality particularly our joyful Iranian parties. Dear Yaser and Neda, many thanks for your help and support. I had very pleasant moments and talks with you. Dear Kamal and Vida, my youngest friends, many thanks for helping me to prepare this thesis. I wish best for you all.

I would like to extend my thanks to other Iranian friends and colleagues; Hamed, Neda(k), Negar, Niloufar, Shima, Marziah, Nahid, Massoud, Fatemeh and Maryam(f) (My sisters). I had a great time with you in these years.

A heart-felt thank you goes to Payman, Nazanin, Arash, Sohail and Nafiseh for their invaluable friendship and unconditional help, always. I, together with Farshad, had very pleasant moments with you. I cannot forget our trip to the Switzerland. Cheers!

Thanks to my Chinese friends in Utrecht (Yang, Sun, Jia, Jian and Jason) for the many pleasure time we spent together and help you gave me.

It is a pleasure to thank many of my colleagues at Utrecht Univesrity Merel, Filis, Erik (T&O), Markus, Amir (V&G), Isil, Albert, Sytze, Audrey, Luis, Andhyk, Burcin, Kristel, Dandan and Yinan, Jan Jaap, Amr, Anna,Yvonne, Edu, Bo, Luann, Feilong, Jos, Mohammad, Maripaz, Maarten, Grzegorz and Kimberley for the nice talks and good times. I wish you all the Bests.

I most want to thank my best friend Farshad for his kind heart, generosity, all the meaningful moments, laughs and fun we had together. Dear Farshad, thanks for sharing with me all the ups and down of these years, all dinners and our endless chats. Our discussions helped me to sharpen my arguments and have improved the content of my reports and this thesis in every aspect.

I would like to express my profound gratitude to my big family Mazdak, Laleh, Mani, Mehrad, Mehrzad, Mahrokh, Massoud, Mahan, Amir Ali, Maryam, Samar, Maral, Reza and Neda for their love, support and especially their understanding. Hopefully I will be able to make it up to you someday.

I would like to thank my parents-in-law and my wife's grandparents for their support. During these years you have shown your dignity by your help, support and patience. Amo Akbar, khale Eli and Neda Joon, thank you for all support and help during these years, and I hope I will be able to make it up to you someday.

The degree to which I am indebted to my parents is quite impossible to express. I am deeply grateful to them for supporting me whenever and wherever, both mentally and financially, and for always guiding me with some wise words. I sincerely hope that you will remain to be around for many, many more years.

Most importantly, I owe unending thanks to my wife Azita for all her love, backing and encouragement without which I would not have accomplished that what I have today.

Dear Azi, No words express how grateful I am for your love and how very much I love and appreciate you. I've been far from you for more than 4 years but every second you have been in my heart. Thanks for everything my wife/friend and professor.

Finally, I would like to thank everybody who was important to the successful realization of thesis, as well as expressing my apology that I could not mention personally one by one.

Thank you all for everything.

Mazda

Curriculum Vitae

Mazda Rad-Malekshahi was born on the 19th of September 1981 in Kermanshah, Iran. After finishing high school, in 2000, he was admitted at faculty of Pharmacy of Tehran University of Medical Sciences. He obtained his Pharmacy Doctorate degree (PharmD.) in 2007 after defending his thesis under the supervision of Prof.dr. R. Dinarvand. After 3 years working in public and hospital pharmacies as well as the R&D department of Rose pharmed Co. (Parsroos Co.). In 2010, he joined the department of pharmaceutics at Utrecht University, Utrecht, The Netherlands through an awarded scholarship funded by Iran's Ministry of Health. His PhD research was supervised by Prof. dr. Ir. W.E. Hennink and Dr. E. Mastrobattista. This book, *Self-assembled peptide nanostructures: production, structural characterization and invivo application as cancer vaccine*, is the result of his PhD research submitted in July 2015.

List of Publication:

- **Rad-Malekshahi M**, Koen M. Visscher, João P. G. L. M. Rodrigues et al. The supramolecular organization of a peptide-based nanocarrier at high-resolution (Accepted at Journal of the American Chemical Society, DOI: 10.1021/jacs.5b02919)
- **Rad-Malekshahi M**, Matthias Flement, Wim E Hennink, Enrico Mastrobattista. Optimization of the recombinant production and purification of a self-assembling peptide in Escherichia coli. *Microbial Cell Factories*, 13(1). doi:10.1186/s12934-014-0178-0
- **Rad-Malekshahi M**, Ludwijn Lempink, Maryam Amidi, Wim E. Hennink and Enrico Mastrobattista. Biomedical applications of self-assembling peptides. (submitted at Bioconjugated Chemistry)
- **Rad-Malekshahi M**, Maryam Amidi, Wim E. Hennink and Enrico Mastrobattista, Ferry Ossendorp. Self-assembled peptide nanoparticle as therapeutic vaccines: in vivo evaluation in 2 tumor models.(Under preparation)
- Ebrahimnejad P, Dinarvand R, Sajadi A, Jaafari MR, Nomani AR, Azizi E, **Rad-Malekshahi M**, Atyabi F. Preparation and in vitro evaluation of actively targetable nanoparticles for SN-38 delivery against HT-29 cell lines. *Nanomedicine*. 2010 Jun;6(3):478-85.
- Esmaeili F, Hosseini-Nasr M, **Rad-Malekshahi M**, Samadi N, Atyabi F, Dinarvand R., Preparation and antibacterial activity evaluation of rifampicin-loaded poly lactide-co-glycolide nanoparticles, *Nanomedicine*. 2007 Jun;3(2):161-7.
- Talasaz A.H.H., Moghadam S.H., Ghahremankhani A.A., **Rad-Malekshahi M.**, Atyabi F., Dinarvand R., In Situ Gel Forming Systems of Poloxamer 407 and Hydroxypropyl Cellulose or Hydroxypropyl Methyl Cellulose Mixtures for Controlled Delivery of Vancomycin. *Journal of applied polymer science* 109 (4), 2369-2374
- Farnaz Esmaeili; Mohammad Hossein Ghahremani; Seyed Nasser Ostad; Fatemeh Atyabi; Mohammad Seyedabadi; **Mazda Rad Malekshahi** ; Mohsen Amini ; Rassoul Dinarvand Folate-receptor- targeted delivery of docetaxel nanoparticles prepared by PLGAPEG-folate conjugate. *Journal of Drug Targeting*, June 2008; 16(5): 415–423